Investigation of the pyrolysis mechanism at particle level: insights into heterogeneous secondary reactions with the aid of in-situ laser-based spectroscopy

vorgelegt von
Dipl.-Ing.
Hernán Almuiña Villar

an der Fakultät III - Prozesswissenschaften
der Technischen Universität Berlin
zur Erlangung des akademischen Grades

Doktor der Ingenieurwissenschaften
– Dr.-Ing. –

genehmigte Dissertation

Promotionsausschuss:

Vorsitzender: Prof. Dr.-Ing. Dietmar Auhl
Gutachter: Prof. Dr. Frank Behrendt
Gutachterin: Jun.-Prof. Dr.-Ing. Alba Dieguez Alonso
Gutachter: Prof. Dr. Jacobo Porteiro

Tag der wissenschaftlichen Aussprache: 25. Februar 2022

Berlin 2022

Ich erkläre hiermit, dass ich die vorliegende Arbeit selbständig verfasst und keine anderen als die angegebenen Quellen und Hilfsmittel verwendet habe.

Berlin, den 3. April 2022

Acknowledgement

I would like to express my gratitude and thankfulness to those who have made the completion of this thesis possible. I would like to especially thank...

... Prof. Dr. Frank Behrendt, the supervisor of this work, for giving me the opportunity to come to the EVUR chair to do my PhD in the first place, for all the facilities, the continuous support, and the scientific freedom.

... Jun.-Prof. Dr.-Ing. Alba Dieguez Alonso for being my mentor from the very first day, for letting me know how investigation works, and for the continuous support and confidence.

... Prof. Dr.-Ing. Jacobo Porteiro for reviewing this work. A big thank you also goes to all my professors from EEI Vigo, for giving me the necessary education to overcome the scientific challenges during the completion of this thesis.

... Priv.-Doz. Dr. Andrés Anca-Couce, Dr. Norbert Lang, Prof. Dr. Jürgen Röpcke, Dr. Jean-Pierre van Helden, Dr. Frank Hempel, Dr. Corinna M. Grottola, Dr. Peter Sommersacher, Dr. Stefan Retschitzegger, for your contributions to the publications, which build the scientific basis of this thesis.

... Susanne Hoffmann, Uwe Röhr, Ines Preschel, who make this chair work every day. This thesis would not have been completed without your work.

... Marie-Theres Scharl, Eloy Coto Alfonso, Dario Faust Akl, Thomas Mouton, Fabia Herzog, and many other colleagues of EVUR, for the time we have spent learning together. Ivo Schneider, I will be ever grateful for your assistance.

... Basi, Covi, Carlos, Agos, Sandra, Ale, Lena, Jonny, Carmen, Marta, and all my friends in Berlin and Spain, for the good memories all these years.

... Most importantly, I would like to thank my family for their unconditional love and support. My heartfelt thanks also go to Paula, my life partner, who has also become part of my family. Thank you for your patience, love, and helping words.

Dedicatoria

Quiero dedicarle esta tesis a mis padres, por la educación recibida y por ser el mejor ejemplo de superación. A mis abuelos, por estar siempre presentes en la distancia, y a mis hermanas, por el amor y apoyo infinitos.

Gracias.

Abstract

Thermochemical conversion processes represent the main pathway for the conversion of lignocellulosic biomass into more useful energy sources. Among them, pyrolysis plays a key role. Its process conditions will have a major influence on the conversion efficiency and products distribution, not only of the process itself, but also of each of the other thermochemical conversion processes, such as gasification or combustion. Despite gaining great scientific relevance during the last decades, the exact pyrolysis mechanism is still unknown. Therefore, the aim of this thesis is to contribute to the better understanding of the pyrolysis process.

To this end, a particle-level reactor cell has been developed, together with the implementation of advanced laser-based spectroscopic techniques to characterize, on-line and in-situ, targeted volatiles in the pyrolysis gas stream. Infrared laser absorption spectroscopy (IRLAS) has been employed to quantitatively determine permanent gases and water vapor. Laser-induced fluorescence (LIF) spectroscopy has been applied to identify mainly aromatic compounds. Moreover, these optical methods have been combined with simultaneous on-line measurements of both mass and temperature, as well as with further characterization of pyrolysis products by means of gas chromatography, ex-situ (GC-TCD) and off-line (GC-MS).

Through this comprehensive experimental approach, the influence of transport resistances (leading to the presence of heterogeneous secondary reactions), the influence of inorganic species, as well as their synergistic influence on the pyrolysis mechanism has been investigated. Moreover, a pyrolysis particle model has been adapted to the employed experimental conditions to reveal the capabilities and limitations of both numerical and experimental results. An extensive characteriazation of pyrolysis products by means of LIF has also been performed considering different LIF-relevant parameters. Its implementation in advance computational methods is going to be crucial to explore potential improvements in both sensitivity and selectivity of this spectroscopic technique when applied to pyrolysis.

Zusammenfassung

Thermochemische Konversionsverfahren repräsentieren einen zentralen Weg für die Umwandlung von holziger Biomasse in wertvollere Energiequellen. Unter diesen Verfahren spielt die Pyrolyse eine Schlüsselrolle. Die Prozessbedingungen haben hierbei einen großen Einfluss auf die Umwandlungseffizienz und die Produktverteilung, nicht nur des Prozesses selbst, sondern auch der anderen thermochemischen Umwandlungsprozesse, wie Vergasung oder Verbrennung. Obwohl die Pyrolyse in den letzten Jahrzehnten große wissenschaftliche Bedeutung erlangt hat, ist der genaue Mechanismus noch immer unbekannt. Ziel dieser Arbeit ist es daher, einen Beitrag zum besseren Verständnis des Pyrolyseprozesses zu leisten.

Zu diesem Zweck wurde eine Reaktorzelle auf Partikelebene entwickelt. Zudem wurden laserbasierte Spektroskopietechniken eingesetzt, um flüchtige Bestandteile im Pyrolysegasstrom online und in-situ zu charakterisieren. Die Laserabsorptionsspektroskopie im nahen Infrarot (IRLAS) wurde zur quantitativen Bestimmung von Permanentgasen und Wasserdampf eingesetzt. Daneben wurde laserinduzierte Fluoreszenzspektroskopie (LIF) zur Identifizierung hauptsächlich aromatischer Verbindungen eingesetzt. Darüber hinaus wurden diese optischen Methoden mit simultanen Online-Messungen von Masse und Temperatur, sowie mit einer weiteren Charakterisierung der Pyrolyseprodukte mittels Gaschromatographie, ex-situ (GC-TCD) und off-line (GC-MS) kombiniert.

Durch diesen umfassenden experimentellen Ansatz wurde der Einfluss von Stofftransportlimitierungen (die zu heterogenen Sekundärreaktionen führen), der Einfluss anorganischer Spezies, sowie deren synergistischer Einfluss auf den Pyrolysemechanismus untersucht. Darüber hinaus wurde ein Pyrolysepartikelmodell an die verwendeten experimentellen Bedingungen angepasst, um die Möglichkeiten und Grenzen sowohl der numerischen als auch der experimentellen Ergebnisse aufzuzeigen. Eine umfassende Charakterisierung der Pyrolyseprodukte mittels LIF wurde ebenfalls durchgeführt, wobei verschiedene LIF-relevante Parameter berücksichtigt wurden. Die Implementierung dieser in fortschrittliche Berechnungsmethoden, wird entschei-

dend sein, um potenzielle Verbesserungen sowohl der Sensitivität als auch der Selektivität dieser spektroskopischen Methode bei der Anwendung auf die Pyrolyse zu untersuchen.

Contents

List of Figures

List of Tables

Abbreviations

AAEM	alkali and alkaline earth metals
BTX	benzene, toluene, and xylene
CCUS	carbon capture, utilization, and storage
DP	degree of polymerization
EC-QCL	external cavity quantum cascade laser
FID	flame ionization detector
FTIR	Fourier-transform infrared spectroscopy
GC	gas chromatograph
GHG	greenhouse gas
HAA	hydroxyacetaldehyde
HC	heavy condensables
HMF	hydroxymethylfurfural
HPLC	high-performance liquid chromatography
HTC	hydrothermal carbonization
HTL	hydrothermal liquefaction
HTU	hydrothermal upgrading
INP	Leibniz Institute for Plasma Science and Technology
IR	infrared
IRLAS	infrared laser absorption spectroscopy
IRMA	infrared multi-component acquisition
LC	light condensables
LED	light-emitting diode
LGA	levoglucosan
LIF	laser-induced fluorescence
LII	laser-induced incandescence
LMWC	low molecular weight compound
MIR	mid-infrared
MS	mass spectrometer
NDIR	non-dispersive infrared
NIR	near-infrared

OPO	optical parametric oscillator
PAC	polycyclic aromatic compound
PAH	polycyclic aromatic hydrocarbon
PLRC	particle-level reactor cell
PM	particle matter
TCD	thermal conductivity detector
TFI	total fluorescence intensity
TGA	thermogravimetric analyzer
TUB	Technische Universität Berlin
UV	ultraviolet
UV/Vis	ultraviolet-visible

Symbols

Roman letters

Sign	Description	Unit
A	Absorbance	-
c	Speed of light	m s^{-1}
c	Concentration	mol cm^{-3}
E	Energy	J
F	Fluorescence intensity	W
h	Plank's constant	J s
l	Path length	cm
K	Instrumental factor	-
N_A	Avogadro constant	molecule mol^{-1}
P	Radiant flux (light intensity)	W
Q	Quencher concentration	mol cm^{-3}
S_n	n-th singlet excited state of a molecule	-
T	Transmittance	-
T_n	n-th triplet excited state of a molecule	-
TFI	Total fluorescence intensity	counts
v	Frequency	s^{-1}

Greek letters

Sign	Description	Unit
ϵ	Molar absorptivity	cm^3 mol^{-1} cm^{-1}
λ	Wavelength	nm
ϕ_f	Fluorescence quantum yield	-
σ	Absorption cross section	cm^2 $molecule^{-1}$
τ	Lifetime	s
τ_0	Unquenched lifetime	s

Chapter 1

Introduction

Taking urgent action to address the impact of climate change on both environment and society is one of the current major societal commitments. The global warming, with all that this entails, or the increase in both the intensity and frequency of extreme weather events are examples of the consequences that complete inaction on current greenhouse gas (GHG) emissions will have.

In order to change the course of events and combat the adverse effects of climate change, the European Union, on the basis of the Kyoto Protocol, set a series of targets in the short (2020), medium (2030), and long term (2050) for large-scale reductions in greenhouse gas emissions. The effective implementation of the legislation in different policy areas resulted in a 24% reduction compared to 1990 emission levels, meeting the 20% target set for 2020. With a view to continuing the trend, more ambitious targets were set in July 2021, increasing the GHG reduction target from 40% to 55% by 2030. By meeting these objectives, the European Union aims to become the world's first climate-neutral continent by 2050 [1].

To achieve these long-term targets and move towards a climate-neutral society, a coordinated set of efforts are needed in a wide range of key areas. Reducing GHG emissions must be addressed by aligning action in energy and industry sectors, but also in transport, buildings, or agriculture [1]. These efforts should be based, in large part, on promoting innovative low-carbon technologies, such renewable energies, both in a sustainable and efficient manner, together with the development and implementation of carbon capture, utilization, and storage (CCUS) systems.

Renewable energies contributed 19.7% of the final energy consumed in the European Union in 2019, very close to the target of 20% [2]. Furthermore, for the first time, wind and solar power generation surpassed that produced by coal [3]. To continue

this trend and in line with the growing climate ambition, which sets the 2030 target at 40% [1], it is necessary to further increase the presence and contribution of renewables-based energy in such a way that overcomes the current disadvantages compared to the use of traditional fossil fuels. For this purpose, it seems clear that, first of all, each European country should exploit its domestic renewable resources. That is, while some countries may be more suitable for solar power, others may focus on hydroelectric or wind power depending on their geographical and temporal circumstances. In fact, when both factors are favorable, renewable energy sources could be as (and more) efficient and economically competitive as fossil fuels. A great and successful example are solar energy technologies, which, together with solid industrial foundation, are now one of the cheapest technologies in terms of electricity generation [4]. Nevertheless, this also highlights one of the main problems of some renewable resources, i.e. their variable nature. This results in a large difference in energy contribution depending on the amount of sunshine for solar panels, the wind speed for wind turbines, or the level of reservoirs for hydroelectric generators. To address this problem, possible solutions may be the combination of different technologies together with the improvement of energy storage systems to meet the energy demand under different situations.

1.1 Biomass as renewable energy source

Biomass, unlike other renewable energy sources, is available worldwide and lacks many of the disadvantages previously mentioned. Its origin derives from forest, agricultural, aquatic, and waste products, allowing a wide range of possibilities for its exploitation. For centuries, its use was limited to heating and cooking purposes; however, with the development of different technologies, it is capable to generate the same products as fossil fuels, which in addition to heat and energy on demand, can also produce fuels for transportation [5, 6]. It is generally believed that fuel from biomass is renewable, however, this is not always the case if the entire life cycle is evaluated [7]. Only if all activities involved, i.e. harvesting, collection, and final processing are conducted in a sustainable manner, it can be considered CO_2-neutral and therefore one of the main energy sources to achieve the targets towards a sustainable energy supply [6, 8]. Protection of soil quality, account of emissions from forest harvesting, or specific limits on direct GHG emissions are criteria to be considered [9]. Taking into account these requirements, the energy

produced from biomass represents almost 60% of the share of renewable energies in the European Union [9].

Biomass, as primary energy source, can be converted into different forms of energy though several routes: (i) biochemical, (ii) physicochemical, and (iii) thermochemical. The initial feedstock (type, quality) and the final desired products, i.e., form of energy needed, are key factors when deciding which kind of conversion route is required [10].

During biochemical conversion, biomass is decomposed by enzymes or bacteria [8, 10, 11]. Digestion and fermentation are the main processes involved in this conversion pathway. The former can be either aerobic or anaerobic depending on the presence or absence of oxygen, respectively. During aerobic digestion, CO_2, water, heat, and a solid digestate are produced by microorganism when mixed under sufficient oxygen [8, 11]. During anaerobic digestion, however, biomass is converted mainly into CH_4 and CO_2 together with small quantities of other gases (biogas) [8, 10, 11]. Fermentation is widely used to produce bioethanol from sugar and starch crops [10]. Enzymes are employed to convert the initial feedstock into sugars; other microorganisms (such as bacteria or yeast) are used to further convert these sugars into ethanol [10]. Even though fermentation represents one of the most commercially competitive routes for biomass conversion into transport fuels, its production competes directly with food (first generation biofuels) and, taking into account the whole life cycle assessment, often exceeds the emissions of traditional fossil fuels [12]. Similar drawbacks present physicochemical conversion routes to produce vegetable oil from food crops [10]. To address this issue, second, third, and fourth generation biofuels come into play. Lignocellulosic biomass conversion (second generation) through biochemical processes such as fermentation, however, requires either acid or enzymatic hydrolysis pretreatment due to the long-chain polysaccharides. This fact turns this technology to be more complex and therefore more expensive, hindering its competitiveness in the energy market [8, 10]. Both third (biomass derived from algae) and fourth (genetically modified algae) generation biofuels do not currently represent a commercially competitive option [13].

Therefore, different conversion processes are needed in order to optimize both sustainability and conversion efficiency from biomass derived from lignocellulosic materials. This type of biomass includes residual parts of crops (e.g., rice husk, almond shell), agricultural residues (e.g., wheat straw, switch grass) and forestry residues. For this reason, their conversion into different forms of more useful energy is a so-

lution, not only for the substitution of fossil fuels and the reduction of greenhouse gas emissions, but also for the treatment and processing of organic residues.

1.1.1 Thermochemical conversion processes

Thermochemical conversion processes meet the needs required to convert lignocellulosic biomass into other valuable forms of energy. The selection of the appropriate process allows the production of different types of fuels (solid, liquid, or gaseous) that are suitable for subsequent heat and power generation or further upgrading into transport fuels. Unlike the biochemical conversion pathway, which is based on biomass decomposition by microorganisms, the thermochemical conversion requires high temperatures and/or pressures in order to break the chemical bonds of biomass macromolecules. For this reason, these processes are much faster than biochemical degradation.

The main thermochemical conversion processes are pyrolysis, gasification, combustion, liquefaction, and hydrothermal carbonization.

Pyrolysis is the thermal degradation of biomass in the absence of an oxidizing agent, usually at temperatures between 250 - 650 °C [6, 8, 14]. Exceptions can be made by introducing a limited supply of oxygen (normally referred to as oxidative pyrolysis) to provide part of the thermal energy needed to maintain the process, making it allothermal [6], but without allowing gasification to any appreciable degree [14]. By controlling the process parameters, such as heating rate or temperature, pyrolysis can be employed for the production of bio-oil, which can be further upgraded into liquid transport fuel [14], and the production of biochar, for soil amendment purposes [6, 14]. Permanent gases, including light hydrocarbons, are also products of the pyrolysis process and can be used for heat and power generation [8], however, nowadays the goal is maximizing either the solid or the liquid product.

Gasification is the thermal degradation of biomass in the presence of a controlled supply of an oxidizing agent, such as air, CO_2, or steam, at temperatures higher than 700 °C. As defined by the word itself, the final objective is to convert biomass into gaseous products. The desired products are mainly CO and H_2 (usually referred as syngas), however, CO_2, CH_4, and H_2O are also present. Besides the production of syngas for further post-processing in methanol synthesis or the Fischer-Tropsch process [11], the producer gas can be directly burned in gas turbines and engines for heat and power generation [6, 8]. Tar (heavy hydrocarbons and oxygenated compounds), char, and ash are also produced, although in smaller quantities. Due to undesired tar

byproducts (usually aromatic hydrocarbons), a cleaning and conditioning process of the producer gas is necessary for its subsequent use.

Combustion is the complete oxidation of biomass. Unlike pyrolysis and gasification processes, combustion is highly exothermic and its purpose is therefore direct heat production. The combustion of biomass produces hot gases at temperatures between 800-1000 °C that can be also employed to produce power by generating steam and through its subsequent use in a steam turbine [8,10]. The latter has been demonstrated to be a well established technology even for large-scale applications [6]. For small-scale applications the produced gases can be used as energy source for an organic Rankine cycle or a Stirling engine [6,8,10].

Liquefaction or hydrothermal liquefaction (HTL) is the direct conversion of biomass into liquid fuels under a wet atmosphere. Therefore, no drying of the initial feedstock is needed. This process takes place at moderate temperatures (300-350 °C) and high pressures (120-200 bar) [11]. Direct liquefaction is usually related to high hydrogen partial pressures [10,15] and the presence of a catalyst to enhance the conversion efficiency [8,15]. Hydrothermal upgrading (HTU) is also defined as the direct conversion of biomass into the liquid phase but without hydrogen [10]. The oxygen content in the final product has to be taken into account and removed in order to produce high quality liquid fuel [15].

Hydrothermal carbonization (HTC) is the conversion of biomass into solid carbon fuels. This process is realized at moderate temperatures (180-220 °C) and saturated pressure to biomass which is suspended with water [16]. As for hydrothermal liquefaction, no drying of the initial feedstock is needed. Its use may be interesting for biomass with lower quality, such as high moisture, heterogeneity, and therefore low calorific value [16]. The ratio biomass to water is a key parameter that must be kept relatively high to improve the selectivity of the process [16].

As it can be observed, there are several options for the conversion of biomass into various forms of energy on small, medium, and large scales. Each process is aimed at maximizing solid, liquid, or gaseous products depending on their subsequent application, i.e., heat and power generation, upgrading into transport fuels, or chemicals synthesis. Thermochemical conversion processes represent, moreover, both the present and the future in terms of lignocellulosic biomass exploitation, which, as explained above, must be prioritized over other sources that may compete with food crops. However, there is still a need for a continuous improvement in terms of conversion efficiency and sustainability, as well as ensuring economic competitiveness with other more conventional technologies. Clearly, this has to go hand in hand

with policy measures to ensure that renewable energies can continue to thrive, with financial support in science and research to achieve a high degree of technological development.

This work is focused on investigating the pyrolysis of woody biomass. This process is key in the thermochemical conversion pathway since it can be treated as a process in itself, as explained above, but also represents a fundamental stage in the other conversion technologies, e.g., gasification, combustion, or HTC. Conversion efficiency, product yields, and contaminant emissions will strongly depend on the way in which the pyrolysis step occurs [6, 17]. Therefore, its correct understanding is fundamental to optimize these processes.

To this end, the state of the art concerning the pyrolysis process is discussed in Chapter 2, with particular attention on the kinetic mechanism and presenting the open questions that need to be investigated in order to reach a better understanding of the pyrolysis process. Furthermore, an overview of the employed methods for volatiles characterization is also introduced, with special emphasis on the online and in-situ implementation of advanced laser-based spectroscopic techniques, whose successful application represents a major novelty and breakthrough in the field of pyrolysis. In Chapter 3, the motivation for this work is explained in a more concrete way and according to the open research questions presented in Chapter 2. In addition, a list of the published works is presented, specifying the work performed in each one of them, which allowed to build the scientific basis of this thesis. The results obtained, all of them published in peer-reviewed journals, are presented from Chapter 4 to 7. Chapter 8 presents an article which is in preparation for submission, and Chapter 9 current work in progress.

Chapter 2

State of the art

2.1 Pyrolysis

Pyrolysis is the thermochemical decomposition of biomass in the absence of an externally supplied oxidizing agent typically at temperatures between 250-650 °C. During pyrolysis, the long-chain macromolecules of biomass are broken down into smaller molecules of liquid (at ambient conditions) and gas products, formed together with a carbonaceous solid product called char [14]. The distribution of these products will be strongly determined by the process conditions and can be optimized depending on its subsequent application. For instance, moderate temperatures and short residence time of volatiles in the reaction zone will maximize liquid yields [18]. On the contrary, long residence times will favor: (i) char yields at low temperatures [14], and (ii) gas yields at high temperatures [14]. When treated as a process itself, and with a view to more commercial and economically competitive applications, pyrolysis can be employed to produce either bio-oil, by prioritizing liquid products, or biochar, by maximizing the solid yield. Furthermore, as previously mentioned, pyrolysis is also an essential stage in other thermochemical conversion processes, such as gasification, combustion, or hydrothermal carbonization, and will influence their products quality and distribution, conversion efficiency, and pollutant emissions [6, 17, 19]. A deep understanding of the pyrolysis process will help the further development and optimization of the thermochemical conversion of biomass to be implemented in reactor design and scale-up into commercial-scale applications [8, 20]. For this reason, a complete and detailed description of the pyrolysis mechanism is essential, which, nowadays and in spite of gaining great scientific relevance in recent years [20], is still unknown.

The following section will define each of the pyrolysis products and their prioritization according to the type of process used. The large number of species involved in the pyrolysis process, together with the heterogeneity and complexity of their chemistry, is one of the main factors that hinders its correct understanding. Therefore, a proper definition and classification is necessary for the development of a model that can accurately predict the products yields and composition for the subsequent process optimization.

2.1.1 Pyrolysis products

The products of pyrolysis can be clustered into char, tar, and gases.

Char is carbonaceous and porous material representing the solid fraction of biomass pyrolysis. It is mostly composed of carbon, but it can also contain oxygen and hydrogen [14]. Moreover, ash-forming compounds such as sulphates, carbonates, silicates, or phosphates, are also present [8]. The composition and structure of char will strongly depend on the initial feedstock, especially in terms of ash content, and the process operating parameters, such as temperature, heating rate, residence time, or pressure. However, the maximum temperature to which biomass is subjected will be one of the most important parameters determining its physical and chemical characteristics [21, 22]. With increasing temperature, the carbon content will increase at the expense of oxygen and hydrogen [22] increasing therefore the energy density. A decrease of oxygen-containing functional groups will occur together with a change from an aliphatic to a more aromatic structure [8]. The surface area tend to increase reaching its maximum (300-500 m^2/g depending on the biomass type) at temperatures between 700-800 °C [8, 21]. At higher temperatures, the solid starts to shrink and changes to a more graphite-like structure, thus reducing its porosity [8, 22].

Tar is a concept whose definition is challenging. Usually, in the field of pyrolysis, it is referred to organic compounds that are liquid at ambient temperature. It encompasses a large number of species, in the range of several hundred, with very complex chemistry [21, 23]. As reviewed by Anca-Couce [8], these products can be clustered into different groups depending on their chemical structure and functional groups:

- **Sugars** are carbohydrates, usually with higher molecular weight than compounds from other groups, that are produced from cellulose (e.g., levoglucosan) and hemicellulose (e.g., xylose).

- **Carbonyls** are organic compounds with a carbon atom double bonded to an oxygen atom (C=O). This includes ketones (R-C(=O)-R), aldehydes (R-C(=O)H), and carboxylic acid (R-C(=O)OH) moieties.
- **Alcohols** are organic compounds with a carbon atom bonded to a hydroxyl functional group (-OH).
- **Heterocyclic** are cyclic compounds that have at least two different elements as part of its ring. In pyrolysis, they are usually furanic compounds with one oxygen atom.
- **Phenolics** are organic compounds with a hydroxyl group (-OH) attached to an aromatic ring. Species with methoxy moieties (-O-CH_3), such as guiacols and syringols, are also common. They are mainly produced from lignin.
- **BTX and PAHs** are aromatic compounds with single ring (benzene, toluene,xylene) or multiple rings (e.g., naphthalene, phenanthrene). They are mainly produced from lignin, although they can also be produced during secondary decomposition of cellulose and hemicellulose.

In addition to the listed groups, **water vapor**, as a pyrolysis product (i.e., not water from drying), has to be taken into account. It may not be considered as a tar product itself, but as a part of the liquid products.

A different classification was made by Evans and Milne [24–26], more based on the process rather than chemistry, in which the different tar compounds are divided into primary, secondary, and tertiary tars. This classification was given according to the origin of each of the compounds in terms of the way in which they are produced. That is, primary tars are organic species that are produced from the primary decomposition (depolymerization) of cellulose, hemicellulose, and lignin [8]. Those can be sugars, deriving from the cellulose and hemicellulose structure, or phenolics, mostly guaiacols and (in the case of hardwood) syringols, coming from the aromatic structure of lignin [8]. Carbonyls and heterocyclic compounds coming from ring opening reactions and the cleavage of side branches are also included in this group. Furthermore, sugar or phenolic oligomers are also considered as primary tars. These compounds deriving from primary pyrolysis, depending on several process conditions (e.g., residence time, pressure), may undergo secondary decomposition either through heterogeneous (in the solid matrix) or homogeneous (in the gas-phase) tar cracking reactions. The latter are reported to be relevant above 500 °C [8, 27]. A schematic representation, based on [14], is presented in Fig. 2.1.

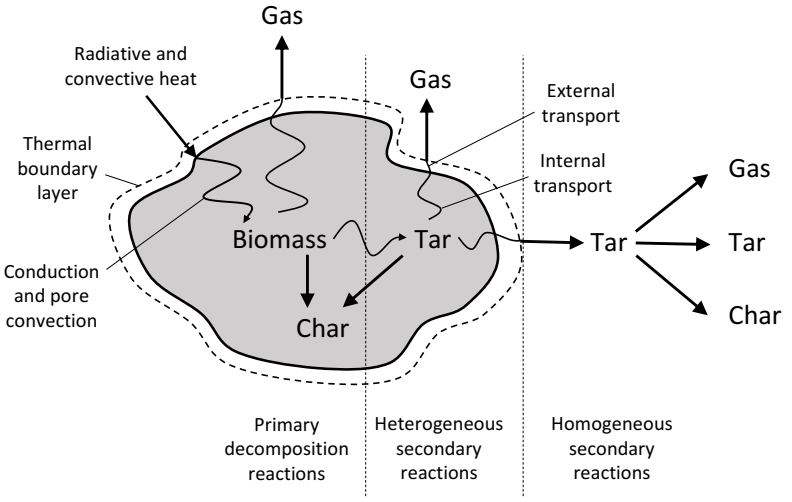

Figure 2.1: *Schematic representation of pyrolysis in a biomass particle (based on [14]).*

After the secondary decomposition of primary tars to form secondary tars, these may further react to form tertiary tars. The latter are reported to be aromatic compounds, such as PAHs and BTX [24]. These are mostly produced at high temperatures (> 700 °C) [21], however, in smaller quantities, they can be produced at lower temperatures (< 500 °C) from hollocelulose and lignin under conditions enhancing the presence of secondary reactions [6, 28–30]. Secondary tars are intermediates between primary and tertiary tars [8, 24]. They usually come from lignin decomposition, since primary tars from cellulose and hemicellulose tend to crack into permanent gases [8]. Examples are phenol or cresol, after demethoxylation of primary phenolic compounds (i.e., guaiacols, syringols) [24–26].

Gas species are mainly composed of CO_2, CO, CH_4, and H_2. In smaller quantities also other light hydrocarbons, such as ethane and ethylene, are produced. These non-condensable gases can be generated from primary or secondary decomposition [14]. However, different gas compounds are produced from heterogeneous or homogeneous secondary reactions. While mainly CO_2 (together with smaller quantities of other gases) is produced from heterogeneous secondary reactions, CO and H_2 are mostly formed at higher temperatures from homogeneous gas-phase reactions [8].

As previously stated, by optimizing and controlling the process parameters, different types of products can be prioritized. Maximum temperature, heating rate, pressure, and residence time of the volatiles in the reacting zone are key factors defining the products distribution. Usually, the different pyrolysis processes are classified in terms of the applied heating rate, however, other parameters such as residence time also go hand in hand and are fundamental in determining the desired product.

- **Slow pyrolysis** is characterized for slow heating rates (1-100 °C/min). It is the oldest technology in the pyrolysis field [14] and the typical process in order to maximize the solid product (charcoal) [6, 14]. For this reason, long residence times (from several minutes to hours [14, 21]), to enhance charring reactions at the expense of tar products, and low temperatures (< 500 °C), to avoid further decomposition of the char, are employed. If its purpose is to be redirected to the soil for amendment by improving its long-term properties and for carbon sequestration, then it is usually referred to as biochar [6, 8].

- **Conventional pyrolysis** is performed at moderate heating rates (up to 300 °C/min) and mild temperatures (around 600 °C). The residence time of the volatiles in the reacting zone is in the order of several minutes. This process encompasses all three types of products (char, liquid, and gas) [14].

- **Fast pyrolysis** is performed at fast heating rates (up to 1000 °C/min). It is employed to maximize the liquid product, therefore, short residence times (0.5 - 2 s), mild temperatures (up to 550 °C), and rapid quenching of the products are needed in order to avoid secondary tar cracking reactions [6, 14]. This liquid product, usually referred to as bio-oil, can be further upgraded into transport fuels or directly employed for heat or power generation [6, 8].

- **Flash pyrolysis** is characterized for very fast heating rates (> 1000 °C/min) together with high temperatures (900-1300 °C/min) [21]. Due to the high reaction temperatures, secondary tar cracking reactions together with further char devolatilization are enhanced, maximizing therefore gases at the expense of liquid and solid products.

It is clear, as explained so far, that a correct selection of the parameters in the pyrolysis process is fundamental to determine products yields and distribution. However, there is another factor that, although not as influential, must also be considered: biomass composition. Biomass encompasses a wide range of different feedstocks. Its composition will vary depending on several aspects and will affect the complex chemical reaction network deriving in different final yields [20]. For instance, biomass with a high lignin content will produce more char, while another with high cellulose content will yield higher liquid products (e.g., sugars) and produce less char. In the following section each of the components of which the biomass is composed will be defined.

2.1.2 Biomass composition

Biomass has a complex structure, and its correct characterization is challenged by the wide heterogeneity of the feedstock [7, 20]. Lignocellulosic biomass can be classified mainly into agricultural and forestry residues. The former consists of residual parts of crops or agricultural by-products such as rise husk, wheat straw, or almond shell. Herbaceous biomass such as switchgrass or miscanthus may also be clustered in this group [7]. Forestry biomass, also referred to as woody biomass, is formed from branches, chips, or foliage from any kind of wood species. At the same time, it can be divided into hard- and softwood. Hardwood originates from angiosperm trees (beech, oak wood) or flowering plants [8, 20]. Generally, it is more dense and its structure more complex than that of softwood [20]. Softwood includes gymnosperms tree (spruce, pine wood) or non-flowering plants [8, 20].

Lignocellulosic biomass is formed of three main macromolecules: cellulose, hemicellulose, and lignin. Moreover, it also contains smaller amounts of other organic substances (extractives) and inorganic species. The composition of biomass is highly variable and depends on several factors. Although the most important is the type of biomass (for instance, herbaceous vs woody biomass, hard- vs softwood), other factors such as growth process and conditions, soil characteristics, age of plants, or harvesting and collection processing may also influence [7]. A schematic representation of the main macrocomponents in lignocellulosic biomass is presented in Fig. 2.2.

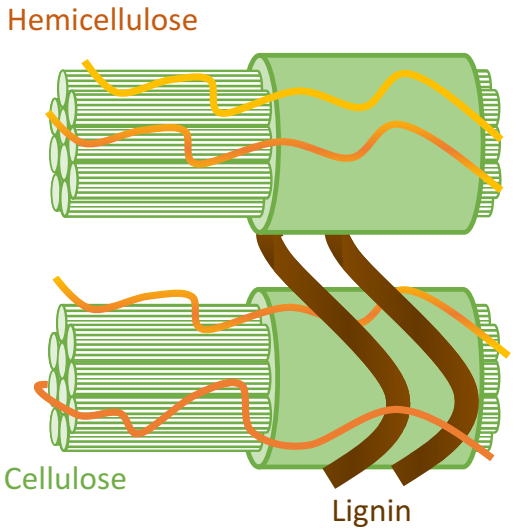

Figure 2.2: *Schematic representation of the main macromolecules in plant cells (hemicellulose, cellulose, and lignin).*

Cellulose is a macromolecular polysaccharide consisting of a liner chain of D-glucose units liked to each other by $\beta(1\rightarrow4)$ glycosidic bonds. Its chemical formula is $(C_6H_{10}O_5)_n$, as shown in Fig. 2.3. It typically has strong crystalline structure, due to the tendency to create intra- and intermolecular hydrogen bonds, and a high degree of polymerization (DP or number of units), in the range of 10.000 [8]. The content of cellulose in lignocellulosic biomass is in the range of 40-50 wt.% [31].

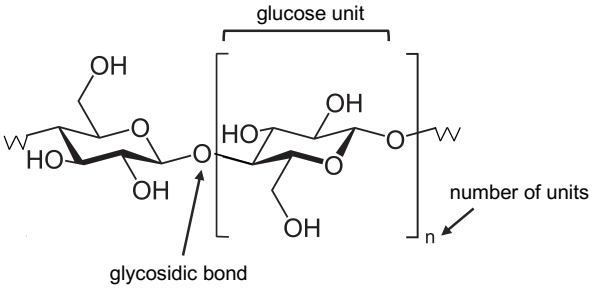

Figure 2.3: *Structure of cellulose*

Hemicellulose is a heteropolysaccharide with an amorphous and more complex structure than that of cellulose [20]. It is mainly formed of hexose sugars (glucose, mannose, galactose, or glucuronic acid) and pentose sugars (xylose and arabinose) with a low number of units, in the range of 50-200 [8, 20, 32]. Due of its heterogeneity together with the insufficient isolation techniques, it is necessary to select a representative compound which is not always able to fully describe its pyrolysis behavior [33]. In the case of hardwood, the most widely used compound is xylan, a polymer formed mainly of D-xylose linked by $\beta(1\rightarrow4)$ glycosidic bonds, as shown in Fig. 2.4. In the case of softwood, glucomannan, a polysaccharide composed mainly of D-mannose and D-glucose sugars, is usually selected as representative compound [8]. The content of hemicellulose in lignocellulosic biomass is in the range of 15-30 wt.% [8, 20, 31].

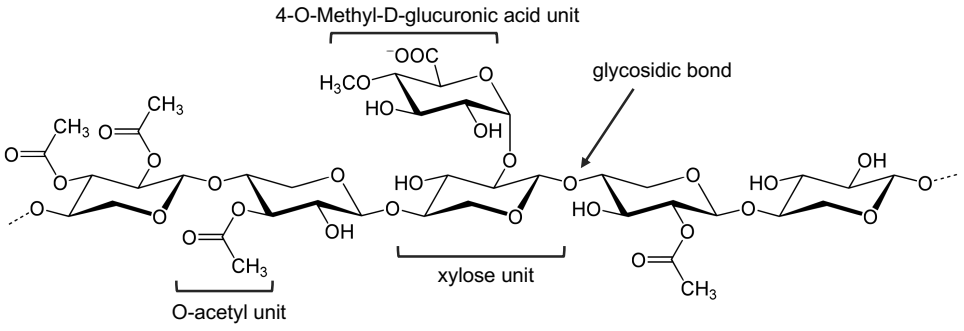

Figure 2.4: *Structure of xylan (representative compound of hemicellulose from hardwood).*

Lignin structure is much more complex than the aforementioned polysaccharides, being a racemic heteropolymer consisting of hydroxycinnamyl alcohol monomers with different degree of methoxylation [34]. The main monomer units are p-coumaryl, conyferyl, and synapyl alcohol, represented in Fig. 2.5. Due to the lack of synapyl units in softwood (contrary to hardwood), no syringols are produced [8,20]. The different monomers are liked to each other through ether (C-O-C), carbon-carbon (C-C), or ester bonds, although the latter is very scarce and found mainly in herbaceous biomass [20]. Hardwood contains more ether bonds than softwood, being carbon-carbon bonds more present in the latter [20]. Such differences strong influence their pyrolytic behavior, with hardwood lignin tending to be more reactive due to the lower thermal stability of ether bonds [20]. The different isolation methods are reported to affect, inevitably, its chemical structure, being therefore its physical and chemical properties strongly influenced by this stage [8, 35, 36]. Alkali lignin is usually employed as model compound due to its mild isolation technique [36], however, other works did also employ organosolv or milled wood lignin [35, 37–39]. The content of lignin vary depending on the type of biomass, while hardwood contains between 18-25 wt.%, softwood can reach up to 35 wt.% [31, 32].

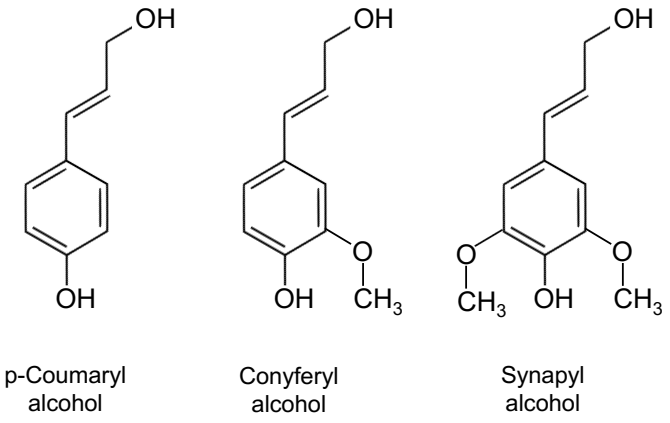

Figure 2.5: *Different types of lignin monomers [8, 23].*

Extractives are organic compounds present in lignocellulosic biomass in lower amounts in comparison to the three main macrocomponents. They can be divided in hydrophobic and hydrophilic depending on their solubility in low-polarity solvents (such as haxane or toluene) and high-polarity solvents (such as water or ethanol), respectively [40]. Hydrophilic are mostly formed of phenolic compounds and hydrophobic of terpenes and fatty acids [21,40]. The content of extractives can slightly differ depending on the type of biomass, but is usually less than 10 wt.% [31, 40].

Inorganics are ash-forming species and represent the largest heterogeneity in terms of biomass composition [7]. Although the amount of ash in wood is generally less than 1% [8], it can range from 0.1% - 20% depending, not only on the type of biomass (woody or herbaceous), but also on other factors such as soil or environmental characteristics [7,21,41]. Most of inorganic constituents (> 90%) are found in water-soluble or ion-exchangeable form [8, 41], being calcium, potassium, magnesium or sodium (i.e., alkali and alkaline earth metalss (AAEMs)) the most abundant ones [7, 8, 21, 41].

The characterization of biomass according to the relative proportion of its different components (i.e., hemicellulose, cellulose, lignin, extractives, and inorganics) is essential for a complete understanding of the pyrolysis mechanism to the point of being able to describe the pyrolytic behavior of biomass through the individual behavior of each of them [8, 20, 32]. In fact, the most detailed reaction mechanisms so far are based on the decomposition mechanism of hemicellulose, cellulose, and lignin assuming no interaction between them [8, 34, 40, 42–45].

It must be pointed out, however, that several works have highlighted the existence of such interactions and their influence on products yields and distribution [8,20,46–49]. Generally, an increase of low molecular weight compounds (LMWCs) has been reported in both cellulose and lignin decomposition [46–49]. With respect to the pyrolytic behavior of cellulose, cellulose-lignin interactions have been reported reported to suppress the tendency for thermal polymerization of macromolecular products [20, 46]. Furthermore, cellulose-hemicellulose interactions have been reported to increase the yields of hydroxyacetaldehyde (HAA) [47] and furans [48], at the expense of sugars formation, such as levoglucosan [47, 48]. Other works, however, reported no significant interaction between cellulose and hemicellulose [49]. With respect to lignin decomposition, it has been shown that, in the presence of the other two polysaccharides, more phenolic compounds are produced [46, 48] at the expense of char [46] and hydrocarbons formation [48].

Although the influence of these interactions has been demonstrated, to date there is no clear consensus and the exact mechanism of interaction is still unknown [20]. Pyrolysis mechanisms based on the absence of such interaction, despite not being strictly correct, usually achieve better results than others describing biomass as a single component [6] especially because of their more accurate products characterization [6, 8]. Consequently, the following section focuses on the most detailed and promising pyrolysis mechanism so far, developed by Ranzi et al. [34], which assumes a linear combination between the three main biomass components. Furthermore,

emphasis will be placed on the main open questions that need to be investigated to contribute to the better understanding of the pyrolysis process and that have created the research basis for this thesis.

2.1.3 Pyrolysis mechanisms and open questions

Despite gaining great scientific relevance in recent years, when modeling of pyrolysis as stage in other thermochemical conversion technologies is considered, mostly global single-step models or models based on simplified competitive schemes are employed. These approaches are able to predict the characteristic time of pyrolysis and product distributions, clustered in three categories: char, tar, and gases [6, 45, 50]. These reaction mechanisms are promising because of their simplicity when coupled with single-particle models describing the different transport phenomena. In this way they can be used for scale-up, design, and optimization of reactors at the industrial level. However, they lack accuracy in determining, for example, the influence of process conditions or initial biomass properties, leading to significant qualitative disagreements on products yields and composition or char reactivity [6, 50]. Such aspects are very relevant, not only for the pyrolysis process itself, but also for other conversion processes since they affect critical sub-processes such as tar formation (critical for gasification), or particle matter (PM) (critical for combustion) [34]. This highlights the lack of a widely applicable detailed pyrolysis mechanism able to correctly predict products composition depending on both biomass properties and process conditions [45, 51].

In this context, one of the most detailed and promising competitive pyrolysis mechanism to date is the one developed by Ranzi et al. [34]. Contrary to one-component models, biomass is described based on its three main macromolecules (cellulose, hemicellulose, and lignin). Due to the complex chemical structure of lignins, in this case, and following the work by Faravelli et al. [52, 53], lignin is approximated by a mixture of three pseudo-components: LIG-C, LIG-H, and LIG-O, which represent its structure being richer in carbon, hydrogen, and oxygen, respectively [34]. As previously explained, these five reference compounds decompose independently from each other, assuming no interaction between them [34]. Up to 22 different compounds are included as products in this reaction mechanism including: the solid residue (char), water vapor, permanent gases, sugars, alcohols, carbonyls (aldehydes, ketones, and carboxylic acids), furans, and phenolics [34]. This comprehensive chemical kinetic scheme showed a good fitting with experimental results (from ther-

mogravimetric analysis and entrained flow reactor experiments) in terms of mass loss and qualitative evolution of a large number of compounds, with activation energies in accordance to those reported in literature for each of the macrocomponents [8,34]. However, some limitations were present, such as notable quantitative deviations in some products yields or the absence of other pyrolysis compounds (e.g., phenolic oligomers deriving from lignin) [8, 54]. Although the authors highlight the use of drastic simplifications due to the large number of intermediates and the complexity of the biomass characterization [34], this reaction mechanism represented a breakthrough in the development of a detailed model based on each of the biomass macrocomponents. In fact, several works further developed this mechanism in order to overcome some of the limitations and extend its applicability to a wider range of conditions [40, 42–45].

The primary pyrolysis kinetic model has been modified and extended together with the inclusion of a secondary gas-phase kinetic scheme in several works from the same group [42,43,55]. The overall kinetic scheme - when accounting for both pyrolysis and combustion of small hydrocarbons, tar, and oxygenated species - encompasses more than 450 species and around 15000 reactions [43]. One of the adaptations/validation of the pyrolysis mechanism was performed by Corbetta et al. [43] at both kinetic and particle level (results in transport-controlled regimes will be discussed later). Despite the relatively good fitting with TGA experiments in terms of mass loss and the semi-quantitative predictions achieved, the authors still highlighted the need of including heterogeneous secondary reactions in order to further improve the model [43].

In this context, Anca-Couce et al. [44], employed Ranzi's pyrolysis scheme and introduced heterogeneous secondary (charring) reactions. This was made in form of a fitting parameter, constant for all reactions, which was tested for values between 0.1 (representing low charring, i.e., kinetic regime) and 0.5 (representing high charring, i.e., particles in the cm-range) [44]. The products from these charring reactions were char, CO_2, H_2, and water. Together with an adaptation of the kinetic reaction scheme, better results were achieved especially regarding the final char yield and some volatiles groups, such as furans, carbonyls, sugars, and water vapor [44]. However, some notable errors were still present in other groups. In order to improve the accuracy of the scheme, different parameters were introduced for each of the macrocomponents. This was presented in the last version of the model [45], in which, together with improvements based on experimental results performed at medium heating rates, the char yield and on-line release of water vapor, permanent

gases (CO_2, CO, CH_4), other light hydrocarbons (C_2H_2, C_2H_4,C_3H_6, and C_3H_8) and total organic condensable species were predicted with good accuracy.

With the aim of extending the applicability of the model to a wider range of biomass types, Debiagi et al. [40] introduced two new reference compounds, complementing the five pseudo-components previously introduced. These two new components represent extractive species which, as described in Section 2.1.2, although not constituting a large part in the biomass composition, can reach up to 10 wt.% depending mainly on the type of biomass [31]. Hydrophobic (fatty acids and triglycerides) and hydrophilic extractives (phenolic compounds) are represented through the new reference species [40]. Compared to previous works, where the pyrolysis mechanism was validated mainly with woody biomass [34, 43–45], the inclusion of extractives allowed to broaden its applicability and to accurately predict the pyrolytic behavior of different biomass feedstocks. In particular, it was validated by thermogravimetric analysis of palm oil shell, wheat straw, softwood bark, and almond shell, whose compositions differ greatly from each other [40].

However, in spite of the great advances in terms of the primary kinetic scheme, secondary reactions (homogeneous and heterogeneous), and the inclusion of extractive species, as pointed out by several authors [40, 43–45], it is still necessary to include further improvements on the model, such as:

- The implementation of the influence of **inorganic species**
- The modeling of **heterogeneous secondary reactions** (instead of fitting parameters, as presented in [44, 45])
- The implementation of the formation of **aromatic species**, such as BTX and PAHs.

These highlights represent the main open questions and constitute the scientific basis of this thesis. The current state of research on the understanding of the influence of inorganics on the pyrolysis mechanism, as well as possible ways to study heterogeneous secondary reactions will be reviewed in this section. In the following section (Section 2.2), the detection and study of aromatic species will be discussed, based on advanced analytical techniques for volatiles characterization.

In order to understand the effect of **inorganic species** on biomass pyrolysis, it is important to study their influence, not only on the overall process, but also on each of the main macromolecules of which lignocellulosic biomass is composed. To this

end, the state of the art regarding the actual mechanism of each macrocomponent (cellulose, hemicellulose, and lignin) - on which the previously introduced pyrolysis mechanism is also based - will be presented, together with the influence of inorganic species on each of them.

2.1.3.1 Cellulose

As previously introduced, cellulose represents the main macromolecule of which lignocellulosic biomass is composed, accounting for up to 50 wt.% of the total mass [31]. During the last decades, its kinetic decomposition mechanism has been extensively investigated. Anhydrosugars (mainly levoglucosan (LGA)), carbonyls, and furans are the main tar products. Primary decomposition of cellulose yields low char, which can be enhanced in the presence of secondary reactions accompanied by permanent gases and water. Moreover, the products distribution is affected by the internal structure of cellulose, being higher LGA yields correlated with higher DP and higher furan yields with lower crystallinity [20]. The current understanding of cellulose pyrolysis can be found in [8], based on several schemes [41, 56–63]. A schematic representation, based on [8], also considering the influence of inorganic species (AAEM) is shown in Fig. 2.6.

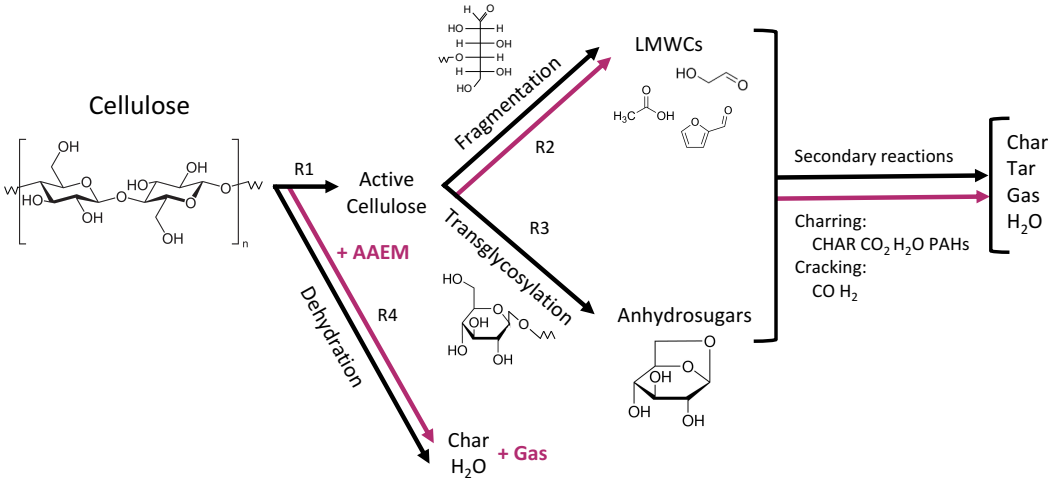

Figure 2.6: *Schematic representation of the current understanding of the cellulose pyrolysis scheme (adapted from [8]).*

Cellulose pyrolysis starts with a first depolymerization reaction (R1) in which a liquid intermediate compound (also referred to as active cellulose) is formed. The cellulose structure starts to degrade at temperatures above 260 °C [8], reducing the number of units (degree of polymerization) through the cleavage of $\beta(1\rightarrow4)$ glycosidic bonds

due to their weak linkage [20]. This preliminary reaction step was first reported by Broido in 1976 [56] and employed in subsequent schemes [34, 57–59]. However, since no volatiles are released during this stage [8], some cellulose decomposition mechanisms do not include it [44, 45, 60]. Following depolymerization, the cellulose pyrolysis scheme can be explained through a competition between two different reaction routes. The first one, fragmentation (R2 in Fig. 2.6), represents the scission of pyran rings through β-elimination, leading to the formation of low molecular weight compounds (LMWCs) and gases [8, 34, 58–60]. The second one, transglycosylation (R3 in Fig. 2.6), results mainly in LGA and other anhydrosugars [8,34,58–60]. Even though the formation of furans, included in LMWCs, was also postulated through secondary reactions of products from transglycosylation, recent findings supported their direct formation through the scission of pyran rings (i.e., through R2) and further rearrangement [21].

The existence of both competitive reaction pathways (R2 and R3), resulting in the production of LMWCs and sugars has been reported in most of the studies of the cellulose decomposition scheme. However, there are disagreements concerning the formation of char. As shown in Fig. 2.6, two different routes for char formation are generally defined. Some authors argue that char is only formed from secondary reactions within the solid matrix through repolymerization of levoglucosan and other products from the transglycosylation pathway [8, 59, 60], and also through the ring fragmentation pathway [8, 44, 59, 60]. However, other schemes do also include char from primary decomposition through dehydration reactions (R4) [34, 41, 58, 62, 64–66]. In some cases, the latter is only associated with slow heating rates and low temperatures (< 300 °C) [58, 65, 66].

The study of the influence of inorganic species on the cellulose decomposition mechanism reveals remarkable trends. Generally, it is reported that: i) it promotes charring reactions, leading to the enhancement of char yields [21, 41, 60–63, 67]; ii) it inhibits the transglycosylation reaction pathway, hindering therefore the production of anhydrosugars (such as LGA) [8,21,41,58,61–63,67]; and iii) it enhances the formation of LMWCs and gases, derived from ring fragmentation reactions [21, 59–61, 63].

The selectivity towards the ring-opening reactions pathway, enhancing the formation of LMWCs at the expense of sugars, has been first explained by Piskorz et al. [58] in a way that inorganic species might delay unzipping reactions of cellulose chain ends. This fact would inhibit the formation of LGA-ends and promote reducing-ends after the cleavage of glycosidic bonds. Cations (coming from inorganic species) would interact with the ring oxygen, leading to the formation of carbonyls and furans after

ring opening [21, 24]. In a deep insight into the understanding of cellulose pyrolysis and following the reducing- and levoglucosan-end mechanism, Mamleev et al. [60], claimed that the presence of a liquid intermediate was needed in order to promote heterolytic (ionic) reactions. This liquid intermediate, formed mainly of oligomers and high-boiling liquid products from transglycosylation, filling the cavities of the cellulose matrix, would act as an electrolyte and, together with the presence of a catalyst, could initiate and accelerate (catalyze) ionic reactions leading to the formation of LMWCs and gases after β-elimination [60]. A schematic representation of the preferred reaction pathways for cellulose pyrolysis in the presence of AAEMs is shown in Fig. 2.6. Although it seems clear that inorganic species promote the formation of char, LMWCs, and gases, there are some discrepancies as to whether these changes are due to effects on the primary decomposition mechanism, to a promotion of secondary reactions between intermediate products, or to a combination of both [41]. Therefore, in the schematic representation, both possibilities have been considered taking into account different studies from the literature [21, 41, 60–62, 67].

Besides influencing the products composition, the presence of inorganic species also affects the devolatilization rate and heat of reaction. The catalytic effect of AAEMs on the pyrolysis scheme results also in an shift of both the onset [21, 62, 68] and the maximum of cellulose decomposition towards lower temperatures [21, 68].

2.1.3.2 Hemicellulose

Contrary to cellulose pyrolysis, information regarding the pyrolysis scheme of hemicellulose is scarce. Due its complex and amorphous structure, it has been studied to a lesser extent. Moreover, as explained in Section 2.1.2, as result of the heterogeneity of its composition (based on pentose and hexose sugars), together with the insufficient isolation techniques, it is usually required to select a representative compound which cannot fully describe its pyrolysis behavior [33]. Xylan, a polysaccharide based on pentose (xylose) sugars, has been usually employed to model hemicellulose pyrolysis (e.g., [34, 44]). However, although it may be representative for hardwood hemicellulose, it does not properly describe the pyrolytic behavior for softwoods [8]. In fact, glucomannan, a polysaccharide based on hexose (manose and glucose) sugars, should be selected as representative compound of hemicellulose from softwoods. Although the products composition is similar from a qualitative perspective regardless of the type of monosaccharides present in the hemicellulose structure, their relative composition may differ [21]. Furans (mainly furfural), ketones (mainly 1-hydroxy-2-propanone and furanone), and anhydrosugars are the main tar products [20, 21].

Moreover, hexose sugars also produce hydroxymethylfurfural (HMF) [8, 20, 20, 21]. Other moieties such as acetyl groups or uronic acids mainly produce carboxylic acids (formic and acetic acid) and CO_2 [21]. A schematic representation of the actual understanding of hemicellulose pyrolysis is shown in Fig. 2.7, adapted from [34], and based on other works from the literature [21, 44, 69, 70].

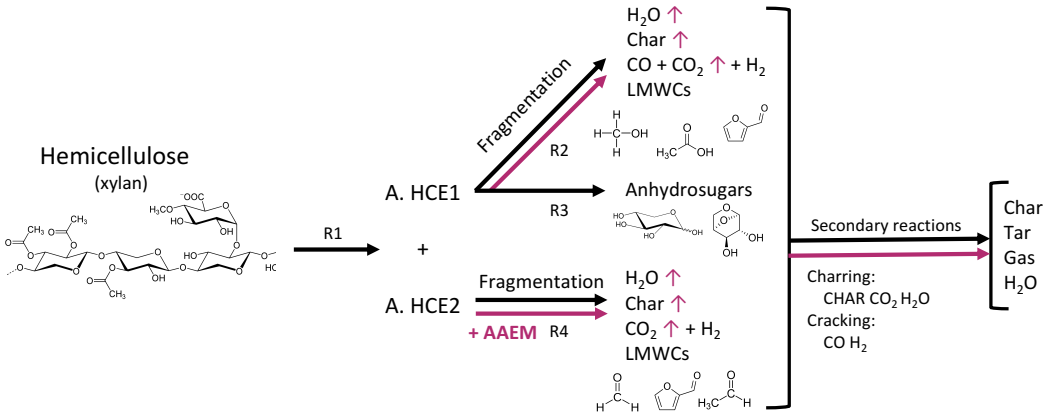

Figure 2.7: *Schematic representation of the current understanding of the hemicellulose pyrolysis scheme (based on [34]).*

Due to its similarity with cellulose, its pyrolysis mechanism can also be explained as a competition between sugar formation (furanose- and pyranose-ring sugars for pentoses and hexoses, respectively) and fragmentation reactions [8, 33, 69]. However, it is usually described as a two-step mechanism [34, 44, 70, 71]. In the kinetic scheme developed by Ranzi et al. [34], hemicellulose decomposes first into two different forms of active hemicellulose, analogous to the formation of the liquid intermediate in cellulose pyrolysis (active cellulose). The two active forms of hemicellulose (A. HCE1 and A. HCE2 in Fig. 2.7) decompose successively, reproducing the two-step decomposition previously introduced [34, 44]. The first active hemicellulose, similar to cellulose pyrolysis, decomposes through a competition between two different reaction pathways [34, 44]. One (R2) leading to the formation of char and LMWCs, products from fragmentation reactions (i.e., ring-opening), and the other one (R3) resulting in the formation of anhydrosugars (usually 1,4-anhydropentoses or 1,6-anhydrohexoses [20]). Following the decomposition of the first active cellulose, the second one would decompose into char and volatiles, similar to R2, deriving from ring fragmentation reactions [34, 44].

In experiments performed with xylan, Shen et al. [72] also relied on a two-step mechanism to explain the devolatilization process, which was clearly differentiated by the presence of two distinct peaks in the devolatilization rate curve. The first peak

was reported to be related to the cleavage of glycosidic bonds and side chains moieties (such as 4-O-methylglucuronic acid and O-acetyl units [72]), thus accompanied by sugars, LMWCs (such as acetic acid), and gases. The second peak was attributed to further fragmentation reactions [72, 73]. This work is also in good agreement with recent results from Zhou et al. [69]. In this case, the formation of sugar-intermediates was confirmed, followed by the formation of char, LMWCs (such as furans and carbonyls), and gases, together with the further decomposition of sugar-intermediates [69].

From a more mechanistic point of view, it was reviewed by Giudicianni et al. [21] that xylan decomposes to xyloses and anhydrosugars (e.g., 1,4-anhydro-D-xylopyranose). The former through the rupture of glycosidic bonds followed by inclusion of H^+ and OH^- (from other products already present [33]) and the latter through glycosidic bond cleavage and further rearrangement [21, 33, 72]. These intermediate products can be immediately further decomposed either via ring-opening reactions, resulting in char and LMWCs, or through dehydration, producing anhydrosugars/dianhydrosugars [21]. The formation of furans from depolymerization and dehydration (and not via fragmentation and rearrangement) has also been considered by some authors [33, 72].

Most of the studies investigating the influence of inorganics on the pyrolytic behavior of hemicellulose are performed with Xylan as model compound [21]. Generally, the presence of AAEM is related to higher char and CO_2 at the expense of sugars [8, 21, 33]. In particular, inorganic species enhanced the formation of furfural, propionic acid, acetaldehyde, water, CO_2, and char, inhibiting the formation of xylose and an/dianhydroxylose [21, 33, 73–75]. Due to the similarity with cellulose structure, this is associated with the preference for the fragmentation reaction pathway over sugar formation. Dehydration reactions are also enhanced with increasing inorganic content [21]. However, there are some discrepancies with other species. In some studies, for example, increasing trends were observed for acetic acid and decreasing trends for formic acid with increasing sodium content [33], but no clear trends were found in other works [21,75]. There is also no significant variation of the CO total yield with the presence of inorganic species [8, 21], however, as reported by Giudicianni et a. [21], this may be due to a counterbalance by an increase in the low temperature range coming from carbonyls from dehydration of side-chain units and a decrease at high temperatures in favor of CH_4 and H_2.

2.1.3.3 Lignin

Lignin structure is much more complex than that of cellulose and hemicellulose. It is composed of p-hydroxyphenyl, guaiacyl, and syringyl units deriving from p-coumaryl, coniferyl, and sinapyl alcohols, as previously introduced. In the lignin matrix, the different monomers are linked to each other through different types of bonds, mainly ether and carbon-carbon bonds. Due to the differences in the dissociation energy of each of them, pyrolysis of lignin does not have a clear decomposition stage, reacting over a broad temperature range (150-700 °C) [8]. The rupture of ether bonds (mostly β-O-4), due to its weak linkage, start to occur between 200-250 °C [8, 20]. In fact, for this reason, hardwood lignin, which contains more ether bonds than softwood, exhibits a weaker thermal stability [20]. The cleavage of aliphatic side chains then follows, occurring at 300 °C and above, together with the weakly bonded methoxy groups [8]. Carbon-carbon bonds, in contrast, have lower reactivity compared to ether bonds and are thermally cleaved at temperatures above 370 °C [8, 20]. During the whole temperature range, the aromatic structures are further rearranged and condensed forming the solid fraction [6]. In fact, char, in pyrolysis of lignocellulosic biomass, derives mainly from lignin [6, 8].

Similar to hemicellulose, when employing different techniques to isolate native lignin from biomass, its chemical structure is inevitably affected [35]. Among all isolation methods, alkali lignin, due to its mild extraction, is usually employed as model compound to investigate its pyrolysis behavior [35, 36]. Phenolic compounds, due to its highly aromatic structure, are the main volatile products, also accompanied by water, carbonyls, alcohols, and permanent gases [8]. A schematic representation of the lignin pyrolysis mechanism proposed by Zhou et al. [76], is shown in Fig. 2.8. Lignin structure is taken from Faravelli et al. [53].

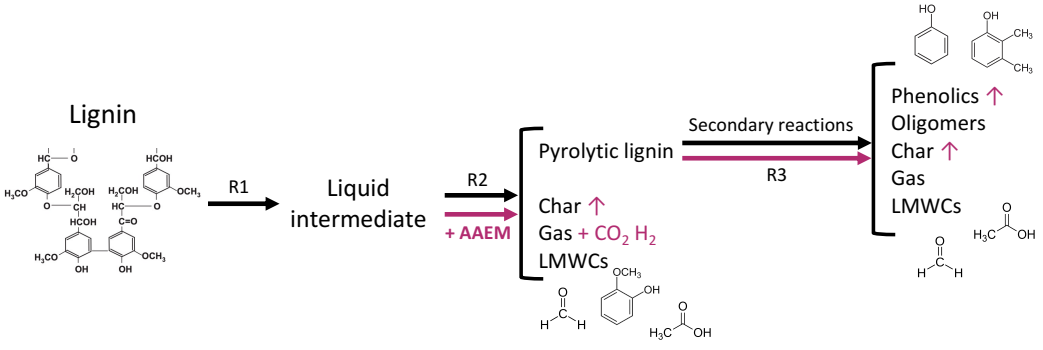

Figure 2.8: *Schematic representation of the lignin pyrolysis scheme (adapted from [76]).*

With the aim of simplifying the structure of the lignin depending on its elemental composition (being richer in carbon, hydrogen, or oxygen), Faravelli et al. [53] proposed a kinetic mechanism assuming lignin as a combination of LIG-C, LIG-H, and LIG-O, respectively. LIG-C is therefore more representative of softwood lignin due to its richer carbon content and absence of methoxyl groups [8, 20, 53], while LIG-H and LIG-O are more suitable to describe hardwood lignin. These reference components decompose through homolytic (radical) reactions releasing gases and forming intermediate compounds which are, at the same time, involved in substitutive additions and cross-linking reactions with a continuous char formation [34, 53]. The final products are mainly phenolics, char, and gases. The model encompasses more than 100 molecular and radical species with around 500 reactions [53], however, it does not consider the formation of a liquid intermediate, as represented in Fig. 2.8, and also does not include secondary reactions [8].

The effect of inorganic species on lignin pyrolysis has been studied by several authors with no clear consensus. Jakab et al. [38] reported that the presence of Na^+ in pyrolysis of spruce milled wood lignin enhances char formation and facilitates the fragmentation of functional groups. Moreover, decarboxylation and dehydration reactions are promoted together with the production of H_2 at the expense of CO and formaldehyde. These effects on product yields did not significantly affect the mass loss behavior. Further studies from the same group [39] reported, however, different results when employing $ZnCl_2$ as catalyst. Both water and formaldehyde shifted towards lower temperatures upon addition of $ZnCl_2$, together with a slight acceleration of the mass loss. The promotion of dehydration and demethoxylation was confirmed when doping with NaCl without significant shift of the temperature-dependent evolution profiles. Similar trends were reported by Giudicianni et al. [36]. Upon addition of KCl, the production of CO was hindered while H_2 and charring reactions were promoted. However, the differences were reported to be less than 10% and no acceleration of mass loss was observed. On the contrary, inorganic species have been reported to have a significant influence on lignin devolatilization when pyrolyzing lignocellulosic biomass, shifting considerably the conversion rate towards lower temperatures to an even greater degree than for cellulose and hemicellulose [8, 77].

Therefore, as it can be observed, there are still certain discrepancies, not only with respect to the effect that inorganic species may have on the kinetic scheme of each of the macrocomponents, but also on the mechanism itself. The complexity of the overall pyrolysis process has hindered its accurate understanding. Furthermore,

such complexity is not only based on the correct description of the large number of chemical reactions occurring at rapid rates and high temperatures, but also on the synergistic combination with other intra-particle phenomena occurring simultaneously: heat and mass transfer, together with phase changes [54], as represented in Fig. 2.9, and evolution of the physical structure. Moreover, as previously introduced, the wide heterogeneity of the biomass feedstock and the complexity of its structure increases the challenge [7, 20]. That is, for the development of a model that can accurately describe biomass pyrolysis and thus achieve a high degree of understanding of the process, it is necessary to solve a very complex multicomponent, multiphase, and multiscale problem [40, 54]. However, as reviewed by Pecha et al. [54], little attention has been paid, for example, on characterizing the phase change and, although the existence of a liquid intermediate has been reported for a long time [78, 79], only few studies highlight its importance on the reaction mechanism and products distribution [54, 60, 76, 80]. The correct definition of transport parameters, condensed phase thermodynamics, and reaction kinetics is challenging but fundamental for the coupling of these intra-particle phenomena into models that aim to correctly predict the pyrolysis behavior of different biomass feedstocks [54].

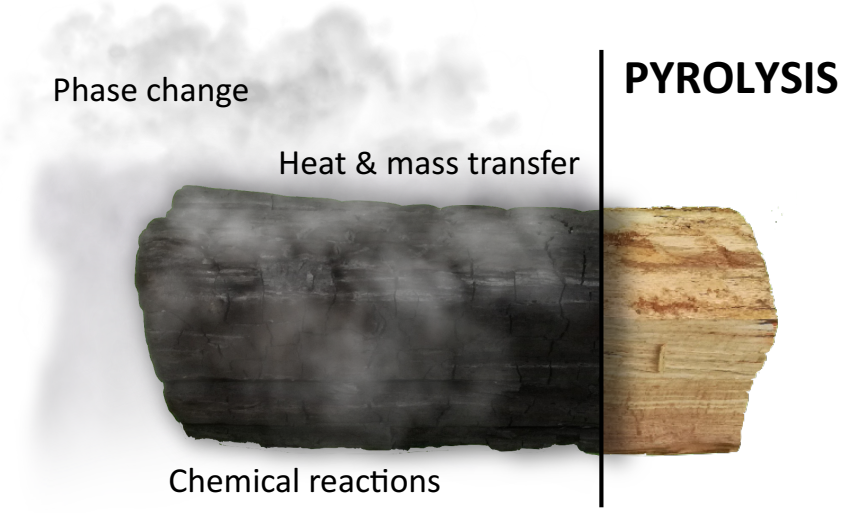

Figure 2.9: *Synergistic combination of intra-particle phenomena occurring simultaneously during biomass pyrolysis (based on [54]).*

Following the development of an intrinsic kinetic mechanism, which has been shown to still have open questions, coupling with heat and mass transport phenomena would be necessary to be able to include, in this way, the influence that secondary

reactions may have on the overall process. This could be done, for example, by introducing residence time dependence of the volatiles in the reaction zone [6]. For instance, in a system with transport limitation phenomena (i.e., reactor scale), the retention time will be increased enhancing therefore the presence of secondary reactions. This will result in significant changes in products distribution as well as in the thermochemistry of the process. These secondary reactions can occur either homogeneously (in the gas-phase) or heterogeneously (in the solid surface) [8]. While an acceptable maturity level has been achieved for kinetics of homogeneous secondary reactions (e.g., [42,43]), **heterogeneous secondary reactions**, are hardly included in pyrolysis models [6], and, if they are, it is in the form of fitting parameters [44,45].

Homogeneous tar cracking reactions have been reported to occur at high temperatures (> 500 °C) and produce mainly CO and H_2 [8]. In fact, Gomez-Barea and Leckner [27] determined, with a retention time of 0.5 s and taking into account different tar cracking kinetics from the literature, that the tar conversion for all tar compounds was $< 10\%$ at temperatures below 500 °C and up to 50% at temperatures between 600 and 700 °C. On the other side, heterogeneous secondary reactions are relevant at temperatures below 500 °C and slow heating rates [44, 45]. In this context, both heterogeneous tar cracking and charring reactions can occur [30, 44]. However, as explained by Anca-Couce et al. [44], the difference between both is not fully understood and tar cracking may also be involved in charring. Even though it is known that char, CO_2, and water are the main products, the complex pathways of both heterogeneous tar cracking and charring are still not clear. Secondary reactions and their possible products are also considered in the schematic representations of the pyrolysis schemes of cellulose (Fig. 2.6), hemicellulose (Fig. 2.7), and lignin (Fig. 2.8). However, further investigation is required in order to gain deeper understanding of the complex chemical reactions behind them.

A possible approach to investigate the presence of heterogeneous secondary reactions is the utilization of transport-controlled regimes, such as the investigation of the pyrolysis conversion of thermally thick particles, increasing, in this way, the retention time of the volatiles inside the char matrix. In this field, Zobel and Anca-Couce [30, 81] developed a single particle reactor where the mass loss measurement was combined with temperature measurements inside and in the close vicinity of the particle characterizing, on-line and in-situ, the released volatiles with LIF. They concluded that: (i) the particle size strongly affects the composition of the condensable gas species leaving a beech wood particle; and that (ii) when het-

erogeneous secondary reactions are promoted, the production of char is enhanced together with the production of PAH, resulting in a higher exothermicity.

Ciuta et al. [82] carried out intra-particle gas sampling during pyrolysis of thermally thick particles. To this end, a sampling probe was inserted in the center of the particle through a opening bore [82]. Gases leaving the pyrolyzing particle were measured in a micro gas chromatograph (micro-GC). In principle, this approach offers potential to gain knowledge of the pyrolysis mechanism and the formation of intermediate species. Nevertheless, it is necessary to take into account that a sampling probe in the center of the particle will affect the flow fields as well as avoid further secondary reactions of the volatiles catalyzed by the char surface in their way out of the particle. Permanent gases and some small hydrocarbons, up to C3, were characterized. It was observed that the gas production is higher for big particle size (31.8 mm diameter) than for small particle size (19 mm diameter) and that the process is exothermic for temperatures higher than 300 °C upon DSC analysis.

Combination of such experimental results with detailed particle models can help to gain a deeper mechanistic understanding of the pyrolysis process. Corbetta et al. [43] developed a single particle model (1-D, spherical), implementing the detailed pyrolysis mechanism proposed by Ranzi et al. [34] with the inclusion of homogeneous secondary reactions of the pyrolysis volatiles [42], as well as the physical transport model developed by Park et al. [83]. Transport phenomena at reactor scale were also included in a second version of the model to account for the reactions outside the particle. This particle model was validated with three sets of experimental data: i) poplar spheres heated in a turbulent preheated nitrogen flow with heating rates of 50 °C/min up to 470 °C and ex-situ species characterization with Fourier-transform infrared spectroscopy (FTIR) and a GC coupled to a thermal conductivity detector (TCD). Permanent gases, light hydrocarbons, and 3 carbonyl species (formic acid, acetic acid, and formaldehyde) were measured; ii) beech cylinders heated mainly by radiation with heating rates up to several hundred °C/min and at temperatures between 468–1050 °C with on-line ex-situ characterization of permanent gases and light hydrocarbons (up to C2), together with off-line characterization of methanol, water, and up to C3 hydrocarbons [84]; iii) maple spheres heated mainly by radiation up to 606 °C with characterization of temperature profiles at the surface, center and R/2 of the particle and char yields [83]. The validation of gas phase reactions was done with experimental data from Norinaga et al. [85]. As claimed by the authors, the model is partially predictive for thermal aspects and for the characterization of the released species for a wide range of temperatures.

However, notable deviations were measured in some key compounds. In fact, underestimation of water and CO_2 yields, together with overestimation of levoglucosan yield could be attributed to absence of heterogeneous secondary reactions in the model. This issue was indeed highlighted by the authors confirming that, in order to improve the model predictions, the inclusion of heterogeneous secondary reactions would be needed. Other advances in physical aspects such as the anisotropy in the biomass properties and the inclusion of particle break-up would also be required.

Bennadji et al. [86, 87] also studied the pyrolysis behavior of wood particles at conditions enhancing secondary charring reactions. They measured the temperature inside the particles (wood cylinders of 1.9 cm diameter [86] and wood spheres of 3.81 and 2.54 cm diameter [87]) and characterized, on-line and ex-situ, permanent gases, methane, methanol, formic acid, acetic acid, and formaldehyde.. First of all, they reported that the exothermic behavior coming after the main devolatilization is caused by the decomposition of an intermediate solid [86]. Moreover, it was concluded that the main influence of particle size is on the timing of the heating and devolatilization processes, as well as less important on the char and individual gaseous species yields [87]. They suggested that the reduction of some yields with increasing particle size could be related to the presence of intra-particle reactions of pyrolysis products (such as formaldehyde and acetic acid) to form secondary char. Such differences between particle sizes were not well captured by the model. Therefore, as highlighted by the authors [87], further improvement of the work would require the inclusion of both extractives as another biomass component (which was included in [40]) and intra-particle reactions of tar (i.e., heterogeneous secondary reactions).

As it can be seen, pyrolysis models which do not include the influence of secondary reactions under conditions promoting them are not able to predict volatiles composition [43, 86, 87], char yields [88], or other properties such as char oxidation reactivity [89]. The implementation of charring reactions in the form of adjustable parameters, as previously reviewed, improved these results [44, 45]. However, only char, CO_2, H_2, and water were considered as products [44, 45]. On the other hand, other works also reported the presence of polycyclic aromatic hydrocarbons (PAHs) as products of these heterogeneous secondary reactions [6, 28–30]. Therefore, a deeper knowledge of the final and intermediate products involved, as well as the complex chemical reactions between them, is needed [45]. To this end, a complete characterization of pyrolysis products is fundamental.

The following section will focus on different analytical techniques usually employed to characterize all pyrolysis compounds. This is especially challenging due to the characterization of tar products, which, as previously introduced, encompasses a large number of species (in the range of several hundred) with a very complex chemistry [21,23–25]. This may lead to certain species not being detectable under certain conditions, especially compounds present in very low concentrations or highly reactive and volatile species. For this reason, a combination of different techniques able to cover the detection of the broad spectrum of pyrolysis products should be considered. Special emphasis will be placed on the implementation of advanced spectroscopic techniques, in particular laser-induced fluorescence (LIF), for the detection of **aromatic species**, such as PAHs and BTX. The importance of correctly detecting such compounds lies not only in their subsequent implementation in more detailed pyrolysis mechanisms, but also in the study of secondary reactions, since these compounds are (almost exclusively [8]) considered to be products of these.

2.2 Volatiles Characterization

Different techniques are needed in order to characterize all pyrolysis products. They can be divided into off-line and on-line measurement techniques. The former are characterized by condensing the liquid products in a liquid solvent (e.g., isopropanol) or by extracting part of the produced gas for subsequent analysis. The latter, however, permit the products characterization during the transient evolution of the process. Although off-line methods are time-consuming and require prior preparation, some on-line methods (especially gas analyzers or micro-GCs) need to be protected from certain compounds and therefore require prior condensation of the liquid compounds. These liquid samples can then be further analyzed. Both technologies can therefore be combined in order to reach a high characterization.

Off-line analytical methods

Most off-line technologies are used to determine tar products. To this end, as previously mentioned, their condensation (usually in organic solvents) is required. Similar methods as the standardized "tar protocol"(CEN/TC BT/TF 143 [90]) for gasification are employed to fulfill this requirement. This method is based on 6 different impinger bottles filled with isopropanol and introduced in two different baths. One containing impinger bottles 1, 2, and 4 at temperatures between 35 and 40 °C,

and another with impinger bottles 3, 5, and 6 at temperatures between -15 and -20 °C [90]. A similar approach adapted to pyrolysis is employed in the present work to analyze the composition of the condensable volatiles.

After condensation, the most common technology is gas chromatography (GC) [8, 91]. This technique is based on the separation of compounds due to their physical and chemical properties and their interaction as they pass through a long (several m) and narrow (hundreds of µm) tube, known as column [92]. The column is usually made of fused silica (if referred to the most used capillary columns) and a microscopic layer of viscous liquid inside called "stationary phase", which is the one interacting with the sample [92]. The different compounds are characterized qualitatively by the retention time in the column. Comprehensive two-dimensional gas chromatography (GC x GC), performing the separation on two capillary columns, has recently been employed to improve the number of compounds to be identified compared to traditional GC analysis [20, 91]. Both qualitative and quantitative characterization are afterwards performed by means of a detector which is coupled to the GC.

The most commonly used detectors are MS and flame ionization detector (FID). Mass spectrometry is used to measure the mass-to-charge ratio (m/z) of the molecules (compounds) present in the sample. For this, the different molecules are first ionized and the results displayed as ion intensity vs m/z. Each molecule is identified by comparing the measured masses with its known mass spectrum. In the case of a flame ionization detector, each of the compounds leaving the column is mixed with hydrogen to be burned. The hydrogen flame create ions which generate a current between electrodes placed adjacent to the flame [92]. Quantification is made based on the current generated for each compound. Carbonyls, alcohols, heterocyclic, and aromatic compounds can be identified with these technologies [8,91,93]. In fact, over 300 different pyrolysis species have been reported to be detected so far using GC-MS and GC-FID [24,25,33,67,91,93]. Sugars (with the exception of levoglucosan) and lignin oligomers, however, can not be detected and other analytical methods, such as high-performance liquid chromatography (HPLC), are required [8, 91]. Moreover, peak co-elution, insufficient chromatographic resolution, or the lack of mass spectra of some compounds (in case of GC-MS) are some of the challenges that these techniques need to face when employed to characterize pyrolysis products [91].

Therefore, it seems clear that, although they represent one of the most widely used analytical techniques, they only provide partial information and need to be combined with other technologies.

On-line analytical methods

Several on-line techniques can be employed to support and extend the information obtained from the off-line analytical methods. If the sampling interval is short enough, some on-line technologies permit the study of the transient evolution of the process, which is fundamental to obtain detailed information about the reaction mechanism. Moreover, they avoid possible mischaracterization due to the sampling and preparation procedures [6]. Interaction between compounds (such as repolymerization), evaporation of high volatile species, or high reactivity of oxygenated compounds are the most common problems when sampling tar pyrolysis products for off-line analysis [6].

Based on the off-line methods previously introduced (GC-MS and GC-FID), advanced experimental technologies have been developed by coupling such methods to a micro-pyrolyzer (Py-GC-MS/FID) and to a thermogravimetric analyzer (TG-MS) [20]. As reviewed by Wang et al. [20], Py-GC-MS/FID has been recently employed in several studies to quantitatively investigate the pyrolysis products composition and try to better understand the reaction chemistry [33, 67]. The volatiles leaving the micro-pyrolyzer are first separated in the GC, then qualitatively identified by the MS detector, and finally quantified by the FID. Although direct quantification by means of the MS has also been employed [35, 63, 76]. The small sample masses (in the mg-range) together with the short residence times of the volatiles in the micro-pyrolyzer (few ms) allows the investigation of the primary pyrolysis mechanism, however, it limits the study of secondary reactions. Moreover, it does not permit a continuous analysis, therefore, it cannot be employed to determine the temperature- or time-dependent products evolution [20].

These disadvantages have been partially solved by the use of TG-MS [20]. This experimental method is able to monitor the mass loss and associate the main volatiles formation to their corresponding release temperature [20]. However, there are limitations when studying fast heating rates or isothermal conditions, since biomass usually decomposes before reaching the desired temperature. Moreover, as in the case of Py-GC-MS/FID, this experimental analysis method is usually employed to investigate the primary pyrolysis mechanism and its application to the study of secondary reactions is limited. Similar drawbacks are present in the thermogravimetric analyzer when coupled with Fourier-transform infrared spectroscopy (FTIR). The latter is a spectroscopic technique based on measuring the absorbed infrared (IR) radiation over a broad spectrum, usually between 500 and 4000 cm^{-1}. Each molecule will absorb light at a specific region, therefore, identification mainly based on their

functional groups can be performed. Carbonyls (C=O), ethers (C-O-C), alkanes (C-C), hydroxyl containing groups (-OH, alcohols or acids), and aromatics can be detected in different regions of the recorded spectra [20, 94]. Moreover, unlike the aforementioned methods, it can also measure permanent gases (CO_2, CO, and CH_4) and water vapor [20]. However, it cannot detect homodiatomic species (such as H_2) and to distinguish between compounds with the same functional group may be complicated [20]. Several studies employed this spectroscopic technique coupled to a TG to study the primary pyrolysis mechanism [35,47,48,65,72,95–97]. Furthermore, this spectroscopic principle has also been employed to characterize pyrolysis products at particle level and several attempts can be found in the literature [43, 45, 86].

Another of the most widely used methods for the detection of permanent gases (including H_2 as opposed to FTIR) is GC-TCD [8]. This technique, as its name suggests, is based on the separation of compounds by gas chromatography, being their further quantification performed by means of a thermal conductivity detector (TCD) coupled to the GC. Its principle relies on measuring the thermal conductivity of the gas sample and comparing it with the thermal conductivity of a reference gas (carrier gas). Usually nitrogen or helium are employed [92]. Since relatively large differences in thermal conductivity are needed, this method has lower sensitivity compared to others, although by selecting different columns and carrier gases this can be improved for specific compounds. Furthermore, due to its sampling interval, in the order of several minutes, it is often employed to determine the temperature- or time-dependent evolution of volatiles only for slow pyrolysis [6, 28, 29, 36, 43, 62, 74, 75, 97]. Fast processes are limited by temporal resolution and information may be lost between measurements.

As it can be observed, there are several off-line and on-line techniques available in order to characterize most of the pyrolysis products. However, off-line methods only focus on the final yields and the exact pyrolysis reaction mechanism can only be speculated on the basis of these results [20]. When studying a transient process it is also very important to characterize each of the final and intermediate products in terms of the time/temperature they are generated. Therefore, on-line methods with high temporal resolution should be preferred for the development of a detailed reaction mechanism. Laser-based spectroscopic techniques can be employed to face these drawbacks. Contrary to the previously introduced analytical methods, which employ gas sampling in an external gas measurement cell to characterize compounds in an ex-situ manner, the fact that they are partly predestined for an in-situ approach avoids possible further reactions or condensation of targeted

species. Furthermore, their non-intrusive nature avoids possible disturbances of the flow field due to extraction methods when applied in-situ.

Typical non-intrusive and in-situ optical methods are, for instance, raman scattering or infrared absorption spectroscopy. The former may be limited in pyrolysis due to interferences that the fluorescence signal emitted from aromatic compounds has on Raman signals. Infrared absorption spectroscopy can be applied in a broadband manner using FTIR. However, as previously reviewed, its application in pyrolysis has been performed mainly in an ex-situ manner and its in-situ implementation is scarce. Although there are some attempts in the literature [20, 98, 99], its low selectivity may lead to difficulties in distinguishing targeted species with the same functional groups (such as light hydrocarbons [20]), or the overlapping of the absorption spectrum due to the large number of species. Therefore, narrowband laser absorption spectroscopy is preferred, since it allows for both higher selectivity and sensitivity. This optical method has been employed in several fields, such as medical applications or combustion studies, both in the mid-infrared (MIR) [100–102] and the near-infrared (NIR) [103–105] spectral range, but its application to the pyrolysis process represents a novelty. In particular, IRLAS in the MIR spectral range is better suited for pyrolysis since the most important gas species possess strong ground state absorptions leading to more precise characterization of volatiles [106]. Therefore, IRLAS has been used to quantitatively characterize permanent gases (CO_2, CO, and CH_4) and water vapor, as well as formaldehyde qualitatively, in several publications which are part of this thesis. It must be highlighted, however, that these experiments, with their respective data processing, were carried out in their entirety by the Leibniz Institute for Plasma Science and Technology (INP) in Greifswald. Their results have been used in the present work to draw relevant conclusions on the pyrolysis mechanism.

Laser-induced fluorescence (LIF) spectroscopy is also characterized for being an online, non-intrusive technique, which can also be applied in an in-situ manner. Its high sensitivity, up to ppb in the gas phase [107, 108], together with its high selectivity, which allows the identification of compounds depending on their emission spectra, makes it an optical method with great potential for the characterization of certain pyrolysis products. However, the targeted species differ from the previous techniques mainly due to the different energy of the excitation source. In the present work, LIF has been implemented in the pyrolysis process at particle level for the detection of aromatic species, such as BTX, phenolics, and PAHs. The following section focuses on this experimental principle, along with its application in the field. As previously

mentioned, this aims to achieve a better understanding of the formation and origin of these species, and to contribute in the further development of a detailed pyrolysis mechanism that takes into account heterogeneous secondary reactions.

2.2.1 Laser-induced Fluorescence

Experimental principle

Fluorescence can be explained as the emission of light from any substance when an excited electron comes back from the exited singlet state to the ground state [109]. To understand the definition of this spectroscopic principle, several concepts must first be clarified. The excitation is induced by earlier absorption of light, in this case, provided by a laser. When a molecule absorbs light, i.e. photons, the energy increases. This energy (E) is going to be defined following Eq. 2.1:

$$E = hv = \frac{hc}{\lambda} \tag{2.1}$$

where h is Plank's constant (J s) and v the frequency (s^{-1}). Moreover, E can also be defined as a function of c, speed of light (m s^{-1}), and λ, wavelength (m). Depending on the energy absorbed by the molecule, i.e., depending on the frequency or wavelength of the applied light, different absorption types can be distinguished, as shown in Fig. 2.10.

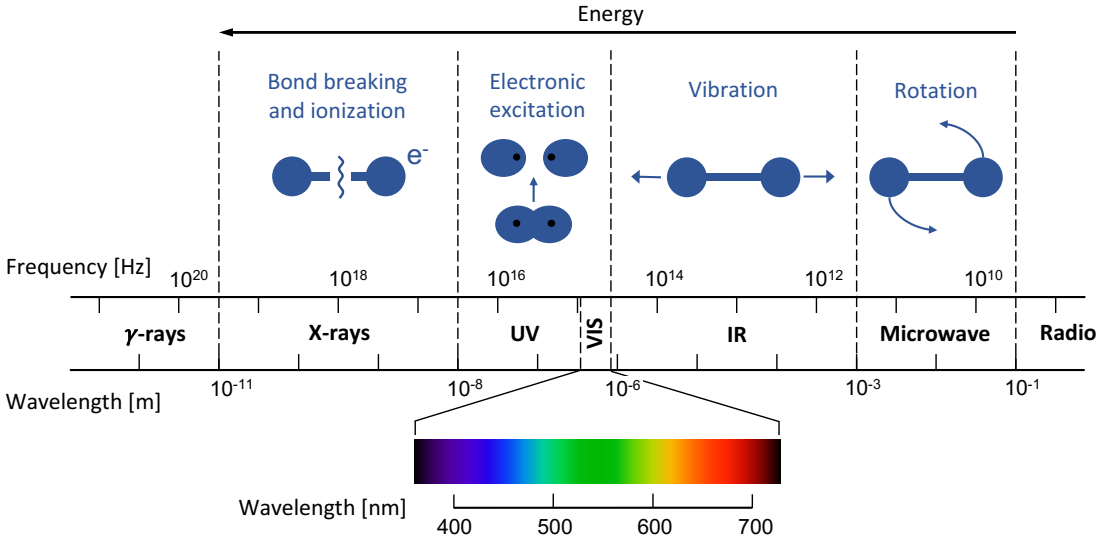

Figure 2.10: *Electromagnetic spectrum, defining the absorption regions as a function of radiation energy (adapted from [110]).*

The highest energy region of the electromagnetic spectrum (X-rays) will cause bond breaking and ionization of the molecules [110]. Electronic absorption is observed in the ultraviolet-visible (UV/Vis) region, promoting electrons to higher energy orbitals [110]. Vibrational absorption is produced in the infrared (IR) region. Spectroscopic techniques such as FTIR and IRLAS are based on this phenomenon. Finally, microwave radiation will stimulate rotation of molecules (rotational absorption) [110]. The higher the energy applied, the more types of absorption can be observed. For instance, absorption in the UV/Vis spectrum causes electronic, rotational, and also vibrational transitions.

When a molecule absorbs light, the irradiance of the beam from the excitation source decreases. Irradiance (P) is defined as the energy per second per unit of area of the beam and transmittance (T) as the ratio between the irradiance before (P_0) and after (P) absorption (Eq. 2.2) [110].

$$T = \frac{P}{P_0} \tag{2.2}$$

At the same time, both concepts are related to the absorbance (A) following Eq. 2.3:

$$A = \log_{10}\left(\frac{P_0}{P}\right) = -\log_{10}\ T \tag{2.3}$$

The importance of absorption, in fact, comes from the definition of absorbance, since it can be directly related to the concentration through the Beer-Lambert law (Eq. 2.4) [110, 111]:

$$A = \epsilon l c \implies T = 10^{-\epsilon l c} \tag{2.4}$$

where ϵ is the molar absorptivity ($\mathrm{cm^3\ mol^{-1}\ cm^{-1}}$), l is the path length where absorption takes place (cm), and c is the concentration of the light-absorbing substance ($\mathrm{mol\ cm^{-3}}$) [110,111]. All spectroscopic techniques involving light absorption are based on quantifying the concentration of the light-absorbing species by this equation, including fluorescence spectroscopy.

In order to induce a molecule to fluorescence, enough energy to promote electronic transitions is needed. Therefore, an excitation wavelength in the UV/Vis range must be employed (see Fig. 2.10). Once the molecule absorbs light in this specific wavelength range, the electron configuration changes from a bonding (σ, π) or non-bonding (n) orbital to an anti-bonding (σ^*, π^*) orbital. An schematic representation

of the different molecular orbitals (deriving from p-orbitals) considering the energy levels for the electronic transitions is shown in Fig. 2.11.

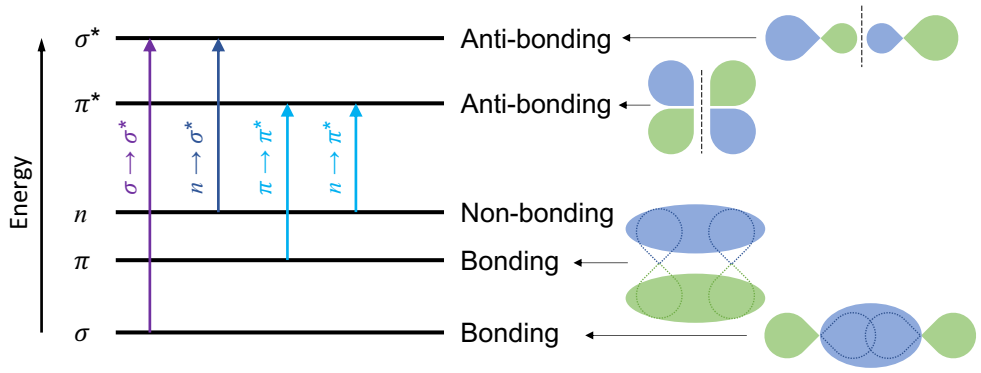

Figure 2.11: *Molecular orbital scheme considering energy levels and orbital shapes.*

As it can be observed, $\sigma \rightarrow \sigma^*$ transitions, such as the ones needed to excite C-H bonds (e.g., from CH_4) or C-C bonds (e.g., from C_2H_6), require the highest energy. In fact, this transition requires more than twice the energy compared to the other transitions. Excitation energies employed by conventional ultraviolet (UV) spectroscopy are usually not enough and vacuum-UV is needed (< 180 nm). In this range, atmospheric compounds (e.g., O_2) do also absorb radiation [111]. Molecules with lone pair (n) electrons, such as saturated compounds with heteroatoms (e.g., CH_3OH), may undergo excitation through $n \rightarrow \sigma^*$. However, as also shown in Fig. 2.11, they do also demand high excitation energy, although lower than that of $\sigma \rightarrow \sigma^*$. Energies in the deep-UV (up to 230 nm) are employed to promote this electronic excitation [111, 112]. For this reason, most applications of absorption spectroscopy (especially fluorescence) focus on transitions for both n and π electrons to the excited state π^*, since the energy required is lower and wavelengths in the UV/Vis region can be employed [111]. Typical pyrolysis products with this electronic transitions will be analyzed in the following section.

After electronic excitation to higher energy states induced by absorption, the excited electrons will loose their gained energy returning to the ground state. If this process is radiative, i.e. emitting photons, it is called luminiscence. The latter term can be classified into two categories: fluorescence and phosphorescence [109]. On the contrary, non-radiative processes may also occur, i.e. without emission of light, such as vibrational relaxation or internal conversion. These processes that occur between absorption and emission can be explained with the Jablonski diagram, shown in Fig. 2.12 [109, 111].

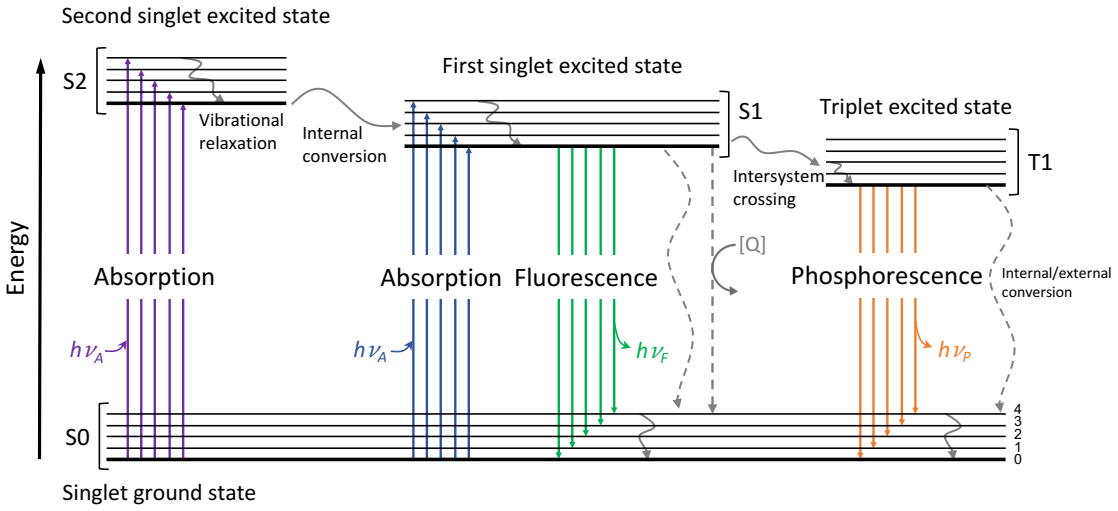

Figure 2.12: *Jablonski diagram (based on [109, 111]).*

As observed in Fig. 2.12, after absorption, the first processes that usually take place are relaxation and internal conversion (both non-radiative) to the lowest vibrational level of the first excited state (S_1) [110]. Both occur really fast, in the order of 10^{-12} s [109]. This fact explains why the fluorescence emission spectrum, i.e., radiative transition from the lowest vibrational level of the exited state (S_1) to the ground state, is independent from the excitation wavelength. This property is also known as Kasha's rule [109]. Due to this energy loss, both fluorescence and phosphorescence emit less energetic light than the absorbed one, also defined as Stokes shift [109], and have therefore longer wavelengths. The emission rates of the fluorescence phenomenon are in the order of 10^8 s^{-1}, being the lifetimes in the range of 10^{-8} s [109, 111]. The lifetime is defined as the average time that the molecule remains in the excited state before returning to the ground state. This transition, $S_1 \rightarrow S_0$, is spin allowed, due to opposite spins between electrons. However, molecules in first singlet state (S_1) may undergo spin conversion (parallel spins) to the first triplet state (T_1) [109]. This conversion is referred to as intersystem crossing and is more probable when vibrational levels of the two stages overlap [111]. The presence of heavy atoms may also promote this conversion [109]. Phosphorescence is the emitted light from the triplet state (T_1) to the ground singlet state (S_0). Usually, T_1 has lower energy than S_1, therefore, phosphorescence emit at longer wavelengths. The transition from the triplet state to a singlet is much less probable than singlet-singlet conversion. Therefore, lifetimes are much longer compared to fluorescence, in the order of 10^{-3} - 10^0 s [109, 111].

A similar equation to the one introduced for absorption, following Beer-Lambert law, also exists for fluorescence. The emitted light after absorption, in the form of fluorescence (F), can be described as:

$$F = \phi_f K(P_0 - P) \tag{2.5}$$

where ϕ_f is the quantum efficiency (or quantum yield) of the fluorescence process, K is an instrumental factor depending on parameters such as geometry, and $(P_0 - P)$, as mentioned above, is the difference between the irradiance of the excitation source before and after the sample [111]. By combining Eq. 2.3 and 2.2, it can be obtained:

$$F = \phi_f K P_0(1 - \frac{P}{P_0}) \implies F = \phi_f K P_0(1 - 10^{-\epsilon l c}) \tag{2.6}$$

as before, ϵ is the molar absorptivity ($\mathrm{cm^3\ mol^{-1}\ cm^{-1}}$), l is the path length (cm), and c is the concentration of the fluorescent substance ($\mathrm{mol\ cm^{-3}}$) [113]. By approximating Eq. 2.6 with a first order Taylor polynomial around the origin ($c = 0$), a linear correlation between F and c can be obtained:

$$F \approx \phi_f K P_0 \ln(10) \epsilon l c \tag{2.7}$$

indicating that the fluorescence intensity should be directly proportional to the concentration of the fluorescent compound when both path length and concentration are maintained sufficiently small ($\epsilon c l < 0.05$) [111, 113, 114].

Moreover, the molar absorptivity (ϵ) can be defined as:

$$\epsilon = \frac{N_A \sigma}{ln10} \tag{2.8}$$

where σ is the absorption cross section of the compound ($\mathrm{cm^2\ molecule^{-1}}$) and N_A the Avogadro constant [111]. Therefore, it can be concluded from Equations 2.7 and 2.8 that, in order to characterize the evolution of volatiles in pyrolysis by means of the emitted fluorescence signal, a selection of these must first be done according to their capacity to absorb energy, and therefore, their absorption cross section (analyzed in the following section).

The fluorescence emission, however, will not only be determined by the absorption phenomenon, but also by the ability of the molecules to emit the energy. This will

be defined by the quantum yield (or quantum efficiency), which is the ratio between emitted to absorbed photons [109]. Therefore, molecules with the highest quantum yields (close to the unity) will show the brightest emission [109]. In this case, non-radiative decay rate would be much lower than that of radiative decay. There are several parameters affecting the quantum yield. For instance, high temperatures will promote deactivation from the excited state by external conversion (radiationless process) due to the higher probability of collisions between molecules [111]. The presence of heavy atoms (i.e., iodine, bromine [109, 111]) will also decrease fluorescence quantum yields. In fact, they may promote intersystem crossing to triplet state with a corresponding decrease in fluorescence emission [111]. These processes, which decrease fluorescence intensity, are called quenching. Moreover, when the radiationless energy loss is due to energy transfer from an excited state to other molecules, it is defined as collisional (or dynamic) quenching. For this, the concentration of certain compounds (quenching agents, e.g., O_2) has to be large enough to ensure deactivation by collision with the fluorescent compound molecules. The influence of collisional quenching in the fluorescence signal can be described by the Stern-Volmer equation [109, 111]:

$$\frac{F_0}{F} = 1 + K[Q] = 1 + k_q \tau_0 [Q] \tag{2.9}$$

where F_0 and F are the fluorescence signals before and after the presence of the quencher agent, K is the Stern-Volmer quenching constant, k_q is the bimolecular quenching constant, τ_0 is the unquenched lifetime, and $[Q]$ is the concentration of the quenching agent [109]. This process is also illustrated on the Jablonski diagram (Fig. 2.12).

Fluorescence of pyrolysis products

Pyrolytic volatiles composition, as reviewed in Section 2.1.1, can be classified into sugars, carbonyls, alcohols, furans, phenolics, and aromatic hydrocarbons (BTX and PAHs). From these groups, PAHs have been reported to have the highest absorption cross section and most of the studies are focus on them [30, 115]. However, other compounds such as phenolics, ketones, or aldehydes will also absorb energy in the UV range and might therefore influence the fluorescence emission spectra of pyrolysis gas. Representative compounds from each group have been selected based on those with the highest absorption cross section [112] of those obtained from GC/MS analyses of both the literature [24, 93] and previous results of this research group.

Table 2.1: *Clustered classes of pyrolysis volatiles divided into aromatic and aliphatic compounds.*

Aromatic Compounds					
PAHs	BTX	Phenols	Carbonyls	Furans	Quinones
Phenylbenzene	Benzene	Phenol	Benzaldehyde	Furfural	Benzoquinone
Naphthalene		Xylenol	Dimethylbenzaldehyde	Furan	Dimethylbenzoquinone
Phenanthrene		m-Cresol	Benzophenone	Mehylfurfural	
Anthracene		o-Cresol	Acetophenone	Methylfuran	
Pyrene		p-Cresol			
Aliphatic Compounds					
Acids			Carbonyls	Alcohols	
Glyoxylic Acid			Formaldehyde	Ethanol	
Propanoic Acid			Acetaldehyde		
Formic Acid			Hydroxyacetaldehyde		
[(a)]Benzoic Acid			Acetone		
			Hydroxyacetone		
			2-Butanone		
			Hydroxybutanone		
			3 and 2-Pentanone		
			3-Cyclopenten-1-one		

[(a)] Aromatic acid

Moreover, as previously introduced, it is known that UV/Vis radiation, between 200 nm and 700 nm, will mainly produce $n \rightarrow \pi^*$ transitions, typical from carbonyls (due to C=O bonds), and $\pi \rightarrow \pi^*$ transitions, from cyclic aromatic compounds (C=C bonds), being the latter more likely. For this reason, the representative species, shown in Tab. 2.1, and their absorption cross sections, plotted in Fig. 2.13, are divided into aromatic and aliphatic compounds.

It can be observed in Fig. 2.13 that the range in which aromatic compounds are found, in terms of their absorption cross section, is clearly higher to that of aliphatic compounds. Moreover, alcohols do not absorb energy which leads to fluorescence at wavelengths longer than 180 nm, due to the high energy needed to promote $n \rightarrow \sigma^*$ transitions, typical from single C-O bonds. When considering 266 nm excitation wavelength (one of the main wavelengths employed in the present study), values between 10^{-19} and 10^{-16} cm^2 molecule^{-1} are reported for aromatic compounds, while for aliphatic remain in the order of 10^{-20} cm^2 molecule^{-1} [112]. Among aromatic compounds, furans present the lowest absorption cross section with the exception of furfural which, at 266 nm, have values up to $3{\cdot}10^{-17}$ cm^2 molecule^{-1} [112, 116]. Benzoic acid, due to its aromaticity, is the only compound belonging to acids that present values of almost 10^{-18} [112, 117], being close to that of quinones, phenolics, and aromatic carbonyls. However, benzophenone, being an aromatic carbonyl, shows at 266 nm values in the range of the group of polyaromatic hydrocarbons, which, over the whole UV-range, present the highest absorption cross sections [112].

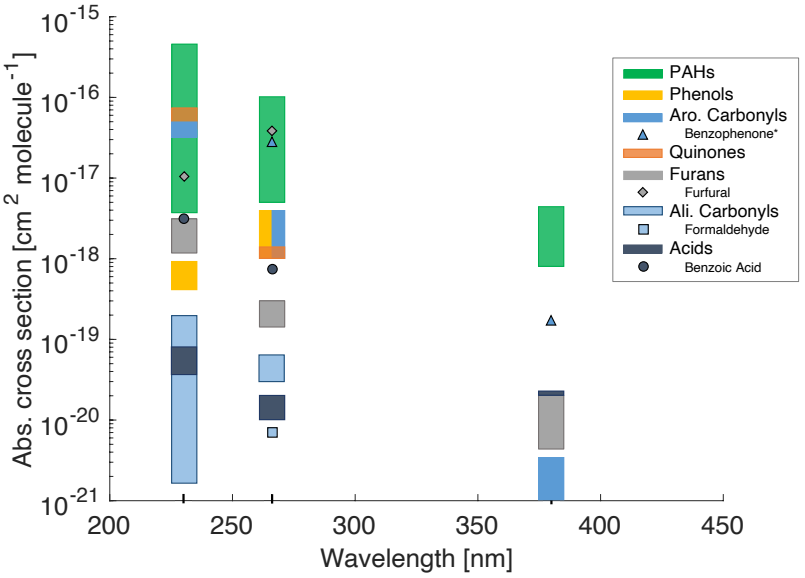

Figure 2.13: *Comparison of absorption cross sections (data obtained from the literature [112]).*

It must be considered that, although similar trends are reported for the studied spectral range, some groups of compounds may show important variations in the absorption spectrum depending on the excitation wavelength. This is clearly noticeable, for example, at 230 nm, where quinones or some aromatic carbonyls (e.g., benzaldehyde) present higher absorption cross sections than some PAHs. Moreover, when employing longer excitation wavelengths, such as 380 nm, the energy applied might not be enough to promote electronic transitions. This is the case for one- and two-aromatic ring species. Other compounds compounds, such as furans or aromatic carbonyls, although being able to absorb light at 380 nm, present low absorption cross sections.

The emission spectrum will be characteristic of each compound (mostly dependent on its functional group) and directly related to its absorption spectrum. The mirror-image rule, also known as Franck-Condon principle, highlights the symmetric nature between absorption and emission spectra. Such behavior results from the similar vibrational levels and therefore similar transitions involved in both absorption and emission [111]. This effect can be clearly identified in Fig. 2.14, where the absorption and emission spectrum of anthracene is plotted.

In this case, each peak represents the transition from the lowest vibrational level of S_0 to a vibrational level of $S_1(0, 1, 2...)$ for absorption, and the transition from the lowest vibrational level of S_1 to a vibrational level of $S_0(0, 1, 2..)$ for fluorescence. Or in other words, each peak represents one of the vertical lines of absorption and

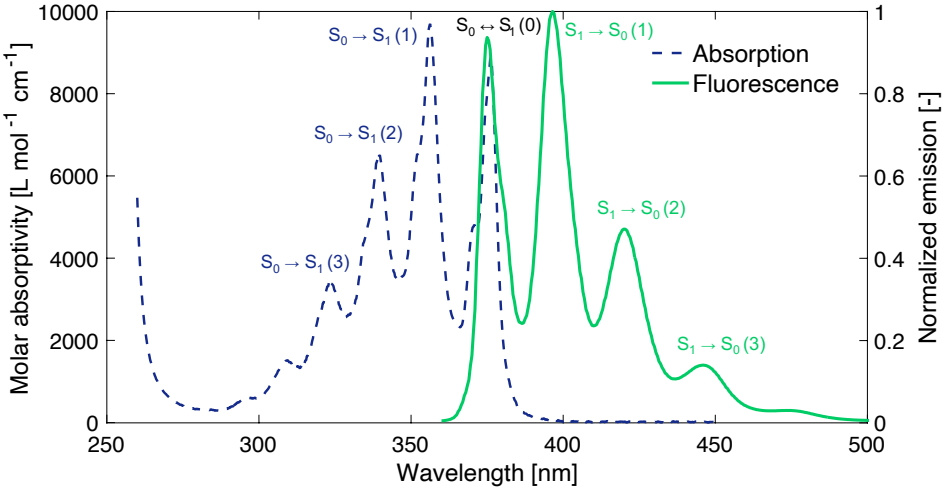

Figure 2.14: *Absorption and emission spectrum of anthracene (data obtained from [118]).*

fluorescence represented in the Jablonski diagram, Fig. 2.12. Since the spacing between vibrational levels of S_0 and S_1 is similar, absorption and emission spectrum will be mirrored around the transition $S_0(0) \longleftrightarrow S_1(0)$, which will have the same energy for both. It must be however highlighted that there are exceptions to this rule due to several reasons [109, 111].

The fact that after absorption, the excited molecule undergoes rapid vibrational relaxation, thus emitting from the lowest vibrational level of the excited state ($S_1(0)$), means that the emission spectra will be independent from the excitation wavelength [109]. Consequently, each spectral range of emission can be assigned to a compound or group of compounds. Under conditions of the present study, i.e., measuring in the gas phase and at high temperatures ($>$ 300 °C), the fluorescence emission spectrum of most of the compounds are broad and structureless. Therefore, both the onset and endset of the spectrum together with the maximum peak position need to be considered to identify the different species present in the pyrolysis gas stream. One-ring aromatic compounds, i.e., benzene, toluene, and xylene (BTX) and phenolics, are reported to emit between 270 and 340 nm, peaking at around 290 nm and 310 nm, respectively [6, 28, 29]. An important characteristic to take into account when studying the fluorescence emission of aromatic compounds is that, the higher the number of rings, the more the spectrum shifts towards longer wavelengths (red-shifted). While the position of the naphthalene peak is at 340 nm, the emission of pyrene starts at this wavelength and peaks at around 380 nm [28, 29, 119]. As previously introduced, these compounds are expected to contribute the most to the fluorescence spectrum mainly due to the great efficiency related to their $\pi \rightarrow \pi^*$

transition [111]. However, their formation in the slow pyrolysis process is expected to be much lower compared to other species such as ketones or aldehydes. For this reason, the potential contribution of both aromatic and aliphatic carbonyls to the fluorescence emission also need to be considered.

Substitutions of a carbonyl group (C=O) on an aromatic ring will promote the lower energetic transition $n \rightarrow \pi^*$. This fact is reported to inhibit the fluorescence typical from aromatic hydrocarbons [6, 111, 120]. Compounds such as benzaldehyde or benzophenone present broad emission spectra with maxima at longer wavelengths (around 420 nm) compared to that of aromatic hydrocarbons. Moreover, aliphatic ketones and aliphatic aldehydes have been reported to show also similar qualitative fluorescence behavior [6]. However, the quantum yield for this electronic transition is significantly lower, leading therefore to less intense signals.

State of technology

Laser-induced fluorescence (LIF), due to its online and non-intrusive nature, has been largely applied in chemical and biological sciences [109]. The re-emitted fluorescence intensity, after energy absorption, is, under certain conditions, proportionally related to the concentration of the excited molecules, as previously introduced. Consequently, the evaluation of the spectral fluorescence signal can provide an extremely precise quantification of the amount of fluorescence-emitting species. Its high selectivity and sensitivity, in the range of tens ppb in gas phase [107, 108] and up to ppt when measured in liquid phase [121], has been of special interest in fields such as, pollution monitoring [122], kinetics and mechanisms of reactions [123], and thermochemical conversion processes such as combustion [120, 124, 125] or gasification [114, 126, 127].

The implementation of this technology in the field of combustion is widely known, specifically for evaluation and analysis of flame structures or the detection of pollutants mainly coming from incomplete combustion, such as oxygenated compounds [120, 128]. Moreover, in combination of laser-induced incandescence (LII), it is largely used for the characterization of particle formation [124] and identification of polycyclic aromatic hydrocarbons, main precursors of soot formation [125]. Following this last potential application, LIF has been also used in gasification processes, giving information about the total content of tars through the detection of PAHs. Karellas and Karl [126] were able to quantify, by means of an ex-situ cell, the tar content (up to 8 g/m^3) of the product gas by calibrating the emitting signal through

offline analysis, in this case the standardized tar protocol. The authors pointed out, however, that problems in quantification may appear when measuring too intense signals, due to high tar content. Baumhakl and Karellas [127], with a similar approach, measured the total amount of tar by means of fluorescence spectroscopy using, however, a light-emitting diode (LED) as light source. A good correlation between tar content (up to 20 g/m^3) and fluorescence intensity could be only made with a 365 nm LED, being the power of the 265 nm LED too weak. It should be remembered that, as introduced above, for there to be a linear correlation between fluorescence signal and concentration, the latter must be sufficiently small. Or in other words, the absorption has to be very small compared to the applied energy or power. Moreover, the fact that only 355 nm excitation source could be employed, left a clear gap in terms of quantification, since smaller molecules, such as benzene and naphthalene, cannot be induced to fluorescence with the selected wavelength. Following a similar experimental approach, Borgmeyer and Behrendt [114] developed an optical online tar analysis system using a 280 nm LED (30 mW). The authors pointed out that advances in the development of light-emitting diodes made it possible to achieve sufficiently high powers for their application in the field of gasification, solving one of the main problems of previous works employing the same analytical technique. The calibration of the system was performed with pure PAHs (naphthalene, phenanthrene and fluoranthene) and mixtures of them. Tar concentrations up to 10 g/m^3 were successfully measured.

Fluorescence spectroscopy has been also applied in pyrolysis, although scarcely, for both, in-situ and ex-situ, characterization of volatiles. However, in contrast to other fields, its application has been done in a qualitative manner. At particle level, Brackmann et al. [115] associated a broad-band fluorescence spectra, in the range from 300 to 500 nm, to the presence of larger (two-, three-ring aromatic) hydrocarbons, although no clear qualitative identification of compounds could be performed. Only the presence of formaldehyde could be detected by employing a 355 nm excitation wavelength due to its characteristic emission spectra. In the same way, Zobel and Anca-Couce [30] stated that both particle size and heating rate were strongly influencing the fluorescence spectra, assuming the presence of PAHs due to heterogeneous secondary reactions of primary volatiles. Prins et al. [129] employed two-photon excitation at 230 nm to identify CO and a 355 nm laser source to detect formaldehyde from wood at fast heating rates and temperatures up to 700 °C. Both characterizations were performed qualitatively. However, it should be noted that both fluorescence signals were attributed to the targeted compounds in their

entirety. As mentioned above, not only these compounds can be induced to fluoresce in this wavelength range. For example, it is unlikely that the fluorescence signal at an excitation wavelength of 355 nm derives only from formaldehyde. In fact, many other species such as aromatic hydrocarbons or aromatic carbonyls, especially at high temperatures, may also contribute to the emission spectrum.

At reactor level, Dieguez-Alonso et al. [28, 29] studied, on-line and ex-situ, the pyrolysis fluorescence behavior of wood and its macrocomponents. The fluorescence emission spectra for holocellulose was attributed to the formation of carbonyl groups and two-ring PAHs when secondary reactions were present. On the other hand, in the case of lignin, the single spectra showed a typical one-ring phenolic and small PAHs shape (emission between 300 and 340 nm), being red-shifted with the enhancement of secondary reactions and attributed to the release of bigger PAHs. In the case of wood, it was also observed, following the latter hypothesis, an increase in bigger PAHs (3-, 4-ring) when secondary reactions were promoted, for example, with higher residence times. Therefore, it was concluded that the fluorescence emission at low temperatures deriving from the slow pyrolysis of wood at reactor level was mainly related to primary products coming from lignin decomposition, i.e., phenolic (one-aromatic ring) compounds such as guaiacols, while at higher temperatures more and bigger PAHs were produced from secondary reactions.

As it can be observed, most of the studies using LIF are focused on the fluorescence behavior of PAHs and quantification has been made following this trend. However, in pyrolysis, unlike in gasification processes where the quantification of tar content (mainly PAHs and BTX) has been successfully performed, the product gas has a large quantity of different volatiles (carbonyls, alcohols, furans, phenols, PAHs, BTX). This fact results in a great challenge for semi-quantification by means of LIF, since not only PAHs, but also compounds such as carbonyls (ketones and aldehydes), furans, or phenolics may be induced to fluorescence. In the present work, fluorescence spectrocopy has been applied, on-line and in-situ, to determine the evolution of these species in slow pyrolysis at particle level. The first publications (Chapters 4 and 5) are mainly based on the qualitative analysis of the species that could be induced to fluorescence with different excitation wavelengths (266 and 355 nm), basing the conclusions on the literature and previous publications of this research group. For verification and comparison with the results obtained, the fluorescence emission of pure aromatic species was also measured in Chapter 6.

In Chapter 8, with the implementation of a new experimental setup, semi-quantification of the total amount of fluorescence-emitting species was achieved and

applied to the study of the slow pyrolysis of wood and its macrocomponents. This was performed by correcting each fluorescence emission spectrum by the energy of its corresponding laser pulses. Previous verification of the linearity between the fluorescence signal and the laser energy was performed for the case with the highest concentration of fluorescence-emitting species. The experimental campaign for each sample was performed in a short period of time to ensure the same experimental conditions (optics alignment, ambient temperature, positioning of the sample holder in the cell, etc). It must be highlighted, however, that this semi-quantification was in terms of the total fluorescence intensity (i.e., total amount of species) and not based on individual compounds.

In order to improve the semi-quantification of individual compounds, not only the single fluorescence emission spectrum must be considered, but also other LIF-relevant parameters such as fluorescence lifetime, dynamic quenching, and temperature. To this end, in Chapter 9 a selection of different pyrolysis products, based on their absorption cross sections, has been made. The influence of this fluorescence parameters on each compound has been measured in the same experimental setup built for single-particle pyrolysis experiments. These results will be crucial for the potential improvement of the LIF measurements sensitivity. Furthermore, together with the introduction of new excitation wavelengths, it will help to towards a better species identification and differentiation. This chapter, however, describes actual ongoing work and needs to be further developed.

Chapter 3

Motivation of this work

The aim of this work is to contribute to improve the understanding of the pyrolysis conversion of woody biomass. As it has been introduced, despite gaining great scientific relevance in recent years, the exact mechanism is still unknown. Its further development will be indicative of a complete understanding of the process and is necessary not only for application as a process itself, but also as a key sub-process of other thermochemical conversion technologies, such as combustion or gasification.

The previous review has highlighted some of the main open questions that hinder the comprehensive development of the pyrolysis mechanism: heterogeneous reactions, the formation of aromatic species, and the influence of inorganics. The study of these research questions through various scientific publications has created the basis for this thesis.

A possible approach for the study of heterogeneous secondary reactions is to work in transport-controlled regimes. For this purpose, a particle-level reactor was developed, allowing the investigation of the process in the thermally thick regime. Under these conditions, there is a strong influence of transport resistances on the chemistry. Therefore, its correct understanding will help the coupling of both intra-particle phenomena in more accurate models. Besides conventional on-line measurements of both mass loss and temperature, characterization of volatiles in the reactor cell was performed on-line and in-situ by means of advanced laser-based spectroscopic techniques: IRLAS and LIF. The implementation and development of the first optical method (IRLAS) was carried out at the Leibniz Institute for Plasma Science and Technology (INP) in Greifswald by co-authors belonging to this research institute. The second spectroscopic technique (LIF) was carried out at the Technische Universität Berlin (TUB). To this end, twin particle reactors adapted to each of the measurement principles were developed. IRLAS was employed for identification of

permanent gases (CO_2, CO, and CH_4) and water vapor. LIF was applied to track the evolution of fluorescence-emitting species. The latter also allowed to focus on the formation of aromatic species (such as PAHs and BTX), which represents not only one of the open research questions, but also an indicator of the presence of heterogeneous secondary reactions. A more detailed description of the experimental setup, the application of these techniques, and the results obtained are presented in Chapter 4.

In Chapter 5 a numerical model (developed by Anca-Couce et al. [44, 45]) was adapted to the experimental conditions employed in the previous chapter. The pyrolysis scheme coupled to the particle model takes into account the presence of heterogeneous secondary reactions in the form of adjustable parameters. Experimental and numerical results are presented to define the capabilities and limitations of both. In addition, the need to include the formation of aromatic species in the pyrolysis mechanism is revealed.

In order to continue the investigation of the open research questions regarding the pyrolysis mechanism, the influence of inorganic species has been studied in Chapter 6. As previously reviewed, the influence of inorganics has been the subject of study for decades, however, discrepancies still exist as to their influence on the pyrolysis scheme. Moreover, most studies focus on the intrinsic kinetic level and few works investigate their influence in the presence of transport limitation phenomena. For this purpose, the same analytical techniques were used in the particle reactor for different materials (washed and doped). Off-line characterization of liquid products was performed by means of a GC-MS. The results obtained provided the basis for the research in the following chapters.

The combined influence of inorganics and transport resistances on the pyrolytic behavior of woody biomass has been studied in Chapters 7 and Chapter 8. The investigation performed in Chapter 7 was the result of an experimental campaign within the framework of a collaboration project (BRISK2). Therefore, the experimental setup, including particle reactor, TGA, and analytical methods, were developed and operated in Bioenergy and Sustainable Technologies (BEST) in Graz (Austria). In this case, particles of different sizes were doped and washed in order to reach different levels both inorganic content and transport resistances. The particle reactor allowed for intermediate and fast heating rates. Volatiles characterization was performed on-line and ex-situ by means of FTIR spectroscopy and a non-dispersive infrared (NDIR) gas analyzer. The experiments were performed by myself under the supervision of the co-authors belonging to this research center. The results ob-

tained have been employed to derive relevant conclusions of the effect of inorganics and transport limitations on the pyrolysis mechanism.

This study was continued at the Technische Universität Berlin, introduced in Chapter 8. In this case, a new particle reactor was developed which allowed to extend the possibilities in terms of measurement techniques and pyrolysis conditions. In addition, different analytical methods for a complete characterization of volatiles were installed. The installation and development of a new spectroscopic setup also allowed the semi-quantitative characterization of the total amount of fluorescence-emitting species. The quantification of water vapor was carried out, in agreement with previous works, by means of IRLAS by the INP. In addition, a micro-GC was installed for ex-situ characterization of permanent gases. The liquid products were condensed, and their subsequent characterization is part of future work. These improvements were applied to perform a comprehensive study of the synergistic influence of inorganics and transport limitation phenomena on the slow pyrolysis of wood, but this time based on each of the macrocomponents of which the biomass is composed. The detailed study of each of them can explain, to some extent, the pyrolytic behavior of wood. In addition, these experimental results can be used for the development of more detailed models based on the decomposition of each of the macrocomponents.

Finally, Chapter 9 describes the work performed for the improvement of the semi-quantification of individual compounds by means of LIF spectroscopy. In this case, up to 23 representative species of the pyrolysis products have been measured in the same experimental setup as the pyrolysis experiments. A calibration of the system has been carried out taking into account different LIF-relevant parameters. Although the whole experimental campaign is finished, further work is in progress and still needs to be developed.

3.1 List of publications

This cumulative thesis is based on different articles published in peer-reviewed journals (Chapters 4 to 7). The article in Chapter 8 is in preparation for submission to *Energy Conversion and Management* and has not been published yet.

Chapter 4

Pyrolysis behavior of thermally thick wood particles: time-resolved characterization with laser based in-situ diagnostics. N. Lang, C. Rupp, **H. Almuina-Villar**, A. Dieguez-Alonso, F. Behrendt, and J. Röpcke. *Fuel*, 210 (Supplement C): 371-379, 2017. https://doi.org/10.1016/j.fuel.2017.08.077

• Installation, development, and operation of the particle reactor at the TUB, as well as pyrolysis experiments, LIF analysis, and data curation were carried out by Hernán Almuiña Villar.

Chapter 5

Laser-Based Spectroscopy Diagnosis and Detailed Numerical Models to Gain Understanding on the Slow Pyrolysis Behavior of Thermally Thick Wood Particles. **H. Almuina-Villar**, A. Anca-Couce, N. Lang, J. Röpcke, F. Behrendt, and A. Dieguez-Alonso. *Chemical Engineering Transactions*, 65: 109-114, 2018. https://doi.org/10.3303/CET1865019

• Pyrolysis experiments, LIF analysis, adaptation of the numerical model (developed by A. Anca-Couce) to the experimental conditions, data curation and visualization, and writing original draft of the manuscript were carried out by Hernán Almuiña Villar.

Chapter 6

Application of laser-based diagnostics for characterization of the influence of inorganics on the slow pyrolysis of woody biomass. **H. Almuina-Villar**, N. Lang, A. Anca-Couce, J. Röpcke, F. Behrendt, and A. Dieguez-Alonso. *Journal of Analytical and Applied Pyrolysis*, 140: 125-136, 2019. https://doi.org/10.1016/j.jaap.2019.03.004

• Materials preparation, pyrolysis experiments, LIF analysis, data curation and visualization, and writing original draft of the manuscript were carried out by Hernán Almuiña Villar.

Chapter 7

Combined Influence of Inorganics and Transport Limitations on the Pyrolytic Behaviour of Woody Biomass. **H. Almuina-Villar**, P. Sommersacher, S. Retschitzegger, A. Anca-Couce, and A. Dieguez-Alonso. *Chemical Engineering Transactions*, 80: 73-78, 2020. https://doi.org/10.3303/CET2080013

• Materials preparation, TGA and pyrolysis experiments, data curation and visualization, and writing original draft of the manuscript were carried out by Hernán Almuiña Villar.

Chapter 8

Synergistic influence of inorganics and intra-particle transport resistances on the pyrolysis mechanism of woody biomass based on its macrocomponents. **H. Almuina-Villar**, C. M. Grottola, F. Hempel, N. Lang, J.-P. H. van Helden, F. Behrendt, and A. Dieguez-Alonso. In preparation for submission to *Energy Conversion and Management*.

• Installation, development, and operation of the new particle reactor at the TUB, materials preparation, pyrolysis experiments, conceptualization, data curation and visualization, and writing original draft of the manuscript were carried out by Hernán Almuiña Villar.

Chapter 4

Pyrolysis behavior of thermally thick wood particles: time-resolved characterization with laser based in-situ diagnostics

This chapter is the peer-reviewed version of the article published in *Fuel* with the title "Pyrolysis behavior of thermally thick wood particles: time-resolved characterization with laser based in-situ diagnostics", N. Lang, C. Rupp, H. Almuina-Villar, A. Dieguez-Alonso, F. Behrendt, and J. Röpcke. *Fuel*, 210 (Supplement C): 371-379, 2017. https://doi.org/10.1016/j.fuel.2017.08.077.

4.1 Abstract

Infrared laser absorption spectroscopy (IRLAS) and laser-induced fluorescence spectroscopy (LIF) are applied in the present study for online in-situ characterization of volatiles products in the close vicinity of a single pyrolyzing wood sphere. These advanced analytical techniques are combined with online measurements of temperature and mass evolutions in order to gain further insight into the complex processes occurring during slow pyrolysis of thermally thick wood particles. Three different heating rates (5, 10, 20 °C/min) and two wood types (beech, pine) were used. Time-resolved absolute concentrations of the main permanent gases CO_2, CO, CH_4 and H_2O were measured applying IRLAS. From the LIF measurements the qualitative temporal release of polycyclic aromatic hydrocarbons (PAHs) could be deduced. Different behaviors regarding the release of volatiles, temperature evolution and conversion rates were observed for both wood species, which could not be ascribed only to the different content of cellulose, hemicellulose and lignin. According to the measured

volatiles evolution an enhancement of heterogeneous catalytic tar cracking seemed to be present with higher heating rates for both wood types. However, the evolution of exothermicity and PAHs release differed for both wood types indicating different reaction pathways. An analysis of possible reaction pathways including secondary reactions is performed taking into account all experimental findings about the in-situ composition of the volatiles and the evolution of the PAHs as well as the exothermicity. The differences in the pyrolytic behavior of both species can be related to both the chemical and physical properties of the raw materials.

4.2 Introduction

Pyrolysis is a key stage in any thermochemical conversion process such as combustion or gasification with a direct impact on the conversion efficiency, product quality and emissions, since gas and char yields as well as char reactivities are highly affected by this stage [17]. In order to improve the performance of these technologies a deeper knowledge of this process is required. In particular, due to its complexity, the exact pyrolysis mechanism is still not known [51].

In early stages of biomass pyrolysis research, the impact of transport limitations on pyrolysis mechanisms, including kinetics, reaction enthalpies and product distributions, was deeply investigated, specially for cellulose [59, 64, 130]. Diverse mechanisms were proposed with competitive reactions leading to different product distributions and properties of these products; with kinetic parameters and heats of reaction. Despite this, when modelling pyrolysis, especially in processes such as combustion or gasification, mostly global single-step models, multi-component devolatilization models and models based on simple competitive schemes have been used [51, 131]. Global single-step and multi-component devolatilization models can predict mass loss rates but not products distributions, since the latter needs to be known or assumed [131]; models based on competitive schemes allow to predict product distributions lumped in char, gas and tar based on reaction conditions [50]. Secondary (cracking) reactions of tar are sometimes also included in these models depending on temperature and residence time of volatiles at this temperature [131].

However, as already shown in early literature and recently reviewed by Anca-Couce [8], the presence of heterogeneous secondary reactions can also have a strong influence on products distribution and composition, as well as on reaction enthalphies. This will have a significant impact on aspects such as gas phase reactions

and char reactivity [19, 89, 131]. Therefore, models based on detailed mechanisms that account for such reactions are needed. On this path, Anca-Couce et al. [44] developed a detailed kinetic scheme in which these secondary charring reactions were included. With this model, the mass loss rate of 20 different volatiles were calculated and compared with literature.

Parallel to the development of such models, experimental investigations are needed for a deeper understanding of the pyrolysis mechanisms and model validation. This experimental work should not be only on a kinetic regime, as is common for the determination of reaction kinetics, but also at a level where transport limitations lead to a different extent of heterogeneous secondary reactions. In such experiments, the initial mass of the samples (particle size or sample size) is typically in the range of hundreds of milligrams up to several grams causing them to behave thermally thick, i.e., in a transport regime. As highlighted by Wang et al. [88], pyrolysis models which do not consider the influence of particle size, sample size and pressure (experimental parameters which can influence transport phenomena) are not able to predict char yields. This holds also for other properties, such as char oxidation reactivity [89], or composition of the volatiles [87]. It has been shown experimentally that an increase in particle size enhances the char and the fixed-carbon yields [88,132,133], as well as the proportion of aromatic carbon - improving therefore char stability, whereas the formation of tar is decreased [132]. This may be attributed to an enhanced intra-particle residence time of the volatiles, increasing the interactions between them and the solid matrix and, therefore, leading to the formation of char through secondary reactions [88, 132]. Regarding the influence of pressure, it has been reported in literature [133] that an increase leads to both an increase in biochar yields and in fixed-carbon content. This was found to be attributed to: (1) the longer intra-particle residence time of the volatiles enhancing secondary reactions; (2) the higher concentration of the volatiles increasing secondary reactions as well; and (3) the more significant catalytic effect of char and inorganic species. In this study, the authors showed this increase in char and fixed-carbon yields for a constant gas flow rate, gas mass flow rate and superficial velocity, i.e., for different retention times of the vapor volatiles within or in close vicinity of the particle and for different concentrations of the volatiles. This was accompanied by changes in the char morphology with higher pressures as well [133].

Other experiments at particle level with similar experimental approach to the present one have been also reported in literature, investigating the temperature and mass loss behavior [83] and the heat of reaction [134]. To further identify heterogeneous

secondary reactions, Zobel and Anca-Couce applied laser-induced fluorescence (LIF) spectroscopy for the detection of polycyclic aromatic hydrocarbons (PAHs) [30, 81]. However, a deeper characterization of the volatiles produced during pyrolysis is still needed in order to better understand the reaction mechanims. Furthermore, selective online characterization techniques with high temporal resolution should be preferred in order to target species originating potentially from different reaction pathways. In addition, in-situ measurements provide data which should not be affected by possible further reactions of the targeted species in an ex-situ experimental arrangement.

For a single particle only a few attempts were reported in the literature, in which the product gas composition was analyzed with a Fourier-Transform-Infrared (FTIR) spectrometer [86, 95, 96]. Although the achievable time-resolution is limited, online measurements with acquisition rates of about 30 mHz have been reported [96]. Quantification of the data is typically performed with additional measurements using pure compounds, introducing the typical uncertainties associated with such procedures. Moreover, all these measurements use gas sampling methods with an additional gas cell to collect or to extract the product gas in an ex-situ manner.

In contrast, laser-based spectroscopy methods are predestined for an in-situ approach. To analyze the composition of the product gas in close vicinity of a pyrolysing particle infrared laser absorption spectroscopy (IRLAS) is well suited. Due to its ability to allow for sensitive and fast concentration measurements it has been used since several decades in different applications, e.g., environmental monitoring, combustion studies, medical applications and plasma diagnostics in the near-infrared (NIR) spectral range [103–105] and in the mid-infrared (MIR) spectral range [100–102], respectively. In particular, if high sensitivities are needed, the application of IRLAS in the MIR spectral range is preferable because of the order of magnitude stronger absorption cross sections of the molecules in the MIR compared to the NIR. Typical laser sources employable for IRLAS in the MIR spectral range are lead salt lasers and quantum cascade lasers (QCL). Whereas the former exhibit narrower laser linewidths suitable for chemical selectivity the latter are more powerful and easier controllable. In both cases the spectral tuning range is often limited to only a few transitions of a probed molecule. With the development of so-called external-cavity QCLs (EC-QCLs) the tuning ranges are extended typically to 200 cm^{-1} enabling multi-component detection, including molecules with broader absorption structures or condensed phase species. Fore more information on the developments and applications of EC-QCLs the reader is referred to various articles and the references therein [135–137].

In this paper, we report on the application of IRLAS for the quantitative characterization of the product gas composition in real-time and in-situ. Both lead salt lasers and an EC-QCL are employed for the monitoring of the main species CO_2, CO, CH_4 and H_2O in the product gas in close vicinity of a single pyrolysing wooden sphere. Furthermore, laser-induced fluorescence (LIF) measurements were performed in-situ to characterize the species that emit fluorescence at an excitation wavelength of 355 nm, such as PAHs. From this analysis information is obtained about the importance of intra-particle heterogeneous cracking of primary and secondary tar species. Both optical approaches were complemented with measurements of the mass loss of the particle and temperature profiles both inside the particle and outside close to its surface. In the experiments two different wood types were investigated, beech and pine.

4.3 Experimental

4.3.1 Setup

For both LIF and IRLAS twin particle cell reactors (PLRC) were developed and adjusted to each measurement principle. Validation between both systems was performed. Fig. 4.1 illustrates the combined realization of both optical diagnostic methods at the PLRC (in reality in separate reactors) in addition to mass and temperature measurements.

The LIF setup is a further development of a previously introduced experimental setup [30, 81]. Briefly summarized, volatiles leaving the pyrolysing particle are excited at a wavelength of 355 nm (third harmonic of a Nd-YAG laser) and the emitted fluorescence is detected in the perpendicular direction to the laser beam using a spectrograph (Princeton Instruments, SpectraPro 2300i) with an ICCD camera (LaVision, NanoStar). The TFI, normalized to its maximum value is analyzed in the present study and compared to the conversion rate and to the evolution of the volatiles. The TFI is determined for each time step according to:

$$TFI = \int_{355nm}^{510nm} I(\lambda) d(\lambda) \tag{4.1}$$

and can be correlated with the release of species produced in secondary reactions (such as PAHs). For more details the reader is referred to [30].

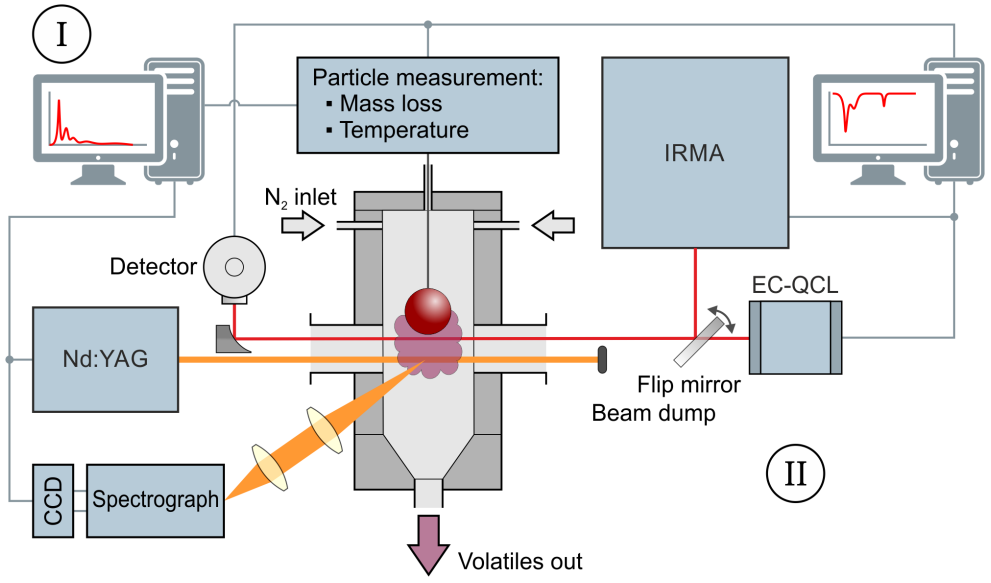

(a)

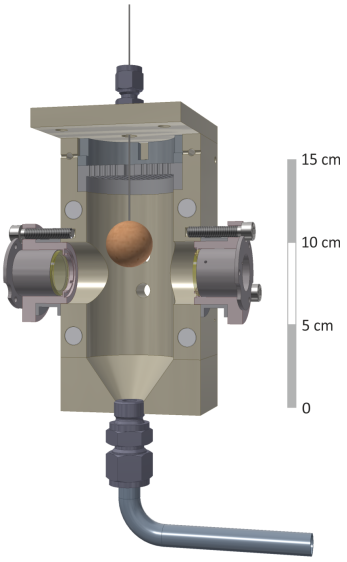

(b)

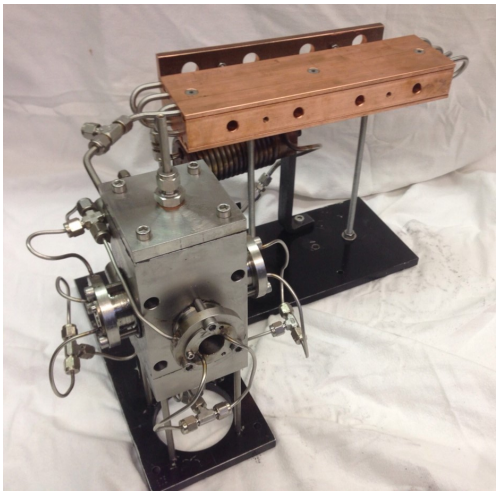

(c)

Figure 4.1: *(a) Combined scheme of each individual experimental setup for both (I) the LIF and (II) the IRLAS measurement systems. The mass evolution and temperature measurements of the particle were performed simultaneously with a special mounted thermocouple directly connected to a balance. (b) Detailed view of the particle-level reactor cell (PLRC) itself. (c) Picture of the PLRC with preheating modules for both the process gas and the window purge gas.*

The IRLAS setup is designed to determine the absolute concentration of the main permanent gases and H_2O leaving the particle in-situ and time-resolved. CO_2, CO and CH_4 were detected using a compact IRMA system. The IRMA system contains four independent laser stations to operate cw lead salt lasers in a way, that they can be temporally multiplexed. The temperature of each laser is controlled independently at millikelvin precision in the range between 30 and 100 K, providing a narrow-band emission of the laser in the spectral region between 3 and 20 µm. The optical beam paths of the IRMA system are designed such that it has the possibility for the simultaneous use of four different lasers on the same beam path to the reactor. A more detailed description of the IRMA system, the software used for the data analysis and its application for in-situ process monitoring can be found in [137,138]. To measure the strong vibrational transitions of H_2O the IRMA system has been optically combined with a cw EC-QCL (Daylight Solutions, 41058-MHF-011) via a flipping mirror. This EC-QCL can be scanned over about 80 cm^{-1} without mode hops. The spectral range to detect H_2O at 1780.7 cm^{-1} enabled also the probing of an adjacent vibrational transition of NH_3 at 1779.7 cm^{-1}. The infrared laser beam used to probe the volatiles leaving the particle had a diameter of about 15 mm and was guided in an evacuated common beam path with KBr windows to the PLRC. Passing through the reactor the laser beam interacts for a length of 5 cm with the gas inside the PLRC and is focused outside the reactor by an off-axis parabolic mirror onto a liquid nitrogen cooled HgCdTe infrared detector (Infrared Associates).

In both setups the particle is hanging in the middle of the cell, around 10 mm above the laser beams, see Fig. 4.1. The particle is connected with a specially prepared thermocouple (type K, $\varnothing$ = 1 mm, 250 mm long) to a balance (setup I: Sartorius AG, BP 121S; setup II: A&D Company, FX-120) which enables the simultaneous measurement of both the mass and the temperature in the center of the particle. The temperature in the cell was measured about 5 mm below the hanging particle with another thermocouple of the same type. Fused silica windows are used in the LIF setup and wedged $BaCl_2$ windows in the IRLAS setup with 25 mm in diameter. In the IRLAS setup the windows were purged from both sides with additionally preheated N_2 to ensure inert conditions for the window material and to avoid deposition on the inner surface. Furthermore, in order to suppress the influence of background absorptions from the ambient atmosphere the optical path in the IRLAS setup had to be purged permanently with nitrogen or evacuated where possible.

4.3.2 Experimental conditions

In the experiments two different types of wood spheres were investigated, beech and pine (as representative of hardwood and softwood), both with diameter of about 25 mm. Elemental and proximate analyses as well as apparent density are presented in Table 4.1.

Table 4.1: *Proximate and ultimate analysis for beech and pine wood.*

(%wt.,db)	Beech	Pine
Volatiles	85.60 ± 0.20	84.95 ± 1.29
Ash	0.41 ± 0.01	0.24 ± 0.06
Fixed. carbon[a]	13.98 ± 0.20	14.80 ± 1.26
C(%)	48.35 ± 0.14	49.84 ± 0.43
N(%)	0.09 ± 0.00	0.09 ± 0.05
H(%)	6.87 ± 0.04	6.71 ± 0.36
S(%)	0.06 ± 0.02	0.19 ± 0.08
O(%)[b]	44.65 ± 0.15	43.07 ± 0.55
Apparent density, g/cm^3	0.708 ± 0.034	0.554 ± 0.048

[a] Fixed carbon is obtained by difference 100 %-(Volatiles(%)+Ash(%)).
[b] Oxygen content is calculated by difference: 100 %-(C(%)+N(%)+H(%)+S(%)+ash(%)).

For IRLAS the molecular transitions used for the determination of the species concentration and their spectral position were identified with the help of an etalon of known free spectral range and well-documented reference gas spectra [139]. The relationship between the measured transmission $T(\nu)$, defined by the ratio of the incident and transmitted laser intensity, $I_0(\nu)$ and $I(\nu)$, and the concentration n of an absorbing species is given by the Lambert-Beer law:

$$\int_{line} \ln T(\nu) d\nu = \int_{line} \ln \left(\frac{I(\nu)}{I_0(\nu)} \right) d\nu = n \times S(T) \times L \tag{4.2}$$

where $S(T)$ is the temperature dependent line strength of a single transition and L the absorption length. Table 4.2 summarizes the spectral positions together with the predominant vibrational mode of the molecule they belong to. In addition, the number of rotational transitions taken into account in the spectral line fit is given as well as the total line strength at room temperature from the HITRAN database [139]. Knowing all transitions contributing to a spectral absorption feature the resulting line profile can be calculated and numerically fitted to the measured profile taken into account all line broadening coefficients and the temperature dependent line strength by using Eq. 4.2. The latter can be calculated from the known line strength at room

temperature and the measured gas temperature in the reactor. The adjustable fitting parameter is the unknown concentration n in the molecular ground state. For data analysis a software package, TDLWintel, is implemented in the IRMA system which allows the determination of CO_2, CO and CH_4 concentrations in real-time by using such non-linear least-squares fit routines [140]. In case of the H_2O measurement with the EC-QCL the data had to be post-processed with self-written scripts.

Table 4.2: *Spectral position and predominating vibrational mode of the species detected by IRLAS (IRMA: CO_2, CO, CH_4; EC-QCL: H_2O). In addition the number of rotational transitions taken into account in the fit is given and the total line strength at room temperature [139].*

Species	Spectral position [cm^{-1}]	Vibrational mode	Rotational transitions	Total line strength ($T_0 = 296$ K) [cm^2 cm^{-1}]
CO_2	2335.3	ν_3 asymmetric stretch	89	4.28×10^{-20}
CO	2119.7	ν_1 asymmetric stretch	1	3.71×10^{-19}
CH_4	3131.5	ν_3 asymmetric stretch	122	1.63×10^{-19}
H_2O	1780.7	ν_2 bend	3	2.58×10^{-20}

Typical examples of the measured spectra and the result of the analysis by fitting the spectral absorption features are given in Fig. 4.2 and 4.3. Each spectrum was measured with an accumulation time of 1 s. In case of CO_2, CO and CH_4 this results in an average over 1000 single spectra, in case of H_2O over 80 single spectra, respectively. Fig. 4.2 (a) shows a transmission spectrum of CO together with the result of a spectral line profile fit to determine the concentration of CO according to Eq. 4.2. The agreement between both is very good. In contrast to the spectra of CO_2, CH_4 and H_2O this line profile consists of only one rovibrational transition. In case of the probed transition of CH_4, 122 individual rovibrational transitions contribute to the measured spectral feature shown in Fig. 4.2 (b). Because of the atmospheric pressure in the PLRC and the temperature in the range of 20 and 550 °C, the line profiles of each individual transition are additional broadened and start to overlap. Therefore, the single transitions cannot be resolved spectrally and the resulting spectrum shown in Fig. 4.2 (b) is observed.

The same effects cause the measured spectrum of CO_2 to be broadened larger than the probed spectral range. In consequence, the non-absorbed laser intensity I_0, the so-called baseline of the spectrum, is no longer detectable as shown in Fig. 4.3 (a).

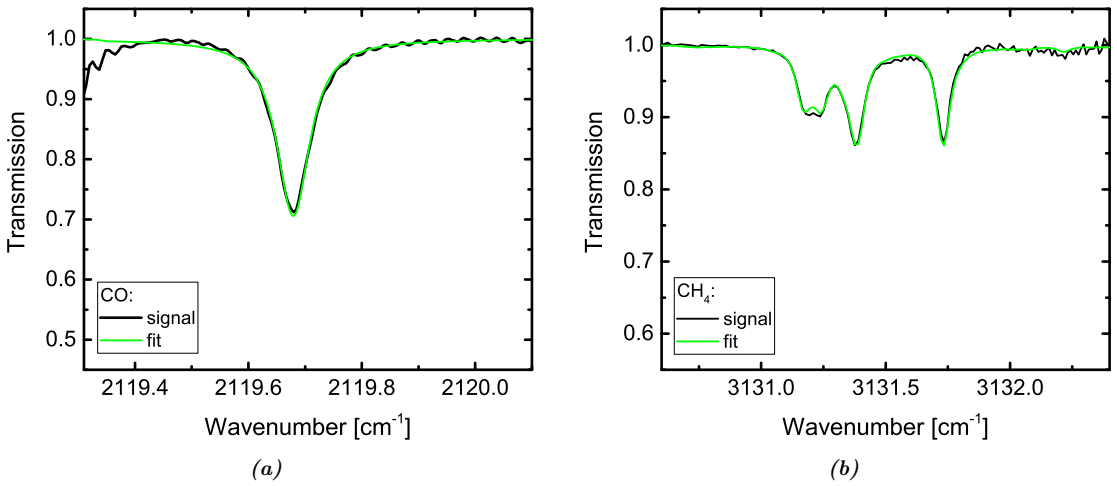

Figure 4.2: *(a) - transmission spectrum of CO at 2119.7 cm^{-1} consisting of a single rotational transition together with the result of the spectral line profile fit. (b) - transmission spectrum of CH_4 at 3131.5 cm^{-1} containing several strong overlapping peaks. For the fit in this spectral range up to 122 transitions were taken into account. In both figures the measured data are plotted in black, the fitted spectra in green.*

Therefore, the baseline had to be measured separately in the beginning of the experiment. The measured spectra during the pyrolysis process were divided by this background spectrum to get the transmission spectrum. Changes in the background or in the sensitivity of the detector during the pyrolysis process leads to errors in the determination of the concentration which was compensated with an additional degree of freedom in the fit of the baseline. However, the uncertainty of the resulting concentration values of CO_2 according to Eq. 4.2 is because of this being significantly larger compared to CO, CH_4 and H_2O and is estimated to be about 30 %.

Fig. 4.3 (b) shows typical transmission spectra of H_2O measured at different temperatures. The spectrum measured at 23 °C (green) belongs to the residual water content in the optical path of the IRLAS system despite its careful purging. Therefore, each measured H_2O spectrum during the pyrolysis process, an example measured at 390 °C is shown in addition in black in the left graph of Fig. 4.3, had to be corrected by such a background spectrum measured once before the pyrolysis is started. Assuming that the H_2O absorption in the optical path is only changed because of H_2O molecules evaporating out of the particle, the difference in the absorption spectra was used to determine the water concentration in the PLRC.

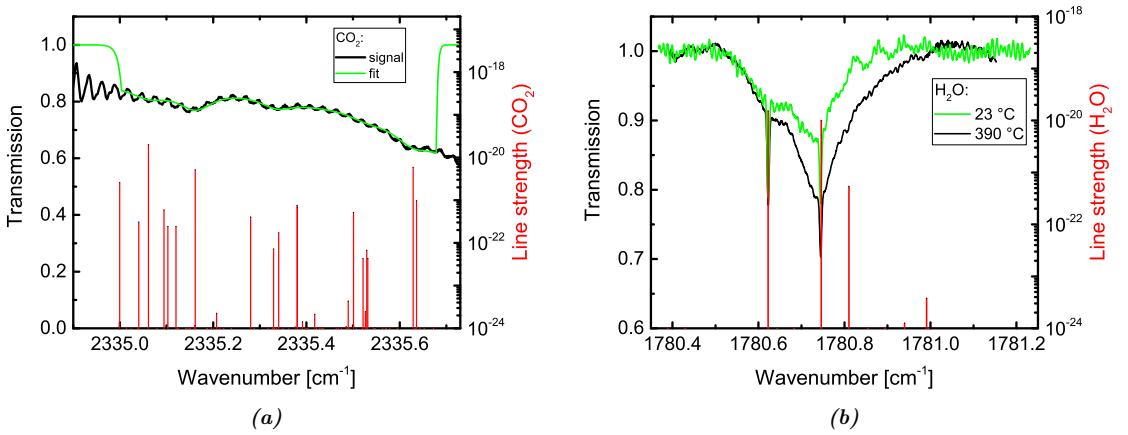

Figure 4.3: *(a) - transmission spectrum of CO_2 at 2335.3 cm^{-1} consisting of several strong overlapping rotational transitions indicated by the stick diagram of their line strengths. The background intensity I_0 had to be measured separately before the pyrolysis process starts. The measured data are plotted in black, the fitted spectra in green. (b) - transmission spectrum of H_2O at 1780.7 cm^{-1} measured for two different temperatures. The green spectrum at 23 °C shows the residual H_2O content in the IRLAS sytem without running pyrolysis, the black spectrum the overall H_2O absorption in the IRLAS system during the pyrolsis process at 390 °C.*

4.4 Results and Discussion

As a first step the comparability of both experiments was assessed so the results can be combined. To this end, the common properties measured in both setups were compared: mass, temperature in the middle of the particle and its outside temperature in close vicinity. In Fig. 4.4 (a), these properties are shown during pine (black) and beech (red) wood pyrolysis at a heating rate of 10 °C/min (setup I – solid lines, setup II – discontinuous lines). In Fig. 4.4 (b), the corresponding conversion rate $d\alpha/dt$ for both experiments is presented, where α is defined according to:

$$\alpha = 1 - \frac{m - m_f}{m_o - mf} \tag{4.3}$$

with m being the actual, m_0 the initial and m_f the final mass of the particle, respectively. It can be seen that in both experimental setups the results are quite similar ensuring that the findings from the LIF measurements and the IRLAS measurements can be combined with each other.

The evolution of the temperature in the middle of the particle exhibits a well pronounced exothermicitiy for both types of wood although, in case of beech this effect starts earlier and is more pronounced than in the case of pine. The exothermicity is recognized when the temperature in the middle of the particle exceeds the temperature in the atmosphere near the particle. With respect to the conversion rate,

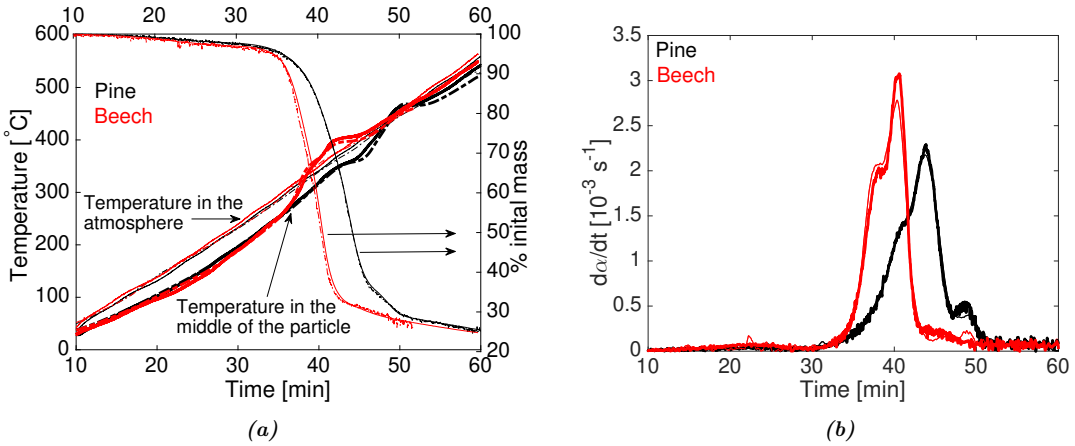

Figure 4.4: *Comparison between experimental setup I – solid line and setup II – discontinuous line. Results are shown for pine (black) and beech (red) pyrolysis at a heating rate of 10 °C/min. (a) time evolution of mass (represented as % of the initial mass), temperature in the middle of the particle (bold line) and in the atmosphere near the particle (thin line). (b) conversion rate as a function of time.*

both wood types present quite different behaviors which will be discussed in detail in the following sections.

4.4.1 Mass loss

In Fig. 4.5, the conversion rates for (a) beech and (b) pine at different heating rates are presented. As previously noted, the behavior of both wood types differs significantly, as the maximum of the mass loss rate occurs at higher temperatures for pine than for beech and the shape of the $d\alpha/dt$ curve is different for both cases. In the case of beech, the shoulder on the left of the main peak is more pronounced (especially a heating rate of 5 °C/min). Furthermore, in the case of pine, a second peak appears at temperatures around 450 °C, in particular, at a heating rate of 10 °C/min, see also Fig. 4.4 (b). This indicates that both wood types follow different reaction pathways. In order to gain further insight into the reaction mechanisms involved, information about the composition of the volatiles and their release yields is required, which is presented in the next section. It is noted that with higher heating rates the maximum of the conversion rate shifts to higher temperatures. This phenomenon has been frequently reported in literature [141, 142] and can be explained due to a coupling of heat transfer limitation and reaction kinetics.

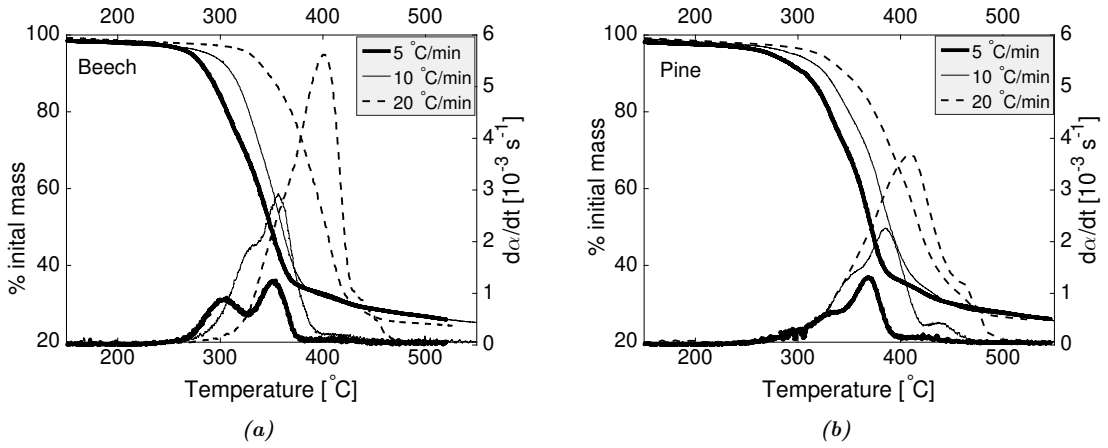

Figure 4.5: *Percentage of the total initial mass (left y-axis) and $d\alpha/dt$ (right y-axis) as a function of temperature inside the cell, in the close vicinity of the particle for beech (a)) and pine (b)) at three different heating rates (5 °C/min 10 °C/min and 20 °C/min).*

4.4.2 Volatiles evolutions

In Fig. 4.6 the evolution of CO_2, CO, CH_4 and H_2O are plotted together with $d\alpha/dt$ as a function temperature in close vicinity of the particle for both pine and beech pyrolysis at heating rates of 5 and 10 °C/min, respectively. The time-resolved in-situ characterization of these species and their correlation with the conversion rate and the temperature allows us to gain further understanding of the pyrolysis mechanisms. H_2O is the most abundant volatile component among the ones characterized in the present study, caused by the drying of the particle at low temperatures and as a product of pyrolysis at higher temperatures. It is also found that H_2O follows qualitatively the behavior of the conversion rate curve, i.e., it reflects the shoulder caused by the decomposition of hemicellulose as well as the maximum of the conversion rate, which is attributed to the decomposition of cellulose as reported by Anca-Couce et al. [143]. CO_2 follows a similar qualitative trend of H_2O and, as a primary volatile is produced during the decomposition of hemicellulose. The decomposition of cellulose mainly produces CO as permanent gaseous product and starts at higher temperatures as reported by Yang et al. [97]. At temperatures above 400 °C, CH_4 and CO are the main gaseous products, resulting from the decomposition of lignin and potentially due to the presence of secondary reactions. The maximum release rate of CH_4 occurs at around 425 °C, which is significantly later compared to the peak of the loss rate and the release of the other species monitored. All these species are products of primary pyrolysis, but can also be due to secondary reactions. According to a recent pyrolysis mechanism and adapted model reported by Anca- Couce et al. [44], char together with H_2O and to a lesser extent CO_2 are

products of secondary charring reactions, while CO and H_2 are mainly products of secondary cracking reactions. Secondary cracking reactions can be either homogeneously or heterogeneously. The former can be neglected in the present study due to the low temperatures at which CO and CH_4 are produced (below 500 °C the extent of homogeneous secondary reactions is very low [144]), whereas the latter are not distinguishable from heterogeneous charring reactions [44]. Using the measured concentrations values for H_2O, CO_2, CO and CH_4, the released amount of mass of each could be calculated. In Table 4.3 the mass yields in dry basis are summarized for pyrolysing beech and pine particles at 5 and 10 °C/min up to a final temperature of 525 °C. In the case of H_2O, to exclude the contributions from drying of the particle the mass values considered here are obtained for temperatures higher than 200 °C.

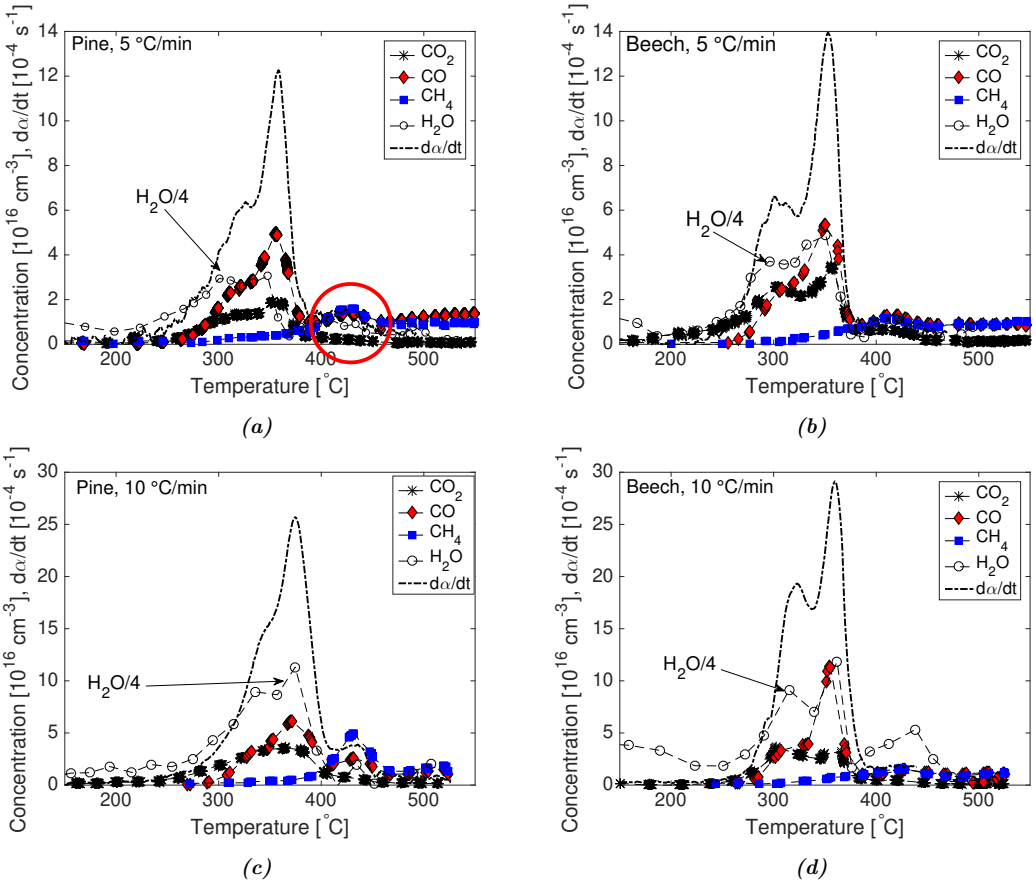

Figure 4.6: *Evolution of CO_2, CO, CH_4, H_2O, and $d\alpha/dt$ as a function of the temperature in the atmosphere in close vicinity of the particle: for pine at a heating rate of (a) 5 °C/min and (c) for 10 °C/min; for beech at corresponding conditions in graph (b) and (d), respectively. The rise of the conversion rate together with the increase in CO and CH_4 concentration at about 420 °C is marked with a red circle in graph (a) exemplarily. The values of the H_2O concentration are scaled down by a factor of 4 for better comparability.*

The total yields of CO, C_4H and H_2O are consistent with other values reported in literature [43, 89], from ex-situ measurements. In contrast, the findings of the values

Table 4.3: *Released mass yields of CO_2, CO and CH_4 in dry basis for pyrolysing beech and pine at heating rates of 5 and 10 °C/min up to a final temperature of 525 °C.*

	Beech		Pine	
	5 °C/min	10 °C/min	5 °C/min	10 °C/min
CO (%mass, db)	6.1	4.3	5.3	4.1
CO_2(%mass, db)	2.9	3.3	2.1	4.3
CH_4(%mass, db)	1.6	1.0	2.8	2.7
H_2O(%mass, db)	16.4	20.7	17.1	18.4

for CO_2 are lower than the ones typically reported in literature for these conditions. However, it must be taken into account that those are not in-situ measurements in close vicinity of the particle. In addition, the concentration values and therefore also the released mass yield of CO_2 have a significant higher uncertainty compared to the values for CO, CH_4 and H_2O as described in Section 4.3.2. Besides, the yield of CH_4 is higher for pine than for beech, which is consistent with the higher content in lignin in softwoods, since CH_4 is produced mainly from lignin and secondary reactions [29]. Comparing the CH_4 yields for different heating rates results in a slight reduction with increasing heating rates for beech. With respect to other volatiles, it is observed that in case of pine the CO yield decreases with increasing heating rate, while the CO_2 yield increases respectively. Although it is known that CO is a product of homogeneous tar cracking reactions, such contribution should be negligible at temperatures below 500 °C according to Anca-Couce and co-workers [44]. Therefore, contributions from homogeneous tar cracking reactions to the observed CO release are seen to be irrelevant for the reported experiments. In fact, according to Boroson et al. [145] both CO and CO_2 are products of heterogeneous cracking reactions, i.e., the cracking of tars in contact with the hot char, changing their composition. Furthermore, CO_2, H_2O and char are also the main products of heterogeneous charring reactions, enhanced by bigger particle size, pressure and the presence of inorganics [132]. However, the distinction between both reaction types is not completely understood and the former could be part of the later as well [44]. At high heating rates, the volatiles produced in the center of the particle interacts with hot catalytic char on their way out of the particle and undergo heterogeneous reactions which produce further CO_2. The production of H_2O seems to be also enhanced with higher heating rates, although the relative change is much smaller and could be due to other experimental factors, such as drying not being finished at higher heating rates.

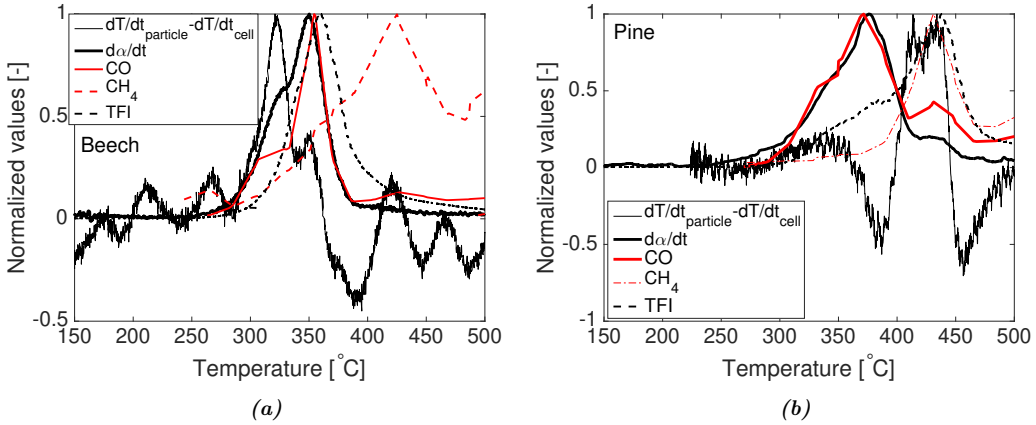

Figure 4.7: *(a) Comparison between the normalized values of $dT_{particle}/dt - dT_{cell}/dt$ and the normalized evolutions of $d\alpha/dt$, TFI, CO and CH_4 concentrations for (a) beech and (b) for pine at a heating rate of 10 °C/min.*

According to literature [146], PAHs are produced during slow pyrolysis at temperatures even below 500 °C and their production has been related to the presence of heterogeneous secondary reactions [28, 30, 81]. In the present study, the release of secondary reactions products, such as PAHs is characterized with the TFI, as defined in Section 4.3.1 and further explained in [30]. In Fig. 4.7 (a) and (b) the normalized TFI as a function of temperature in the close vicinity of the particle at a heating rate of 10 °C /min is shown for beech and pine, respectively. While in the case of beech the peak of TFI is slightly delayed with respect to $d\alpha/dt$, for pine it appears at significantly higher temperatures. This indicates that secondary reactions leading to the formation of PAHs are in the case of pine significantly delayed, i.e. occur at higher temperatures compared to beech. The release of PAHs has been also related with exothermicity [81]. An appropriate way to point out exothermicity graphically is plotting the difference of the temporal gradient in temperature inside the particle $dT_{particle}/dt$ and in the atmosphere around it dT_{cell}/dt as a function of the temperature in the PLRC. In Fig. 4.7 (a) and (b) the results are presented for beech and pine together with the corresponding evolution of CO and CH_4. All quantities are plotted normalized to its maximum.

For beech pyrolysed at a heating rate of 10 °C/min a first peak of exothermicity is observed at temperatures around 300 °C in close vicinity of the particle, which can be correlated with the degradation of hemicellulose [147]. The subsequent valley has been attributed in the literature to the combination of the simultaneous degradation of cellulose and lignin together with convective cooling, whereas the second exothermic peak is correlated to the degradation of lignin residue [147]. But, as can be seen in Fig. 4.7 (a), the second exothermic peak in beech decomposition coincides

approximately with the peak of the reaction rate which is usually attributed to the decomposition of cellulose. Furthermore, this exothermic peak also coincides with the maximum release of CO and H_2O (see also Fig. 4.6). Because of the maximum of the TFI evolution being also in the same range of temperatures these observations are seen as an indication that this exothermicity is correlated to the presence of heterogeneous secondary reactions of volatiles produced during primary pyrolysis. Therefore, there is a temporal overlap between the primary decomposition of cellulose and lignin and secondary reactions of their products (mainly lignin phenolics) leading to the observed PAH formation. Around 425 °C a third mild exothermic peak is observed coinciding with the release of CH_4 and therefore could be attributed to further degradation of the lignin residue, as reviewed by Di Blasi et al. [147].

For pine, however, the release of CO resembles almost exactly the curve of the conversion rate, accompanied by a significant endothermicity, associated with cellulose decomposition. At lower temperatures a very mild exothermicity occurs which could be related to the decomposition of hemicellulose. This is also consistent with the lower content of hemicellulose in softwood compared with hardwood. At higher temperatures, CH_4 is produced, coincident with the release of PAHs as well as with a strong exothermicity. This sequence is in accordance with the one reviewed by Di Blasi et al. [147].

In comparison to beech the differences in the evolution of the TFI and in the exothermicity peaks suggest, that in case of pine the two reasons for the observed exothermicity, i.e. secondary reactions leading to PAHs formation and further degradation of the lignin structure, identified by the release of CH_4, occur at the same time. Because of this, the exothermicity peak is more significant in case of pine than in case of beech. In the same temperature range of about 400 °C the conversion rate curve exhibits a shoulder which is attributed to the pyrolysis of lignin. It has been shown in literature that some stages in the decomposition of lignin, such as the cleavage of methoxyl groups occur at higher temperatures for softwood lignin compared to hardwood lignin [8]. In addition, a significant peak in the TFI evolution is observed indicating the potential formation of PAHs from phenolic volatiles during heterogeneous secondary reactions. A similar behavior regarding this delayed mass loss in pine in coincidence with an exothermic peak was also observed for experiments with beech leached particles (although without measurements of the gas composition [81]).

4.5 Conclusions

In the present study an approach for time-resolved in-situ characterization of slow pyrolysis at particle level is presented. Advanced spectroscopic techniques (IRLAS and LIF) are combined with mass and temperature measurements to gain further insights into the complex pyrolysis mechanisms. The evolution of the volatiles CO, CO_2, CH_4 and H_2O characterized quantitatively by means of IRLAS, as well as the evolution of PAHs characterized qualitatively by means of normalized TFI have been correlated with conversion rates and temperature evolutions of pyrolysing beech and pine wood spheres. Different release rates have been found for these species, which suggests different reaction pathways depending on wood type and heating rate. Higher heating rates seem to increase the production of CO_2 for both wood types due to heterogeneous catalytic cracking of primary volatiles. With respect to the exothermicity, it is present at all experimental conditions although to different extents. For beech, three exothermic regimes are observed. The first one is correlated to the decomposition of hemicellulose. The second one, at temperatures slightly higher than 350 °C is attributed to a temporal overlapping of primary decomposition of cellulose and lignin on one side and heterogeneous secondary reactions of the primary volatiles, such as phenolics on the other side. This would lead to the formation of PAHs as it was measured with LIF. The third exothermic regime is seen to be associated to further decomposition of the lignin residue which is linked to the release of CH_4. In contrast, in the case of pine, an endothermic region is observed in the same temperature range as the occurrence of the maximum of the conversion rate. For temperatures between 400 and 450 °C an exothermic region is observed which is in coincidence with the formation of PAHs and the release of CH_4. As shown by the mass loss curves the decomposition of the lignin is delayed for pine in comparison to beech. This results in the heterogeneous reactions of the primary products leading to PAHs formation to occur at the same time with further changes in the lignin structure resulting in an enhancement of the exothermicity. A similar behavior was observed for leached beech spheres. Therefore, both chemical and physical properties play a significant role in the different reaction pathways. These novel experiments bring new insights about heterogeneous secondary reactions within a single pyrolysing thermally thick particle as shown by different volatiles composition, exothermic regions and release of PAHs.

Chapter 5

Laser-based spectroscopy diagnosis and detailed numerical model to gain understanding on the slow pyrolysis behavior of thermally thick wood particles

This chapter is the peer-reviewed version of the article published in *Chemical Engineering Transactions* with the title "Laser-Based Spectroscopy Diagnosis and Detailed Numerical Models to Gain Understanding on the Slow Pyrolysis Behavior of Thermally Thick Wood Particles", H. Almuina-Villar, A. Anca-Couce, N. Lang, J. Röpcke, F. Behrendt, and A. Dieguez-Alonso. *Chemical Engineering Transactions*, 65: 109-114, 2018. https://doi.org/10.3303/CET1865019

5.1 Abstract

The slow pyrolysis behavior of thermally thick wood particles is investigated at 5, 10 and 20 °C/min, combining an advanced single-particle experimental approach with a detailed numerical model. Infrared laser absorption spectroscopy (IRLAS) and laser-induced fluorescence spectroscopy (LIF) are used to characterize on-line and in-situ the evolution of the following volatile products in the close vicinity of the pyrolysing particle: CO_2, CO, CH_4, H_2O, CH_2O and fluorescence-emitting species with excitation wavelengths of 266 and 355 nm, such as polycyclic aromatic hydrocarbons (PAHs). The numerical particle model is coupled with a detailed pyrolysis kinetic scheme, being able to predict with good accuracy mass loss, temperature evolution and online release of species such as H_2O and CO. Model predictions are

in some cases even better than for the medium heating rate conditions for which the model was initially tested, showing its wide applicability. Furthermore, the model can be improved including PAHs release, for which experimental data is presented, and the delayed release of CH_4, which is not correctly described by the model at low heating rates.

5.2 Introduction

Pyrolysis is a key stage in any thermochemical conversion of biomass [51], influencing aspects of the process, such as technology design and scale-up or emissions [17]. Despite its relevance, and due to its high complexity, enhanced by the interaction of chemical pathways and physical transport phenomena, the exact pyrolysis mechanism is still unknown [51]. In fixed-bed thermochemical conversion processes (gasification, combustion, slow pyrolysis), particle sizes in the centimeter scale are typically used [87, 148], which can have a strong influence on the pyrolysis mechanism [43, 87, 149] due to the presence of intra-particle secondary reactions, along with intra-particle temperature gradients. The current understanding of pyrolysis reaction mechanisms has been recently reviewed by Anca-Couce [8], pointing out that the kinetic schemes based on the one developed by Ranzi et al. [34], treating biomass as five components (cellulose, hemicellulose and three types of lignin), are the most detailed.

Ranzi's scheme has been applied in several single-particle models, reproducing the pyrolysis of thermally thick wood particles. Corbetta et al. [43] developed a single-particle model adapting Ranzi's scheme and including homogeneous secondary reactions of the pyrolysis volatiles [42], as well as the transport model developed by Park et al. [83]. Although the model [43] showed promising results for mass loss, temperature evolution and characterization of the released species, as highlighted by the authors, its further improvement would require the inclusion of heterogeneous secondary reactions. This adaptation of Ranzi's scheme [43] was also used by Bennadji et al. [87]. It was pointed out that future improvement of the kinetic scheme should include intra-particle tar reactions, as well as a reevaluation of kinetic parameters for the early evolution of gas species [87]. Anca-Couce et al. [44] adapted Ranzi's scheme to include the presence of secondary char-forming reactions, relevant in pyrolysis of thermally thick particles, as previously mentioned. In a recent study, Anca-Couce et al. [45] compared detailed experimental results at particle level with the results of a particle model using three different versions of Ranzi's scheme:

(1) the adaptation of Ranzi's scheme by Anca-Couce et al. [44] including secondary charring reactions (Version 1); (2) the adaptation of Ranzi's scheme by Corbetta et al. [43], including secondary charring reactions (Version 2); and (3) an improvement of Version 2, mainly regarding char yield and composition, as well as the release of light hydrocarbons, based on experimental results (Version 3) [45]. Version 3 (called in the following RAC V3) showed the best results, which included temperature in the centre and surface of the particle, mass loss and dynamic evolution of CO, H_2O, CO_2, CH_4, other light hydrocarbons and light condensable species (formaldehyde, acetic acid, methanol, ethanol, acetaldehyde and acetic acid), characterized on-line and off-situ with Fourier-transform infrared absorption (FTIR), and levoglucosan, measured off-line by gas chromatography – mass spectrometry (GC-MS). Despite the achieved improvements, the authors highlighted the need to include the influence of inorganic species on the pyrolysis mechanism, the description of secondary charring reactions with Arrhenius equations (instead of fitted parameters) and the formation of PAHs (polyaromatic hydrocarbons), BTX (benzene toluene xylene) and soot, accompanied by a more detailed characterization of the volatile products and validation under different conditions.

Quantification of volatiles in single-particle pyrolysis experiments has been done predominantly in an ex-situ manner, either online or offline, usually applying FTIR and chromatography techniques [45, 96]. However, in order to correctly characterize the volatiles produced during pyrolysis, in-situ techniques should be preferred, with the objective of avoiding possible further reactions of the targeted species. Zobel and Anca-Couce [30] applied laser-induced fluorescence (LIF) spectroscopy to detect PAHs formed during pyrolysis of thermally thick wood particles. Lang et al. [149] combined two laser-based spectroscopy techniques (IRLAS - infrared laser absorption spectroscopy - and LIF) to analyze the volatiles composition in the close vicinity of a pyrolysing particle.

The objective of the present study is to compare the experimental characterization (particle mass and temperature evolution; release of volatile species) of a single pyrolysing wood particle with the results obtained from the particle model developed by Anca-Couce et al. [45], using the adaptation of Ranzi's pyrolysis kinetic scheme (RAC V3) carried out by Anca-Couce et al. [45]. The particle model was adapted in the present study to meet the conditions used in the experiments. For the experimental characterization of the volatiles release, the innovative approach, based on the combination of two laser-based spectroscopy techniques (LIF and IRLAS), previously introduced, was used. These experiments were performed with beech wood

spheres, with a diameter of 25 mm, at three heating rates: 5, 10 and 20 °C/min. The experimental results have been published in Lang et al. [149]. Moreover, the experimental and modeled volatiles evolution reported by Anca-Couce et al. [45] are also used in the present study for comparison. In Anca-Couce et al. [45], medium heating rates (> 150 °C/min) and smaller particles (spruce cylindrical pellets with a diameter of 8 mm and a length of 19 mm) were employed. This novel comparison between numerical and experimental results under different conditions, including different experimental setups, will bring new insights into the pyrolysis reaction mechanism and the influence of secondary charring reactions.

5.3 Experimental and model description

The experimental setup used to perform the single particle pyrolysis experiments has been presented elsewhere [149]. Dried beech spheres (Ø = 25 mm; mass around 5.5 g) were used. Characterization of this material is given in Table 5.1. Three heating rates, 5, 10 and 20 °C/min were applied until a final temperature of 600 °C. Moreover, the experimental results published by Anca-Couce et al. [45] were employed in the present study for comparison purposes. These experimental results were obtained from pyrolysis of spruce pellets (Ø = 25 mm, L =9 mm; mass around 1.5 g), conducted at higher heating rates (> 150 °C/min) until a final temperature of 550 °C. The particle model used in the present study has been developed by Anca-Couce et al. [45]. This model uses the adaptation (RAC V3) of Ranzi's kinetic scheme developed by Anca-Couce et al. [45], based on an earlier adaptation of Ranzi's kinetic scheme developed by Corbetta et al. [43].

In the RAC V3 scheme, secondary charring reactions are included, as well as further adjustments (volatiles composition and stoichiometric factors) in Corbetta´s scheme, based on comparison with experimental data from Anca-Couce et al. [45]. The introduction of secondary charring reactions was done in the form of fitting parameters, X_{CEL}, X_{HCE}, X_{LIG} and $X_{G\{\}}$, introduced in Table 5.2 [45, 150]. They represent the extent of these reactions in cellulose, hemicellulose and lignin pyrolysis, as well as secondary reactions in the char formed at lower temperatures ($X_{G\{\}}$). Biomass is treated as five independent pseudo- components: cellulose, hemicellulose and three types of lignin (depending on the proportion of C, H and O).

To meet the experimental conditions pertinent to the experimental results presented in this study [149], several model parameters were modified with respect to the

Table 5.1: *Raw materials properties.*

(%wt.,db)	Beech	Spruce [45]
Volatiles	85.60 ± 0.20	-
Ash	0.41 ± 0.01	0.40
Fixed. carbon[a]	13.98 ± 0.20	-
Moisture	-	8
C(%)	48.35 ± 0.14	50.15
N(%)	0.09 ± 0.00	-
H(%)	6.87 ± 0.04	6.23
S(%)	0.06 ± 0.02	-
O(%)[b]	44.65 ± 0.15	-
Apparent density, g/cm^3	0.708 ± 0.034	1.120

[a] Fixed carbon is obtained by difference 100 %-(Volatiles(%)+Ash(%)).

[b] Oxygen content is calculated by difference: 100 %-(C(%)+N(%)+H(%)+S(%)+ash(%)).

ones presented by Anca-Couce et al. [45], shown in Table 5.2. No homogeneous tar cracking reactions in the reactor were considered due to the low temperatures. Other model parameters remained unchanged.

5.4 Results and discussion

In Fig. 5.1, the comparison between experimental and numerical results is presented for the time-dependent evolution of the solid mass fraction and the temperature in both center and surface of the particle. The experimental temperature evolution at 10 °C/min and the experimental mass loss evolution at 5, 10 and 20 °C/min have been already published in a recent work of this group [149]. It is important to clarify that while the model gives the temperature on the particle surface, experimentally this was measured in the close vicinity of the particle, i.e., a few mm from the particle surface. This could explain the differences between model and experiments at low temperatures. The experimental mass loss evolutions and solid yields (Fig. 5.1, right) were well predicted by the model, specially at the lowest heating rates, 5 and 10 °C/min. With respect to the temperature in the center of the particle, the model was able to reproduce the exothermicity present in all cases, identified when the temperature in the center of the particle exceeded the temperature on the surface of the particle. This exothermicity was also stronger with higher heating rates and, at each heating rate, two exothermic regimes were identified. These were associated to hemicellulose decomposition and to the overlapping of primary cellulose

Table 5.2: *Single-particle model parameters changed in the present study with respect to Anca-Couce et al. [45].*

Properties	Present study	Anca-Couce et al. [45]
Porosity	0.53	0.2
Cellulose[a] [%]	42	44
Hemicellulose[a] [%]	31.5	26
Lignin-C[a] [%]	13	17.5
Lignin-H[a] [%]	1.6	9.5
Lignin-O[a] [%]	11.9	3
X_{CEL}	0.2	0.05
X_{HCE}	0.2	0.1
X_{LIG}	0.3	0.15
$X_{G\{\}}$	0.4	0.2
$T_{heating}$[b] [°C]	T_{amb} – 600	550
Gas velocity[c] [m/s]	0.03 – 0.10	0.35
Geometry	Sphere (Ø = 25 mm)	Cylinder (Ø = 8mm; L = 19 mm)

[a] Taken from Gauthier et al. [84]

[b] The temperatures measured in the particle-level reactor were taken as boundary conditions. For convective heat transfer, the temperature measured in the atmosphere, in the close vicinity of the pyrolysing particle, was used. For radiation, an average of the temperatures measured in the particle-level reactor walls (externally heated) was used

[c] Temperature-dependent gas velocity

decomposition and lignin, and linked with heterogeneous secondary reactions of the primary volatiles [149].

In the detailed kinetic scheme coupled to the particle model, used in the present study and developed by Anca-Couce et al. [45, 150], the presence and extent of exothermic heterogeneous charring reactions were determined by a factor "X" for each pseudo-component. This was the only factor "fitted" in the present model, to get a good agreement between model and experiments, regarding final char yield and temperature evolution.

The "X" factors for all pseudo-components increased with respect to the values used by Anca-Couce et al. [45], and they were very similar to the values suggested for high charring conditions in Anca-Couce et al. [150]. This indicates that the extent of secondary charring reactions during pyrolysis of a beech particle (in Lang et al. [149]) was higher than for pyrolysis of a spruce particle (in Anca-Couce et al. [45]), where the heating rates were higher (> 150 °C/min) and the particle size smaller, as presented in Section 5.3.

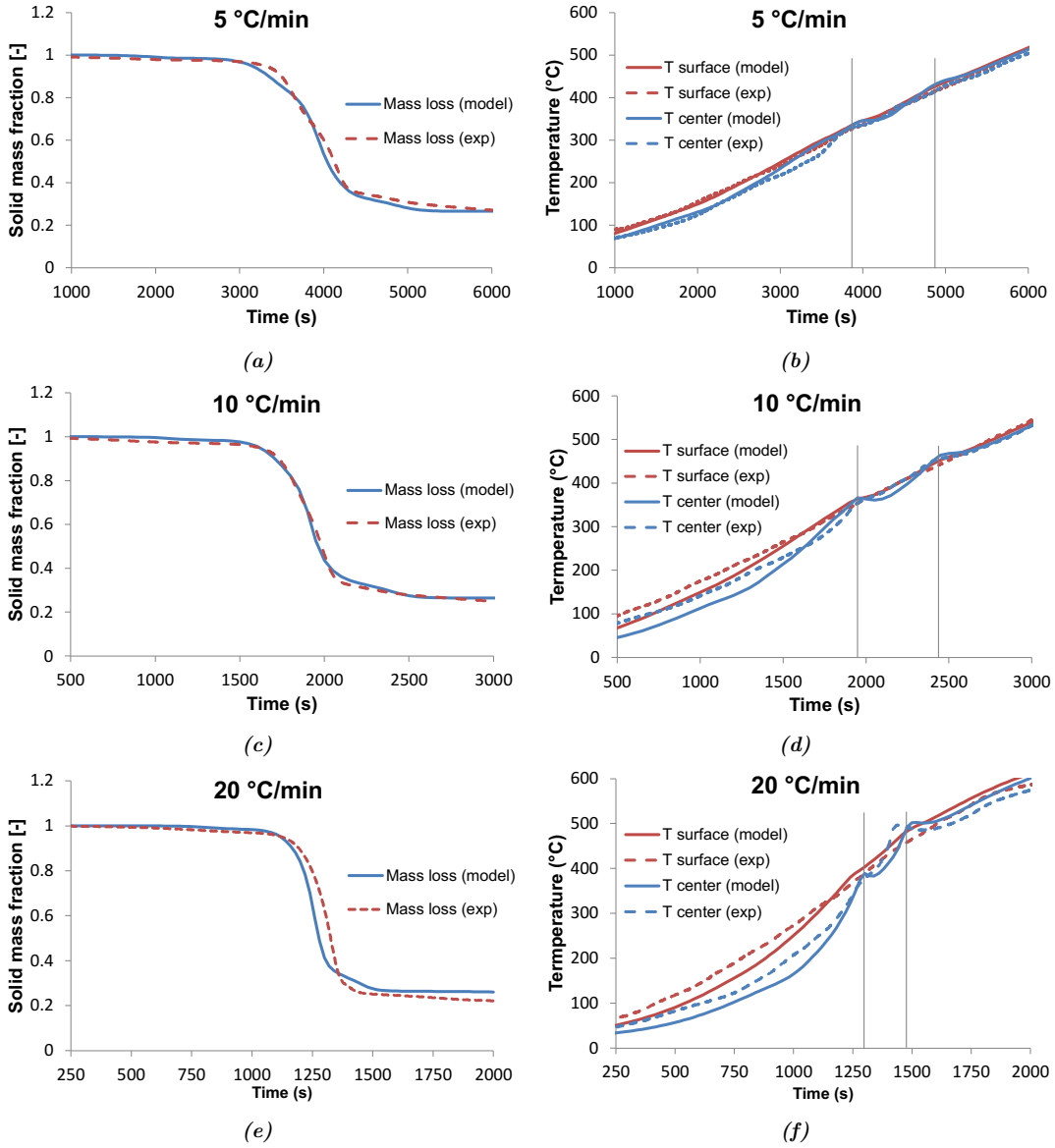

Figure 5.1: *Comparison of mass loss (left) and temperature evolution (right) between experimental (dashed lines) and numerical (solid lines) results for pyrolysis of a beech particle at 5, 10 and 20 °C/min. For temperature comparison, red lines represent the surface temperature and blue lines the temperature in the center of the particle. The experimental results for mass loss and temperature evolution at 10 °C/min have been published in a study of this group [149]. Vertical lines distinguish the exothermic regions.*

In Fig. 5.2, a comparison between numerical and experimental results for release of H_2O (a), CO_2 (b), CO (c), CH_4 (d) and CH_2O (e) during pyrolysis of beech at 5 °C/min is presented. The concentration of these species was determined with IRLAS in the close vicinity of the particle, as introduced in Section 5.3. Both numerical and experimental results from the present work are also compared with the numerical and experimental results from Anca-Couce et al. [45]. The differences in heating rate and initial mass explain the difference in the release values, expressed in g/s, between the two sets of results. The mass yields of the measured volatile species are also compared in Table 5.3.

Table 5.3: *Mass yields of the main characterized volatile species during pyrolysis of beech at 5 °C/min. The experimental results from the "present study" have been published in a recent work of this group [149].*

Yields	Present study		Anca-Couce et al. [45]	
(wt.%)	Experimental	Model	Experimental	Model
H_2O	16.4	14.2	18.0	16.4
CO	6.1	6.3	4.8	6.2
CO_2	2.9	14.4	11.6	11.4
CH_4	1.6	1.3	1.5	1.4

For H_2O and CO there is remarkable good agreement between numerical and experimental results (Fig. 5.2 and Table 5.3) in the present study, even better than those for A-C (Anca-Couce et al. [45]. This supports the applicability of the model for a wide variety of experimental conditions. For CO_2 and CH_4 the fitting was not as good. One of the reasons is the technical limitations of the IRLAS technique to measure CO_2, due to the influence of temperature in these measurements [149]. This could lead to a lower measured CO_2 yield and will be addressed in future work of this group. For CH_4, however, these limitations were in principle not present. CH_4 yields were predicted with a good accuracy (Table 5.3), but CH_4 was released mainly at the end of the experiment, i.e. at high conversions, which was not completely captured by the model, specially for the results of this study at low heating rates. The pyrolysis reaction scheme has been already adapted in Anca-Couce et al. [45] to account, to some extent, for this delayed release at medium heating rates (A-C in Fig. 5.2, d). The novel results at low heating rates in this study show, however, that further modifications are still needed in order to correctly predict the delayed release of light hydrocarbons. The CH_4 evolution is presented normalized for a better comparison between model and experiments, so that CH_4 release, especially at low heating rates, is clearly seen, as it takes place mainly at the end of

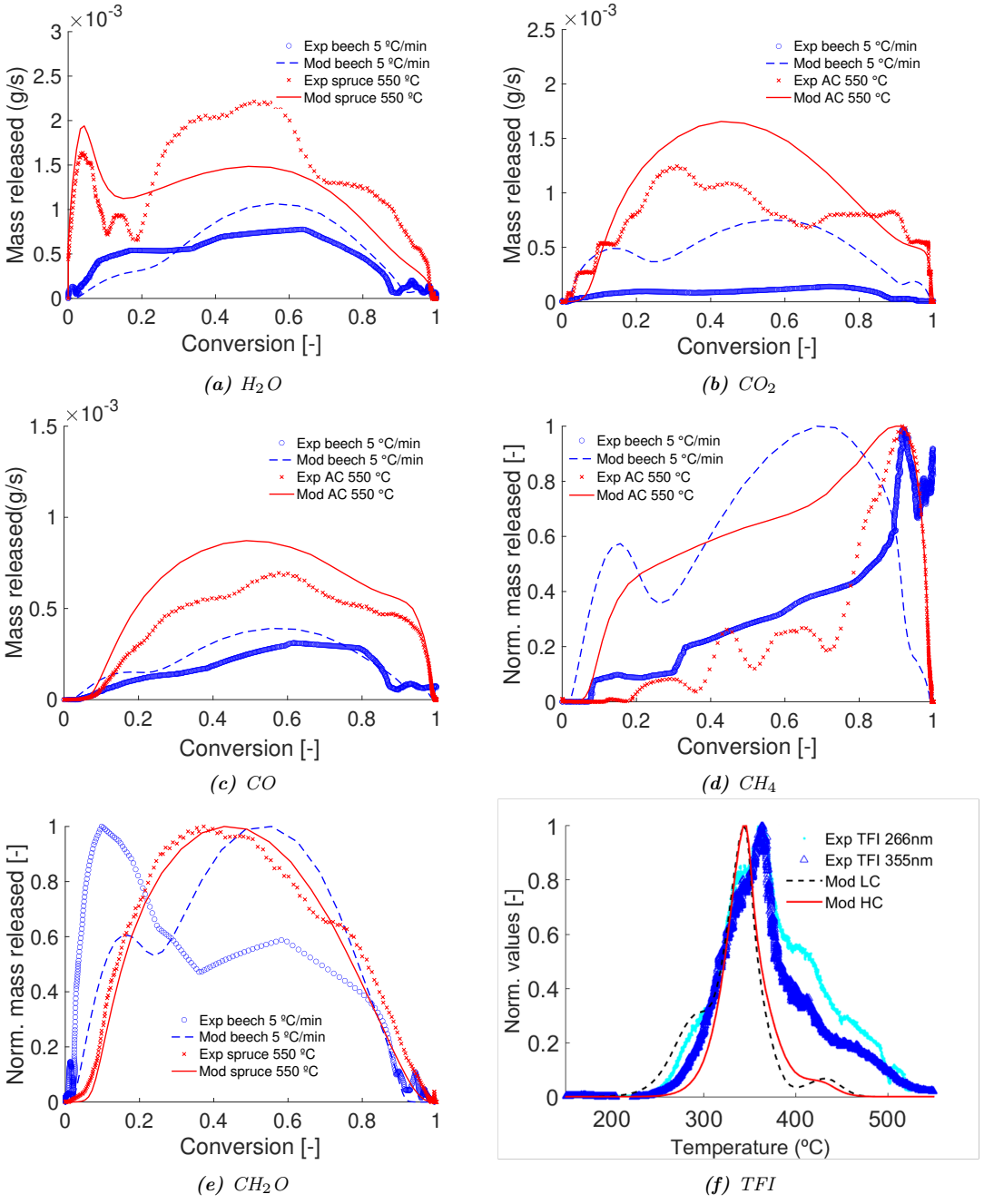

(a) H_2O *(b)* CO_2 *(c)* CO *(d)* CH_4 *(e)* CH_2O *(f)* TFI

Figure 5.2: *Comparison for (a) H_2O, (b) CO_2, (c) CO, (d) CH_4 (normalized), (e) CH_2O (normalized) production between numerical and experimental results. The experimental results (blue circles) of the present study were published in Lang et al. [149], except for CH_2O. In red, the results from Anca-Couce et al. [45] are shown. (f) Comparison between the evolution of fluorescence-emitting species determined with 355 and 266 excitation wavelengths and the numerical results for light condensables (LC) and heavy condensables (HC) from the present study.*

the experiment, in a period with a small variation in total conversion, and slowly, achieving low values in g/s.

In Fig. 5.2 (e) the normalized values of formaldehyde (the time-dependent evolution was measured in this study, but not the absolute concentration) are also compared. It is possible to see that the behavior was different in both cases. In the present study, there were two regions of emission, one at low conversion, coincident with hemicellulose decomposition and a second one at higher conversion, coincident with the emission of CO and other species, i.e., with the main decomposition of cellulose. The model can qualitative predict these two regions observed in the experimental results at a low heating rate. In the case of A-C's results, only one region was present, probably due to the merging of the two aforementioned regions at higher heating rates. In Fig. 5.2, (f) the qualitative evolution of species that can emit fluorescence when excited at 266 and 355 nm is compared with the model derived evolution of light condensables (LC) (carbonyls and alcohols, including formaldehyde and other species) and heavy condensables (HC) (5-hydroxymetylfurfural, phenolics and sugars). The fluorescence emitting species at these excitation wavelengths should be mainly PAHs [28, 149]. It is then observed that the emission of PAHs, coming from secondary reactions, was delayed with respect to the emission of the pyrolysis condensable volatiles. This data can be employed to further improve pyrolysis models including PAHs release.

5.5 Conclusions

A detailed experimental characterization of the slow pyrolytic behavior of a thermally thick wood particle (beech) is compared with the results of a particle model, including a detailed pyrolysis scheme, with 22 volatile species, and accounting for the influence of secondary charring reactions. The experimental characterization was performed with an innovative experimental approach, combining two spectroscopy techniques (IRLAS and LIF). The model was able to properly predict mass loss, temperature in the center and surface of the particle and the evolution of volatile species, such as H_2O and CO, in conditions enhancing secondary charring reactions. The obtained results were in some cases even better than for the medium heating rate conditions for which the model was initially tested, with a lower extent of secondary charring reactions. This shows the wide applicability of the model and the suitability of volatiles characterization with sensitive on-line and in-situ techniques. The results also show that although the total yield of CH_4 was well predicted, the

delayed CH_4 release was not correctly described by the model at low heating rates. Experimental data for future model improvements including PAHs release were also provided.

Chapter 6

Application of laser-based diagnostics for characterization of the influence of inorganics on the slow pyrolysis of woody biomass

This chapter is the peer-reviewed version of the article published in *Journal of Analytical and Applied Pyrolysis* with the title "Application of laser-based diagnostics for characterization of the influence of inorganics on the slow pyrolysis of woody biomass", H. Almuina-Villar, N. Lang, A. Anca-Couce, J. Röpcke, F. Behrendt, and A. Dieguez-Alonso. *Journal of Analytical and Applied Pyrolysis*, 140: 125-136, 2019. https://doi.org/10.1016/j.jaap.2019.03.004

6.1 Abstract

The influence of inorganic species content on the slow pyrolysis of thermally thick wood particles was investigated with the application of laser-based spectroscopy techniques. Infrared laser absorption and laser-induced fluorescence were used to characterize, on-line and in-situ, the release of permanent gases (CO and CH_4) and the formation of species emitting fluorescence, respectively. These advanced methods were combined with the continuous monitoring of mass and temperature and with off-line GC-MS and elemental analyses of the liquid and solid fractions. The experiments were performed using spherical particles of beech, H_2O- and HCl-washed beech, KCl-doped beech and pine. The pyrolytic behavior of washed beech (with lower content in inorganic species) was found to resemble much closely the one of

pine, rather than the one of beech, probably due to the pine low content in K. Both washed beech and pine showed a more clear separation between cellulose and lignin decomposition, being the lignin decomposition, and potentially the presence of heterogeneous secondary reactions, shifted to higher temperatures. The composition of the species emitting fluorescence was also affected by the removal of inorganics, resulting in more red-shifted spectra (i.e. higher emission wavelengths). K was observed to catalyze the pyrolysis reaction, accompanied by a strong exothermic behavior, coincident with the release of fluorescence-emitting species (e.g. PAHs) and, therefore, with the presence of secondary charring reactions. Moreover, at the end of the pyrolysis process, further reactions in the char, enhanced by the presence of K, were detected, with no further mass loss or temperature gradient, leading to the further formation of fluorescence-emitting species (e.g. PAHs). For KCl-doped beech, the fluorescence spectra were more blue-shifted (i.e. lower emission wavelengths) in comparison to the rest of the materials. Higher content in inorganic species resulted also in higher char yields, lower major carbohydrates yields and slightly higher guaiacols, syringols and phenols yields. This indicates an enhancement of charring reactions, in good agreement with the higher exothermicity, as well as in fragmentation reactions and in the lignin reactivity with higher presence of inorganic species.

6.2 Introduction

The current understanding of the pyrolysis reaction mechanism for cellulose and lignocellulosic materials has been recently reviewed by Anca-Couce [8]. According to this review, one of the most promising detailed pyrolysis mechanisms up to now to describe the pyrolysis of lignocellulosic biomass is the one proposed by Ranzi et al. [34], where biomass is treated as five components which decompose independently: cellulose, hemicellulose and three types of lignin. This mechanism has been further adapted by Corbetta et al. [43], including as well gas phase reactions at the particle level, and by Anca-Couce et al. [44], including heterogeneous secondary reactions (in the form of fitting parameters). However, it still presents important limitations as highlighted by Anca-Couce et al. [45] including, among others: a) kinetic schemes for heterogeneous secondary reactions are not included, b) the influence of inorganic species on the pyrolysis mechanism is not taken into account, c) the interactions between biomass components and their pyrolysis products are not included. While kinetics for homogeneous reactions of lignocellulosic pyrolysis tars have been

reported in literature to an acceptable maturity level [42, 85, 151–153], the determination and implementation in pyrolysis kinetic schemes of heterogeneous secondary reactions is less developed [144, 145, 154–157], although a better understanding of the presence of these reactions has been achieved [28, 81, 89, 149]. Moreover the impact of inorganic species on the pyrolysis mechanism of lignocellulosic materials in general, and on heterogeneous reactions in particular, needs to be better understood and characterized, both qualitatively and quantitatively.

The influence of inorganic species on the pyrolytic behavior of cellulose has been widely investigated. Already in 1995 Antal and Varhegyi [59], after a comprehensive review of the topic, reported that two main competitive reaction pathways are active during pyrolysis of cellulose, one leading to the formation of levoglucosan as major product and the other one leading to the formation of glycolaldehyde and other fragmentation products, favored by higher temperatures and heating rates. This second fragmentation route was observed to be also enhanced with the addition of alkali and alkaline earth species, favoring as well char formation. Mamleev et al. [60] reported the enhancement of fragmentation and dehydration reactions, leading to char formation, upon addition of alkali salts to cellulose. Their two-level kinetic model assumed that first transglycoxylation reactions occur, leading to the formation of tar.Volatile acids present in this tar can catalyze several heterolytic reactions, including depolymerization by the acid-catalyzed β-elimination. The enhancement of the β-elimination pathway results in lower levoglucosan yields. A competition between cross-linking reactions, leading to the formation of char, and fragmentation reactions, leading to the formation of gases and light volatiles is established then between intermediate products in the liquid phase. The latter is favored by high temperatures. Both can be enhanced by the presence of alkali species, as previously introduced, although the origin of this catalytic behavior is not clear so far [60]. The enhancement of dehydration reactions upon addition of potassium in cellulose pyrolysis was also reported by Trendewicz et al. [41], enhancing the formation of char, water and permanent gases, while leading to a strong inhibition of levoglucosan formation and to lower oil yields with reduced heating values. It has been also reported that the mechanism behind the catalytic effect of inorganic species on cellulose pyrolysis was mainly ionic, being acidity/alkalinity of secondary importance [41, 158]. Based on experimental data of Avicel cellulose pyrolysis doped with K (in the form of K_2CO_3, with concentrations 0.01 - 1 % mass) in kinetic regime (4 mg sample), combined with on-line volatiles characterization in a MBMS, Trendewicz et al. [41] proposed a modification of Ranzi's kinetic scheme [42]. With

the aid of Principle Component Analysis (PCA) applied on the MBMS data, the principal components were identified. To analyze the impact of inorganics on the cellulose pyrolysis mechanism, two principal components were considered, one representing anhydrogusars (PC1) and a second one representing fragmentation products (hydroxyacetaldehyde, 5-hydroxymethyfurfural, among others) (PC2). An increase in the activation energies for the reactive pathways leading to the formation of levoglucosan and fragmentation products was observed, although more significantly for the former, upon addition of K. On the contrary the activation energy for the formation of char decreased. It is important to mention that the authors [41] attributed the increased char formation to the solely effect of inorganics and not to secondary reactions.

LeBrech et al. [68] and Ferreiro et al. [62] reported that the impregnation of cellulose with K resulted in a shift of the beginning of the pyrolysis decomposition towards lower temperatures, higher char yields, lower conversion rate peaks, and a shift to lower temperatures of the maximum of the conversion rate. Ferreiro et al. [62] also proposed a modification of Ranzi's pyrolysis mechanism to account for the influence of KCl on the cellulose decomposition, catalyzing the formation of char and low molecular weight compounds, while inhibiting the formation of levoglucosan. LeBrech et al. [68] applied in situ ^{1}H NMR spectroscopy to characterize the amount of fluid ^{1}H NMR, referred to as mobility. As already highlighted by Mamleev et al. [60], to promote acid catalyzed reactions two factors are required: the presence of an ion-conductive medium, i.e. an electrolyte, and the presence of donor of mobile protons. The liquid tar (intermediate species) [60] formed during the pyrolysis process that fills the cavities in the cellulose matrix, also referred to as liquid intermediate, e.g. by LeBrech et al. [68], acts as the electrolyte. LeBrech et al. [68] observed that when cellulose is doped with K, the ^{1}H mobility is reduced. This reduction could be due to the inhibition of cellulose depolymerization (transglycoxylation reactions as presented by Mamleev et al. [60] to form the liquid tar) or due to an enhancement of homolytic scission due to the presence of K [68]. As hypothesized by Kuzhiyil et al. [159], the mechanism behind the influence of alkali and alkaline earth metals on the pyrolysis pathways involving ring scission lies on the formation of coordinate bonds between inorganic species and oxygen of nearby hydroxyl groups of the glucose ring, leading to its instability and finally to homolytic ring scission. The increase in the formation of radicals could then reduce the number of mobile protons, due to their interaction and stabilization [68]. During pyrolysis of pure cellulose, the mobility starts and reaches its maximum before any significant mass loss takes place. This

shows the formation and presence of the liquid intermediate phase, previously discussed [68]. However, in the case of K-doped cellulose, the mobility profile was very similar to the mass loss rate profile, indicating the formation of lighter species, product of the fragmentation reactions, that are volatilized more easily.

The authors [68] also analyzed the ^{1}H mobility during oak, Douglas fir and miscanthus pyrolysis. For miscanthus lower mobility was observed, in good agreement with the higher content in inorganic species as previously described. With respect to the two woody species, a delay in the ^{1}H mobility signal was observed for Douglas fir with respect to oak, although the maximum values were similar in both cases, despite the lower content in inorganics. This delay was also consistent with the delayed in the mass loss rate, which the authors attributed to the different hemicellulose composition, being more stable (glucomannan, C_2 pyranose) for Douglas fir than for oak (xylan, C_5 pyranose), and to the difference in inorganics content and composition. Finally, the pyrolysis behavior of both woody species and demineralized miscanthus was reported to be globally endothermic, while for miscanthus and K-doped miscanthus, the behavior was more thermoneutral, attributed to the enhancement of cross-linking reactions (exothermic) due to the presence of inorganic species [68]. Di Blasi et al. [160] also investigated the influence of K, including different K chemical states, on the exothermicity of wood pyrolysis. The authors also observed that the addition of K shifted the beginning of the conversion process and the maximum of the mass loss rate towards lower temperatures. The basicity of the K-containing species, as well as the total K content, also contributed to this shifting towards lower temperatures. The impact of K on the pyrolysis process was attributed by the authors [160] to a combined effect of alkaline pretreatment followed by catalysis. Guo et al. [161] observed as well a reduction in the initial and peak temperature when pyrolyzing K-doped pine in a TGA, resulting in lower apparent activation energy at initial pyroylsis stages. A very interesting result was the increase in activation energy at higher conversion degree, attributed by the authors to a change in the structure of the solid. Upon FTIR characterization of the produced char, it was observed that K may increase the polycondensation reaction of aromatic nucleus and promote the aromaticity and stability of the solid [161]. This was accompanied by an increase in gas yield (specially H_2 and CO_2) and a decrease in tar yield, observed at reactor level [161].

Most literature regarding pyrolysis mechanisms and the influence of inorganic species is focused on cellulose. However, there are similarities between cellulose and the other macrocomponents in lignocellulosic biomass, specially with respect to hemicel-

lulose. The present work aims at contributing to the understanding of the impact of inorganic species on the pyrolysis behavior of lignocellulosic biomass and the extent of heterogeneous secondary reactions, mainly in a qualitative manner. To this end, results of mass loss rate, exothermic/endothermic regimes, main gas species release and formation and release of species emitting fluorescence were combined. Moreover, tar condensation and off-line GC-MS analysis of the condensed volatiles were performed to gain further insight into their composition. The pyrolysis experiments were performed in a particle level reactor, using beech, washed beech, KCl-doped beech and pine as materials. For characterization of gas and aromatic species, infrared laser absorption spectroscopy (IRLAS) and laser-induced fluorescence (LIF) were applied, respectively. This experimental approach has been developed in a previous work of this group [149] and initially applied to the characterization of the pyrolytic behavior of beech and pine. The novelty in this work lies on the application of these advanced techniques to get further insights into the complex pyrolysis process regarding the global influence of inorganic species and secondary reactions at particle level.

6.3 Experimental

6.3.1 Experimental setup

The experimental setup used for the slow pyrolysis experiments is shown in Fig. 6.1, where the combined realization of the (I) laser-induced fluorescence (LIF) setup and the (II) infrared laser absorption (IRLAS) setup is presented (separated setups). Validation between both setups was performed. The particle cell is heated through 4 electrical heating cartridges symmetrically placed in the reactor walls. The particle hangs in the middle of the cell from a specially prepared thermocouple connected to a scale, allowing in this way, the continuous recording of mass and temperature in the centre of the particle. Moreover, another thermocouple records the temperature in the close vicinity of the particle (a few millimeters below the particle). The particle is positioned always with the main fibers orientation parallel to the horizontal plane. The composition of the volatiles is characterized on-line also a few millimeters below the pyrolysing particle.

For the LIF measurements, the third (355 nm) and fourth (266 nm) harmonics of a Nd-YAG laser (Quanta-Ray LAB-150) are used to excite and track targeted species in the volatiles stream leaving the pyrolysing particle. The emitted fluorescence

is detected in the perpendicular direction to the laser beam, coupling a spectrograph (Princeton Instruments, SpectraPro 2300i) with an ICCD camera (LaVision, NanoStar). This fluorescence is characterized through the total fluorescence intensity (TFI), normalized to its maximum value, and compared to the conversion rate and volatiles evolution. To determine the total fluorescence intensity (TFI) for each time step, each fluorescence spectrum was integrated according to Eq. 6.1. For experiments performed with an excitation wavelength of 266 nm, $\lambda_i = 266$ nm and $\lambda_f = 455$ nm. For experiments performed with an excitation wavelength of 355 nm, $\lambda_i = 355$ nm and $\lambda_f = 510$ nm

$$TFI = \int_{\lambda_i}^{\lambda_f} I(\lambda) d(\lambda) \tag{6.1}$$

The IRLAS setup is designed to determine the concentration of the main permanent gases leaving the particle on absolute scale, in-situ and time-resolved. A compact and mobile infrared multi-component acquisition system (IRMA) is used. A more detailed description of the IRMA system and the software used for the data analysis and its application for in-situ process monitoring can be found in [137, 138]. For further details on the experimental setup and the optical diagnostic methods the reader is referred to [149].

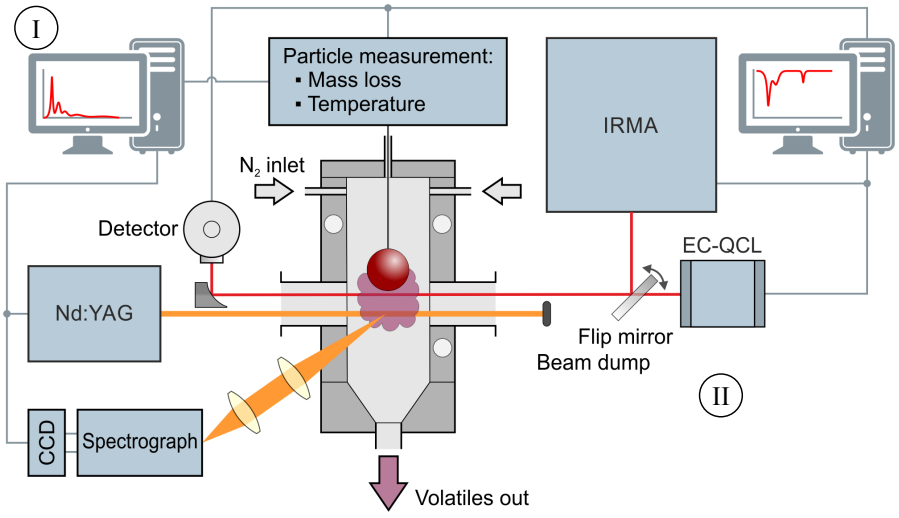

Figure 6.1: *Combined scheme of each individual experimental setup for both (I) the LIF and (II) the IRLAS measurement systems.*

6.3.2 Experimental conditions and analyses

Spherical particles (25 mm in diameter) were used to conduct the pyrolysis experiments. According to the treatment they are classified as follows:

- Beech wood
- Beech wood washed with H_2O
- Beech wood washed with HCl
- Beech wood doped with KCl
- Pine wood

The pyrolysis experiments were performed at two different heating rates (5 and 10 °C/min) up to a final temperature of 600 °C, with a N_2 flow rate of 3.5 Nl/min.

For beech wood washed with H_2O, the particles were washed with deionized water in vacuum during 24 h, dried for 24 h and washed again in vacuum for 24 h. For beech washed with HCl, the particles were washed during 24 h with a highly diluted HCl solution, followed by a second washing with deionized water, also during 24 h. For KCl treatment, approximately 100 g of beech wood were soaked in vacuum during 24 h in a solution of 9 g of KCl in 800 ml of deionized water. This was done after two washing steps with deionized water during 24 h (x 2) to remove other inorganic species. All particles were dried for over 24 h before performing the pyrolysis experiments. The ash content and elemental analysis of the raw materials are presented in Table 6.1.

Table 6.1: *Ash content and elemental analysis for beech, pine, H_2O-washed beech, HCl-washed beech, and KCl-doped beech.*

(wt.%, db)	Beech	Pine	H_2O-Beech	HCl-Beech	KCl-Beech
Ash(%)	0.41 ± 0.01	0.24 ± 0.06	0.27 ± 0.01	0.08 ± 0.03	0.77 ± 0.11
C(%)	48.35 ± 0.14	49.84 ± 0.43	46.32 ± 0.03	47.98 ± 0.54	48.22 ± 0.47
N(%)	0.09 ± 0.00	0.09 ± 0.05	0.10 ± 0.02	0.09 ± 0.01	0.05 ± 0.01
H(%)	6.87 ± 0.04	6.71 ± 0.36	6.11 ± 0.17	6.31 ± 0.04	6.54 ± 0.11
O[(a)](%)	44.65 ± 0.15	43.07 ± 0.55	47.07 ± 0.10	45.47 ± 0.58	44.24 ± 0.47
Bulk density (g/cm^3)	0.708 ± 0.034	0.554 ± 0.048	0.692 ± 0.053	0.660 ± 0.039	0.701 ± 0.050
Ca(mg/kg)	1204 ± 39.88	1241 ± 50.05	680.59 ± 38.59	460.27 ± 2.66	387.1 ± 15.63
K (mg/kg)	812.78 ± 23.61	137 ± 1.52	294.17 ± 13.99	168.4 ± 4.15	6606.25 ± 286.13
Mg(mg/kg)	379.85 ± 10.08	212.98 ± 3.43	182.33 ± 5.15	69.41 ± 1.16	98.64 ± 3.98
Mn(mg/kg)	148.43 ± 4.08	101.38 ± 1.48	82.65 ± 1.13	26.82 ± 0.41	85.13 ± 12.80
Na (mg/kg)	6.41 ± 0.77	9.12 ± 0.30	13.23 ± 8.59	5.74 ± 0.50	5.37 ± 2.80
Fe(mg/kg)	22.88 ± 1.21	7.50 ± 1.49	37.18 ± 2.11	4.36 ± 0.28	11.85 ± 1.89

[a] Oxygen content is calculated by difference: 100 %-(C(%)+N(%)+H(%)+S(%)+ash(%)).

The elemental composition (%C, %N, %H, and %O, given in wt.%, dry basis) was characterized in an elemental analyzer (Elemental Vario EL III). Inorganic elemental composition analysis was performed with ICP-OES (inductively coupled plasma - optical emission spectrometer, Varian 720-ES) after digestion in a microwave (Multiwave 3000, from Anton Paar) with nitric acid and hydrogen peroxide. The composition of the condensable volatiles, collected in a cold trap with isopropanol after the particle level reactor, was further analyzed in a GC-MS (HP G1800C GCD, Agilent) using a GC capillary column (Ultra 2, crosslinked 5% Ph-Me-Silicone 25 m x 0.2 mm x 0.33 μm) and He as carrier gas. The used temperature ramp was: 50 °C during 4 min, 15 °C/min up to 90 °C, holding for 5 min, 9 °C/min up to 320 °C, holding for 2 min. The column pressure was 100 kPa. The MS was operated in electron ionization mode, scanning a m/z range from 45 to 450. Standard mass spectra with an electron ionization energy of 70 eV were recorded.

It is important to mention that the condensable volatiles collected in the isopropanol trap, and therefore analyzed in the GC-MS, were only a fraction of the total condensed volatiles, due to condensation in other cold points upstream of the isopropanol trap. Nevertheless, all experiments were performed in the same conditions and repeated several times, which allows for comparison of the volatiles composition for the different materials. However, this may explain the low yields observed. The volatile species were quantified with respect to a known concentration of an internal standard (fluoranthene) introduced in all samples.

6.4 Results and discussion

6.4.1 Influence of inorganic species on the pyrolysis process

A comparison of the pyrolysis behavior for beech, H_2O- and HCl-washed beech, KCl-doped beech, and pine is presented in Fig. 6.2. These experiments were performed at a constant heating rate of 10 °C/min. The conversion rate is plotted together with the temporal evolution of the total fluorescence intensity (TFI), obtained with an excitation wavelength of 266 nm), CO and CH_4 release, as well as with the evolution of the thermal regimes versus the temperature in the close vicinity of the particle. The normalized curves (with respect to their maximum) are plotted for an easier comparison of the results. The presence of exothermic or endothermic regimes is characterized by the difference of the temperature time derivative in the centre ($dT/dt_{particle}$) and in the close vicinity (dT/dt_{cell}) of the particle. Positive values

are attributed to exothermic regimes while negative values to endothermic/thermally neutral ones. It should be taken into account that intra-particle temperature gradients are present due to the size of the particles, leading to a potential overlap of the conversion stages. However, looking at the experimental data (Fig. 6.2), it is still possible to distinguish the three conversion stages associated to cellulose, hemicellulose and lignin pyrolysis.

6.4.1.1 Beech, washed beech and pine

In a previous work of this group [149], it has been shown that the pyrolytic behavior of beech and pine differ with respect to the temperature-dependent thermochemistry, conversion rate and volatiles evolution. For a better comparison between all measurements, the results in Fig. 6.2 have been divided in several zones (I, II and III), based on the different phases of the conversion process. As discussed in [149], for beech (shown in Fig. 6.2 (a)) three exothermic regimes were observed. The first (and highest) exothermic regime, highlighted in Fig. 6.2 (a) as zone I, was associated with the decomposition of hemicellulose, also reported by Di Blasi et al. [147]. The second one, zone II, was associated with the primary decomposition of cellulose and lignin, together with the presence of heterogeneous secondary reactions of primary volatiles. As discussed by Di Blasi et al. [147], this overlap in cellulose and lignin decomposition can be endothermic or thermally neutral (observed in their results). However, the contribution of heterogeneous secondary reactions is not negligible, leading potentially to a change from endothermic to exothermic behavior, as observed in [149]. Finally, in zone III, the third exothermic regime, significantly milder, was attributed to further decomposition of the lignin residue, as discussed by Di Blasi et al. [147]. For pine (shown in Fig. 6.2 (b)), a first very mild exothermic peak was also observed in zone I and attributed to the decomposition of hemicellulose [149]. However, unlike beech wood, this was followed by an endothermic valley in zone II, consistent with cellulose decomposition. A second very exothermic peak was observed at higher temperatures (zone III), attributed to lignin decomposition and secondary reactions of primary volatiles coming from lignin decomposition [149].

In the present work, the study is extended to characterize the influence of inorganic species on the slow pyrolysis process. The results for H_2O-washed beech and HCl-washed beech are presented in Fig. 6.2 (c) and (d), respectively. The higher acidity in HCl-washed beech led to a more efficient removal of inorganic species, as it is shown in Table 6.1. The pyrolysis behavior was, however, quite similar in both cases. In zone I, a first exothermic peak was observed, as in the case of beech and pine wood,

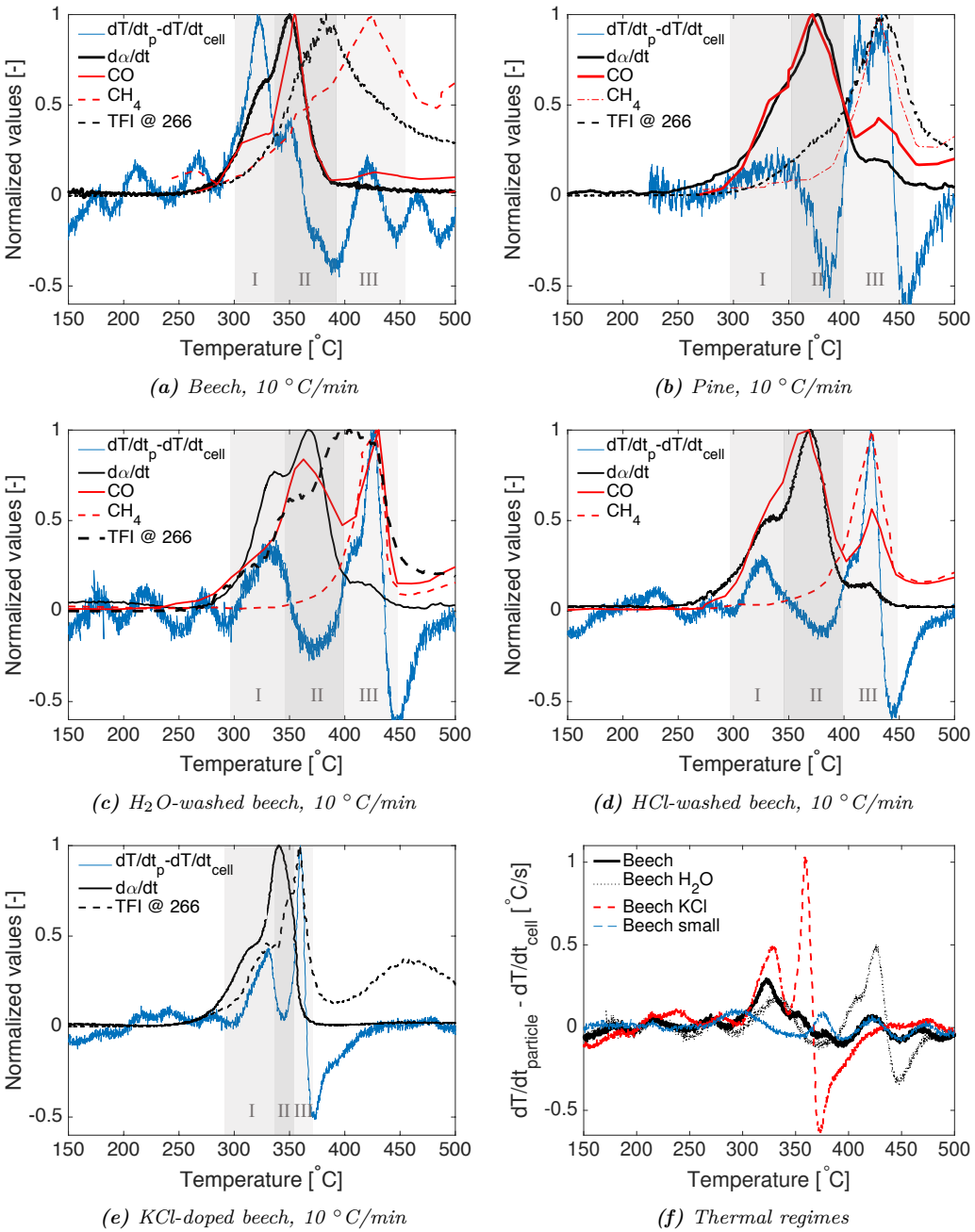

(a) Beech, 10 °C/min

(b) Pine, 10 °C/min

(c) H_2O-washed beech, 10 °C/min

(d) HCl-washed beech, 10 °C/min

(e) KCl-doped beech, 10 °C/min

(f) Thermal regimes

Figure 6.2: *Comparison of conversion rate, TFI (at 266 nm), CO and CH_4 release, and $dT/dt_{particle}$ - dT/dt_{cell} versus the temperature in the close vicinity of the particle for: (a) beech (adapted from [149]), (b) pine (adapted from [149]), (c) H_2O-washed beech, (d) HCl-washed beech (TFI not measured), and (e) KCl-doped beech (CO and CH_4 not measured). (f) $dT/dt_{particle}$ - dT/dt_{cell} for beech, H_2O-washed beech, KCl-doped beech and beech with diameter of 15 mm.*

coincident with hemicellulose decomposition. This was followed, already in zone II, by an endothermic/thermally neutral valley and a second strongly exothermic peak in zone III. It is possible to see that this behavior is more similar to the one of pine, rather than to the one of beech, previously introduced. While for beech wood a mild exothermic behavior was observed in zone II, in the case of pine and washed beech an endothermic/thermally neutral valley was observed. This may suggest that for beech the presence of inorganic species (specially alkali and alkaline earth metals) catalyzed the pyrolysis process, leading in zone II to an overlap of cellulose and lignin decomposition, as well as of heterogeneous reactions of the produced volatiles. However, for H_2O- and HCl-washed beech, a more pronounced shoulder in the conversion rate at high temperatures was observed, typically associated with lignin decomposition. This indicates the shifting of lignin decomposition to zone III, similar to the behavior observed for pine. This could be attributed to the absence of the catalytic effect associated with inorganic species for both washed beech and pine. As it is shown in Table 6.1, in both cases the content of inorganics, specially species such as K, was very similar and significantly lower than for beech.

Different behavior can also be observed when analyzing the permanent gases normalized release. In the case of CO, two clear release zones were observed for pine and H_2O- and HCl-washed beech. The first one is related to the main decomposition of hemicellulose and cellulose, highlighted as zones I and II, and also coincident with the first exothermic and endothermic/thermally neutral regimes. The second peak in CO release occurred simultaneously with the second exothermic peak at a later stage of the pyrolysis process (zone III), previously attributed to lignin decomposition and heterogeneous secondary reactions of primary products. This behavior also resembles more closely the one of pine. In the case of beech, however, only one significant peak of CO release was observed in zone II, occurring simultaneously with the overlapped decomposition of cellulose and lignin. The release of CO in zone III was minor. In all cases, CH_4 was mainly observed between 400 and 450 °C (measured in the close vicinity of the particle, zone III), being coincident with the last exothermic regime associated with further decomposition of lignin. However, in the case of beech wood, in which lignin decomposition overlapped cellulose decomposition, CH_4 release at lower temperatures was also significant in comparison to the maximum release. The small CH_4 peak observed for beech at temperatures around 275 °C was probably due to an artifact in the spectroscopic measurement.

The TFI signals were obtained with excitation wavelengths of 266 nm and 355 nm, while in Lang et al. [149] only an excitation wavelength of 355 nm was used. Further

insights into the interpretation of the collected fluorescence signal are provided in Section 6.4.2. In previous studies, the fluorescence signal using these excitation wavelengths was associated with the formation of PAHs, among other species, such as phenolics, ketones and aldehydes [28,29,149,162]. As it can be seen in Fig. 6.2 (a) and (b), the TFI peak maximum for beech occurred at lower temperatures (around 375 °C in the close vicinity of the particle, zone II) than in the case of pine (at about 425 °C, zone III). These results were already reported in [149] and attributed to the difference in the presence of heterogeneous secondary reactions between beech and pine. While in the former an overlap of secondary reactions with cellulose and lignin decomposition occurred, for the latter these heterogeneous secondary reactions happened together with the decomposition of lignin. In the case of H_2O-washed beech, the TFI peak was observed in a wider temperature range, being its maximum located at an intermediate temperature (approximately 400 °C) between beech and pine. At higher temperatures, the TFI decayed simultaneously with the CO (second peak) and CH_4 evolutions, as well as with the shift from exothermic to thermally neutral regime, supporting the relation between all these variables.

The TFI with an excitation wavelength of 266 nm was not measured for HCl-washed beech. However, due to the similar behavior with H_2O-washed beech, the LIF signal is expected not to differ significantly.

6.4.1.2 KCl-doped beech

To further prove the influence of inorganic species, specially K, beech particles were first H_2O-washed and then doped with KCl. As shown in Table 6.1, this resulted in samples with a K content of approximately 0.65 wt.%, in dry basis. It can be observed in Fig. 6.2 (e), that there was a shift to lower temperatures in the conversion rate and a narrowing of the temperature range in which this took place, occurring zones I, II and III between 300 and 375 °C. The catalytic effect of K in wood pyrolysis was already reported in literature, as reviewed in Section 6.2. In the present study, a first exothermic regime was observed in the same region (zone I), followed by an endothermic/thermally neutral valley in zone II, coincident with the maximum of the conversion rate. At temperatures higher than 350 °C, in zone III, a very strong exothermic region was observed, which was also coincident with the maximum of the TFI evolution. In this case, both exothermic regimes were stronger than for the other materials, as it can be seen in Fig. 6.2 (f). For the sake of comparison, a small particle (15 mm in diameter) was also pyrolyzed in the same conditions, not observing the same strong exothermic regimes as for the big particles.

This indicates that smaller particle size may lead to a lower presence of heterogeneous secondary reactions and, consequently, lower exothermicity.

With respect to the TFI evolution, a first shoulder was observed in zone I, as for washed beech and pine wood, coincident with the first exothermic peak maximum. This was followed by a rise in the fluorescence signal during the maximum of the conversion rate, being the maximum of the TFI in zone III, coincident with the second exothermic peak, as previously introduced. Noteworthy to mention is the wide fluorescence peak observed at higher temperatures, with its maximum at around 460 °C. At these temperatures, no significant mass loss was detected and there was no noticeable temperature gradient between the inner part of the particle and the atmosphere close to the particle. Therefore, this signal could be related to further reactions in the char, enhanced by the presence of alkali metals and leading to the formation of different species, including PAHs [68, 163].

6.4.1.3 Product yields

Higher content in inorganic species, and specially in K, resulted in higher char yields, as it is shown in Table 6.2, although the contribution of K (in mass) to the final char yield for KCl-doped beech experiments may not be negligible. The higher char yields are in good agreement with the catalytic effect of K on dehydration reactions, leading to enhanced char formation, as discussed in literature [41, 60, 68]. For pine, despite the low content in inorganic species, a char yield similar to the one for beech was observed, which can be attributed to the higher lignin content of softwoods. With respect to the yields of the main condensable volatiles (clustered in groups, see Table 6.3), it was observed that a lower content in inorganic species resulted in higher yields of major carbohydrates, as shown in Fig. 6.3. Among these major carbohydrates is levoglucosan.

Table 6.2: *Char, liquid and gas yields at 10 °C/min for beech, H_2O- and HCl-washed beech, KCl-doped beech and pine. The gas yield was determined by difference (n.d. - not determined).*

Yields (wt.%, db)	Char	Liquid (tar + water)	Gas (by difference)
Beech	23.55 ± 0.11	53.47 ± 1.88	22.29 ± 3.35
Pine	23.67 ± 0.56	53.46 ± 1.96	22.62 ± 2.26
Beech H_2O	22.11 ± 1.43	51.77 ± 3.78	26.12 ± 3.30
Beech HCl	22.43 ± 0.54	56.14 ± 0.21	21.05 ± 0.43
Beech KCl	26.06 ± 0.54	n.d.	n.d.

Table 6.3: *Clustered classes of pyrolysis volatiles condensed and characterized off-line by GC-MS.*

Minor carbohydrates	Major carbohydrates	Furans
Propanoic acid	1,4:3,6-Dianhydro-.alpha.-d-glucopyranose	2-Furancarboxaldehyde
2-Hydroxycyclopent-2-en-1-one	Dehydroacetic Acid	2-Furanmethanol
Propanoic acid, 2-methyl-, 2-methylpropyl ester	Levoglucosan	2(5H)-Furanone
2-Cyclopenten-1-one, 2-hydroxy-3-methyl-		2-Furancarboxaldehyde, 5-methyl-
		2-Furancarboxylic acid, 1-methylethyl ester
		2-Furancarboxaldehyde, 5-(hydroxymethyl)-

Phenols	Guaiacols	Syringols	BTX
1,2-Benzenediol	Guaiacol	Syringol	Benzene
1,2-Benzenediol, 3-methyl-	Eugenol	[b]4-Methyl-2,5-dimethoxybenzaldehyde	Toluene
Phenol, 2,3,5,6-tetramethyl-	Isoeugenol	Phenol, 2,6-dimethoxy-4-(2-propenyl)-	Ethylbenzene
Hydroquinone	Vanillin	Benzaldehyde, 4-hydroxy-3,5-dimethoxy-	p-Xylene
2-Pentanone, 1-(2,4,6-trihydroxyphenyl)	Homovanillic Acid	Ethanone, 1-(4-hydroxy-3,5-dimethoxyphenyl)-	
	Phenol, 2-methoxy-4-propyl-	Benzaldehyde, -3,4,5-trimethoxy-	
	Phenol, 2-methoxy-4-methyl-		
	1,2-Benzenediol, 3-methoxy-		
	Phenol, 4-ethyl-2-methoxy-		
	[a]Ethanone, 1-(3-methoxyphenyl)-		

[a] Despite not having an -OH group, Ethanone, 1-(3-methoxyphenyl)- is clustered as Guaiacol
[b] Despite not having an -OH group, 4-Methyl-2,5-dimethoxybenzaldehyde is clustered as Syringol

As discussed in Section 6.2, inorganic species, specially alkali metals, catalyze the fragmentation pathway in pyrolysis, leading to an enhanced formation of low molecular weight compounds, at the expense of other species such as levoglucosan. Therefore, higher inorganic species content results in lower levoglucosan yields, as observed in this study (Fig. 6.3). It is also to expect that heterogeneous secondary reactions, fostered by the presence of transport limitations (thermally thick regime), further contribute to the formation of char and low molecular weight compounds, at the expense of major carbohydrates. Moreover, no syringols were observed in pine pyrolysis, in good agreement with the lack of syringyl units in softwood lignin [8].

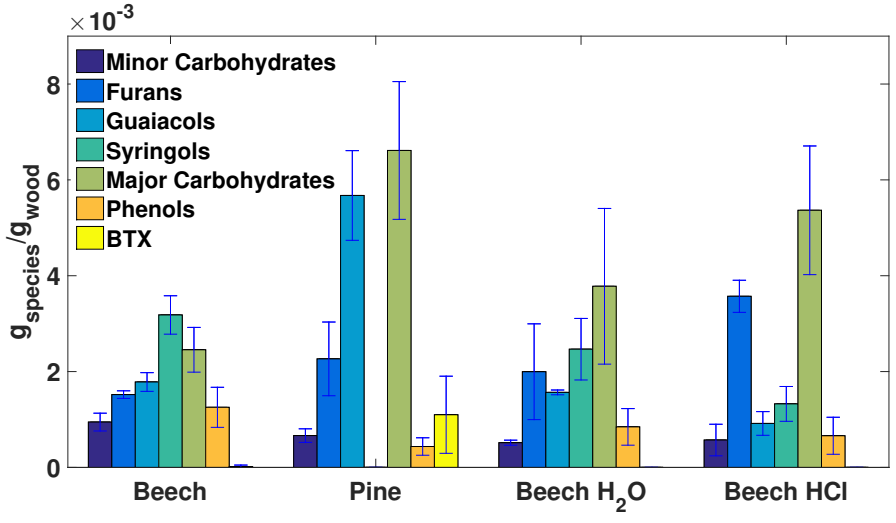

Figure 6.3: *GC-MS analysis of condensable volatiles retained in a cold trap with isopropanol.*

For beech, higher yields in guaiacols, syringols and phenols were also detected, in comparison to H_2O- and HCl-washed beech. It has been reported in literature [160] that higher phenols yields are obtained with higher content of alkali species, due to the increase in lignin reactivity and breakage of ether and C-C bonds. This increase in lignin reactivity due to the presence of alkali species can also be recognized in the overlapping of lignin and cellulose decomposition for beech, and more significantly, for KCl-doped beech. Noteworthy to mention is that BTX (benzene, toluene, xylene) were barely detected in beech pyrolysis. This could be related to the fraction of the tar analyzed in the GC-MS, as explained in Section 6.3.2.

6.4.2 LIF results

6.4.2.1 TFI evolution with 266 nm and 355 nm as excitation wavelengths

The comparison of conversion rate with TFI evolution using 266 nm and 355 nm as excitation wavelengths is shown in Fig. 6.4 for: (a) beech at 5 °C/min, (c) beech at 10 °C/min, (e) H_2O-washed beech at 10 °C/min, (b) pine at 5 °C/min, and (d) pine at 10 °C/min. A change in the TFI evolution for both wood species can be observed. For pine, the temperature-dependent TFI evolution at both excitation wavelengths was quite similar, being the maxima of these curves delayed to higher conversion temperatures in comparison to beech. These maxima were also coincident with the shoulder associated to lignin decomposition, as introduced in Section 6.4.1. For beech, however, different behaviors were observed. At 5 °C/min, the 266-TFI followed the same evolution as 355-TFI up to approximately 380 °C. At higher temperatures the 355-TFI decayed, while a shoulder was observed for 266-TFI, followed by a milder decay in comparison to 355-TFI. This may indicate the release of species that can be detected with an excitation wavelength of 266 nm but not with 355 nm. With a heating rate of 10 °C/min this behavior was more extreme, leading to a shift of the 266-TFI maximum by approximately 10 °C towards higher temperatures, followed by a much slower TFI decay at higher temperatures. For H_2O-washed beech, a shift of both TFI curves towards higher temperatures was observed. This behavior was stronger for 266-TFI evolution than for 355-TFI. The reason for the different TFI evolutions using both excitation wavelengths lies on the species that can be characterized with each excitation wavelength, as previously mentioned, and is further discussed in Section 6.4.2.3.

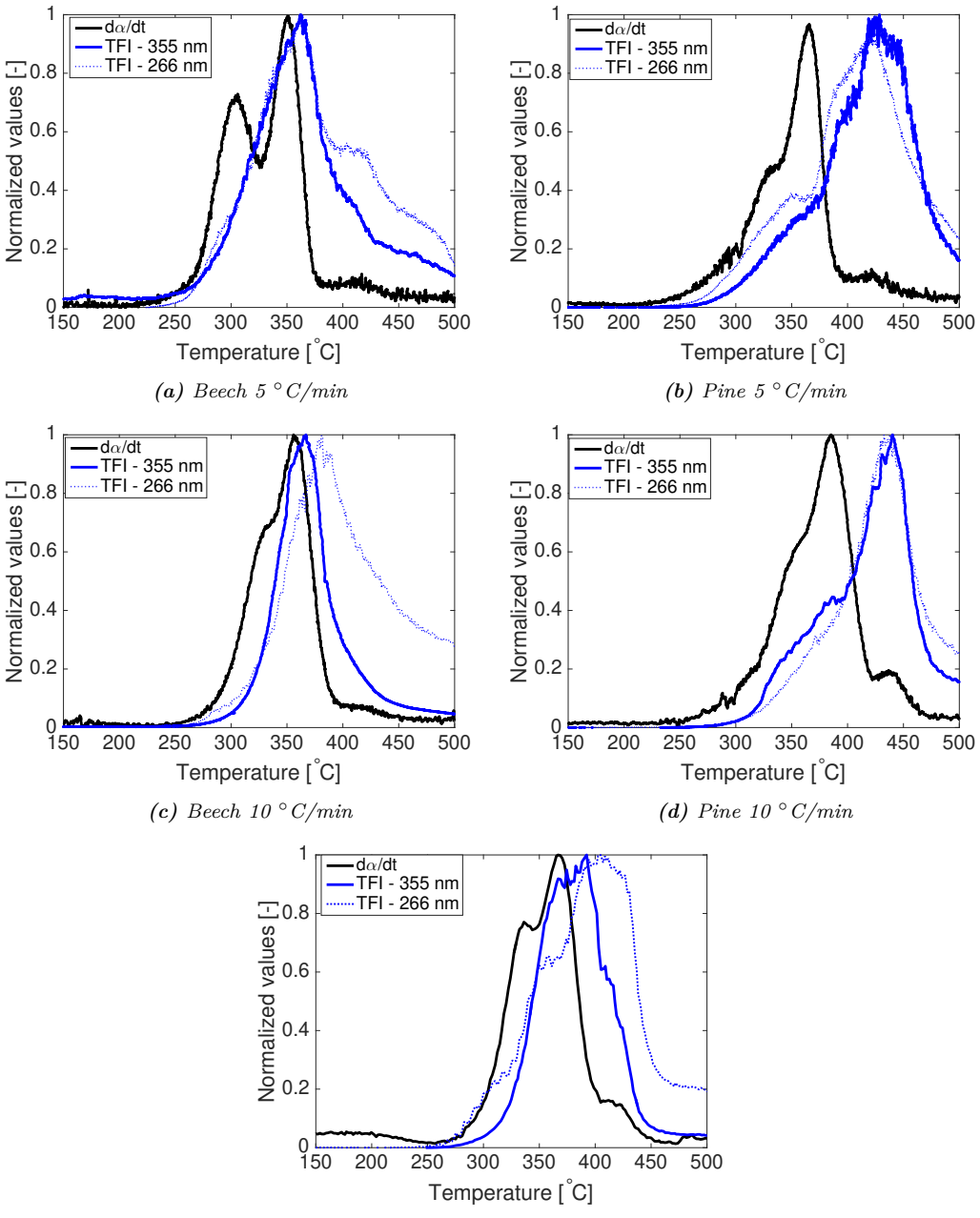

(a) Beech 5 °C/min

(b) Pine 5 °C/min

(c) Beech 10 °C/min

(d) Pine 10 °C/min

(e) Beech H_2O 10 °C/min

Figure 6.4: *Comparison of conversion rate and TFI evolution using 266 and 355 nm as excitation wavelengths versus the temperature in the close vicinity of the particle for: (a) beech at 5 °C/min; (b) pine at 5 °C/min; (c) beech at 10 °C/min; (d) pine at 10 °C/min and (e) H_2O-washed beech at 10 °C/min.*

6.4.2.2 Behavior of single species

The final objective of applying LIF spectroscopy is to track the evolution of PAHs, expected products of secondary reactions [28,29]. However, with the excitation wavelengths used in the present study, not only PAHs, but also other species present in the pyrolysis volatiles can be excited, emitting fluorescence in the same region as PAHs. This issue has been already discussed in previous studies of this group [28,29]. Examples of these species are those containing carbonyl groups, such as ketones and aldehydes (which can be aliphatic or aromatic), as well as 1-ring aromatic compounds, e.g. phenols or guaiacols. The probability that these species get excited at the used excitation wavelengths will depend on their absorption cross sections in the applied experimental conditions. Naphthalene has been reported to have an absorption cross section at 266 nm in the range of 1.25-1.35$\times 10^{-17}$ cm^2/molecule, with temperatures from 227 to 627 °C in N_2 [112,164] at atmospheric pressure, observing no significant variation with measurement temperature. Grosch et al. [165] measured similar values from ambient temperature up to 500 °C at 266 nm excitation wavelength. The absorption cross section for phenol was reported to be approximately one order of magnitude lower [112,165]. Aromatic aldehydes (e.g. benzaldehyde) were reported to have absorption cross sections in the range of 10^{-19}-10^{-18} cm^2/molecule from ambient temperature up to approximately 90 °C [112] (temperatures significantly lower as in the present study). For aliphatic aldehydes and ketones, the absorption cross sections have been reported to be even lower, in the range of 10^{-20} cm^2/molecule from ambient temperatures up to temperatures similar to the ones used in the present study [112]. For anthracene, Thöny and Rossi [166] reported an absorption cross section in the range of 1.41-1.13$\times 10^{-17}$ cm^2/molecule at 355 nm in air. For other PAHs such as phenathrene or pyrene, literature shows disagreement in the values, ranging in the order of 10^{-18}-10^{-17} cm^2/molecule for both excitation wavelengths [112]. Based on the absorption cross sections, with an excitation wavelength of 266 nm it would be possible to see different compounds containing carbonyl groups, such as ketones and aldehydes, 1-ring aromatic compounds (e.g. guaiacols and phenols), as well as PAHs of 2-, 3-, 4-rings, and larger. With 355 nm as excitation wavelenght it is not possible to detect compounds such as naphthalene or phenol (main fluorescence emission range at lower wavelengths than 355 nm). With respect to species containing carbonyl groups, although typically lower absorption cross section values are reported at 355 nm than at 266 nm, it is for example well known that formaldehyde is easy to detect with 355 nm (validated experimentally in the present study, data not shown).

Nevertheless, not only absorption cross section, but also other parameters such as fluorescence lifetime, quantum yields, and influence of quenching substances play a very important role in the fluorescence emission, as well as in the part of this emission that can be captured with the applied experimental setup.

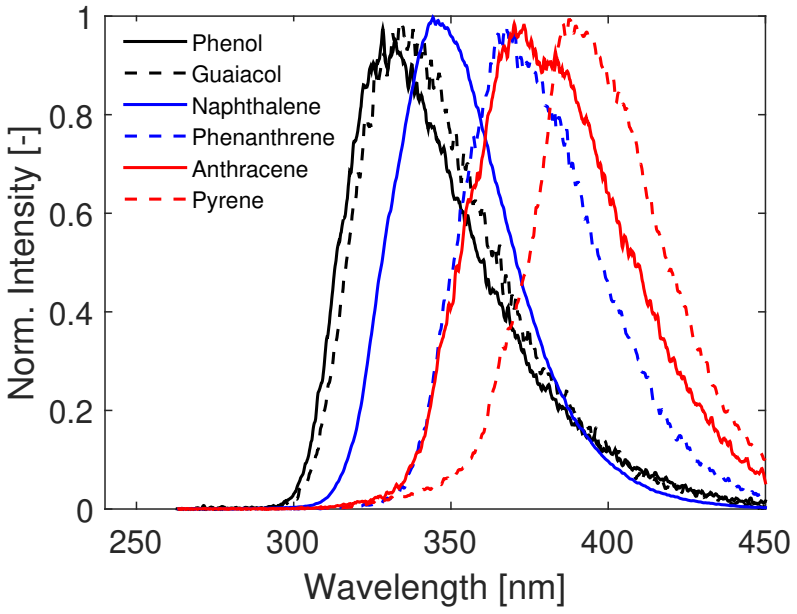

Figure 6.5: *Fluorescence spectra of pure species (phenol, guaiacol, naphthalene, phenanthrene, anthracene, and pyrene) with an excitation wavelength of 266 nm*

In Fig. 6.5, the fluorescence spectra of representative species from these groups are presented, obtained with the same experimental setup used for the wood pyrolysis measurements. As it can be observed in Fig. 6.5, and also reported in literature [28,167], the bigger the aromatic compound, the more shifted the fluorescence spectrum to higher wavelengths (red-shifted), being each compound class (1-, 2-, 3-, and 4-rings aromatic compounds) in a different region of the spectrum [29]. This red-shifting behavior depending on the number of rings is an important characteristic to take into account when analysing the fluorescence spectra of the pyrolysis volatiles, since the peak position or curve trend may be related to some specific groups or species. In complex gas mixtures with a large number of species, such as the ones produced in pyrolysis, other characteristics such as quantification or identification of the functional groups attached to aromatic compounds is not possible due to the broad spectra and signals overlapping [29]. It should also be noted that, even though the spectra are represented with normalized values in Fig. 6.5, these species have different fluorescence intensities. This is specially remarkable when comparing guaiacol or phenol spectra with the naphthalene spectrum, which is smoother.

Other species such as ketones and aldehydes, as previously introduced, could also contribute to the fluorescence signal [29]. However, taking into account their lower absorption cross sections, the contribution to the global signal is expected to be much lower for the same concentration as the PAHs. It has to be taken into account though that the concentration of these species in the volatiles stream is significantly higher than for PAHs. It is also important to take into account the emission wavelength range for data analysis. Although in the present study fluorescence spectra of these species have not be investigated, in previous works of this group, as well as in literature, it has been shown that emission spectra of typical ketones and aldehydes, using an excitation wavelength of 266 nm, peak at approximately 400 nm or even higher wavelengths [29, 120]. With an excitation wavelength of 355 nm, PAHs of 3- and 4-rings, as well as formaldehyde have been measured in the present study (data not shown).

6.4.2.3 Comparison of fluorescence spectra for pyrolysis experiments

In Fig. 6.6, the fluorescence spectra obtained with an excitation wavelength of 266 nm, at different temperatures during the pyrolysis process (10 °C/min), are shown for (a) beech, (b) pine, (c) H_2O-washed beech, and (d) KCl-doped beech. For all cases, the onset of the fluorescence signal occurred at approximately 300 °C (measured in the close vicinity of the pyrolysing particle), as it can be seen also in the TFI curve (Fig. 6.4), and continued until the end of the experiment. It is important to clarify that, although the spectra are plotted with normalized values for comparison purposes, they have different intensities, also observable in the TFI evolution at that specific temperature, i.e., low TFI value means low spectrum intensity.

As it can be observed in Fig. 6.6, there are significant differences between the pyrolyzed materials. For beech wood, Fig 6.6 (a), the fluorescence signal started with a noisy spectrum (low TFI value), which had its peak maximum at approximately 340 nm. Since this spectrum corresponded to early stages of the pyrolysis process, highlighted as zone I in Fig. 6.2 (a), the species contributing to the fluorescence signal should be mainly primary tars, such as guaiacol or phenol (see Fig. 6.5), expected to be mainly produced during early primary decomposition of lignin; or species containing carbonyl groups, such as ketones and aldehydes [28]. Extractives could also contribute to this early fluorescence signal. The presence of aldehydes is further confirmed by the fluorescence spectra collected with an excitation wavelength of 355 nm (data not shown), observing the typical fluorescence structure of formaldehyde at 300 °C (in the close vicinity of the particle).

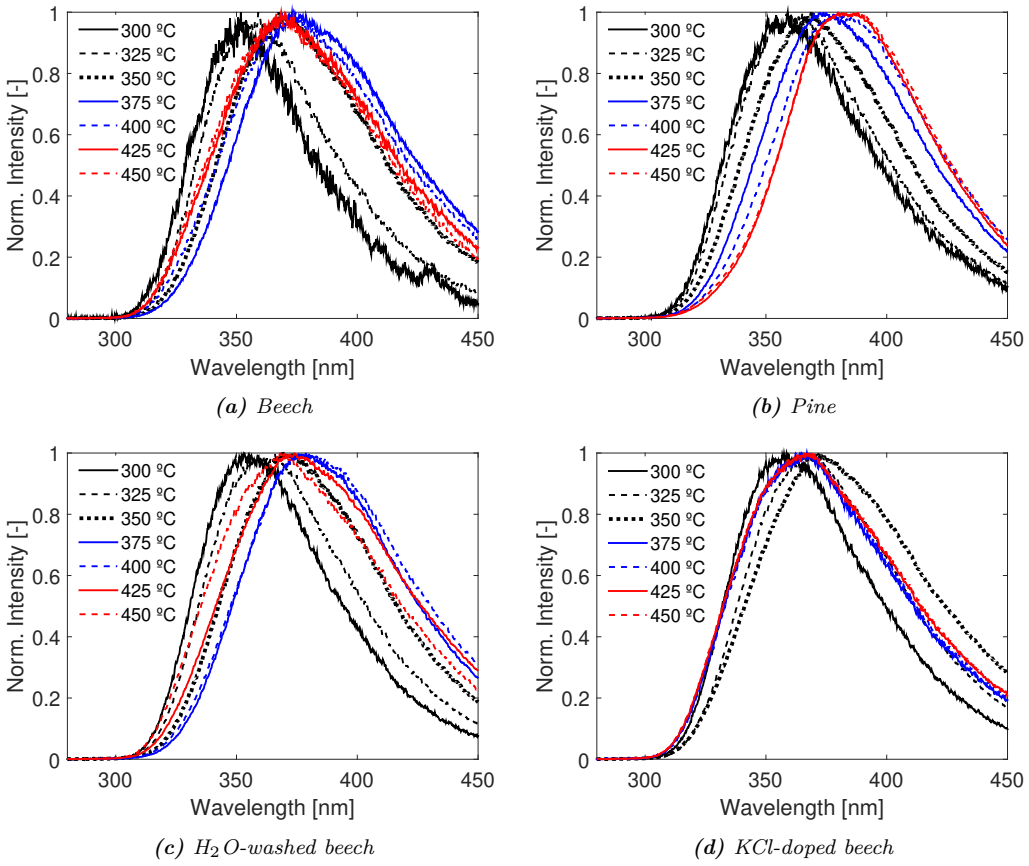

(a) Beech *(b) Pine*

(c) H_2O-washed beech *(d) KCl-doped beech*

Figure 6.6: *Pyrolysis fluorescence spectra at 10 °C/min with an excitation wavelength of 266 nm at different temperatures measured in the close vicinity of the particle for: (a) Beech; (b) Pine; (c) Beech H_2O-washed; (d) Beech KCl-doped*

With increasing temperature, the fluorescence intensity increased (see also TFI evolution, Fig. 6.4 (c)) and the spectrum peak position shifted to higher wavelengths (Fig. 6.6 (a)). At approximately 375 °C, corresponding to zone II (primary decomposition of cellulose and lignin together with heterogeneous secondary reactions of primary volatiles) in Fig. 6.2 (a), the spectrum peak position reached its highest value, around 370 nm. The maximum of the 266-TFI curve was also reached at this stage. At temperatures higher than 375 °C, being already in zone III, the TFI decreased and the spectrum shifted to slightly lower wavelengths, remaining practically constant until the end of the pyrolysis process. This suggests that the composition of species emitting fluorescence in zone III (further decomposition of the lignin residue, increase in CH_4 release rate) did not change significantly. The mild blue-shift in the fluorescence spectra at temperatures higher than 375 °C was also coincident with a rapid decay of the 355-TFI evolution (Fig. 6.4 (c)). Taking into account that with an excitation wavelength of 355 nm PAHs such as naphthalene are not detected, this (combination of blue-shift in the fluorescence spectra at 266 nm together with the

rapid decay in 355-TFI) may suggest the formation of smaller PAHs mainly during the further decomposition of the lignin residue.

The formation of PAHs in the temperature range of 400-600 °C for cellulosic materials [168, 169] and tobacco [170] has been reported in literature. Hajaligol et al. [168] highlighted that, in order to reduce the potential presence of homogeneous secondary reactions (gas-phase cracking of pyrolysis volatiles), the raw material was pre-charred (in the temperature range of 300-360 °C, depending on material) and further pyrolyzed at 400, 500, and 600 °C. Similar approach was followed in the other other studies [169, 170]. Samples in the order of 10s to 100s mg were used. The formation of PAHs was mainly detected in the temperature range of 400-600 °C, although very small amounts were also measured at 350 °C by [170]. Moreover, inorganic species were reported to increase the yields of PAHs [168], as well as to shift their maximum release to lower temperatures [170]. In all cases, the formation of PAHs was attributed to a direct pathway occurring within the char matrix. In particular, Hajaligol et al. [168] reported that elimination (of substituents/bridges) and dehydrogenation reactions led to condensation and fusion of the aromatic structure into larger polycyclic aromatic clusters. This is consistent with the fact that they evaluated mostly pre-charred samples, using as well small sample sizes.

It has been also reported in literature that vapor-solid interactions [59], or vapor-liquid interactions as reviewed more recently by Mamleev et al. [60], are the main pathway for char formation during pyrolysis of cellulose, also known as charring reactions. Therefore, these reactions (namely charring reactions or heterogeneous secondary reactions) could contribute to the formation of PAHs as well. Moreover, it has been observed [171] that char (produced by pyrolysis, with slow heating rate and N_2 atmosphere) washing with organic solvents resulted in PAHs extraction, with higher extraction yields for lower char production temperatures (in the range of 400-700 °C). This suggests that the PAHs may be formed during pyrolysis but retained in the solid structure, either adsorbed or condensed, until release at higher temperatures. Based on this evaluation, both heterogeneous secondary reactions (charring reactions) and further solid residue transformation may contribute to the formation of PAHs at low temperature. For beech pyrolysis the former would be mainly located in zone II while the latter mainly in zone III. Hajaligol et al. [168] also showed that the release of aromatics (e.g. toluene, indene, and first peak in naphthalene) occurred simultaneously with the release of CH_4. This is consistent with the results observed for beech pyrolysis (Fig. 6.2 (a)), where the main peak

in CH_4 release occurred in zone III, with no significant mass loss and attributed to further reactions in the lignin residue.

In the case of pine, a continuous red-shifting of the fluorescence spectra was observed (Fig. 6.6 (b)) during the pyrolysis process. At 350 and 375 °C (zone II), the fluorescence spectra observed for pine were practically identical to the ones for beech, indicating the formation of very similar fluorescence-emitting species in both cases (see Fig. 6.7 c) and (d)). This was also coincident with the maximum of the conversion rate. At higher temperatures, however, when for beech a blue-shift in the fluorescence spectra took place, for pine the red-shifting continued. At the same time, both 355- and 266-TFI evolutions followed qualitatively the same behavior (see Fig. 6.4 (d)). This indicates that the species emitting fluorescence can be detected using both excitation wavelengths, being consistent with the formation of larger (more than 2-rings) PAHs. It could be argued that other species such as aromatic ketones and aldehydes (e.g. methylbenzaldehyde, benzophenone, acetophenone), phenols, or guaiacols, products of lignin decomposition, could be the source of fluorescence. However, taking into account the lower adsorption cross sections of these species with 355 nm excitation wavelength in comparison to 266 nm [112], the detection of PAHs formation would be more plausible.

In Fig. 6.6 (c), it can be seen that fluorescence spectra during H_2O-washed beech pyrolysis followed qualitatively a similar behavior as for beech (see Fig. 6.6 (a)). However, when comparing the single spectra at different temperatures in Fig. 6.7, it can be observed that the spectra of H_2O-washed beech had an intermediate behavior (with respect to emission wavelengths) between beech and pine. Moreover, as for the beech, the 266-TFI evolution was slightly delayed with respect to 355-TFI evolution (Fig. 6.4 (e)), although both appeared slightly shifted to higher temperatures with the removal of inorganic species.

For KCl-doped beech, the fluorescence spectrum at 300 °C resembled the one for H_2O-washed beech. This behavior may be related to the fact that in both cases, extractives, which mainly decompose at the beginning of the pyrolysis process, were removed from the solid during the washing procedure. At around 350 °C, the maximum red-shift in the fluorescence spectra was observed, approximately at the same time as the 266-TFI maximum. Since this increase in the fluorescence intensity occurred simultaneously with a strong exothermic peak (much stronger than for the other cases), the release of species emitting fluorescence could be attributed mainly to the enhancement of heterogeneous secondary reactions by the catalytic effect ofK. At 375 °C a blue shift in the fluorescence signal was observed, remaining the spec-

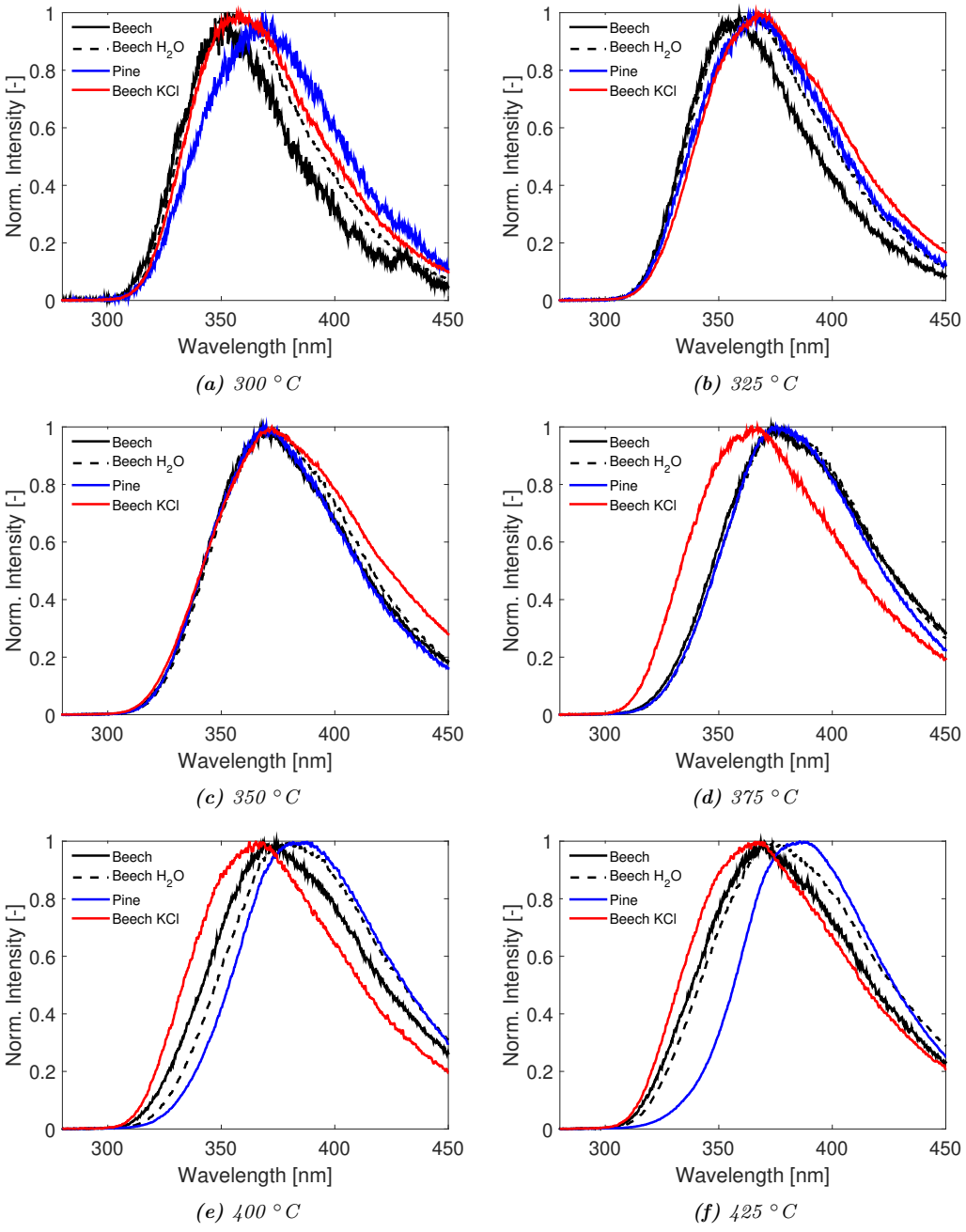

(a) 300 °C *(b) 325 °C*

(c) 350 °C *(d) 375 °C*

(e) 400 °C *(f) 425 °C*

Figure 6.7: *Comparison of pyrolysis fluorescence spectra obtained with an excitation wavelength of 266 nm at different temperatures measured in the close vicinity of the particle*

tra practically unchanged until the end of the process. This was coincident with a second peak in the 266-TFI evolution (Fig. 6.2 (e)), when no further mass loss was detected, suggesting the release of PAHs during further transformation of the char, catalyzed by K. This behavior is consistent with the results reported by Guo et al. [161], discussed in Section 6.2, indicating that K may increase the polycondensation reaction of aromatic nucleus, promoting the aromaticity of the char. For KCl-doped beech it is then possible to distinguish the two phenomena potentially contributing to the emission of PAHs at low temperature: heterogeneous secondary reactions and further transformations in the solid matrix, as previously discussed.

Further work is needed to get a deeper insight into the composition of the species emitting fluorescence.

6.5 Conclusions

The influence of inorganic species on the pyrolytic behavior of beech wood and the comparison with the pyrolytic behavior of pine wood under the same conditions has been investigated. To this end, spectroscopy techniques (IRLAS for characterization of permanent gases and LIF for characterization of species emitting fluorescence, including PAHs) were combined with mass and temperature measurements.

The differences between beech and pine wood pyrolysis behavior observed in the present study may be attributed to the varying content in inorganic species, specially K, rather than to the different content and structure of their macrocomponents. This is supported by the removal of inorganic species from beech, resulting in a pyrolytic behavior similar to the one for pine, with a delayed lignin decomposition (lower lignin reactivity). This was accompanied by the release of CH_4, a second peak in the release of CO, a delay/widening of the TFI curve (tracking the production and emission of species emitting fluorescence), and a strong change in the process thermochemistry (very similar to the one for pine), suggesting that heterogeneous secondary reactions of primary volatiles were also shifted to higher temperatures, partially due to the delayed release of lignin primary volatiles. Moreover, the removal of inorganic species resulted in lower char yields and higher major carbohydrates yields, consistent with a reduced presence of secondary charring reactions. Lower guaiacols, syringols and phenols yields were also observed, which could be attributed to the lower lignin reactivity.

Addition of K catalyzed the pyrolysis process, shifting the maximum of the conversion rate towards lower temperatures and leading to a strong overlapping of cellulose and lignin decomposition, including as well heterogeneous secondary reactions of primary volatiles. The strong exothermicity observed supports the enhancement of heterogeneous secondary reactions, such as charring, reported to be exothermic in literature.

The release of species emitting fluorescence, represented via the TFI evolution, is considered to be an indication of the presence of heterogeneous secondary reactions (vapor-solid/liquid interactions), since PAHs are expected to play an important role contributing to the collected fluorescence signal. Their strong fluorescence emission in the conditions of the present study (excitation wavelength, emission spectra considered) is well known. However, other species such as ketones or aldehydes, typical products of pyrolysis, could also contribute to the fluorescence signal, specially due to their high concentration. In this work, the use of two different excitation wavelengths aided with the qualitative interpretation of the fluorescence spectra. However, further work is necessary to get a better qualitative, or even semi-quantitative, characterization of the species emitting fluorescence.

Formation of PAHs at low temperature (400-600 °C) has been attributed in literature to reactions within the char matrix, mainly due to further carbonization and aromatization of the solid. However, PAHs can be also product of heterogeneous secondary reactions, such as charring reactions. This is further supported by the influence of inorganic species on the TFI evolutions in regions where mass loss was significant. The fluorescence signal observed at higher temperatures, when no significant mass loss was recorded, and specially strong for KCl-doped beech, could be due to PAHs release from further solid conversion.

Chapter 7

Combined influence of inorganics and transport limitations on the pyrolytic behavior of woody biomass

This chapter is the peer-reviewed version of the article published in *Chemical Engineering Transactions* with the title "Combined Influence of Inorganics and Transport Limitations on the Pyrolytic Behaviour of Woody Biomass", H. Almuina-Villar, P. Sommersacher, S. Retschitzegger, A. Anca-Couce, and A. Dieguez-Alonso. *Chemical Engineering Transactions*, 80: 73-78, 2020. https://doi.org/10.3303/CET2080013

7.1 Abstract

A deeper understanding and quantification on the influence of inorganic species on the pyrolysis process, combined with the presence of heterogeneous secondary reactions, is pursued in this study. Both chemical controlled and transport limited regimes are considered. The former is achieved in a tthermogravimetric analyzer (TGA) with fine milled biomass in the mg range, while the latter is investigated in a particle level reactor with spherical particles of different sizes. To account for the influence of inorganics, wood particles were washed and doped with KCl aqueous solutions, resulting in K concentrations in the final wood of around 0.5% and 5% on dry basis. Gas species and condensable volatiles were measured online with Fourier transform infrared (FTIR) spectroscopy and a non-dispersive infrared (NDIR) gas analyzer. The removal of inorganic species delayed the pyrolysis reaction to higher temperatures and lowered char yields. The addition of inorganics (K) shifted the devolatilization process to lower temperatures, increased char and water yields, and

reduced CO production among others. Higher heating rates and temperatures resulted in lower char, water, and light condensable yields, but significantly higher CH_4 and other light hydrocarbons, as well as CO. The increase in these yields can be attributed, at least in part, to the gas phase cracking reactions of the produced volatiles. Larger particle size increased the formation of char, CH_4 and other light hydrocarbons, and light condensables for low and high pyrolysis temperatures, while reduced the release of CO_2 and H_2O. This novel data set allows to quantify the influence of each parameter and can be used as basis for the development of detailed pyrolysis models which can include both the influence of inorganics and transport limitations when coupled into particle models.

7.2 Introduction

The different reaction pathways during the pyrolysis process (pyrolysis mechanism) have a significant influence on products yields and composition, as well as on products properties relevant for their further application [8]. Many studies have been performed to understand the relation between initial feedstock properties, pyrolysis conditions and products distribution and composition. Nevertheless, an accurate description of the pyrolysis mechanisms that can be globally applied is still missing due to the high degree of complexity of the reaction pathways involved and the numerous factors affecting their evolution [8, 45].

Alkali metals, with potassium being one of the most relevant, have been reported to play an important role on both devolatilization kinetics and products composition. Their catalytic effect in biomass results in a preference of the ring fragmentation reactions at the expense of sugar formation reactions (depolymerization, transglycoxylation) for both cellulose and hemicellulose. The former would lead to the formation of low molecular weight compounds and furan-ring derivatives, while the latter would lead mainly to levoglucosan and similar compounds [41, 67, 67, 68]. The presence of alkali species may as well catalyze dehydration reactions at low temperature enhancing char formation [41, 68]. For lignin pyrolysis, alkali species (Na) were shown to catalyze functional groups scission, favoring methanol release (demethoxylation) and dehydration reactions, as well as radicals recombination [39]. It was also shown that alkali species (Na) catalyzed functional groups cleavage in a selective manner, favoring demethoxylation over demethylation of guaiacyl units [38]. At the same time, the formation of CO and formaldehyde was hindered, while decarboxylation and dehydration reactions were favored [38].

Studies in literature with similar approach as the present one also show that alkali species (K) during wood and other biomasses pyrolysis resulted in an overall increase of gas and char yields over liquid condensables [160,172,173]. Secondary charring reactions, i.e. further reactions of the primary volatiles within the solid/liquid matrix (and therefore triggered by transport limitations), have been shown to also influence products distribution and process thermochemistry [89,147,149,160,174]. Almuina-Villar et al. [174] reported that the presence of K at slow pyrolysis led to a partially overlapped primary decomposition of cellulose and lignin, together with heterogeneous secondary reactions of primary volatiles, leading to higher exothermicity and formation of aromatic species, among other species.

The present study constitutes an extension of the work by Almuina-Villar et al. [174], to investigate in detailed the combine action of inorganic species and heterogeneous reactions on the pyrolysis process. To this end, both chemical kinetic controlled (intrinsic kinetics) and transport limited regimes at different conditions, including higher temperatures and intermediate heating rates, have been considered. The former is achieved in a thermogravimetric analyzer (TGA) with fine milled biomass in the mg range, while the latter is investigated in a particle level reactor, with continuous monitoring of temperature and mass, using spherical particles of different sizes at different heating rates. To account for the influence of inorganics, wood particles were washed and doped with KCl aqueous solutions. Furthermore, gas species were characterized online, combining Fourier transform infrared (FTIR) spectroscopy and non-dispersive infrared (NDIR) gas analyses. The data obtained in the present work, besides providing understanding on the combined influence of inorganics species and secondary charring reaction of the pyrolysis process can be also used as complete database for further modification of Ranzi's detailed pyrolysis scheme, following the works by Trendewicz et al. [41] and Anca-Couce et al. [45] among others.

7.3 Experimental

The experimental setup used to perform the single particle pyrolysis experiments has been presented elsewhere [45, 175, 176]. Beech wood spheres of two different sizes (Ø = 10 mm and Ø = 6 mm, referred as big and small particles, respectively) were used. Washed particles (referred as Bw-H_2O) were soaked in deionized water during 16 h in vacuum, dried 8 h at 50 °C in vacuum, and washed again under the same conditions. For KCl doped wood (referred as Bw-KCl_1 and Bw-KCl_2), the particles were, first washed, as for Bw-H_2O, and then soaked in different KCl aqueous solutions

during 16 h in vacuum, resulting in K concentrations in the final wood of around 0.5 wt.% and 5 wt.%. Characterization of the materials is presented in Table 7.1. The single particle reactor was preheated until 500 °C and 900 °C, in order to reach different heating rates and final temperatures in the particles. Detailed online characterization of the produced volatiles was achieved with a multi-component Fourier transform infrared (FTIR) spectroscopy system and with a non-dispersive infrared (NDIR) gas analyzer. Mass and temperature evolution in the center and in the atmosphere around the particle were also characterized. A set of 3 experiments were performed for each case to ensure repeatability of the results. All the results shown are an average of those measurements.

Table 7.1: *Properties for small (Ø = 6 mm) and big (Ø = 10 mm) particles.*

Ø = 6 mm	Bw	Bw-H_2O	Bw-KCl_1	Bw-KCl_2
C (wt.%, db)	48.57 ± 0.12	47.93 ± 0.11	46.90 ± 0.03	43.63 ± 0.12
H (wt.%, db)	6.67 ± 0.03	6.63 ± 0.03	6.53 ± 0.02	6.01 ± 0.02
O[a] (wt.%, db)	44.35 ± 0.15	45.16 ± 0.14	44.97 ± 0.04	41.03 ± 0.11
Inorg. (wt.%, db)	0.24 ± 0.01	0.16 ± 0.02	1.49 ± 0.02	9.21 ± 0.07
K (mg/kg)	708 ± 5	93 ± 8	7459 ± 185	47984 ± 852
Cl (mg/kg)	-	-	6790	43678
Ca (mg/kg)	1019 ± 46	958 ± 125	427 ± 15	177 ± 1
Ø = 10 mm	Bw	Bw-H_2O	Bw-KCl_1	Bw-KCl_2
Inorg. (wt.%, db)	0.25 ± 0.00	0.13 ± 0.00	1.07 ± 0.01	8.47 ± 0.09
K (mg/kg)	885 ± 4	199 ± 2	5243 ± 77	43612 ± 896
Cl (mg/kg)	-	-	4773	403801
Ca (mg/kg)	1032 ± 2	736 ± 3	843 ± 5	198 ± 15

[a] Oxygen content is calculated by difference: 100 %-(C(%)+N(%)+H(%)+S(%)+ash(%)).

To study the chemical kinetics, milled samples from the big particles (Ø = 10 mm) were prepared and afterwards measured in a thermogravimetric analyzer (TGA) in conditions that should ensure a chemical kinetic control regime, i.e. initial mass of around 10 mg and slow heating rates (10 °C/min). The results are shown as the derivative of the conversion ($d\alpha/dt$), being conversion (α) defined as:

$$\alpha = 1 - \frac{m - m_f}{m_o - mf} \tag{7.1}$$

where m_i is the initial mass of the particle, m_f is the final char mass and m is the mass at each time step.

7.4 Experimental results and discussion

7.4.1 Chemical kinetic regime

The conversion rates ($d\alpha/dt$) of raw beech wood (Bw), washed beech wood (Bw-H_2O), and KCl-doped beech wood (Bw-KCl_1 and Bw-KCl_2) in TGA experiments are presented in Fig. 7.1. Doping of wood with KCl significantly affected the pyrolysis chemistry, shifting to lower temperatures the maximum of the conversion rate and the shoulder attributed to the conversion of hemicellulose [8]. Furthermore, the decay of the conversion rate (end of devolatilization process) was shifted as well to lower temperatures, leading to a reduced total devolatilization temperature span (and time). The shoulder at lower temperatures became less pronounced with higher K content as well. All together these results show the catalytic effect of K on the pyrolytic decomposition of biomass macrocomponents, hemicellulose, cellulose and lignin, leading to an increased overlap of the three regions with higher K content. These results are consistent with similar studies from literature [173]. K-doping also increased the char yields, with values of 10.3 wt.%, 12.3 wt.%, 17.0 wt.%, and 25.5 wt.% at 700 °C (expressed on dry, additive free basis) for Bw-H_2O, Bw, Bw-KCl_1, and Bw-KCl_2, respectively.

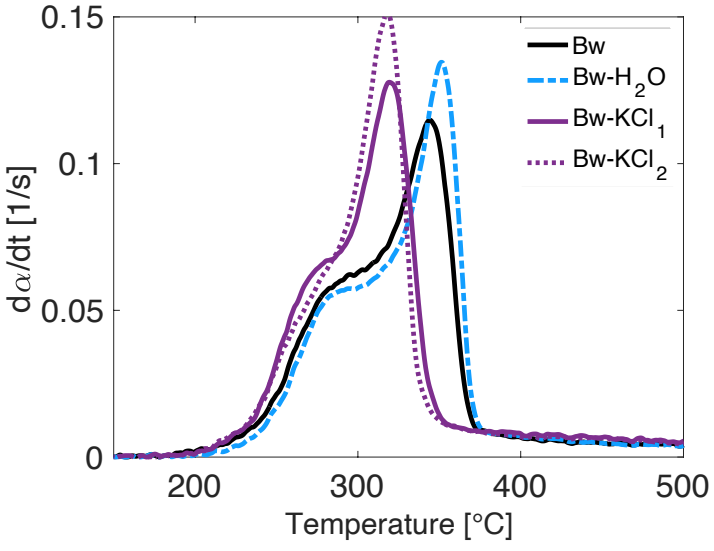

Figure 7.1: *Conversion rate ($d\alpha/dt$) obtained at 10 °C/min*

7.4.2 Mass loss and temperature at particle level

The conversion rate at particle level is presented in Fig. 7.2. Two particle sizes (Ø = 6 mm and Ø = 10 mm) were used to have differences in the potential influence of transport limitations on the pyrolysis process, including enhancement of heterogeneous secondary (charring) reactions. Furthermore, two pyrolysis temperatures (500 °C and 900 °C) were used, which led also to varying heating rates: approximately 300 °C/min and 1350 °C/min for small particles; and 215 °C/min and 900 °C/min for big particles.

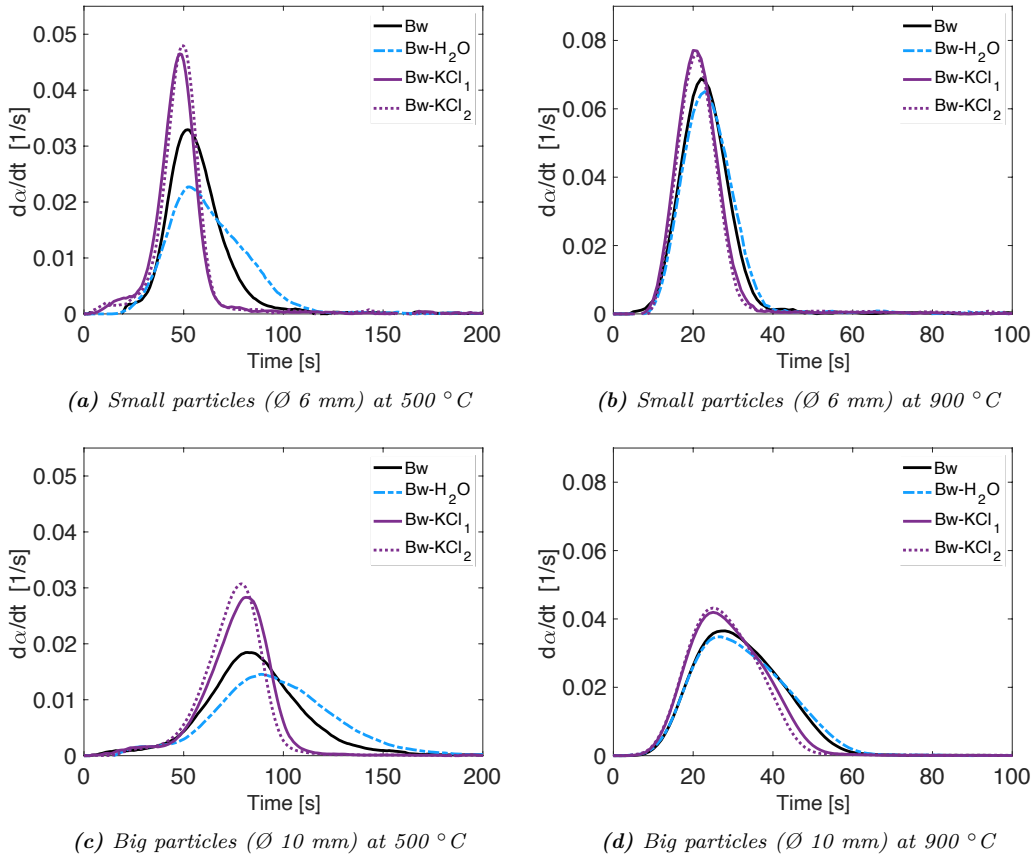

(a) Small particles (Ø 6 mm) at 500 °C

(b) Small particles (Ø 6 mm) at 900 °C

(c) Big particles (Ø 10 mm) at 500 °C

(d) Big particles (Ø 10 mm) at 900 °C

Figure 7.2: *Conversion rate (dα/dt) of: (a) Small particles 500 °C, (b) Small particles 900 °C, (c) Big particles 500 °C, and (d) Big particles 900 °C.*

The addition of KCl also shifted the maximum of the conversion rate to slightly earlier times (and therefore lower temperatures) as for the chemical kinetic controlled (TGA) experiments. A narrowing of the devolatilization process with KCl doping was also observed for the experiments at 500 °C, as for the TGA measurement. However, at particle level it was also observed that the conversion rate curve for Bw-H_2O was notably wider than for Bw, extended in the temperature range associated to lignin decomposition. A similar behavior was also observed by Almuina-Villar et

al. [174] and attributed to the lack of catalytic effect on lignin pyrolysis upon removal of inorganics. Lower temperatures in the center of the particle during most of the devolatilization process for Bw-H_2O could also explain this delayed conversion at higher temperatures. However, the lower temperature at the center of the particle can only be explained by differences in the pyrolysis thermochemistry, since heat transfer outside and inside the particle should not vary for the same experimental conditions depending on K content.

In Fig. 7.3 the different thermal regimes for the experiments previously introduced are presented with the dT/dt in the center of the particle [147]. It is possible to see clear differences between washed, raw, and KCl doped wood. For experiments at 500 °C several peaks are observed. The first one, after the particle heating, is attributed to hemicellulose and the last one to lignin (Fig. 7.3 (a)). For Bw-KCl_1, and Bw-KCl_2, the peaks of $dT/dt_{particle}$ are larger, specially at the end of the conversion, showing a higher global exothermicity during the devolatilization process. This suggests that K also significantly affects the process thermochemistry, catalyzing exothermic reactions, including cellulose and lignin primary decomposition and secondary reactions of their primary products [147, 174].

The last exothermic peak appears earlier (for Bw-KCl_1 and Bw-KCl_2) or delayed (Bw-H_2O) in comparison to Bw, in agreement with the conversion rate curves (Fig. 7.2). For big particle size, the thermal regimes followed the same qualitative behavior as for small particle size for Bw. The last exothermic regime, attributed to lignin/lignin residue decomposition and secondary reactions, was significantly higher for Bw-KCl_1 and Bw-KCl_2, relative to other exothermic peaks, in comparison to the results for small particle size. This suggests that some of the reactions resulting in exothermicity may be also enhanced by the big particle size, i.e., potentially secondary reactions. In the experiments at 900 °C, the patterns for the four cases were very similar. Mainly a clear exothermic peak, coincident with lignin/lignin residue decomposition was observed. It is clear that K catalyzes the wood devolatilization process, shifting it to lower temperatures and leading to an overlapping of the three macrocomponents decomposition. Furthermore, it catalyzes char formation, which has been reported in literature (e.g. Di Blasi et al. [147]) to be an exothermic process. However, looking at the thermochemistry of the process under the different studied conditions, the exothermic influence of K on the pyrolysis process is further enhanced by the presence of transport limitations, probably due to the occurrence of heterogeneous secondary reactions. This could be also understood as heteroge-

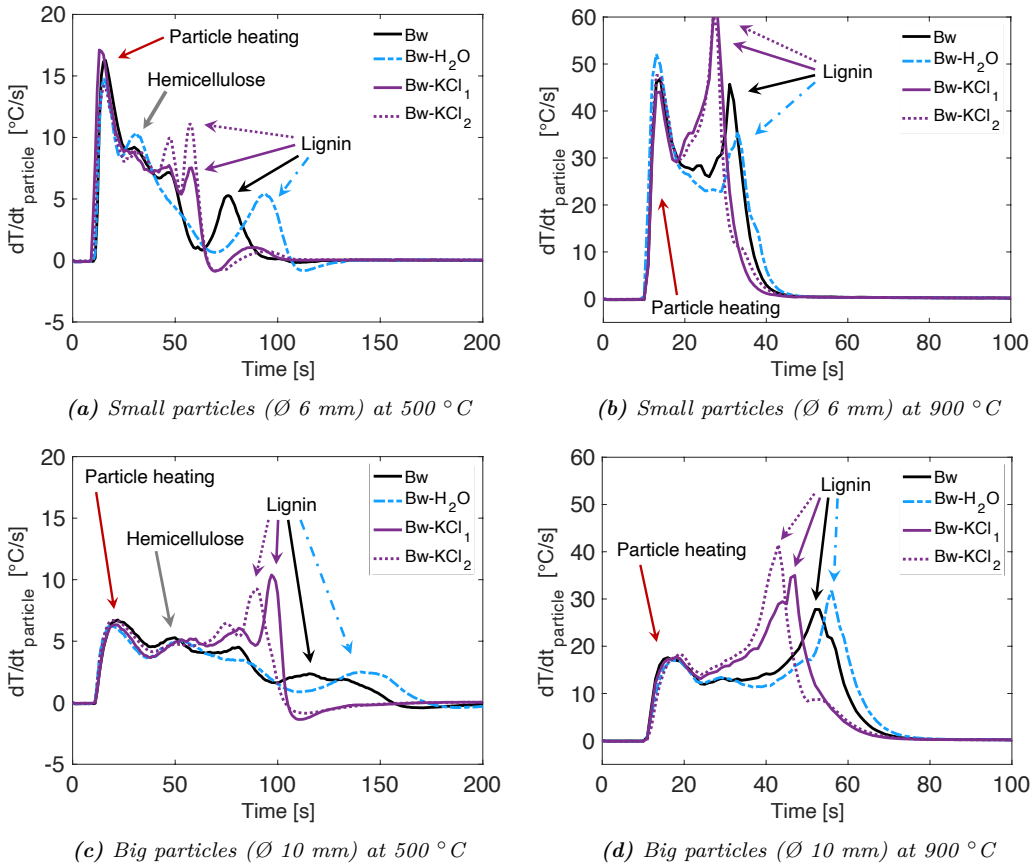

(a) Small particles (Ø 6 mm) at 500 °C

(b) Small particles (Ø 6 mm) at 900 °C

(c) Big particles (Ø 10 mm) at 500 °C

(d) Big particles (Ø 10 mm) at 900 °C

Figure 7.3: *Rate of temperature increase (dT/dt) in the center of the particle for: (a) Small particles 500 °C, (b) Small particles 900 °C, (c) Big particles 500 °C, and (d) Big particles 900 °C.*

neous secondary reactions are favored by K doping. The fact is that both factors act combined and cannot be separated.

7.4.3 Yields at particle level

The product yields for both particle sizes and pyrolysis temperatures are plotted in Fig. 7.4. With increasing pyrolysis temperature (500 °C versus 900 °C), the yields of CO, CH_4, and other light hydrocarbons (LH: ethene, acetylene, propane, propene) increased, while light condensable species (LC: acetic acid, lactic acid, formaldehyde, acetaldehyde, methanol, ethanol) and char yields decreased. CO_2 yields remained quite constant, with values of around 13 – 15 wt.% and H_2O decreased from around 15 wt.% to values in the range of 5 – 10 wt.%, depending on particle size. The decrease of char yields with higher pyrolysis temperatures (900 °C) can be explained by the higher heating rates achieved, which favor the yields of gas and condensable volatiles, as well as by further char reactions that can happen at high temperatures.

The increase in CO, CH_4, and other LH can be explained by an increase in gas phase tar cracking reactions due to high temperatures.

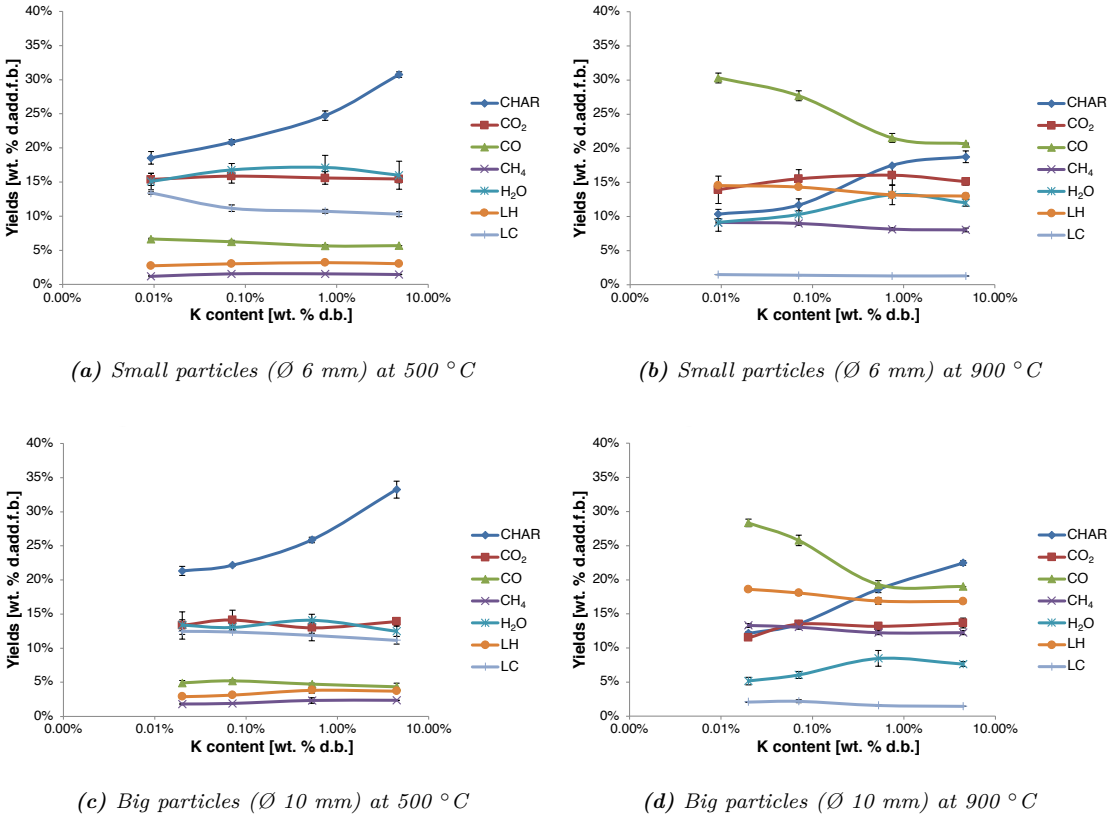

(a) Small particles (Ø 6 mm) at 500 °C

(b) Small particles (Ø 6 mm) at 900 °C

(c) Big particles (Ø 10 mm) at 500 °C

(d) Big particles (Ø 10 mm) at 900 °C

Figure 7.4: *Product yields in dry additive (KCl) free basis with standard deviations for: (a) Small particles 500 °C, (b) Small particles 900 °C, (c) Big particles 500 °C, and (d) Big particles 900 °C.*

Regarding inorganics, their presence in the initial feedstock has been reported to increase char and gas yields at the expense of condensable volatiles [160, 172, 173]. This is also observed in the present study, i.e. the higher the K content, the higher the char yields, due to catalysis of charring reactions, as previously discussed. It must be taken into account that this char yields include also the inorganics species remaining in the char after the pyrolysis process. The organic fraction of this char is lower than the plotted values. Nevertheless, the organic fraction of the char is also increased with higher K content. Bigger particle size also led to an increase in char yields for both pyrolysis temperatures. Therefore, the highest char yields were obtained with K doping and big particle size. Permanent gases (CO and CO_2) remained quite constant at low pyrolysis temperatures with the presence of inorganic species. Only a 1 wt.% decrease in CO for both particle sizes could be observed with the increase in K content. However, at 900 °C, CO production was drastically reduced along with a significant increase in H_2O and only a very slight

increase in CO_2 with K loading. The inhibition in CO release at high temperatures with K doping has been also observed by Demirbaş [177], who obtained similar results by adding K_2CO_3 to the initial feedstock and by Hu et al. [172], who found that washing with H_2O and HCl resulted in higher CO yields at the expense of H_2 and CO_2. With respect to light condensable (LC) species, their yields were slightly increased by particle size and reduced by K content (slightly) and by high pyrolysis temperature (strongly). The latter can be attributed to secondary gas cracking reactions [45].

In Fig. 7.5, light condensables and CH_4 release for Bw-H_2O (a) and Bw-KCl_1 (b), big particle size at 500 °C is presented. Upon addition of K, light condensables release was narrowed, in good agreement with the devolatilization behavior.

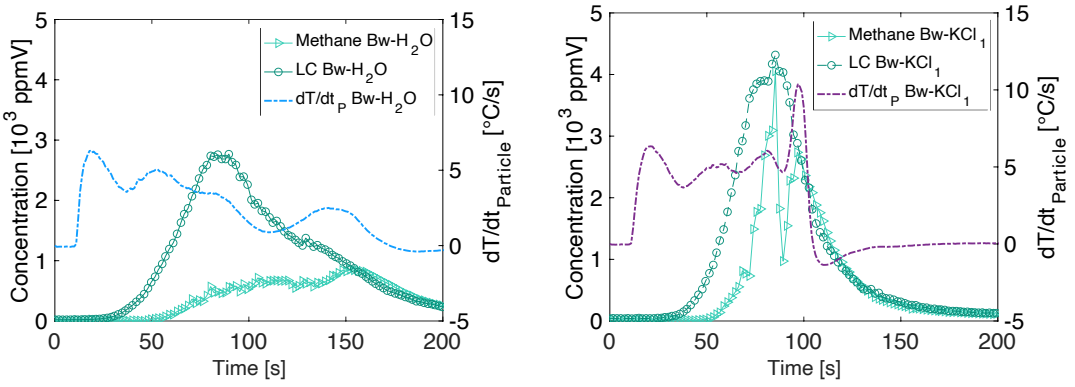

(a) Bw-H_2O (Ø 10 mm) at 500 °C *(b) Bw-KCl_1 (Ø 10 mm) at 500 °C*

Figure 7.5: *Methane and light condensables release together with dT/dtP for: (a) Bw-H_2O and (b) Bw- KCl_1.*

In the case of CH_4 at 500 °C, its formation seems to be slightly promoted with big particle size. At low pyrolysis temperatures, K doping did not significantly affect the total CH_4 yields. However, the time dependent release was strongly modified. In Fig. 7.5 it is shown that for Bw-H_2O the main release of CH_4 was coincident with the final exothermic peak and attributed to lignin/lignin residue decomposition and secondary reactions of primary volatiles, as previously introduced. However, upon addition of K, CH_4 release increased significantly during the main devolatilization process. This indicates an enhancement of lignin reactivity and secondary reactions with the addition of K, potentially favored by bigger particle size. At 900 °C CH_4 decreased with K content. Other light hydrocarbons, such as ethene, acetylene and propane followed the same trend as CH_4 (results of single yields not shown). Jakab et al. [39] discussed that Na doping reduced slightly the production of methane, while enhanced demethoxylation reactions, leading to methanol release.

The formation of CH_4 would require not only the functional group cleavage, but also the availability of transferable H [39] which, as shown by Le Brech et al. [68] is reduced with K doping. Furthermore, CH_4 yields were higher for big particle size than for small particle size, indicating the presence of other reactions within the solid matrix leading to the production of CH_4.

7.5 Conclusion

It has been shown and quantified the combined impact of K doping with the presence of secondary heterogeneous reactions (enhanced by higher transport limitations) on the pyrolysis process. Besides the known catalytic effect of K on charring reactions, leading to higher char and water yields, other relevant patterns have been as well identified and quantified, as it is the suppression of CO release, affected as well by the increased presence of transport limitations. CH_4 formation was observed to be reduced at high pyrolysis temperatures (900 °C) by K doping. The formation of light hydrocarbons and light condensables was favored by bigger particle size for both pyrolysis temperatures. Light condensable yields were reduced with K doping at both temperatures. Regarding thermochemistry, it has been already discussed that both, K doping and heterogeneous secondary reactions lead to an increase in process exothermicity. We have observed that the combined effect of both phenomena increased further this exothermicity, therefore K doping may favor the presence of these secondary reactions. With this work we aim at contributing to the understanding of the pyrolysis process and to complement other studies towards the further advances in the modeling of the process.

Chapter 8

Synergistic influence of inorganics and intra-particle transport resistances on the pyrolysis mechanism of woody biomass based on its macrocomponents

This chapter is in preparation for submission to *Energy Conversion and Management* with the title "Synergistic influence of inorganics and intra-particle transport resistances on the pyrolysis mechanism of woody biomass based on its macrocomponents", H. Almuina-Villar, C. M. Grottola, F. Hempel, N. Lang, J.-P. H. van Helden, F. Behrendt, and A. Dieguez-Alonso.

8.1 Abstract

The combined influence of inorganic species and intra-particle transport limitations on the slow pyrolysis of wood and each of its macrocomponents (cellulose, hemicellulose and lignin) has been investigated. To this end, simultaneous measurements of both mass and temperature were combined with advanced laser-based spectroscopic techniques to characterize, online and in-situ, targeted volatiles in the pyrolysis gas stream. Laser-induced fluorescence (LIF) and infrared laser absorption spectroscopy (IRLAS) were employed to identify fluorescence-emitting species, such as polycyclic aromatic compounds (PACs), and water, respectively. Permanent gases (CO_2, CO, CH_4 and H_2) were characterized by means of a micro gas chromatograph. The experiments were performed with two different initial masses employing pure, washed and KCl-doped samples up to a temperature of 600 °C with a constant heating rate

of 10 °C/min. Inorganic species shift the devolatilization rate of wood towards lower temperatures. Exothermic reactions are promoted by both inorganics and transport limitation phenomena mainly due to their effect on cellulose decomposition and lead to a narrowing and overlap of the three main macrocomponents devolatilization. With increasing inorganic content there is a preference for fragmentation reactions to form light gases. However, when intra-particle resistances are increased, there is an enhancement of charring reactions (e.g. dehydration) which inhibit the formation of other gases such as CO. PACs are mainly derived from lignin during the main devolatilization stage. However, at high temperatures, the contribution to the formation of PAC is related to further reactions in the solid matrix of holocellulose. There is a qualitative correlation between CH_4 formation and PACs release indicating common formation mechanisms. Inhibition of PACs upon addition of K suggest a competition between PACs release and char formation.

8.2 Introduction

In the last decade, initiated by the targets towards sustainable energy supply, pyrolysis has become one of the main routes for biomass conversion. Depending on its application and by controlling the process parameters, it can be used for both the production of bio-oil, which can be further upgraded into liquid transport biofuels, and the production of bio-char, for soil amendment. Moreover, its importance lies not only in being treated as a process on its own, but also as a key stage in other thermochemical conversion processes with significant influence in the overall product distribution and conversion efficiency.

Lignocellulosic biomass is composed of cellulose (40-50 wt.%), hemicellulose (25-30 wt.%), lignin (18-25 wt.% for hardwood and up to 35 wt.% for softwood) [7], and smaller amounts of extractives and inorganic species. Due to its complexity, and despite the achieved progress in the recent years, the exact pyrolysis mechanism remains unveiled. Furthermore, the need to account for the reactions that take place between the primary pyrolysis products, both homogeneously (in the gas-phase) and heterogeneously (in the char matrix), further increases the challenge. One of the most promising pyrolysis kinetic schemes available so far is the one developed initially by Ranzi et al. [34] and updated to include homogeneous secondary reactions [43], the presence of extractives [40], and the presence of heterogeneous secondary reactions in the form of fitting parameters [44, 45, 162]. However, as highlighted by several authors [40, 43, 45], there is still a need for further improvements

of the model such as: (i) the implementation of the influence of inorganic species; (ii) the modeling of heterogeneous secondary reactions; and (iii) the formation of aromatic species such as BTX (benzene, toluene, xylene) and PACs (polyaromatic compounds).

To understand the effect of inorganic species on biomass pyrolysis it is necessary to study their influence on each of the main macromolecules present in the biomass. The current understanding of the cellulose pyrolysis mechanism has been reviewed by Anca-Couce [8]: after a first depolymerization step, in which a liquid intermediate compound is formed, cellulose pyrolysis may be explained as a competition between two different global pathways: transglycosylation and ring fragmentation reactions. The former leads to the formation of mainly levoglucosan and other anhydro-sugars [8, 34, 58–60], while the latter, fragmentation reactions through β-elimination, results in the formation of low molecular weight compounds (LMWCs) and gases [8, 34, 58–60]. Regarding the mechanisms of char formation in cellulose pyrolysis the pathway is, however, less clear. Some authors claim that char is only formed through secondary reactions within the solid/liquid matrix, both through repolymerization of levoglucosan and other oligomers formed by the transglycosylation pathway [8, 59, 60], as well as through the ring fragmentation pathway[8, 44, 59, 60]. Others argue that primary char may be already formed through dehydration reactions, competing with depolymerization reactions, accompanied therefore mainly by water formation [34,41,58,62,64,66]. However, in many cases, this reaction pathway is only associated with slow heating rates or low temperatures ($<$ 300 °C) [58, 66]. When accounting also for the influence of inorganic species, it is reported that: i) it hinders the formation of sugars [8, 41, 58, 62, 67]; ii) it enhances the formation of LMWCs and gases, promoting the ring fragmentation pathway over transglycosylation [59, 60]; and iii) it increases char yields [41, 62, 67]. The delay in unzipping reactions, favored by the presence of alkali or alkaline earth species, has been proposed as a potential mechanism behind the reduction of levoglucosan yields, since it could promote the fragmentation pathway,[58]. However, Mamleev et al. [60] claimed that the presence of a liquid intermediate (tar) in the cavities of the cellulose matrix (acting as an electrolyte), containing a catalyst (potentially volatile acids from cellulose decomposition or inorganic species), may promote heterolytic (ionic) reactions, enhancing therefore the β-elimination pathway. The presence of an intermediate liquid during biomass pyrolysis, which further supports the hypothesis postulated by Mamleev and co-workers has been further proved by Dufour et al. [80] experimentally by in situ ^{1}H NMR spectroscopy. Due to the influence of inorganics

on different pathways in the pyrolysis mechanism, macroscopically both a change in the product distribution as well as a shift in the devolatilization rate towards lower temperatures has been observed [62, 68].

Hemicellulose has been studied to a lesser extent in comparison to cellulose. Because of its heterogeneity, together with the problems inherent to the isolation techniques, it is necessary to select representative compounds which are not able to fully represent its behavior [33]. In the case of hardwood, the most widely used compound is xylan. Hemicellulose pyrolysis mechanism is also discussed as a competition between sugar formation (e.g. xyloses, mannoses) and ring opening (fragmentation) reactions [8, 69]. However, some differences with respect to cellulose need to be highlighted. In general, hemicellulose decomposition yields more char and less sugars than cellulose, being its main products furfural and acetic acid [75]. Moreover, it decomposes at lower temperatures, attributed to its lower degree of polymerization [33]. The presence of inorganic content is reported to increase char and CO_2 yields as well as inhibit the formation of sugars [8,33]. Furthermore, the production of propionic acid, furfural, and other furan derivatives may also be enhanced by the presence of AAEMs [33, 75].

Regarding lignin, even though the different isolation methods are reported to affect inevitably its chemical structure [35], alkali lignin is usually employed as model compound to investigate its pyrolysis behavior [36]. Unlike cellulose and hemicellulose, lignin does not have a clear decomposition stage, reacting over a broad temperature range (150-700 °C). Due to its aromatic structure, phenolics are the main volatile products, accompanied by water, carbonyls, alcohols, and permanent gases [8]. Moreover, it is the main source of char in pyrolysis of lignocellulosic biomass. The effect of inorganic species on lignin pyrolysis has been studied by several authors, but up to now without a clear consensus. The presence of alkali species (e.g. Na [38] or K [36]) has been reported to enhance char formation and favor the fragmentation of functional groups [38], including the promotion of decarboxylation and dehydration reactions with the production of H_2 at the expense of CO and formaldehyde [36, 38]. However, the differences were reported to be less than 10 % and no enhancement of mass loss rates was observed. On the contrary, inorganic species have been reported to have a significant influence on lignin devolatilization within lignocellulosic biomass, shifting considerably the conversion rate towards lower temperatures [77, 174, 178].

As it can be observed, there are still certain discrepancies, not only with respect to the effect of inorganic species on the pyrolysis of each of the macrocomponents, but

also with respect to the possible interactions when applied to the study of pyrolysis of lignocellulosic biomass. Moreover, in thermally thick particles the influence of inorganic species on the pyrolysis mechanism is further affected by the presence of heterogeneous secondary reactions [174].

Heterogeneous secondary reactions occur when the immediate transport of primary pyrolysis products out of the reacting particle is hindered. Charring reactions, at least in cellulose pyrolysis, have been considered as a part of these heterogeneous secondary reactions [8, 59, 60], as it has been previously introduced. Both low temperatures, i.e. below 500 °C, and slow heating rates enhance the occurrence of charring reactions [44]. Furthermore, heterogeneous tar cracking reactions can also occur. Several works have investigated both charring and tar cracking reactions by employing particles in the cm-scale, reporting an increase in char production and process exothermicity as well as a clear influence on the composition of the pyrolysis volatiles [82, 149, 174].

Formation of polyaromatic compounds (PACs) has been reported as a product of these heterogeneous secondary reactions. However, at low temperature, the concentration of these species is rather low, hindering its detection by conventional methods. In this context, this group has published several works employing LIF spectroscopy [28, 29, 149, 162, 174, 178], taking advantage of the fact that it is an on-line non-intrusive technique with high sensitivity (up to ppb in the gas-phase [107]).

Another non-intrusive, in-situ laser-based technique is infrared laser absorption spectroscopy (IRLAS) and has been widely employed to quantify targeted molecular species in reactive gas flows. In particular, using laser sources emitting in the mid infrared (MIR) high sensitivities with reasonable time resolution can be achieved allowing for the quantitative characterization of chemical processes in the gas phase or in gas discharges [102, 135]. Infrared laser absorption spectroscopy (IRLAS) by means of external cavity quantum cascade lasers (EC-QCLs) to measure the water release during the pyrolysis of woody biomass at atmospheric pressure has been previously tested [149]. This is a promising technique to address the lack of knowledge concerning on-line and in-situ water detection during biomass pyrolysis.

As it can be observed, despite the advances made in recent years, there are still some open questions. To the best of the authors' knowledge, the synergistic influence of inorganic species and heterogeneous secondary reactions on the pyrolysis mechanism has not been investigated in detailed yet. In fact, as expressed by some authors [41, 174], the influence that these species may have is still not clear whether they are due to changes in the pyrolysis mechanism itself, to a promotion of the

secondary reactions or to combinations of both. To address this issue, the pyrolytic behavior of both wood and its main macrocomponents (cellulose, hemicellulose, and lignin) has been studied at particle level. To study the influence of inorganic species all samples were washed and doped with KCl. Furthermore, to understand the influence of intra-particle transport limitations on the presence of secondary reactions, different initial masses were used. Simultaneous measurements of both mass and temperature in the center of the sample were combined with advanced laser-based measurement techniques in order to monitor the product gas composition online and in-situ. Infrared laser absorption spectroscopy (IRLAS) was used for quantification of water vapor whereas laser-induced fluorescence (LIF) spectroscopy was employed for characterization of fluorescence emitting species at an excitation wavelength of 266 nm, such as phenolics and PACs. These measurements were complemented with ex-situ characterization of permanent gases (CO_2, CO, CH_4 and H_2) by means of a micro gas chromatograph coupled with a thermal conductivity detector.

8.3 Experimental

8.3.1 Experimental setup

A schematic diagram of the particle level reactor, together with the different measurement techniques applied in this study, is presented in Fig. 8.1. Setup (I) shows the LIF spectroscopic system (located at the Technische Universität Berlin) and used to detect mainly aromatic species, while setup (II) shows the IRLAS system (located at the Leibniz Institute for Plasma Science and Technology in Greifswald) used to measure water. This experimental approach is based on previous works of this group [149, 174, 179]. Furthermore, a micro gas chromatograph coupled to a thermal conductivity detector (micro-GC) was used to measure permanent gases and small hydrocarbons (CO_2, CO, CH_4, and H_2).

The particle level reactor is heated through 4 ceramic heating cartridges (HTH 350W, Rauschert GmbH) symmetrically placed in the reactor walls. In both setups, the sample is located inside a cubic mesh-based sample holder (25 mm length) which hangs in the center of the particle reactor.Inside the sample holder there is a especially prepared thermocouple (type K, Ø = 1.5 mm) that, at the same time, is connected to a scale (BP 121S, Sartorius AG), allowing, in this way, the simultaneous measurement of both mass loss and temperature inside the sample. Moreover, the temperature in the close vicinity of the sample is also recorded

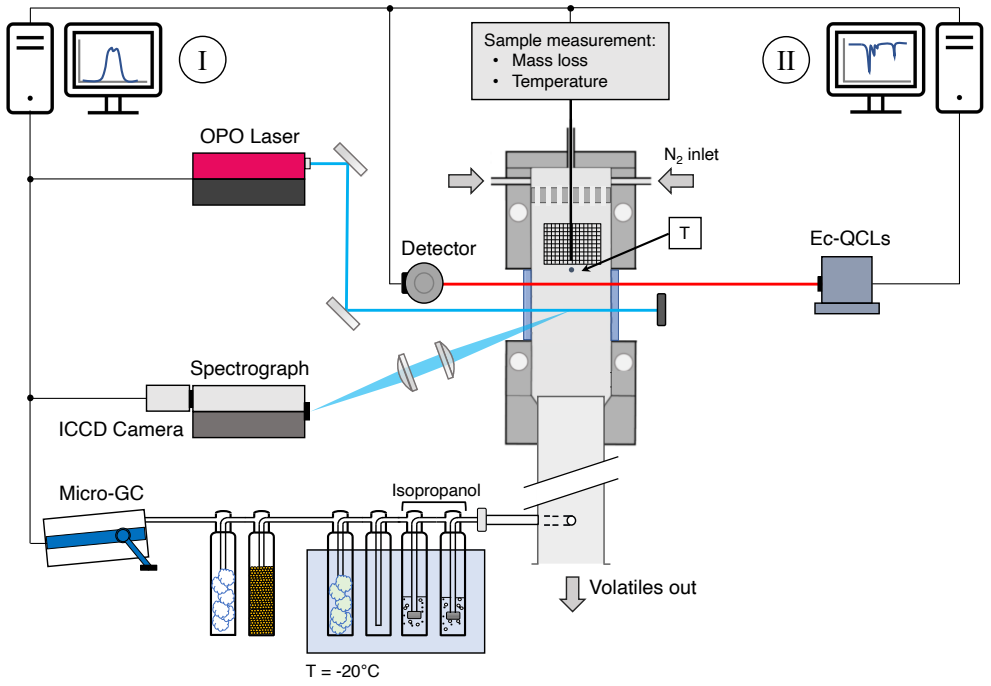

Figure 8.1: *Combined scheme of each individual experimental setup for both (I) the LIF and (II) the IRLAS measurement systems.*

through different thermocouples, represented as "T"in Fig. 8.1, placed in several axial positions in the reactor wall. The nitrogen enters the particle reactor from the top and passes through a porous plate to achieve a laminar flow. The volatiles leave the reactor chamber from the bottom through a heated tube to avoid condensation of tars. The in-situ characterization of the volatiles was performed 1 cm below the sample.

Setup (I) in Fig. 8.1 consists of a LIF spectroscopic system coupled together with an ex-situ characterization of the permanent gases (CO_2, CO, CH_4, H_2 and N_2) by means of a micro gas chromatograph (3000 Micro-GC, Inficon), equipped with a thermal conductivity detector. For the LIF measurements, the volatiles leaving the sample holder are excited at a 266 nm wavelength employing a tunable laser (Opolette HE 355 LD UV, Opotek), which utilizes an optical parametric oscillator (OPO) technology and is equipped with an UV system. The energy of each individual laser pulse is measured, before the cell, by means of an energy monitor (Gentec-EO). The fluorescence light emission is detected in the perpendicular direction to the laser beam by two plano-convex spherical lenses (Thorlabs INC) combined with a fiber optic which is coupled to a spectrograph (SR-303i-A, Andor Technology) and ICCD camera (iStar, Andor Technology).

After leaving the reactor chamber, part of the product gas is guided by means of a gas pump through a condensation system consisting of several impinger bottles placed inside a cold bath (-20 °C). The bottles are filled with isopropanol (x2), silica gel (x1) and cotton (x2), as represented in Fig. 8.1 (I), in order to condense most of the condensable species. Both a gas and a flow meter together with a manometer are installed after the condensation system to ensure a constant flow through all the experiments. Afterwards, the non-condensable gases are measured and its concentration is calculated by also measuring the carrier gas (N_2).

To measure the H_2O concentration in-situ, a cw EC-QCL (Daylight Solutions, 21074-MHF) IR-laser was used in setup (II). Emitting in a range between 1305 – 1415 cm^{-1} vibrational transitions of H_2O could be probed for concentrations down to 1016 cm^{-3} for a total absorption length of only 5 cm. The diagnostic set-up consists of (i) the EC-QCL; (ii) a chopper (New Focus optical chopper 3501), (iii) two liquid nitrogen-cooled HgCdTe detectors for measurement in-situ and reference pathsway (Infrared Associates Inc.), (iv) gold mirrors for beam manipulation, and (v) an oscilloscope for the data acquisition (Teledyne LeCroy HDO 6104).

The identification of the H_2O transition at 1372.27 cm^{-1} as well as the spectral calibration of the tuning behavior of the EC-QCL was performed using a reference gas cell filled with known absorbers (all spectral data were taken from the HITRAN databases [180] and a Ge etalon with known free spectral range. The infrared laser beam passes the particle level reactor through two wedged BaF_2 windows (Korth Kristalle) resulting in an effective absorption length of 5 cm. With a beam diameter of about 5 mm the H_2O concentrations could be measured time-resolved with a distance of about 10 mm to the surface and therefore, in close vicinity of the pyrolyzing material. The transmitted laser intensity was detected using a liquid nitrogen-cooled detector connected to an oscilloscope.

8.3.2 Experimental conditions, materials, and analysis

The pyrolysis experiments were carried out at a constant heating rate of 10 °C/min up to a final temperature of 600 °C with a nitrogen flow rate of 3.5 Nl/min. Two different sample (milled) sizes were used for each macrocomponent and for wood: 1 g, which resulted in a thin layer of a few millimetres inside the cubic sample holder (25 mm length), and 4 g, which resulted in a half full sample holder. Due to limitations in the positioning of the thermocouple in the sample holder, temperature inside the sample was only measured for the experiments conducted with 4 g. For

beech wood experiments, however, single spheres of 25 mm in diameter with a mass of about 5.5 g were used instead of the 4 g milled sample to obtain comparable results with our previous findings reported elsewhere [149, 162, 174].

For each material (cellulose, xylan, lignin, and beech wood), 3 samples with different content in inorganic species, were prepared. For cellulose experiments, Avicel PH-105 microcrystalline cellulose 0.020 mm (SERVA Electrophoresis GmbH) was selected. Preliminary TGA experiments were performed by washing the cellulose with H_2O to confirm that no difference could be found between the washed and pure cellulose due to its negligible inorganic content. After this verification, therefore, instead of washing the material, two levels of potassium content (two orders of magnitude difference as KCl) were used. Cellulose doped samples were prepared by introducing cellulose into stirring deionized water with different concentrations of KCl during 24 h. Afterwards, the sample was filtered employing glass microfibre filters (IDL GmbH & Co. KG) and dried for 8 h at 106 °C in order to ensure complete moisture removal. Both doping procedures resulted in a potassium content of 427 mg/kg and 3427 mg/kg, as shown in Tab. 8.1.

Xylan from beech wood (Sigma Aldrich) was selected as representative compound of hardwood hemicellulose. First, due to its high inorganic content, probably related to its isolation technique, a washing procedure was performed. Raw xylan was therefore soaked into stirring deionized water for 24 h. In this case, however, due to its lower degree of polymerization in comparison with cellulose, xylan was completely dissolved in water. Therefore, a filtering procedure as the one employed for cellulose could not be performed. The samples were dried at 106 °C for several days in order to evaporate the whole water. Consequently, the washing treatment was not efficient on removing potassium and sodium, as shown in Tab. 8.1. However, between 35 % and 45 % of its calcium content was removed. Doping of xylan samples was carried out after the washing procedure by adding them into a stirring solution of deionized water and KCl during 24 h. As for washed xylan, its complete dissolution did not allow any filtering procedure, therefore, samples were dried during several days at 106 °C until the complete moisture removal was ensured. For this reason, most of the KCl remained in the sample, resulting in a higher potassium content (32029 mg/kg, shown in Tab. 8.1).

Alkali lignin (Sigma Aldrich) was washed and doped following the same method as for xylan, implementing, however, filtering of the sample. Almost 50 % of potassium and sodium content was removed through the washing procedure. Moreover, sulphur

content, although still relatively high, was slightly reduced. Doping of the sample resulted, after washing, in a potassium content of 11782 mg/kg, as shown in Tab. 8.1.

Beech wood spheres (25 mm in diameter) were twice washed with deionized water in vacuum during 24 h, following the same procedure described elsewhere [174]. For KCl treatment, around 100 g of beech wood spheres were introduced under vacuum in a solution of 9 g of KCl and 800 ml of deionized water. This was performed, as for the aforementioned samples, after the washing procedure, in order to remove other inorganic species. The doping treatment resulted in a potassium content of 7519 mg/kg.

Ash content and inorganic elemental analysis of all samples are shown in Tab. 8.1. Inorganic elemental composition was characterized in an ICP-OES (inductively coupled plasma - optical emission spectrometer, Varian 720-ES), after digestion in a microwave (Multiwave 3000, from Anton Paar) with HNO_3 and H_2O_2.

Table 8.1: *Ash (wt.%) and inorganic content (mg/kg) of cellulose, xylan, lignin, and beech wood*

Material	Acronym	Ash content [%]	K [mg/kg]	Ca [mg/kg]	Na [mg/kg]	S [mg/kg]
Cellulose	C	0.01 ± 0.00	19 ± 8	-	-	25 ± 2
	C-K1	0.06 ± 0.02	426 ± 43	-	-	12 ± 3
	C-K2	0.37 ± 0.10	3426 ± 293	-	-	7 ± 0.1
Xylan	X-W	3.32 ± 0.06	246 ± 22	4100 ± 270	14393 ± 445	142 ± 10
	X	3.26 ± 0.14	236 ± 16	5916 ± 140	14095 ± 368	159 ± 4
	X-K	6.72 ± 0.16	32029 ± 278	3126 ± 15	12750 ± 158	116 ± 1
Lignin	L-W	1.04 ± 0.11	450 ± 80	-	3072 ± 256	12751 ± 402
	L	2.44 ± 0.02	688 ± 20	-	6952 ± 118	16037 ± 99
	L-K	2.34 ± 0.16	11783 ± 1520	-	4196 ± 187	13828 ± 602
Beech wood	B-W	0.21 ± 0.01	379 ± 41	732 ± 6	21 ± 3	81 ± 3
	B	0.31 ± 0.01	771 ± 133	750 ± 50	16 ± 8	94 ± 4
	B-K	1.05 ± 0.01	7519 ± 258	428 ± 42	17 ± 6	81 ± 12

8.4 Results and discussion

The presentation of results for each material is organized organized as follows: cellulose (C), xylan (X), lignin (L), and beech wood (B). The acronym for each condition is explained with the following example: **X4-W**, being X (sample, xylan) 4 (initial mass, 4g) and W (pretreatment, washed).

The conversion rate, temperature inside the sample, gas release rate (CO, CO_2, CH_4, and H_2) and total fluorescence intensity (TFI), defined in Eq. 8.2) are shown as a

function of the temperature in the atmosphere in the close vicinity of the sample (thermocouple represented as T in Fig. 8.1). The conversion rate (or devolatilization rate) is defined as $d\alpha/dt$, being α as follows:

$$\alpha = 1 - \frac{m - m_f}{m_o - mf} \tag{8.1}$$

where m is the actual mass at each time step, m_0 is the initial mass and m_f is the final mass of the sample.

The total fluorescence intensity (TFI) is calculated by integrating the recorded fluorescence spectrum for each time step, following Eq. 8.2

$$TFI = \int_{270nm}^{520nm} I(\lambda)d(\lambda) \tag{8.2}$$

Each fluorescence emission spectrum is additionally corrected by the energy of its corresponding laser pulses, measured before entering the cell by an energy monitor.

8.4.1 Cellulose

8.4.1.1 Conversion rate and temperature.

The comparison of the conversion rate ($d\alpha/dt$) between pure cellulose and cellulose doped with two levels of potassium (in the form of KCl) is shown in Fig. 8.2 (a), for the experiments performed with 1 g, and in Fig. 8.2 (b), for the experiments conducted with 4 g, both as a function of the temperature in the close vicinity of the sample. Moreover, for the larger sample size, the temperature in the center of the sample is shown in Fig. 8.2 (c).

In the experiments conducted with 1 g, Fig. 8.2 (a), cellulose devolatilization started at 260 °C, reaching its maximum rate at 374 °C (measured in the close vicinity of the sample). When doping with KCl, both the onset and the maximum of the conversion rate shifted towards lower temperatures. In the case of C1-K2 it occurs at 220 °C and 356 °C, respectively. For C1-K1, however, the change was hardly noticeable, being the maximum of the conversion rate just a few degrees lower than for pure cellulose, 371 °C. These findings are in line with other works from literature (e.g. [68]). For the experiments performed with 4 g, Fig. 8.2 (b), the catalytic effect of K on cellulose devolatilization rate was significantly enhanced compared with the smaller sample size (30 °C shifting towards lower temperatures in the case of 4 g

sample versus 18 °C shifting in the case of 1 g sample). The temperature at which the maximum mass loss occurred was 390 °C, 382 °C and 361 °C for C4, C4-K1 and C4-K2, respectively. Moreover, not only the onset but also the end of the conversion phase was clearly shifted towards lower temperatures.

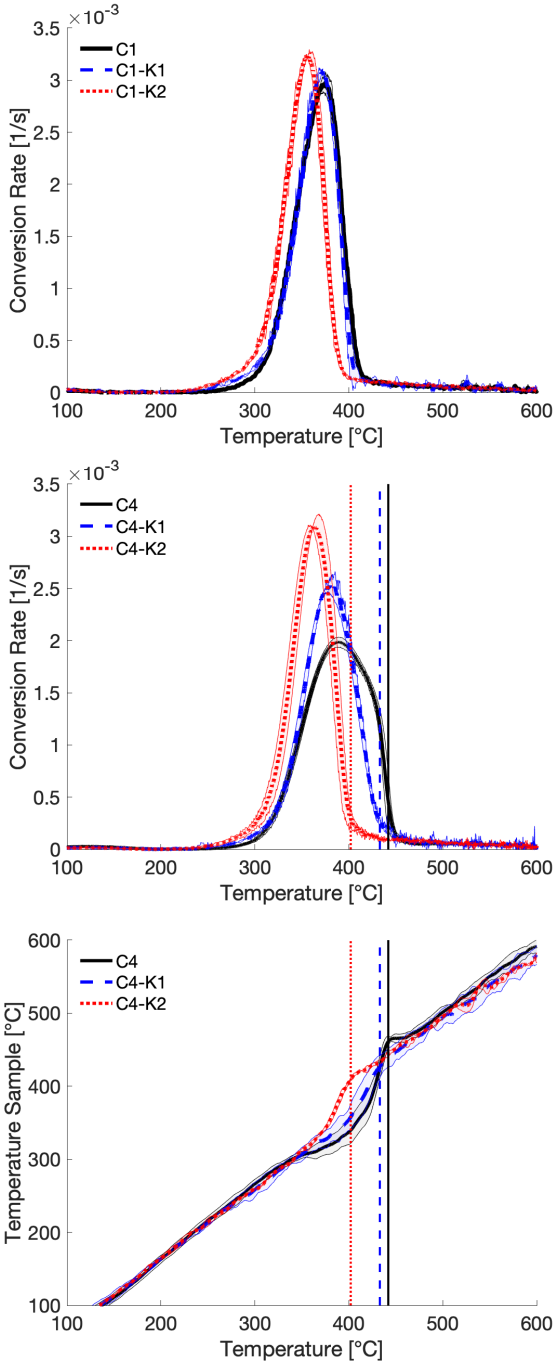

Figure 8.2: *Comparison of conversion rate (a) for 1 g cellulose samples (C1, C1-K1, and C1-K2); and for (b) 4 g cellulose samples (C4,C4-K1, and C4-K2). For the latter samples the observed temperature evolutions in the center of the sample are shown in (c). The shaded areas show the standard deviations. The vertical lines highlight the temperature at which the exothermic regime ends for each case.*

The higher temperatures at which devolatilization took place in the case of 4 g sample can be explained by the larger sample size, enhancing intra-particle heat transport resistance, since the reported temperatures are measured in the close vicinity of the reacting sample. Fig. 8.2 (c) shows the temperature in the center versus the temperature in the close vicinity of the samples for the 4 g experiments. From this, the thermal behavior of the three cellulose species during pyrolysis can be discussed. For pure cellulose, (Fig. 8.2 (c), C4), an endothermic regime clearly dominates during most part of the devolatilization stage (valley in the temperature evolution in the centre of the sample), being exothermic reactions more relevant at the end of the devolatilization (rapid increase in the temperature in the center of the sample with overshoot above the temperature in the close vicinity of the sample). The vertical lines in Fig. 8.2 (b and c) point to the end of the dominantly exothermic regime. When doping cellulose with KCl, the endothermic valley occurring throughout the devolatilization stage became almost thermally neutral for the case of C4-K1, resulting in a globally exothermic regime for the highest KCl concentration sample, C4-K2. The end of the dominantly exothermic regime occurs at the same position relative to the devolatilization for the three cases as indicated by the vertical lines in Fig. 8.2. Furthermore, the overshoot of the temperature in the center of the sample was observed to be nearly the same in all cases.

Based on the phenomenological model proposed by Mamleev et al. [60], and supported by other authors (e.g. [54, 68]), an intermediate liquid phase with high-boiling temperature is formed within the solid matrix during cellulose devolatilization. For pure cellulose devolatilization in the absence of significant intra-particle transport limitations, which mostly undergoes the transglycosylation reaction pathway, this liquid phase would be mostly formed by levoglucosan and other anhydrosugars [60, 68]. This results in a globally endothermic behavior due to the cleavage of glycosidic bonds together with the evaporation of high-boiling liquid products [59, 60, 68], consistent with the temperature evolution observed in Fig. 8.2 (c), C4. To enable the fragmentation pathway, as discussed by Mamleev et al. [60], catalysts (high activation energy pathway possible otherwise only at high temperatures) are needed, which would be products of the cellulose devolatilization itself (volatile acids) or inorganic species [60]. Therefore, the increase in K upon doping would promote the fragmentation pathway with the consequent higher (earlier) production of lighter species, resulting in a shifting of the conversion rate towards lower temperatures. However, the influence of K cannot be understood without discussing the influence of intra-particle mass transport limitations as well. As highlighted by

Mamleev et al. [60] the concentration of this liquid phase in thermogravimetric analysis conditions is not high enough as to provide an effective catalytic environment for the fragmentation pathway. In fact, in thermogravimetric analysis of these same samples [results not published] the opposite behavior was observed, with a shifting of the devolatilization rate towards higher temperatures upon K addition. Similar results have been observed by other authors (e.g. [62]) as well. With an increase in intra-particle mass transport resistance both the accumulation of the liquid phase and the concentration of active catalysts in the liquid phase increases, enabling a more effective impact of K^+ through heterolytic reactions on the devolatilization mechanism resulting in the enhancement of the fragmentation pathway.

At the same time, exothermicity in pyrolysis of cellulose, has been reported to be correlated with char forming reactions [68, 181], via crosslinking, which in the case of pure cellulose should be related to the presence of secondary reactions of primary pyrolysis products enhanced by the intra-particle transport limitations. That is why the more exothermic regime (charring reactions of primary products) occurs after the more endothermic regime of primary devolatilization [8, 60]. This explains the higher char yields obtained for pure cellulose with 4 g, C4 in Tab. 8.2, in comparison with pure cellulose with 1 g, C1 in Tab. 8.2 (15.06 wt.% and 11.67 wt.%, respectively). With respect to K, its major impact on the process thermochemistry is the reduction of the endothermicity during the devolatilization process. This behavior would be the overlap of two different pathways: (i) the reduction of the endothermicity derived from the transglycosylation reactions due to the enhancement of the ring fragmentation pathway; and (ii) the catalyzation of charring reactions, either directly or via the higher production of fragmentation products, favoring for example dehydration reactions [60]. This is also consistent with the higher char yields presented in Tab. 8.2 for C4-K1 and C4-K2.

Table 8.2: *Final char and released mass yields of CO_2, CO, CH_4, H_2, and H_2O in dry basis for cellulose (n.d. - not determined)*

Yield	Cellulose 1 g			Cellulose 4 g		
(wt.%, db)	C1	C1-K1	C1-K2	C4	C4-K1	C4-K2
Char	11.67	13.37	15.42	15.06	16.13	18.76
CO_2	2.92	4.58	5.82	6.09	8.83	9.52
CO	4.21	4.74	5.17	4.37	4.18	4.33
CH_4	0.57	0.61	0.64	0.61	0.63	0.69
H_2	0.03	0.04	0.06	0.05	0.06	0.07
H_2O	n.d	n.d	n.d	15.06	29.31	34. 27

8.4.1.2 Products distribution.

The comparison between the evolution of CO_2, CO, CH_4, and H_2 for 1 g and 4 g samples is shown in Fig. 8.3 and Fig. 8.4, respectively. Table 8.2 lists the final yields for char, permanent gases, and water. The yields (wt.%, db) are calculated by integrating over time the release rate curves (g/min). The highest standard deviations are of 1 %, 0.7 % and 0.08 % for char, major (CO_2 and CO) and minor (CH_4 and H_2) gaseous compounds, respectively.

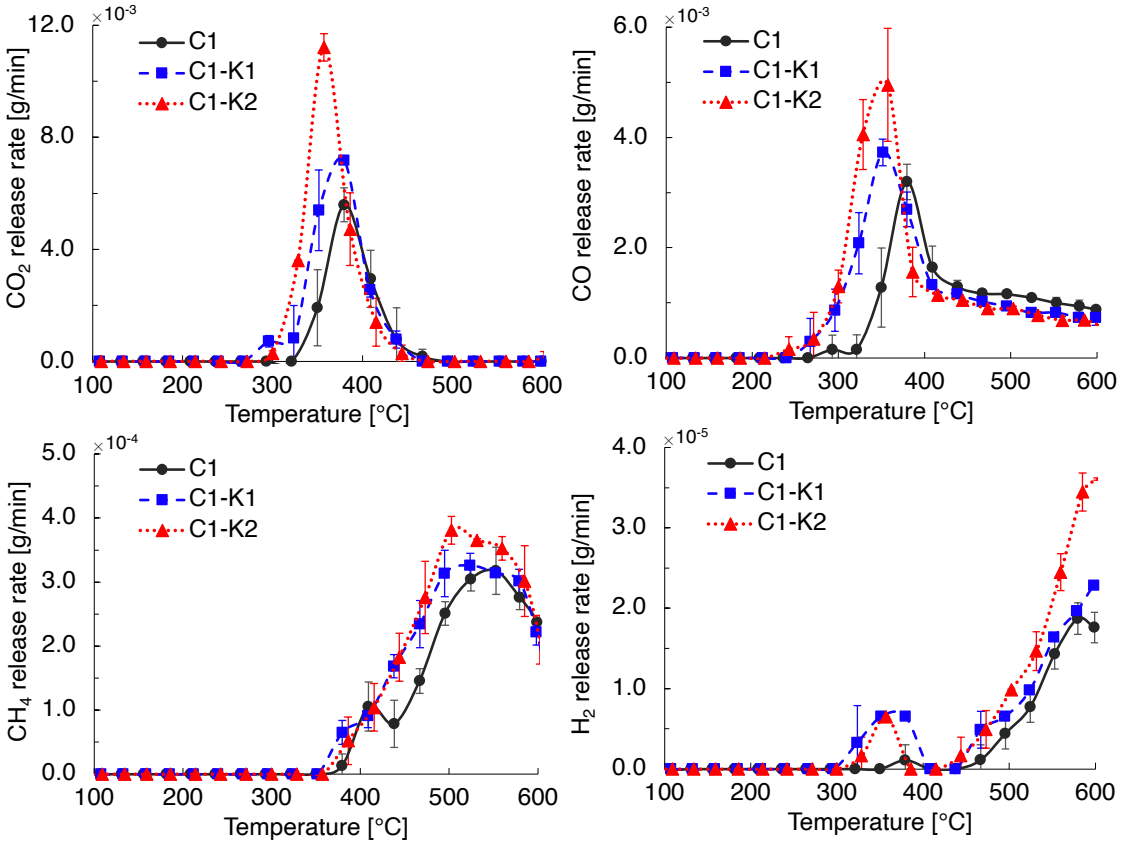

Figure 8.3: *Comparison of release rate of CO_2, CO, CH_4, and H_2 as a function of temperature in the vicinity of the sample for 1 g cellulose (C1) and cellulose doped with different potassium content (C1-K1 and C1-K2).*

For both sample sizes, the major gases released during the main devolatilization stage were CO and CO_2, as it is well known [8]. Both CH_4 and H_2 production was rather low during this stage, increasing at higher temperatures. For pure cellulose, the total gas yield rose with larger sample mass (7.73 wt.% and 11.12 wt.% for 1 g and 4 g, respectively), mainly due to the enhancement of CO_2 (from 2.92 wt.% to 6.09 wt.%). This is consistent with CO_2 being an important product of secondary reactions of primary volatiles within the matrix [45, 60].

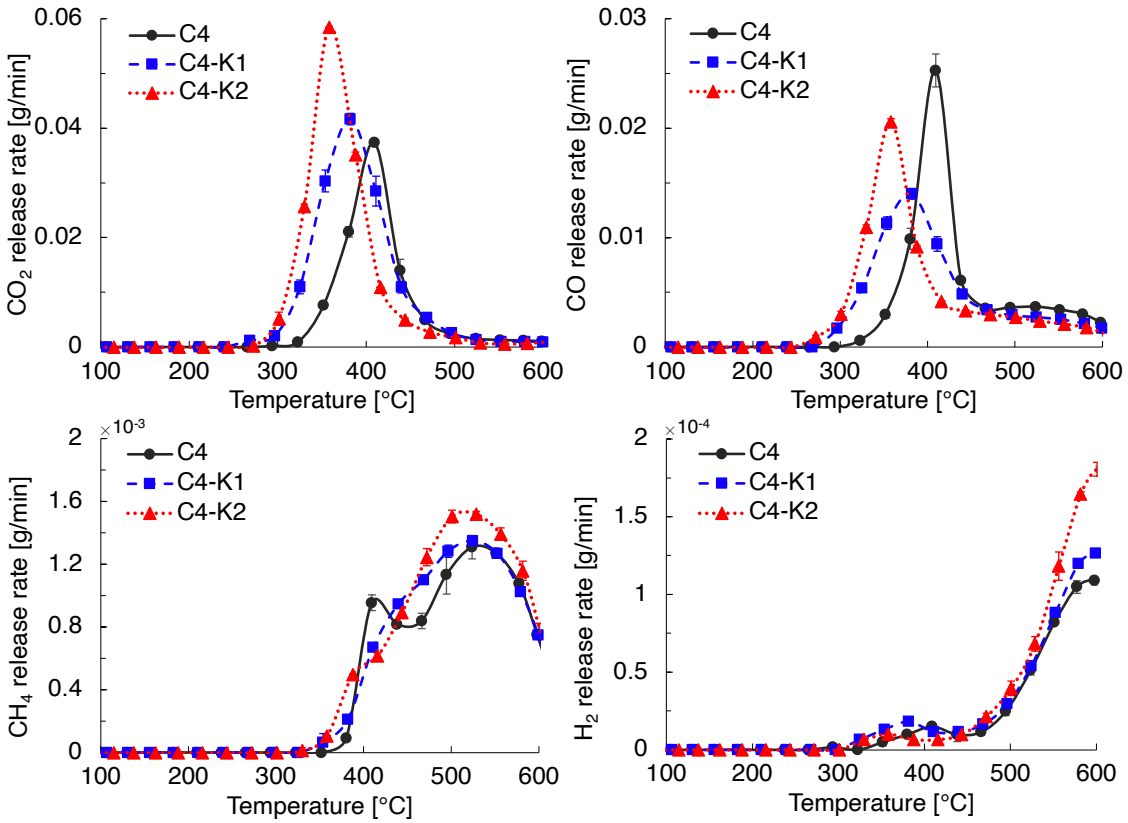

Figure 8.4: *Comparison of release rate of CO_2, CO, CH_4, and H_2 as a function of temperature in the vicinity of the sample for 4 g cellulose (C4) and cellulose doped with different potassium content (C4-K1 and C4-K2).*

When doping with KCl, the catalytic effect observed for conversion rate was reflected also in the release of CO_2 and CO, shifting towards lower temperatures. This effect on CH_4 and H_2 was rather unnoticeable. Regarding yields, K-doping also resulted in an increase of both gas (mainly due to CO_2) and char yields (see Tab. 8.2). The production of CH_4 and H_2 was only slightly promoted by both the increase in sample size and the increase in K content. An increase in water yield was also observed with K-doping in 4 g samples.

The release of gases further supports the previous discussion based on the phenomenological model by Mamleev et al. [60]. In 1 g experiments, the addition of K resulted in the increase of CO due to enhancement of the fragmentation pathway and of char and CO_2 due to promotion of charring reactions. At the same time, larger masses did not significantly affect the release of CO. These results point to a competition between the CO_2 and the CO production pathways with K-doping in the regime where the extent of intra-particle transport limitations are higher (4 g sample). Larger intra-particle transport limitations promote charring reactions, sec-

ondary to both transglycosylation and fragmentation pathways, enhancing therefore the production of char, H_2O, and CO_2. K promote furthermore the fragmentation pathway, but due to the higher intra-particle transport resistances, the open-ring products of this pathway react further in the intermediate phase (potentially together with the intermediate products of the transglycosylation pathway), from now on referred to as carbon pool, to form char, CO_2 and H_2O. This is also in good agreement with the release of CH_4 shown in Fig. 8.4. Its release at lower temperatures can be used to monitor the reactions leading to the production of low molecular weight compounds (LMWCs) and CO. In the case of pure cellulose (C4), a peak of CH_4 release is observed at around 400 °C, coincident with the release of CO_2 and CO. However, upon K addition, this peak disappears. There is hence a preference in the pathway of char and CO_2 in detriment to the LMWCs and CO pathway when K-doped cellulose is pyrolyzed in conditions where the intra-particle transport limitations are very relevant. This is also consistent with the larger exothermicity with K, as discussed in the previous section.

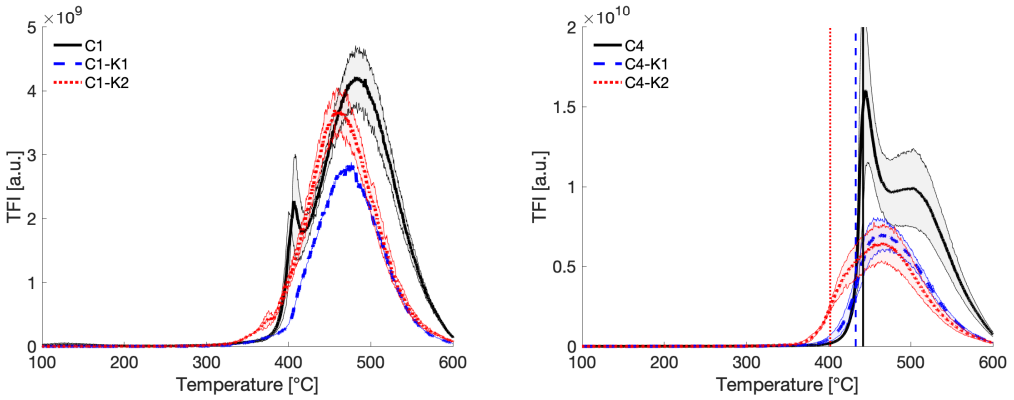

Figure 8.5: *Comparison of the total fluorescence intensity (TFI) as a function of temperature in the vicinity of the sample for: (a) 1 g cellulose (C1, C1-K1, and C1-K2) and (b) 4 g cellulose (C4, C4-K1, and C4-K2). The shaded areas represent the standard deviation. The vertical lines highlight the temperature at which the exothermic regime ends for each case.*

The comparison of the total fluorescence intensity (TFI) as a function of temperature in the close vicinity of the reacting sample is presented in Fig. 8.5. The fluorescence signal was obtained with an excitation wavelength of 266 nm and its intensity was corrected by the energy of its corresponding laser pulses. Therefore, in advancement to our previous publications [28, 29, 149, 174], a semi-quantitative analysis of the total amount of fluorescence-emitting species can be obtained. The species that are

more likely to emit fluorescence at this excitation wavelength are mainly aromatic compounds [28, 29, 174]. Based on the absorption cross section [112], PACs, phenolics, and aromatic carbonyls are, in that order, the species most likely to be excited at 266 nm. However, it is not only the absorption cross section, i.e. the probability of being excited, that has to be taken into account, but it is also important to consider the probability, once excited, of emitting fluorescence, which is defined as the quantum yield. In fact, other individual species, such as furfural, which are also reported to have an absorption cross section in the same range as PACs [112], were not able to emit fluorescence despite being able to absorb laser light at this excitation wavelength. This can be confirmed by experiments performed in this group in the same conditions as the pyrolysis experiments (see Chapter 9). Moreover, even species such as benzaldehyde and benzophenone, i.e. aromatic carbonyls, under conditions of the present work, emitted fluorescence with an intensity 3 orders of magnitude lower than that of PACs. Therefore, the TFI signal presented in this work is assumed to come mainly from PACs.

In the case of pure cellulose, the release of PACs occurred in two differentiated stages. In experiments performed with 1 g, C1 in Fig. 8.5 (a), the release of PACs started with a peak at around 400 °C, corresponding to the end of the devolatilization rate curve, and continued with a broader peak at higher temperatures, reaching its maximum at 480 °C (measured in the close vicinity of the particle). Besides the work of this group on the release of PACs at low temperatures in pyrolysis [149,174], recent publications have also confirmed the presence of aromatic compounds even at 350 °C and above [94]. When using larger mass, C4 in Fig. 8.5 (b), the initial peak was much higher relative to the second stage, indicating a higher release of aromatic species at around 440 °C. For K-doped cellulose, both in 1 g and 4 g experiments, both stages merged in one. This behavior is also consistent with the release pattern of CH_4 as previously discussed.

The formation of (poly) aromatic ring species in cellulose pyrolysis is derived from the secondary reactions occurring in the carbon pool, as previously introduced. Carlson et al. [182] proposed such mechanism for the production of (poly) aromatic species during catalytic pyrolysis of glucose. In the present work, it is assumed that the mechanism of PACs production is closely related with the mechanism of char production via heterogeneous (charring) secondary reactions in the carbon pool, formed by intermediate products from the fragmentation and transglycosylation pathways. The production of CH_4 is qualitatively related to the production of PACs and the first peak in the release of CH_4 can be considered as an indicator of the formation

and further reaction of the LMWCs. With higher initial mass and therefore larger intra-particle transport resistance, the extent of the secondary reactions in the carbon pool are larger, increasing the likelihood of production both PACs and char. This is consistent with the larger TFI in the first stage, at lower temperatures, also coincident with a larger release of CH_4 as well as CO, CO_2, and char, as previously discussed. In the case of C4 further PACs are produced, peaking at around 500 °C, also coincident with CH_4 and H_2 and attributed to further reactions in the solid matrix. Upon doping with K, despite favoring the fragmentation pathway and hence producing more LMWCs, also secondary charring reactions are promoted. It has been postulated above that a competition between the release of CO + LMWCs + CH_4 and the formation of char + CO_2 + H_2O is established, being the latter favored with K-doping in the presence of significant intra-particle mass transport limitations and therefore resulting, for example, in a lesser release of CH_4 at lower temperatures (associated with cracking reactions of intermediate products). In the same way, also the production of PACs is decreased upon K addition. This discussion is summarised in Fig. 8.6 based on the mechanism of Mamleev et al.[60] and taking into account the synergistic influence of K and secondary reactions.

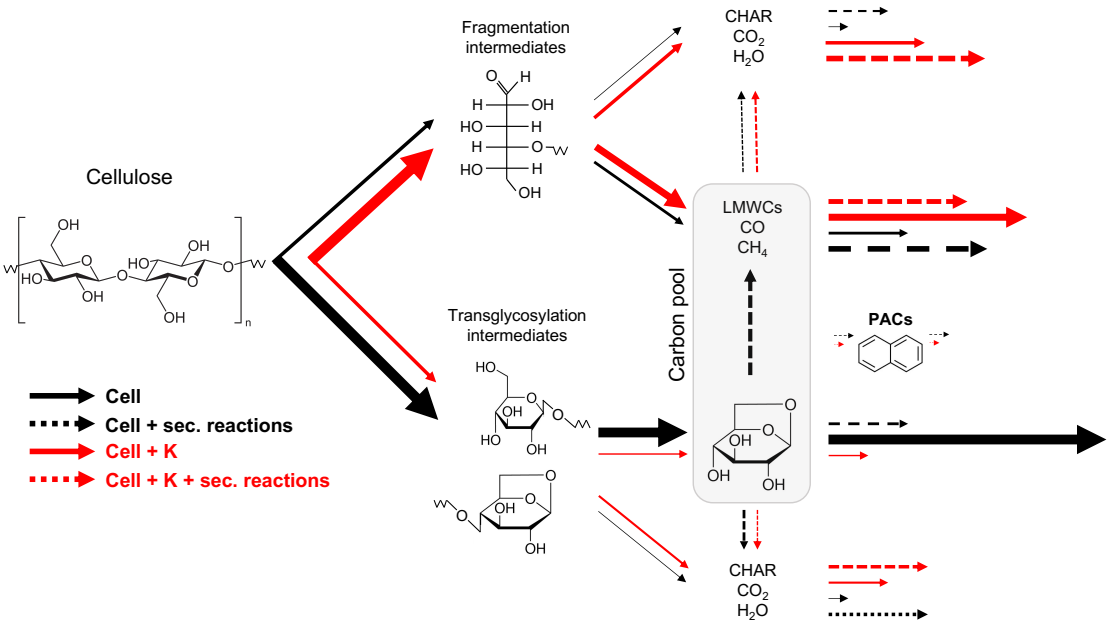

Figure 8.6: *Proposed reaction scheme for cellulose pyrolysis taking into account the synergistic influence of K and secondary reactions. The size of the arrows, as well as the final length, represent the expected yields depending on the presence of K, secondary reactions or a combination of both.*

8.4.2 Xylan

8.4.2.1 Conversion rate and temperature.

The comparison of the conversion rate ($d\alpha/dt$) between washed xylan, xylan, and K-doped xylan for 4 g is presented in Fig. 8.8 (a), together with the temperature evolutions in the centre of the samples (Fig. 8.8 (b)). For 1 g the comparison is available in Fig. 8.7. Both conversion rates and temperature evolutions are plotted versus the temperature in the close vicinity of the sample.

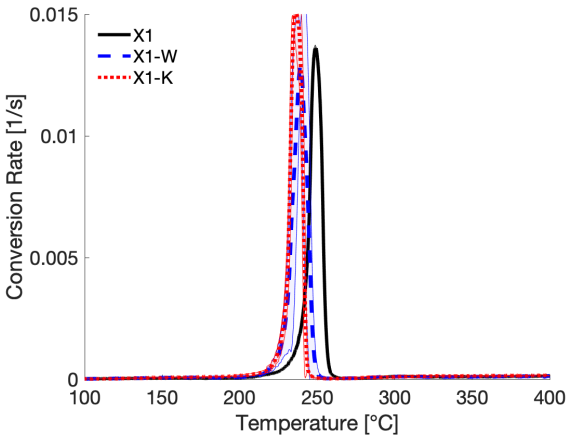

Figure 8.7: *Comparison of conversion rate 1 g xylan (X1), washed xylan (X1-W), and K-doped xylan (X1-K). The shaded areas represent the standard deviation.*

The devolatilization of both K-doped and washed xylan samples are slightly shifted towards lower temperatures in both intra-particle transport regimes (see Fig. 8.7 and Fig. 8.8 (a)). The shape of the devolatilization curve was not significantly affected, though, being noteworthy to mention the very narrow temperature range in which complete reaction of all samples occurred, that is within 20 - 30 °C, from the onset of the devolatilization until no further significant mass loss was detected. An important increase of temperature in the center of the sample was also observed during devolatilization of 4 g samples (see Fig. 8.8 (b)), indicating strong exothermic reactions. This exothermicity could explain, at least partially, the fast devolatilization, since heating rates around 120 °C/min are reached in the center of the sample in this step.

One could conclude, based on the results from Fig. 8.7 and Fig. 8.8 (a), that both doping and washing procedures did not significantly influence the pyrolysis mechanism of xylan, as reflected by the devolatilization curves. This could be potentially explained by its large content in inorganic species, derived from the extraction

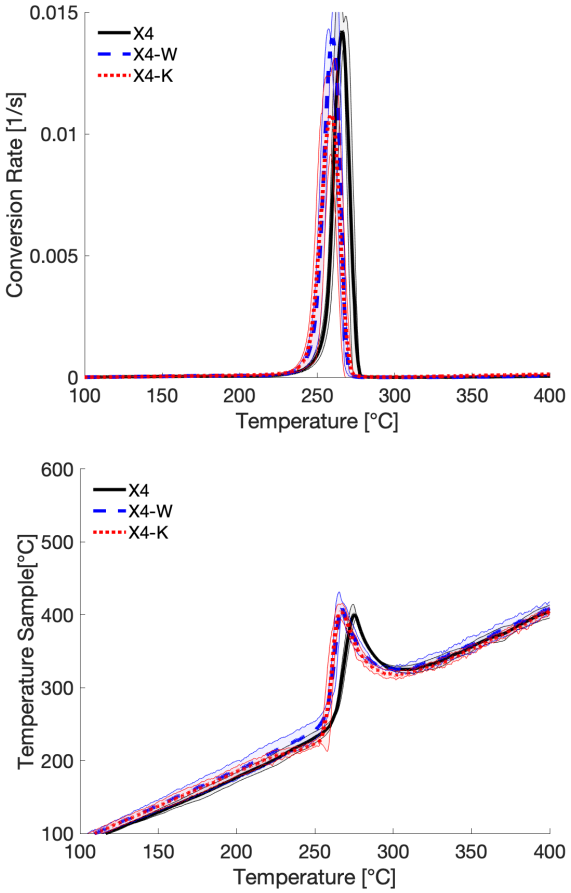

Figure 8.8: *Comparison of conversion rate (a) and temperature inside the sample (b) as a function of temperature in the vicinity of the sample for 4 g xylan (X4), washed xylan (X4-W), and K-doped xylan (X4-K). The shaded areas represent the standard deviation.*

method. However, pyrolysis of the same samples in a thermogravimetric analyzer, with initial masses of 20 mg and N_2 flow rates of 100 ml/min, (see Fig.8.9) presented a different behavior. These results showed a clear influence of the K-doping and washing on the devolatilization rate (Fig.8.9) and heat of reaction (data not shown). Washed xylan (X-TGA-W, Fig. 8.9) presented two distinct peaks in the devolatilization rate curve, between 200 – 300 °C. The devolatilization rate at temperatures above 300 °C was very mild, though. These results are consistent with a multi-step pyrolysis mechanism. It has been often reported in literature that the pyrolysis of hemicellulose, commonly represented through model compounds such as xylan, should be described by a multi-step kinetic model, most conventionally limited to a two-step model [34, 44, 70, 71]. Ranzi et al. [34] proposed a kinetic scheme where hemicellulose converts fast to two active hemicellulose forms, similarly to the formation of active cellulose. The two active hemicelluloses decompose successively, reproducing the two-step decomposition previously introduced [34, 44]. The first

active hemicellulose decomposes through two competitive pathways, one leading to the formation of sugars (e.g., xylose) and a second one, via ring opening, leading to fragmentation products, such as light volatiles and char [34, 44], following the same approach as for cellulose, as discussed in the previous section. The decomposition of the second active hemicellulose would follow the fragmentation pathway as well, leading to volatiles and char [34, 44]. In a recent review by Giudicianni et al. [21] it has been also discussed, from a more mechanistic perspective, that xylan decomposes to xyloses (via glycosidic bond cleavage followed by inclusion of OH^- and H^+, requiring therefore that other pyrolysis products are already present [33]) and anhydrosugars (e.g. 1,4-anhydro-D-xylopyranose) via cleavage of glycosidic bonds and further rearrangement [21, 33, 72], which can be consumed immediately [72]. These products decompose further via two competitive pathways: (I) dehydration, leading to the production of anhydrosugars/dianhydrosugars, and (II) ring fragmentation, leading to light volatiles, furans, and char [21]. The production of furans following the depolymerization and dehydration pathway is also considered [33], and not only via ring scission and further rearrangement [33, 72].

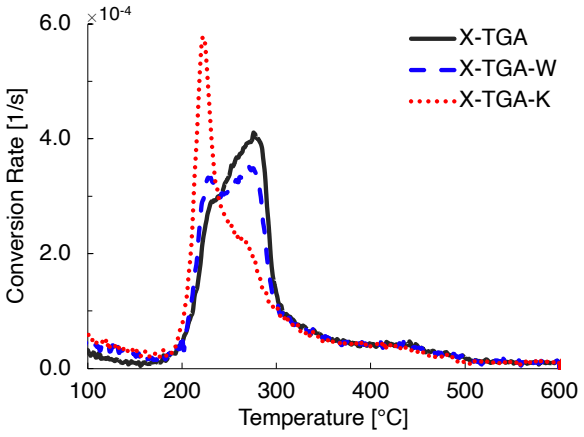

Figure 8.9: *Comparison of conversion rate as a function of temperature for 20 mg xylan (X-TGA), washed xylan (X-TGA-W), and K-doped xylan (X-TGA-K) measured in a thermogravimetric analyzer.*

Accordingly, the first peak in xylan devolatilization has been usually attributed to cleavage of glycosidic bonds as well as side chains (e.g., O-acetylxylan and 4-O-methylglucuronic acid units [72], while the second peak should be related to the ring fragmentation reactions [72, 73]. This is also in good agreement with the results from the excellent work by Zhou et al. [69] for fast pyrolysis of hemicelluloses. These authors showed first the formation of sugars intermediates and di-/anhydrosugars,

followed by the formation of light volatiles, gases, furanic compounds, and char, parallel to a consumption of the sugars intermediates and di-/anhydrosugars.

In the results at TGA level (conversion rate, Fig.8.9), as previously introduced, the washed xylan results showed these two distinct peaks at 230 °C and 277 °C. In the case of raw xylan, the first peak was very mild, rather shoulder, at around 239 °C, while the second peak was higher, indicating higher contribution to devolatilization rate, at around 280 °C. These results present a very similar behaviour to the ones reported by Giudicianni et al. [74, 75]. For washed xylan, the results in the present study (Fig. 8.9) followed qualitatively also the results by Giudicianni et al. [74, 75] and others [73, 183] that is, an increase in the intensity of the first devolatilization rate peak and a decrease in the intensity of the second one, although the results in the present paper are much milder, resulting in the two clear peaks, attributed to the less efficient removal of inorganic species by washing, in comparison to cation-exchange methods [183]. Doping with KCl, resulted in a dramatic increase in the intensity of the first devolatilization rate peak, with maximum at around 224 °C, accompanied by a significant reduction of the second devolatilization rate peak. Once again, these results are in good agreement with other results from literature (e.g., [75] with Na doping, [183] with K doping). Consequently, it can be concluded that the changes in the devolatilization rate curves between washed xylan, xylan, and K-doped xylan in the present work at TGA level are due to the doping with K and removal of inorganic species, and not due to the influence of washing on the xylan structure, since the works by Giudicianni et al. [74, 75] and others [73, 183] used other methods besides wet impregnation and washing.

In the experiments at particle level, both with 1 g and 4 g, these different regions cannot be distinguished any longer and just a sharp peak in the devolatilization rate curves is observed. However, it is still possible to see that washing and K-doping resulted in a shifting of the devolatilization rate peaks towards lower temperatures. It could be interpreted that both washing and K-doping enhanced the devolatilization pathway at lower temperatures, analogously to what was observed at TGA level and by other authors [74, 75, 183]. At the same time, the different behaviour between particle and TGA experiments for all samples (i.e. washed xylan, xylan, and K-doped xylan) indicate a significant influence of intra-particle transport limitations on the pyrolysis pathway. This is two-fold: on one side, the higher temperatures and higher heating rates (above 120 °C/min for 4 g sample) reached in the centre sample due to the strong exothermic behaviour and, on the other side, the possibility of undergoing further secondary reactions due to higher mass transport limitations.

Table 8.3: *Final char and released mass yields of CO_2, CO, CH_4, H_2, and H_2O in dry basis for xylan (n.d. - not determined)*

Yield	Xylan 1 g			Xylan 4 g		
(wt.%, db)	X1-W	X1	X1-K	X4-W	X4	X4-K
Char	25.39	24.23	31. 27	24.65	24.03	30.71
CO_2	13.04	15.65	10.87	18.07	16.19	16.63
CO	5.46	6.40	4.01	6.36	4.42	4.04
CH_4	0.67	0.69	0.63	0.68	0.65	0.67
H_2	0.43	0.41	0.35	0.40	0.38	0.36
H_2O	n.d	n.d	n.d	17.52	14.35	21.47

8.4.2.2 Products distribution.

Gas release is compared for pure xylan, washed xylan, and K-doped xylan in Fig. 8.10 for 1 g samples and in Fig. 8.11 for 4 g samples. In Tab. 8.3 the total mass yields for char, permanent gases, and water are listed. The standard deviations of the total yields are within the range of 0.65% and 0.07% for char and minor gases (CH_4 and H_2), respectively. Higher deviations (up to 2.5 % standard deviations) were observed for CO_2 and CO, attributed to the high devolatilization rates, leading to non-negligible pressure differences within the reactor and to fewer measurement point in the micro-GC within the devolatilization stage. Therefore, these limitations must be accounted for when interpreting the quantitative releases of both CO_2 and CO.

As it can be seen in Fig. 8.10 and Fig. 8.11 for both samples sizes, the major gases produced during the main devolatilization stage were CO_2 and CO. Similar to cellulose decomposition mechanism [8, 33], their release is mainly associated to ring opening reactions [33, 72, 75, 183]. CO_2 production is also associated to decarboxylation of the O-acetyl groups attached to the xylose units in xylan [72]. It has been reported that CO_2 yields increase upon addition of alkali metals and alkaline earth metals [33, 75]. The behaviour of CO upon addition of inorganics is not as clear. In general, it is concluded that is not significantly affected by the addition of inorganics [33, 75], being the main production pathway the further reactions of the intermediate products produced from ring opening reactions, especially decabonylation of aldehydes [72]. With respect to char, it has been also reported that char yields increase with the presence of alkali metals [33, 75], although more intensely with alkaline earth metals [33]. After this sharp devolatilization stage, both CH_4 and H_2 were released for temperature higher than 400 °C, when no further significant mass loss was detected. Their production is usually mainly related to secondary

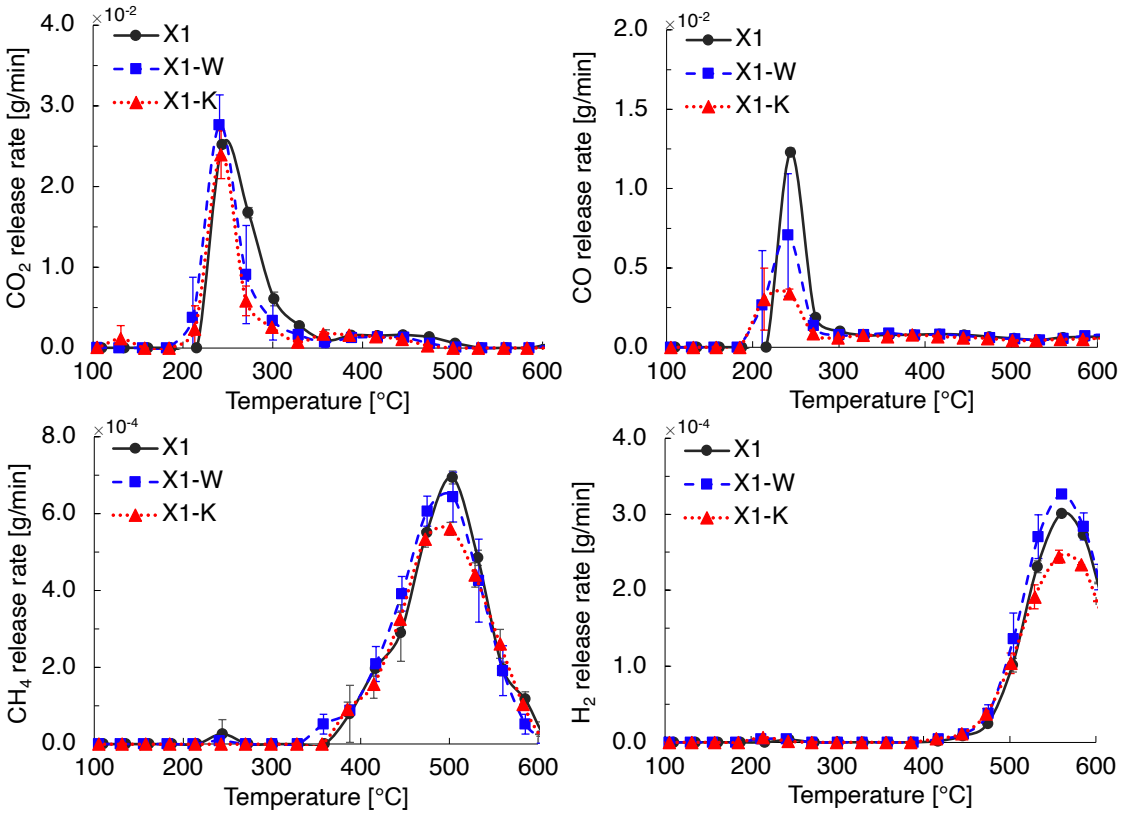

Figure 8.10: *Comparison of release rate of CO_2, CO, CH_4, and H_2 as a function of temperature in the vicinity of the sample for 1 g xylan (X1), washed xylan (X1-W), and K-doped xylan (X1-K).*

reactions within the solid matrix, analogously to the case of cellulose, as discussed in section 8.4.1.2.

Higher char yields were observed for K-doped xylan in comparison to xylan increasing from around 24 wt.% to around 30 wt.% for both sample sizes, as shown in Tab. 8.3. Even higher char yields were observed with the same samples in TGA experiments (in the range of 30 - 35 wt.% [results not shown]). It can be concluded that intra-particle transport limitations do not enhance char yields in xylan pyrolysis, contrary to cellulose pyrolysis, and the lower char yields with increasing initial mass may be explained by the higher heating rates reached in the 1 g and 4 g experiments due to the strong process exothermicity. With respect to the impact of K, in TGA experiments the lowest char yield was observed for washed xylan (X-TGA-W) followed by xylan (X-TGA), and by K-doped xylan (X-TGA-K). This is in good agreement with other results from literature [33,75], showing higher char yields with higher content in alkali and/or alkaline earth species. However, in the 1 g and 4 g experiments, both washed xylan and K-doped xylan showed higher char yields than xylan. The same behavior was observed for H_2O yields. K-doping catalyzes dehy-

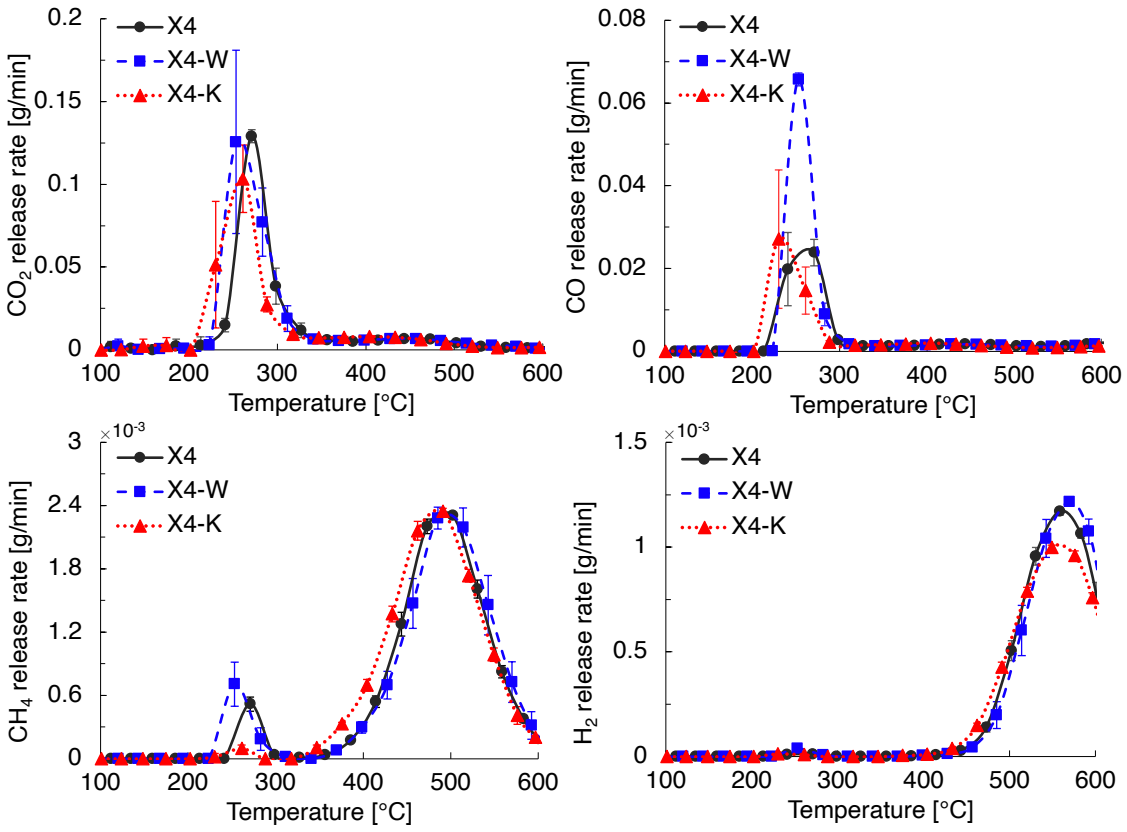

Figure 8.11: *Comparison of release rate of CO_2, CO, CH_4, and H_2 as a function of temperature in the vicinity of the sample for 4 g xylan (X4), washed xylan (X4-W), and K-doped xylan (X4-K).*

dration reactions that compete with the production of LMWCs and other species. This, as previously discussed, results in a shifting of the conversion rates to lower temperatures, which can be also seen as an enhancement of the conversion pathways leading to the first devolatilization peak, attributed typically to breakage of glycosidic bonds and side chains. Higher initial masses and therefore larger intra-particle transport limitations seem to have a similar impact on the conversion as K-doping, supported by the similar conversion rate curve, temperature evolution in the center of the sample, and increase in char and H_2O yields. Regarding CO_2 and CO, no clear conclusion can be derived from the yields in the present work. With respect to CH_4, a very small peak is observed coincident with the release of CO and CO_2 for xylan. However, this peak disappears in the case of K-doped xylan. Similar behavior was also observed for K-doped cellulose (see section 8.4.1.2) and attributed to competition between cracking and charring reactions, being the latter favored by inorganic species. This explanation seems to be also valid in the case of xylan, concluding that K-doping favors direct dehydration reactions on xylan depolymerization products.

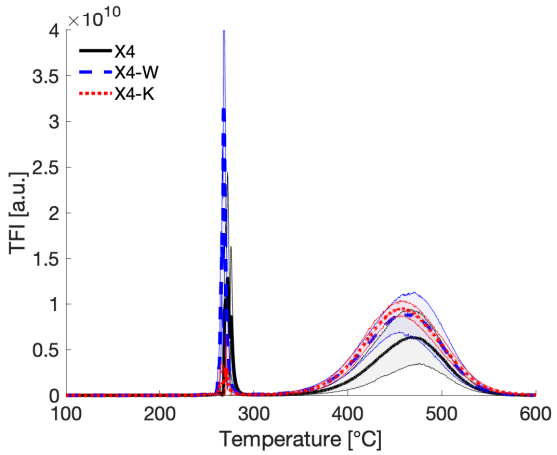

Figure 8.12: *Comparison of the total fluorescence intensity (TFI) as a function of temperature in the vicinity of the sample for 4 g xylan (X4), washed xylan (X4-W), and K-doped xylan (X4-K). The shaded areas represent the standard deviation.*

The comparison of the TFI as a function of temperature for the experiments performed with 4 g is shown in Fig. 8.12. As it can be observed, the release of aromatic compounds occurred in two different stages. The first one is related to the main devolatilization stage, coincident with the exothermic peak, at temperatures of around 270 °C. The second one, however, was detected at a wider temperature range, between 350-550 °C, when almost no mass loss was observed. One may think, however, that the temperature of the first release stage of xylan is too low for the production of polyaromatic compounds. Nevertheless, as shown, in Fig 8.8 (b), temperatures up to 400 °C and heating rates up to 120 °C/min were reached inside the sample, supporting the fact that PACs can be already formed during the main devolatilization stage of xylan. Moreover, as observed for cellulose, its release followed qualitatively the same release pattern as CH_4 (Fig 8.11). The first release stage is associated to the high temperatures and heating rates reached inside the sample during the main devolatilization stage and the second one is related to further reactions in the char matrix. Therefore, for both polysaccharides, cellulose and hemicellulose, the reaction pathway associated to the formation of CH_4 should be accompanied by the release of PACs, too.

8.4.3 Lignin

8.4.3.1 Conversion rate and temperature.

The comparison of the conversion rate ($d\alpha/dt$) between pure lignin, washed lignin, and K-doped lignin for the experiments performed with 1 g is presented in

Fig. 8.13 (a) as a function of the temperature in the close vicinity of the sample. Moreover, the comparison of the temperature in the center of the sample for the experiments performed with 4 g is shown in Fig. 8.13 (b). The conversion rate for the large sample size (4 g) could not be measured due to melting (formation of a liquid intermediate) at the beginning of the devolatilization and its subsequent swelling affecting the mass measurements. Photos of this event are provided in Fig. 8.14.

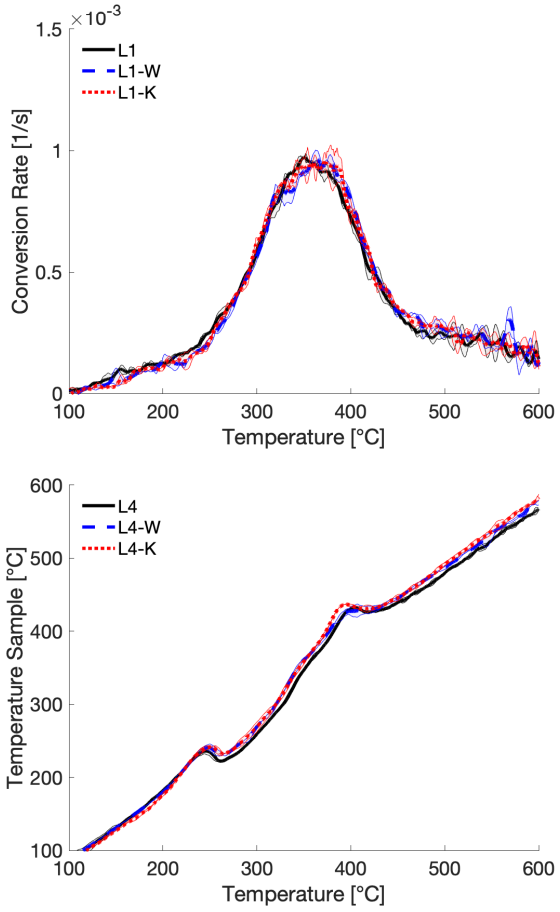

Figure 8.13: *Comparison of conversion rate (a) for 1 g lignin (L1), washed lignin (L1-W), and K-doped lignin (L1-K); and temperature inside the sample (b) as a function of temperature in the vicinity of the sample for 4 g lignin (L4), washed lignin (L4-W), and K-doped lignin (L4-K). The shaded areas represent the standard deviation.*

As shown in Fig. 8.13 (a), and also reported in literature [8], the thermal decomposition of lignin occurred over a wide range of temperatures, starting at around 150 °C up to the final temperature of 600 °C. Such thermal decomposition is mainly associated to the different types of linkages deriving from its complex structure. Cleavage of ether bonds (mostly β-O-4) are reported to occur between 200-250 °C due to its weak linkage and, therefore, low thermal stability [8, 20]. Scission of aliphatic side chains follows at 300 °C together with the cleavage of methoxy groups [8]. Finally, C-C bonds, due to its low reactivity, are thermally cleaved at temperatures above

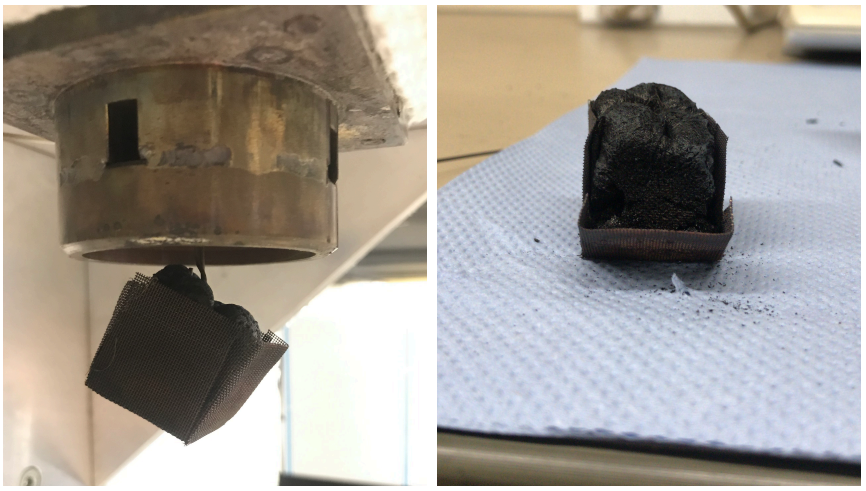

Figure 8.14: *Photos of the char sample after the experiments with 4 g lignin. Photo (a) shows the swollen lignin char stuck to the hanger. Photo (b) is the swollen lignin char with the upper part with bubbled shape.*

370 °C [8, 20]. Moreover, it is known, as in the case of cellulose, that a liquid intermediate is formed, associated to glass transitions and/or cleavage of ether bonds, before devolatilization [76]. The formation of this intermediate liquid phase provides an ionic medium in which dehydration and cross-linking reactions are more likely, promoting therefore char at the expense of lignin oligomers [54,76]. In Fig. 8.13 (b), the formation of the liquid intermediate can be clearly differentiated through the endothermic behavior occurring between 230-260 °C. Furthermore, for the larger sample mass, as previously introduced, a significant melting and swelling was observed in the final char. Such behavior (shown in Fig. 8.14) proves that char is formed directly from a liquid phase and, as reported by Zhou et al. [76], reactive boiling ejection should be considered the main mechanism for oligomeric products. The enhancement of intra-particle transport resistances due to the use of large sample masses likely intensified the effect of both melting and swelling. In fact, similar behavior has been reported in literature when pyrolyzing in transport-controlled regimes with to high heating rates [54]. Increasing the retention time of volatiles in the liquid-solid phase will favor char forming reactions, which explains the higher char yields obtained for pure lignin with 4 g (L4), 49 wt.%, in comparison with pure lignin with 1 g, 46.86 wt.%, as shown in Tab. 8.4.

Neither washing nor K-doping caused a significant change in the devolatilization rate and thermal evolution of lignin. As it can be observed in Fig. 8.13 (b), after the endothermic valley, all samples showed an increase of exothermic reactions being maintained throughout the devolatilization process, starting at temperatures around 270 °C and ending with an exothermic peak at 400 °C. Exothermicity is

associated with the presence of charring reactions [8]. Due to the larger extent of charring reactions in lignin in comparison to other macrocomponents (see Tab. 8.4.) a globally exothermic behavior is observed in all samples. Repolymerization of aromatic compounds is reported to be the main pathway for char formation [21]. With increasing potassium content, a slight increase of the exothermic overshoot was observed together with a shift of approximately 10 °C towards lower temperatures, occurring at 403 °C for pure lignin (L4) and 392 °C for K-doped lignin (L4-K). More char was also formed with increasing inorganic content, as shown in Tab. 8.4, being 48.85 wt.%, 49.03 wt.% and 51.87 wt.% for washed lignin (L4-W), pure lignin (L4), and K-doped lignin (L4-K), respectively. These effects, however, as observed in Fig. 8.13 (a), were not reflected in terms of conversion rate.

Table 8.4: *Final char and released mass yields of CO_2, CO, CH_4, and H_2 in dry basis for lignin*

Yield	Lignin 1 g			Lignin 4 g		
(wt.%, db)	L1-W	L1	L1-K	L4-W	L4	L4-K
Char	47.53	46.86	50.10	48.85	49.03	51.87
CO_2	2.66	2.85	3.05	4.88	5.07	4.94
CO	3.23	2.89	2.42	3.54	3.38	2.79
CH_4	2.14	1.91	1.88	2.50	2.34	2.21
H_2	0.20	0.19	0.20	0.25	0.24	0.24

8.4.3.2 Products distribution.

The comparison of the release rate of CO_2, CO, CH_4, and H_2 for pure lignin, washed lignin, and K-doped lignin is presented in Fig. 8.15 for the experiments performed with 1 g and in Fig. 8.16 with 1 g. The total mass yields for char and permanent gases are listed in Tab. 8.4. The standard deviations of the total yields are within the range of 0.67%, 0.15%, and 0.07% for char, major gases (CO_2 and CO), and minor gases (CH_4 and H_2), respectively.

As it can be observed in Fig. 8.15 and 8.16 only the release of CO_2 followed the conversion rate curve, occurring over a broad temperature range between 200-500 °C. Its production, as reported in literature, is directly linked to the decomposition of carboxyl and ester groups [35]. However, the former pathway should be more likely since the amount of ester bonds in the lignin structure is rather low [20]. The release of CO, however, started at higher temperatures than that of CO_2. As clearly shown in Fig. 8.16, several stages can be differentiated, indicating different formation pathways. A mild first release stage (shoulder) occurred between 290 °C and 390 °C, coincident with the main devolatilization stage. This can be attributed

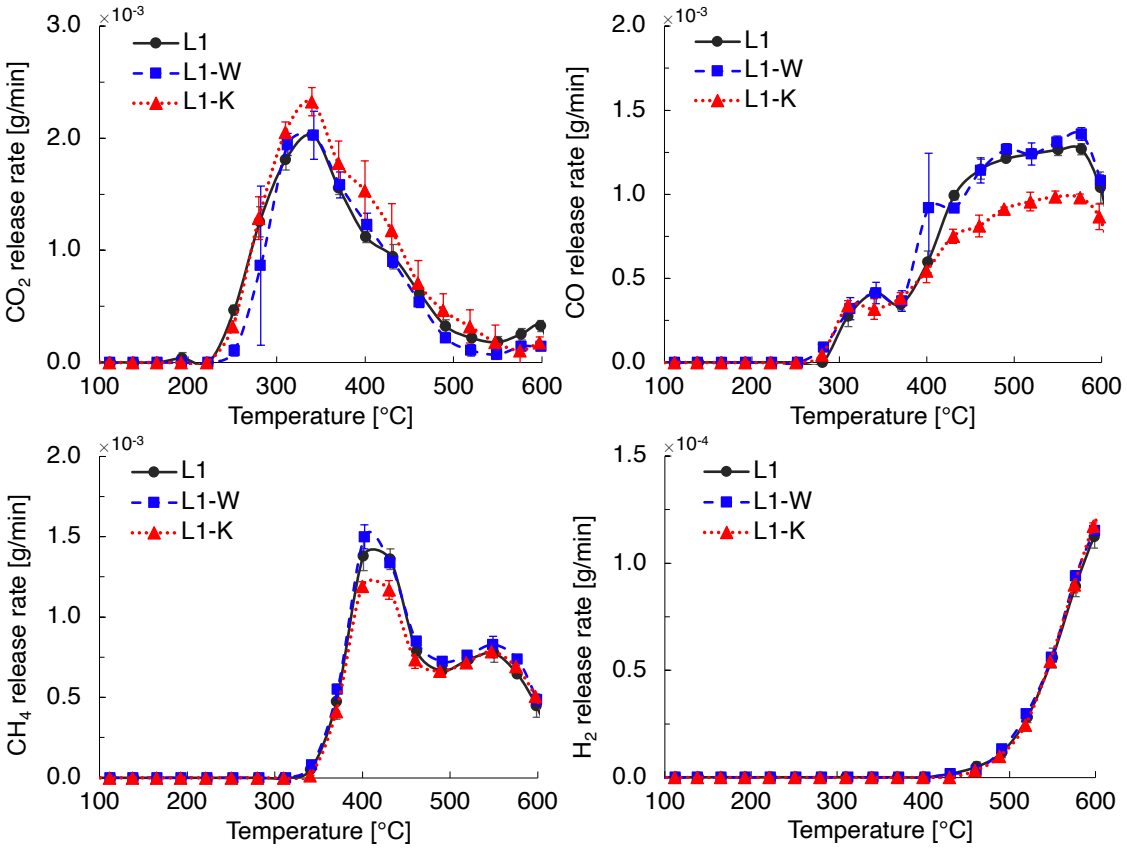

Figure 8.15: *Comparison of release rate of CO_2, CO, CH_4, and H_2 as a function of temperature in the vicinity of the sample for 1 g lignin (L1), washed lignin (L1-W), and K-doped lignin (L1-K).*

to the decomposition of mainly carbonyl groups [35]. At 400 °C a release peak occurred, coincident with the main release stage of CH_4, which indicates that its formation may be related to the demethylation of methoxy groups, as in the case of CH_4 [38]. In fact, Jakab et al. [38] illustrated the formation of CO accompanied by CH_4 through unstable orthoquinone rings as a possible route. The release of CO at higher temperatures, above 430 °C, may be related to further deoxygenation and rearrangement reactions of the aromatic structure [53]. This is accompanied by the release of CH_4, also attributed to further charring reactions [35, 36, 38], and H_2 at higher temperatures when less oxygen is present through dehydrogenation [36, 38].

When secondary reactions are enhanced due to the use of larger sample masses, i.e. 4 g lignin, both char and permanent gases are promoted at the expense of liquid products, as depicted in Tab. 8.4. As previously mentioned in section 8.4.3.1, due to an increased residence time of the volatiles in the solid-liquid phase, char yields increased from 46.86 wt.% to 49.03 wt.% for L1 and L4, respectively. Dehydration reactions and, therefore, the release of H_2O is expected to be also enhanced [54]. Such increase of charring reactions was accompanied mainly by an enhancement of

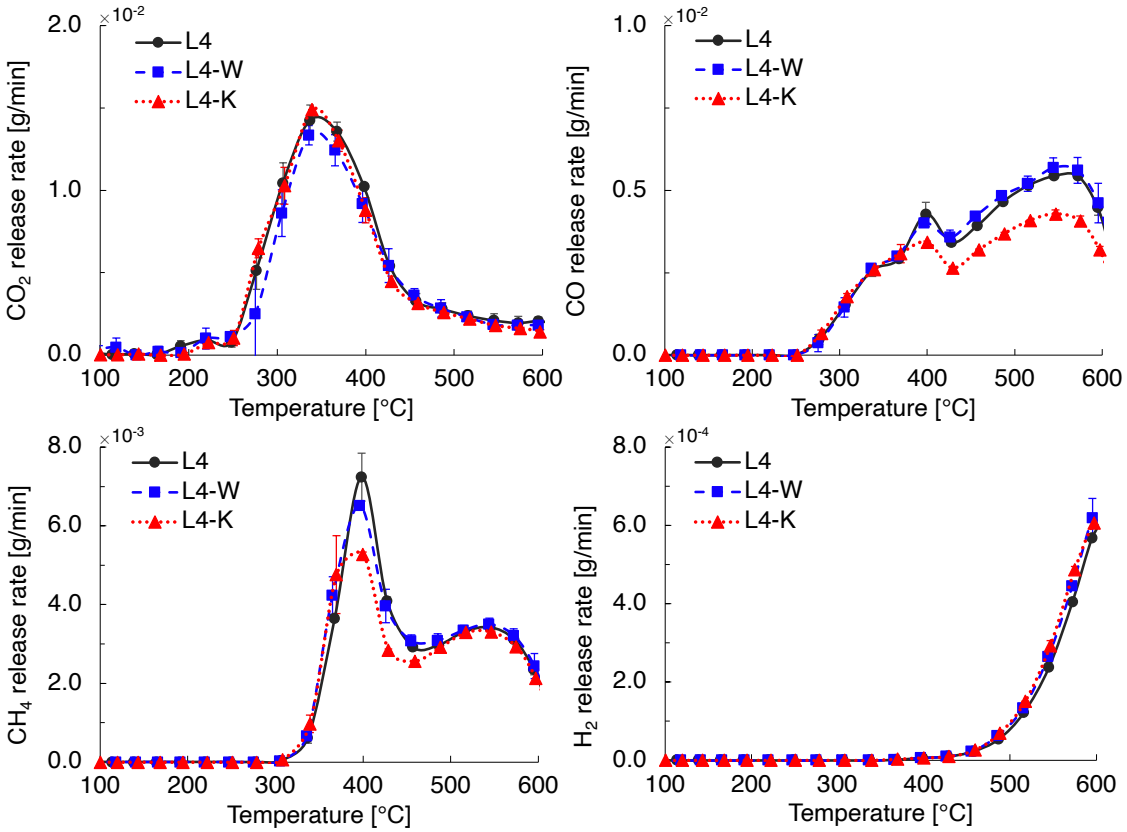

Figure 8.16: *Comparison of release rate of CO_2, CO, CH_4, and H_2 as a function of temperature in the vicinity of the sample for 4 g lignin (L4), washed lignin (L4-W), and K-doped lignin (L4-K).*

decarboxylation reactions leading to higher CO_2 yields, from 2.85 wt.% to 5.07 wt.%, for L1 and L4, respectively. Moreover, to a lower extent, CO (from 2.89 wt.% to 3.38 wt.%), CH_4 (from 1.91 wt.% to 2.34 wt.%), and H_2 (from 0.19 wt.% to 0.24 wt.%) were also promoted, which indicates the preference for fragmentation reactions with the presence of transport limitation phenomena.

Mild effects of inorganic species on the conversion rate with relevant influence on the products composition have been reported in several works [36, 39]. However, other studies did observe, additionally, a catalytic effect of inorganics on lignin devolatilization by shifting the conversion curve towards lower temperatures [37–39]. The difference between lignins and extraction methods [35], the effect of different types of inorganic species [39, 184] or the employed doping procedure [183] may explain the variety of results in the different studies. In this case, despite not observing significant changes in terms of the conversion rate and thermal behavior, the alteration of the inorganic content in lignin by doping and washing procedures left clear trends regarding the evolution of volatiles. For both sample masses, as observed in Fig. 8.15, Fig. 8.16, and as reported in Tab. 8.4, char and CO_2 were promoted with

increasing inorganic content. Metal ions have been reported to decrease the dissociation energy of ether bonds [21] and catalyse the cleavage of functional groups, such as carboxylic units [38,39], which may thus explain the promotion of CO_2. Moreover, H_2O formation is expected to be significantly enhanced through the rupture of free hydroxyl groups [38]. In fact, Jakab et al. [38] observed that up to 80 wt.% of the oxygen could be removed as H_2O when doping with Na^+ ions. The preferred pathway for deoxygenation through CO_2 and H_2O with the presence of inorganic species may therefore explain the clear decrease of CO, especially, at high temperatures. That is, after the increase of CO_2 and, presumably, H_2O, less oxygen would be available in the solid matrix at high temperatures for CO formation. [38]. With respect to CH_4 release pattern, as observed in Fig. 8.15 and 8.16, a decrease of the first release peak is observed with increasing inorganic content. However, the release at higher temperatures seems not to be affected. As previously mentioned, the first CH_4 release stage is associated with demethylation of mainly methoxy groups [38].However, as reported in [39], its formation cannot be determined by the primary bond cleavage alone, but also by the availability of transferable hydrogen, which, as reported by Le Brech et al. [68], decreases upon the addition of K for wood and cellulose. The release of H_2 at higher temperatures was not affected by the presence or absence of inorganic species.

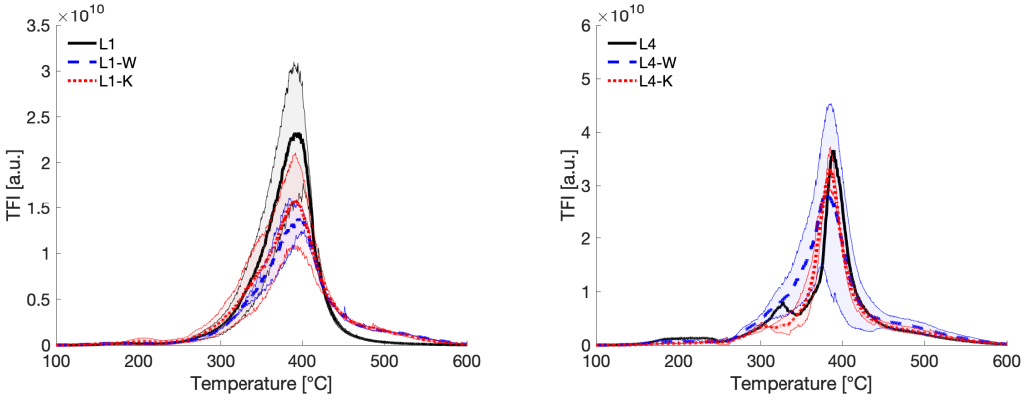

Figure 8.17: *Comparison of the total fluorescence intensity (TFI) as a function of temperature in the vicinity of the sample for: (a) 1 g lignin (L1, L1-W, and L1-K) and (b) 4 g lignin (L4, L4-W, and L4-K). The shaded areas represent the standard deviation.*

The comparison of the TFI as a function of temperature is presented in Fig. 8.17. As it can be observed, the release of aromatic species in the slow pyrolysis of lignin was homogeneous throughout the process and reached its maximum at 390 °C for

both sample sizes. Furthermore, it is important to note that the total production of fluorescence-emitting species was much higher than for cellulose or xylan. This is in line with previous works indicating that PACs production in lignocellulosic biomass is mainly originating from lignin [8, 28]. However, as previously discussed, PACs produced in holocellulose, mainly at high temperatures and related to methane release and charring reactions, cannot be neglected. For lignin, unlike the other macrocomponents (cellulose and xylan), however, the production of PACs cannot be qualitatively related to the release of CH_4, which is one of the main gases produced. In fact, it seems that PACs are formed to a large extent together only with the first release stage of methane, shortly before 400 °C. Afterwards, its production is much lower. Looking at the individual spectra (results not shown), and coinciding with previous results of this group at reactor level [28], it can be observed that the species emitting fluorescence at temperatures below 300 °C are mainly one-ring aromatic species, such as phenols or guaiacols, which, due to the structure of lignin, are expected to be the main products. As the temperature increases, thus being able to reach the dissociation energy necessary to break the bonds of functional groups, such as methoxy units, the total fluorescence significantly increases, and the individual spectra shifts to longer wavelengths. This means that, not only there is a cleavage of functional groups in the aromatic rings (coinciding with the main release of CH_4), but also repolymerization reactions take place to form larger 2-,3-aromatic rings.

The washing procedure and the consequent reduction of inorganic species led to a reduction in the formation of aromatic species for both sample masses, as shown in Fig. 8.17. Furthermore, the increase in potassium content after washing resulted in a slight promotion of aromatic species, thus confirming the observed trend. However, despite the higher inorganic content measured in the doped lignin compared to pure lignin, the TFI measured in the former did not reach the levels obtained with pure lignin, being more noticeable in Fig. 8.17 (a). This may be due to the weaker interaction between the lignin structure and K compared to the inorganics that are organically bound to the structure in the case of pure lignin [183]. Despite this, the trends are consistent with the results obtained for gas evolution. That is, with increasing inorganic content, the cleavage of functional groups is promoted, such as demethoxylation [38], dehydroxylation or decarboxylation [36,38,39], which would lead to an increase in purely aromatic structures, which, with increasing temperature, would also increase the number of aromatic rings.

8.4.4 Beech wood

8.4.4.1 Conversion rate and temperature.

The conversion rates ($d\alpha/dt$) of beech wood, washed beech wood, and K-doped beech wood are shown in Fig. 8.18 (a), for the experiments performed with 1 g, and in Fig. 8.18 (b), for the experiments conducted with a single beech wood particle (Ø = 25 mm, mass ≈ 5.5 g), both as a function of the temperature in the close vicinity of the sample. For beech wood particles, the temperature in the center of the particle is shown in Fig. 8.18 (c).

As it can be observed in Fig. 8.18 (a) and (b), the conversion rate was shifted towards lower temperatures upon addition of K. Not only the onset and the maximum of the conversion rate were affected by this pretreatment, but also the devolatilization occurred in a narrower temperature interval. Despite this, the devolatilization curves for the three different samples pyrolyzed with an initial mass of 1 g still showed the different zones associated with the decomposition of the three macrocomponents (hemicellulose, cellulose, and lignin [174]). However, this was not the case for the samples when pyrolyzed as spherical particles. This could be explained by the intra-particle transport resistances resulting in an overlap of the aforementioned zones. Noteworthy to mention is the fact that K-doping of spherical particles resulted in a much stronger narrowing of the devolatilization curve, both in comparison to the other particles (beech wood (BP) and washed beech wood (BP-W)) as well as to the 1 g sample with the same K-doping (B1-K). This effect cannot be explained solely by the intra-particle resistances to heat transfer nor by the catalytic effect of K. The authors' interpretation is that the presence of transport limitation phenomena, enhancing vapor-liquid/vapor-solid interactions, together with the catalyst would promote specific reactions affecting not only the product composition, but also leading to a stronger overlap of the macrocomponents devolatilization and a shifting of the maximum of the devolatilization rate towards lower temperatures. The removal of inorganic species by washing had, on the contrary, a very mild effect on the devolatilization rate, shifting slightly the maximum of this curve towards higher temperatures, due to the low content in inorganic species.

The temperature evolution in the center of the particle for beech wood particles with different inorganic content resembles the previous results of this group [174]. Briefly summarized, as it can be seen in Fig. 8.18 (c) for pure beech wood (BP), different zones can be recognized. The first zone, characterized by an initial exothermic region between 320-340 °C, was mainly attributed to the devolatilization of hemicellulose,

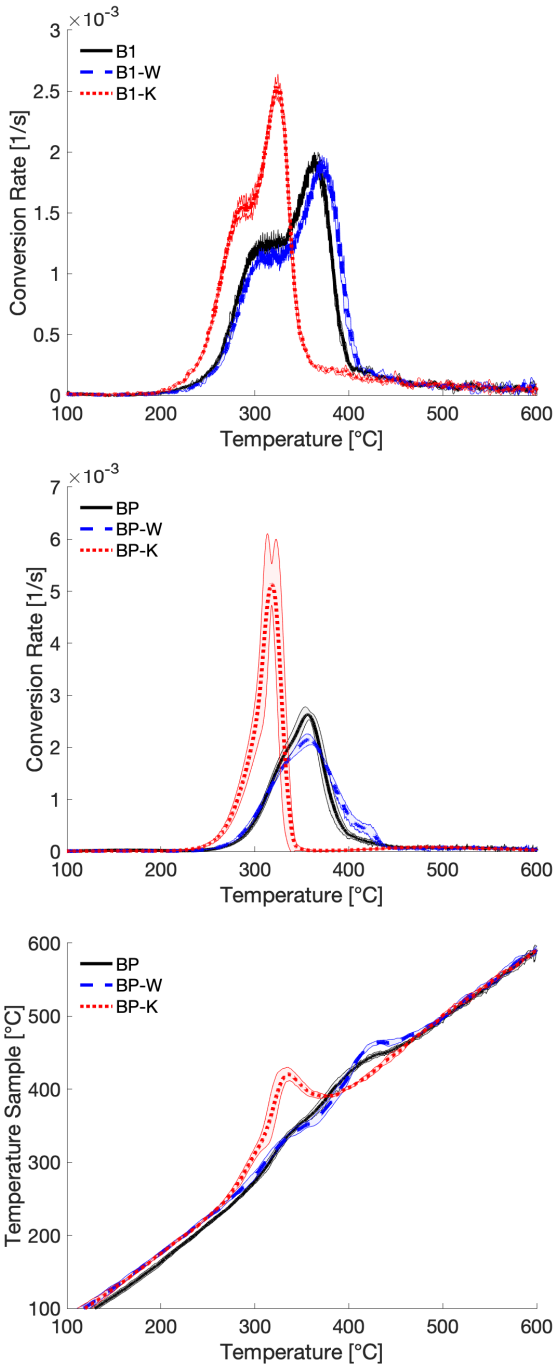

Figure 8.18: *Comparison of conversion rate ($d\alpha/dt$) for (a) 1 g beech wood samples (B1, B1-W, and B1-K); and (b) beech wood particles (BP,BP-W, and BP-K). For the latter samples the observed temperature evolutions in the centre of the particle are shown in (c). The shaded areas represent the standard deviation.*

which, as observed for xylan, has a highly exothermic behavior and a lower thermal stability. The second zone, between 350-400 °C, with a more thermally neutral behavior than the first one, was associated with the primary devolatilization of cellulose together with lignin and the presence of heterogeneous (exothermic) secondary

reactions. Exothermic reactions at temperatures above 400 °C were attributed to further decomposition of lignin residues [174].

When removing the inorganics by washing, BP-W in Fig. 8.18 (b) and (c), the most significant impact was the shift towards higher temperatures, not only of the devolatilization attributed to lignin, but also of the pool of exothermic reactions associated with this process. This is clearly distinguishable in Fig. 8.18 (b) by the final shoulder observed in the conversion rate curve at 420 °C. This resulted in an endothermic valley coinciding with the maximum of the conversion rate, previously attributed to the main decomposition of cellulose, and a final exothermic peak, Fig. 8.18 (c). The shift of both the conversion and the exothermic regime was attributed to the absence of the catalytic effect produced by inorganic species mainly in the decomposition of lignin [174]. However, as observed in the results obtained for cellulose (section 8.4.1.1), there is also a significant exothermic contribution from the secondary charring reactions of cellulose at the end of its devolatilization stage, at around 400 °C. This is also coincident with the final devolatilization shoulder in wood, attributed to lignin decomposition. Consequently, this exothermic regime at higher temperatures in the case of wood has been attributed to lignin decomposition [174]. However, according to the results in the present work for cellulose, it can be concluded that secondary charring reactions in cellulose play also a significant role.

Doping beech wood particles with KCl resulted in a pronounced exothermic behavior, reaching a temperature overshoot of about 100 °C, as shown in Fig. 8.18 (c) for BP-K. As observed for cellulose, higher intra-particle resistances resulted in an enhanced catalytic effect of potassium. It can be then extrapolated, that for wood, the higher intra-particle resistances associated with the real particle wood microstructure would also increase this catalytic effect, explaining the high exothermicity measured in the center of the particle. However, in the individual results for both xylan and lignin the combined impact of intra-particle resistance and K on conversion and exothermicity was not so evident. Therefore, it could be concluded, that the shifting of lignin conversion in wood to lower temperatures upon addition of K is not due (or not only due) to the impact of K on lignin conversion, but due to the high exothermicity derived from the K doping, especially on cellulose, accelerating the lignin conversion. This is further supported by the results of 1 g samples, with much less intra-particle transport limitations and where the lignin conversion does not change with respect to the beech and washed beech samples.

Table 8.5: *Final char and released mass yields of CO_2, CO, CH_4, and H_2 in dry basis for beech wood*

Yield	Beech wood 1 g			Beech wood particle		
(wt.%, db)	B1-W	B1	B1-K	BP-W	BP	BP-K
Char	18.19	19.67	22.05	22.39	23.06	26.59
CO_2	7.25	8.86	10.56	9.39	10.55	10.96
CO	3.82	4.45	5.47	5.16	5.47	5.32
CH_4	0.44	0.45	0.45	1.11	1.12	0.99
H_2	0.06	0.08	0.13	0.07	0.09	0.13

8.4.4.2 Products distribution.

The comparison between the evolution of CO_2, CO, CH_4, and H_2 is plotted in Fig. 8.19 for 1 g milled sample and in Fig. 8.20 for single beech wood particle ($Ø = 25$ mm, mass ≈ 5.5 g). The total mass yields (wt.%, db) for char and permanent gases are listed in Tab. 8.5. The standard deviation of the total yields are within the range of 0.64%, 0.61%, and 0.04% for char, major gases (CO_2 and CO), and minor gases (CH_4 and H_2), respectively.

The production of both char and total gas increased at the expense of liquid products with increasing extent of intra-particle resistances, enabling more secondary charring reactions. As shown in Tab. 8.5, char yield increased from 19.67 wt.% to 23.06 wt.% for B1 and BP, respectively. Furthermore, not only CO_2, which is one of the main products together with H_2O of heterogeneous secondary reactions [8], but also CO and CH_4 increased their yields significantly. Nevertheless, after studying the single macrocomponents independently, these increases could be attributed to different origins. In fact, as observed in the case of cellulose and xylan, neither CO nor CH_4 production was significantly affected by the increased retention time of the volatiles in the reacting sample. This may indicate that the source of the increase of both gases could be more linked to lignin decomposition (see L1 and L4 in Tab. 8.4) and the preference for the cleavage of functional groups, such as decarbonylation reactions, with higher intra-particle transport limitation phenomena. The enhancement of char, CO_2, and H_2O yields are, however, common factors associated to the decomposition of the three different macrocomponents when heterogeneous secondary reactions are promoted.

The products distribution for the different samples according to their inorganic content showed clear trends in accordance with the results obtained for each of the macrocomponents. The overall increase in char production was a common consequence related to the presence of inorganics. In this case, char yield increased from

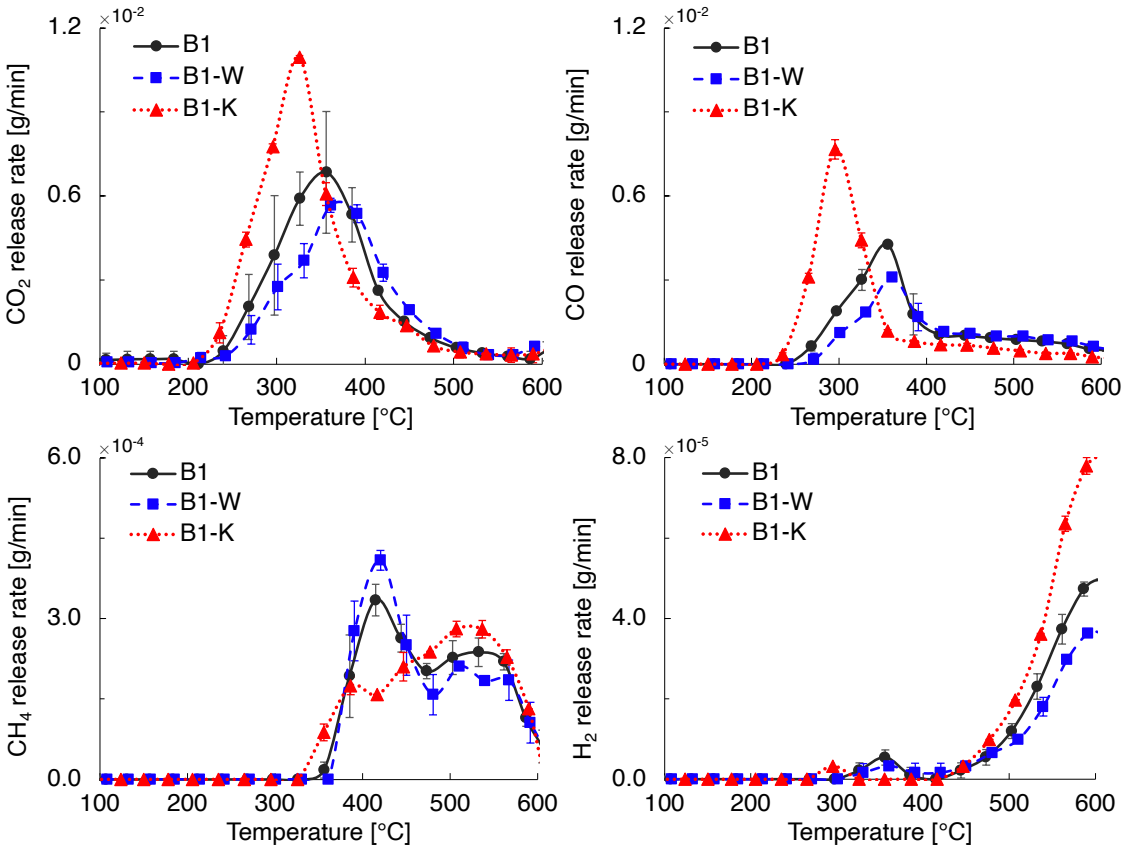

Figure 8.19: *Comparison of release rate of CO_2, CO, CH_4, and H_2 as a function of temperature in the vicinity of the sample for 1 g beech wood (B1), washed beech wood (B1-W), and K-doped beech wood (B1-K).*

18.9 wt.% to 22.05 wt.% between washed and K-doped beech wood, for the experiments conducted with 1 g (B1-W and B1-K, Tab. 8.5), and from 22.39 wt.% to 26.49 wt.%, for beech wood particles (BP-W and BP-K, Tab. 8.5). This can be attributed to a promotion of dehydration [21, 54] and repolymerization reactions of both anhydrosugars and fragmentation products in the case of holocellulose [59, 60], and aromatic compounds in the case of lignin [21]. Together with char formation there was also an enhancement of CO_2 yield for all macrocomponents, which was consequently reflected in the beech wood experiments. In the case of holocellulose, as reported in previous sections, such behavior is associated with a preference for fragmentation reactions, i.e. ring-opening reactions, to form low molecular weight compounds and gases at the expense of anhydrosugars from depolymerization by transglycosylation [67]. As observed in the present work, formation of CO_2 in cellulose was also closely related with the formation of char, increasing as well with higher char yields. Furthermore, decarboxylation of both O-acetyl groups in the case of hemicellulose [72] and aromatic structures in the case of lignin [21] are also

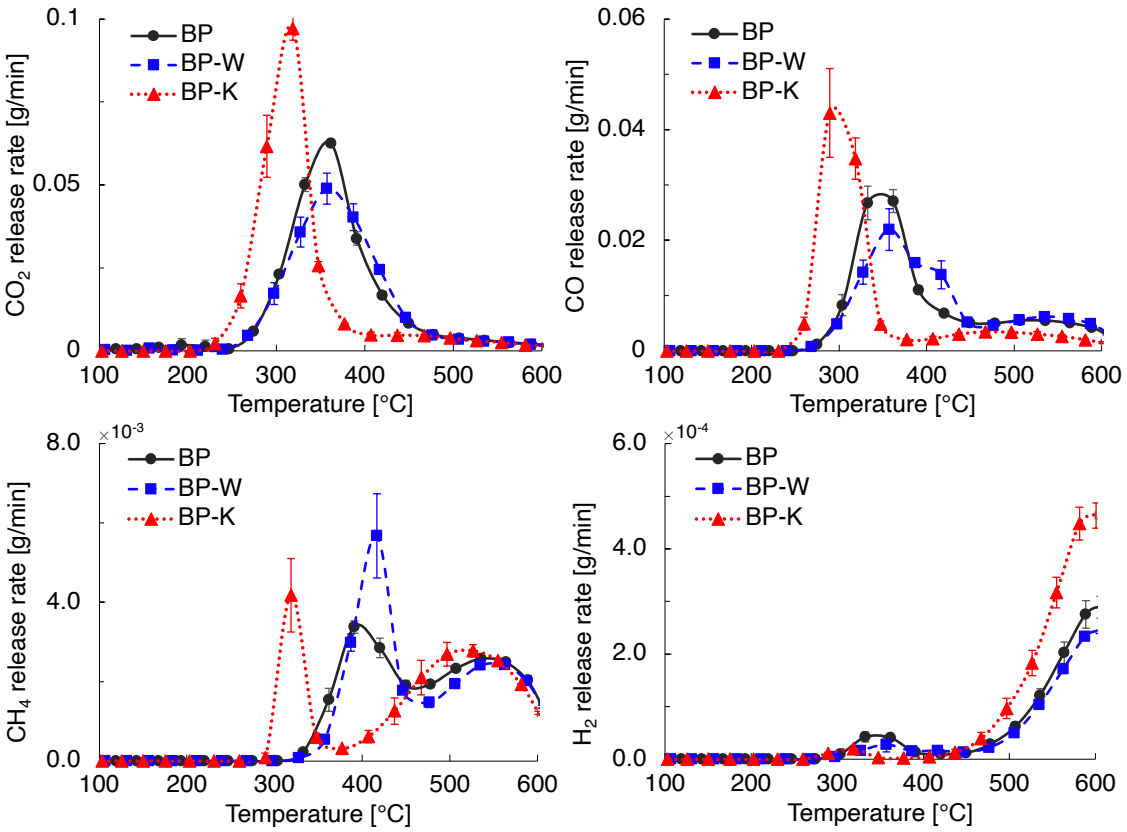

Figure 8.20: *Comparison of release rate of CO_2, CO, CH_4, and H_2 as a function of temperature in the vicinity of the sample for particles of beech wood (BP), washed beech wood (BP-W), and K-doped beech wood (BP-K).*

favoured upon the increase of inorganic compounds. Since its origin is associated with the main devolatilization stage, its release rate curve also shifted towards lower temperatures upon the addition of K, as observed in Fig. 8.20 and Fig. 8.20.

A similar temperature-dependent release rate was also found for CO. Noteworthy to mention is the different release pattern shown by the washed beech wood particles, BP-W in Fig. 8.20, where two peaks can be distinguished, related to their different formation pathway [149,174]. While the first one, coincident with the main devolatilization stage, is mostly associated with holocellulose, the second one, happening together with the final shoulder in the devolatilization rate curve, is linked to lignin decomposition, which, as explained in section 8.4.4.1, was delayed due to the absence of the catalytic effect of inorganics. The influence of inorganic species on CO yield did not show a clear trend. Its production seems to be clearly enhanced with the presence of inorganics when employing 1 g samples. However, with beech wood particles the influence was not so evident. It must be taken into account, as discussed in section 8.4.3, that, in the case of lignin, CO yield is inhibited by the

addition of K, especially at high temperatures, due to the preference for deoxygenation through both CO_2 and water vapour [38]. This is observed for both samples masses, Fig. 8.19 and Fig. 8.20, however, the promotion of ring-opening reactions during the main devolatilization stage in the case of cellulose seems to counteract this effect. Contrary to what was observed for with 1 g, the combined influence of transport limitation phenomena and inorganic species did not quantitatively affect the formation of CO, being 5.47 wt.% and 5.32 wt.% the total yields for B1-K and BP-K, respectively. This may be attributed to the preference for charring reactions, such as dehydration, to form char and H_2O, at the expense of cracking reactions resulting in CO and other LMWCs, as discussed for cellulose in section 8.4.1.

The release of CH_4, as reported in previous sections, takes place at high temperature starting at the end of the devolatilization stage. The first release peak, at temperatures of around 400 °C for both sample sizes, Fig. 8.19 and Fig. 8.20, can be attributed to both cellulose and lignin decomposition. Even though lignin is known to be its main source, deriving from methoxy groups [38], pure cellulose did also show a clear release peak at the end of the devolatilization stage. This was coincident with the exothermic peak and attributed to secondary reactions of LMWCs in the carbon pool. With increasing inorganic content, this first peak is expected to be inhibited due to (i) the reduction of available transferable hydrogen and (ii) the shifted towards lower temperatures. The significant shift of the CH_4 release rate curve for beech wood particles (see BP-K in Fig. 8.20) is related to the overlap of the macrocomponents decomposition, as discussed in section 8.4.4.1. The second release stage, much broader, at higher temperatures, attributed to further charring reactions of all macrocomponents, increased with the presence of inorganic species (especially observed in 1 g samples, see Fig. 8.19). The reduction of the first release stage and the increase of the second one led to a counterbalance of the effect of inorganics on the total CH_4 yield, as shown in Tab. 8.5. Further dehydrogenation of the char matrix at high temperatures was increased with the presence of inorganic species.

The comparison of TFI as a function of temperature is shown in Fig. 8.21 for both sample sizes. In previous works of this group [149, 174], the maximum of the TFI at temperatures of around 375 °C was mainly related to fluorescence-emitting species coming from heterogeneous secondary reactions of primary volatiles derived from cellulose and lignin decomposition. Further release of PACs at higher temperatures was attributed to further decomposition and charring reactions of lignin residue [174]. However, different conclusions can be drawn by looking at Fig. 8.22, where the TFI

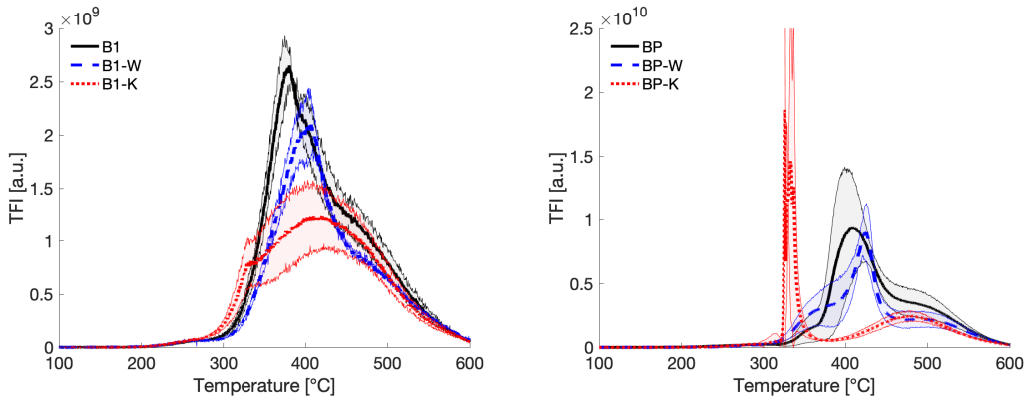

Figure 8.21: *Comparison of the total fluorescence intensity (TFI) as a function of temperature in the vicinity of the sample for: (a) 1 g beech wood (B1, B1-W, and B1-K) and (b) beech wood particles (BP, BP-W, and BP-K). The shaded areas represent the standard deviation.*

for 1 g beech wood (B1) and the TFI calculated based on the individual macrocomponents results (Model) are shown. The composition of beech wood is an estimate obtained from literature, within the range reported for hardwood (42 wt.% cellulose, 31.5 wt.% hemicellulose, and 26.5 wt.% lignin) [162].It should be noted that for a better quantitative comparison the results presented in this figure were carried out in a later experimental campaign, so they may differ from the quantitative results shown in the previous sections. This is due to inevitable changes in the alignment of the spectroscopic system. It seems clear from Fig. 8.22 that the main source of aromatic species, starting at 200 °C and until the maximum of the TFI, are reactions related to lignin devolatilization. During the early pyrolysis stage, between 200-300 °C, it is clear that the species contributing to the fluorescence signal are mainly primary tars, such as guaiacols or syringols, from the primary decomposition of lignin [28, 174]. These compounds, although produced in larger quantities compared to PACs, have an absorption cross section one order of magnitude lower [174], being their contribution to fluorescence much lower and justifying the low intensity measured in this temperature range. From 300 °C onwards, the intensity gradually increased until it reached its maximum shortly before 400 °C, coincident with the first peak of CH_4 release. In this case, the contribution to fluorescence, originating mainly from the decomposition of lignin, is due to 2-, 3-, and 4-ring aromatic compounds formed after the cleavage of functional groups in the aromatic structure, such as the breaking of aliphatic side chains and methoxy groups. Finally, at higher temperatures, when no further mass loss is detected, the origin of the release of PACs are basically secondary reactions in the solid matrix associated with both cellulose and hemicellulose, which, as it can be seen, do have a large contribution to the total fluorescence spectrum.

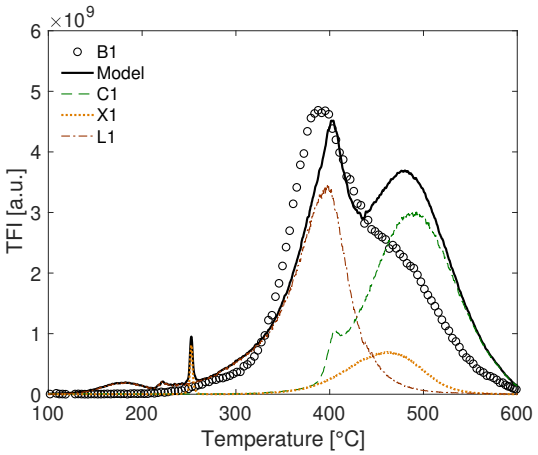

Figure 8.22: *Total fluorescence intensity (TFI) as a function of temperature in the vicinity of the sample for 1 g beech wood (B1), and calculated TFI (Model) based on the TFI of each macrocomponent. The composition of wood is an estimation based on literature [162] (42 wt.% cellulose, 31.5 wt.% hemicellulose, and 26.5 wt.% lignin).*

The close correlation between fluorescence emitting species and CH_4 formation has to be emphasised. Such behaviour was already observed for cellulose and xylan, in which, not only the first CH_4 release peak, associated with the main devolatilization stage, was accompanied with the emission of PACs, but also the second broader release stage at temperatures higher than 400 °C, associated further reactions in the char matrix. For lignin, however, only the first release peak, associated to the cleavage of functional groups in the aromatic structure, was coincident with the emission of aromatic compounds. This fact may indicate the different charring reaction pathways for each of the macrocomponents.

Moreover, this correlation holds also with the presence or absence of inorganics as observed by comparing the TFI in Fig. 8.21 (a) and (b) with the CH_4 release rate curves in Fig. 8.19 and Fig. 8.20, respectively. The shift of the maximum TFI peak is directly related to the shift of the devolatilization rate curve, being larger with the presence of transport limitation phenomena. Furthermore, as shown in Fig. 8.21 (a), there is a clear change in the release pattern of aromatic species with increasing inorganic content, especially noticeable in the first release stage (between 300-400 °C), associated with lignin and, to a lesser extent, cellulose decomposition. The overall inhibition of PACs release upon addition of K can be attributed to the same mechanism as for cellulose, i.e. competition between PACs and char formation.

8.5 Conclusions

In the present work, the influence of inorganic species, intra-particle transport resistances, and their combined interaction on the pyrolysis mechanism has been investigated for wood as well as for its macrocomponents. The experimental results show the different impact of both factors on the devolatilization rate and product composition of each of the macrocomponents, explaining, to some extent, the pyrolytic behavior of wood. The following conclusions can be drawn:

- Inorganic species in the presence of intra-particle transport limitations catalyze cellulose decomposition, shifting its devolatilization rate to lower temperatures. The thermochemistry of the process changes to a more exothermic regime and an increase of char and gas yields due to a preference for the fragmentation reaction pathway are observed. Charring reactions (e.g. dehydration) are preferred when both inorganics and transport limitation phenomena are present, inhibiting CO and CH_4. CH_4 and PACs are released at temperatures above 400 °C following similar release patterns and suggesting that both may be produced through the same reaction mechanism within the solid matrix. There is an inhibition of PACs release upon addition of K, suggesting a competition between PACs formation and char.

- For xylan, both pretreatments (washing and doping) affect the devolatilization rate at the kinetic level by catalyzing both the decomposition of side-chain units and products derived from depolymerization and fragmentation of xylose units. At the particle level, however, these effects are minimized by the strong exothermic behavior governing the decomposition mechanism. As for cellulose, the reaction pathway associated to the formation of CH_4 is accompanied by the release of PACs.

- Lignin devolatilization occurs after the formation of a liquid intermediate which melts and swells throughout the devolatilization stage. By increasing the retention time of the volatiles in the liquid/solid phase, char forming reactions are promoted together with fragmentation reactions to form light gases. Inorganic species favor the cleavage of functional groups, promoting decarboxylation, and H_2O is expected to be enhanced through dehydroxylation and dehydration. At high temperatures CO is inhibited due to the preference for deoxygenation through CO_2 and H_2O. The first release stage of CH_4 associated with the cleavage of methoxy groups decreases potentially due to

the lower transferable hydrogen upon addition of K. PACs release decreases with removal of inorgancis species, contrary to cellulose and xylan. Despite the observed trends in product composition, no significant effects on the devolatilization rate and thermochemistry were observed.

- Increasing K content causes a shift towards lower temperatures of the devolatilization rate curve in the slow pyrolysis of wood. When intra-particle resistances are enhanced, there is a promotion of exothermic reactions, mainly due to the effect of K on cellulose decomposition, that leads to a narrowing and overlap of the three main macrocomponents devolatilization. Char and CO_2 yields are enhanced when both transport limitation phenomena and inorganics are present. The inhibition observed for CO at high temperatures in the case of lignin is also reflected for beech wood, being however counterbalanced by the preference for fragmentation reactions during the main devolatilization stage, associated with holocellulose, with increasing inorganic content. The emission of PACs resembles the CH_4 release rate curve, suggesting similar formation mechanism, as observed for cellulose and xylan. Its formation during the main devolatilization stage is mostly related to lignin decomposition, while, at high temperatures, when no further mass loss is detected, it is associated to further reactions in the solid matrix of both cellulose and hemicellulose. The inhibition of PACs release upon addition of K is attributed to the same mechanism as for cellulose, i.e. competition between PACs and char formation.

Chapter 9

Development of a calibration method for analysis of pyrolysis volatiles via laser-induced fluorescence spectroscopy

The publication where these results are presented is currently work in progress. For this reason, the introduction, experimental setup, and preliminary results will be presented briefly.

9.1 Introduction

Most of the studies employing laser-induced fluorescence focus on identification and characterization of aromatic hydrocarbons, especially PAHs. As it has been reviewed in Section 2.2.1, quantification has been performed under conditions almost free of other substances, or at least under conditions where fluorescence emission could be associated exclusively with such compounds, such as gasification and combustion [114, 124, 126, 127]. In pyrolysis, however, several tar products may be induced to fluorescence besides aromatic hydrocarbons. Carbonyls, phenolics, or furans are main pyrolysis products and have been reported to absorb energy in the UV/Vis range [112]. Although their fluorescence emission is not as efficient as for PAHs (lower quantum yield), they are produced in larger quantities. Therefore, quantification or semi-quantification of individual compounds may be challenging due to the high concentration of different species contributing to the fluorescence signal.

As discussed in previous chapters (Chapters 4 to 6), the qualitative evolution of the different fluorescence-emitting species could be speculated on the basis of their

emission spectra. For instance, while polycyclic aromatic hydrocarbons, depending on the number of rings, emit in the range between 340 and 400 nm, aromatic carbonyls emit around 450 nm. Therefore, only qualitative conclusions could be drawn by studying the evolution of the normalized fluorescence spectra. In the previous chapter, semi-quantification of the total amount of fluorescence-emitting species was achieved by correcting each individual spectrum by the energy of its corresponding laser pulses. This fact, together with previous verification of the linear correlation between the fluorescence signal and the energy of the laser, ensured repeatability of the results in terms of the total fluorescence intensity (TFI). Therefore, normalization was not necessary and the TFI between different experiments could be compared. However, this only provided information on the total amount of species emitting fluorescence. In order to quantify each individual compound, a calibration of the system must be performed. Such calibration, however, should also consider other LIF-relevant parameters and not only the fluorescence emission spectrum of each compound, since overlap between different species emitting in the same spectral range must be considered and to distinguish between certain compounds may be challenging.

To this end, a selection of different pyrolysis products, based on their absorption cross sections, has been made. The influence of different LIF-relevant parameters on the fluorescence emission of each compound have been measured in the same experimental setup built for single-particle pyrolysis experiments. The effect of concentration, temperature, delay (fluorescence lifetime), and dynamic quenching have been considered. These results are fundamental to explore the potential improvement in both sensitivity and selectivity of this spectroscopic technique when applied to pyrolysis. Additionally, together with the introduction of new excitation wavelengths, it will aid in better identification and differentiation of species. This chapter, however, describes current work-in-progress and will be further developed.

9.2 Experimental

9.2.1 Experimental setup

The experimental setup to analyze single species by means of laser-induced fluorescence is depicted in Fig. 9.1. The reactor in which the different compounds are measured was the same designed and developed to study the pyrolysis process at particle level, introduced in Chapter 8. Representative pyrolysis compounds and

synthetic mixtures of them were introduced in order to calibrate the system. A solution of cyclohexane (Carl Roth, $\geq$ 99.9%) with each compound was dosed in the system with a syringe pump (Nemesys, Cetoni) and introduced through a quartz capillary in an oven at 400 °C. By controlling the injection rate of the syringe pump, the concentration of each compound in the gas stream was determined. The generated vapors were mixed with a pre-heated N_2 flow (Air liquid, $\geq$ 99.8 vol%) of 1 l min^{-1}, controlled with a mass flow controller (Red-y, Vögtlin). A gas mixer (Hova-GAS, IAS GmbH) was also employed to introduce a specific amount of O_2 (0.6 %, 1 %, 1,4 vol. %) in the main flow to study the influence of dynamic quenching. The desired mixture was guided through a heating tube (Hillesheim GmbH), maintained at 350 °C, into the particle cell.

The different compounds were excited employing a tunable laser (Opolette HE 355 LD UV, Opotek), which utilizes an optical parametric oscillator (OPO) technology and is equipped with an UV system. The applied excitation wavelength was 266 nm. The energy of each individual laser pulse was measured, before the cell, by means of an energy monitor (EM in Fig. 9.1; Gentec-EO). Therefore, each fluorescence spectrum could be corrected by the energy of its corresponding laser pulses. The fluorescence light emission was detected in the perpendicular direction to the laser beam by two plano-convex spherical lenses (Thorlabs INC) combined with a fiber optic which is coupled to a spectrograph (SR-303i-A, Andor Technology) and ICCD camera (iStar, Andor Technology).

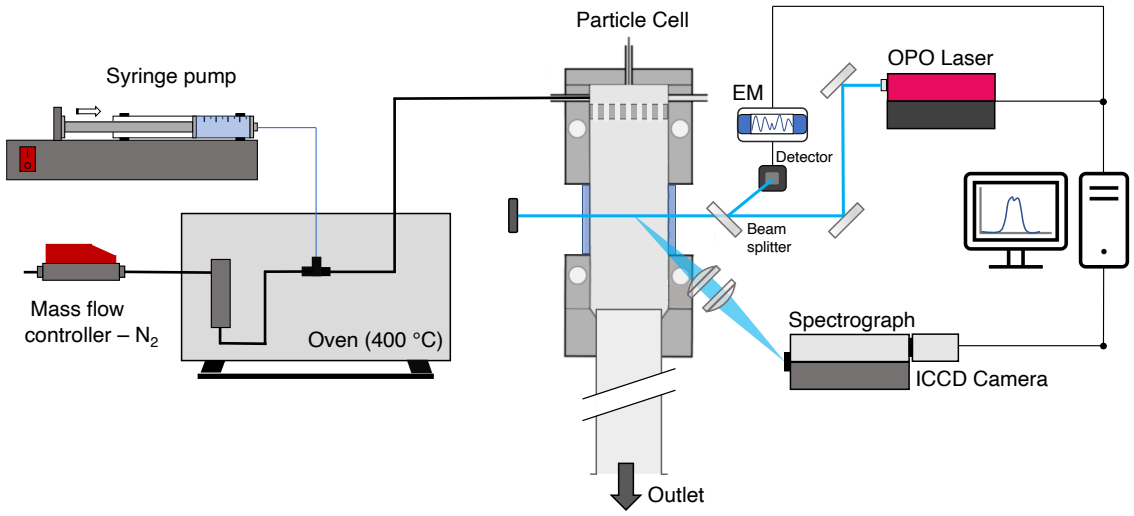

Figure 9.1: *Experimental setup*

Table 9.1: *Selected compounds divided into aromatic and aliphatic.*

Aromatic Compounds					
PAHs	BTX	Phenolics	Carbonyls	Furans	Quinones
Naphthalene Phenanthrene Pyrene Fluoranthene	Toluene Xylene	Guaiacol m-Cresol	Benzaldehyde Benzophenone 2-Hydroxyacetophenone	Furfural Furan Dibenzofuran	Benzoquinone
Aliphatic Compounds					
Acids			Carbonyls	Alcohols	
Glyoxylic Acid [(a)]Benzoic Acid			Formaldehyde Hydroxyacetaldehyde Acetone 2-Butanone 2-Hydroxy-4-methyl-2-pentanone	Ethanol	

[(a)] Aromatic acid

9.2.2 Experimental conditions and analysis

Representative compounds of each group of pyrolysis products were selected based on their ability to absorb energy, i.e. their absorption cross section (See Fig. 2.13 in Section 2.2.1). Tab. 9.1 lists the 23 different compounds that were measured in this experimental setup. Certain species were also measured as a verification despite not expecting any emission (mainly due to low or no absorption), such as ethanol or glyoxylic acid.

The fluorescence signal was recorded at three different temperatures (300, 400, and 500 °C). This range of temperature was selected since it represents the devolatilization stage of woody biomass in slow pyrolysis, as reported in previous chapters. The fluorescence emission in the different pyrolysis experiments was also within the selected range. In fact, above 550 °C almost no fluorescence could be detected. By varying the temperature, its influence on the quantum yield for each compound can be determined. In fact, the quantum yield is expected to decrease with increasing temperature due to the higher probability of deactivation by external conversion (radiationless process) due to collisions with other molecules [111]. This effect, however, may be different for each compound, and its determination is essential for semi-quantification in a transient process such as the one under study.

For each temperature, five concentrations were measured. In this way, the correlation between the emitted fluorescence and the concentration can be obtained. In the range studied, this correlation is expected to be linear, as explained in Section 2.2.1. However, due to the high concentrations used for certain species, due to their low

fluorescence, this may not be fulfilled and the saturation point may be reached. It is therefore important to consider this for further application in the calculation method. As mentioned above, the different concentrations were obtained by controlling the injection rate of the syringe pump.

The temporal decay for the highest concentration for each temperature was also measured. To this end, four different delays (a camera parameter) were employed. Usually, the employed values were: 25, 50, 100, and 200 ns; however, lower values were used for species with shorter lifetimes. It must be highlighted that, although the temporal decay was measured only for the highest concentration for each temperature, the same exponential decay is expected for all concentrations. Therefore, this can be extrapolated for each value. Preliminary tests with naphthalene were performed to confirm this, as shown in Fig. 9.2.

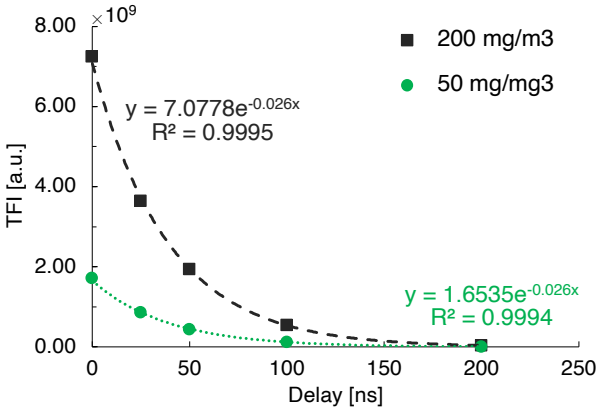

Figure 9.2: *Naphthalene temporal decay for 200 mg/Nm^3 and 50 mg/Nm^3 at 300° C.*

Following the same approach, the influence of dynamic quenching was measured for the highest concentration of each temperature. To this end, a specific amount of O_2 (0.6 %, 1 %, and 1.4 vol. %) was introduced in the main flow. Taking into account all parameters, 36 different conditions were measured for each compound. Moreover, each condition was measured 40 times. Therefore, a large database was obtained from the calibration, with 1440 spectra per compound. For clarity, the experimental scheme is presented in Fig. 9.3.

For the data processing, not only the individual spectra were considered, but also the total fluorescence intensity (TFI), defined as:

$$TFI = \int_{266nm}^{520nm} I(\lambda)d(\lambda) \tag{9.1}$$

being $I(\lambda)$ the intensity of the spectrum as a function of the wavelength (λ).

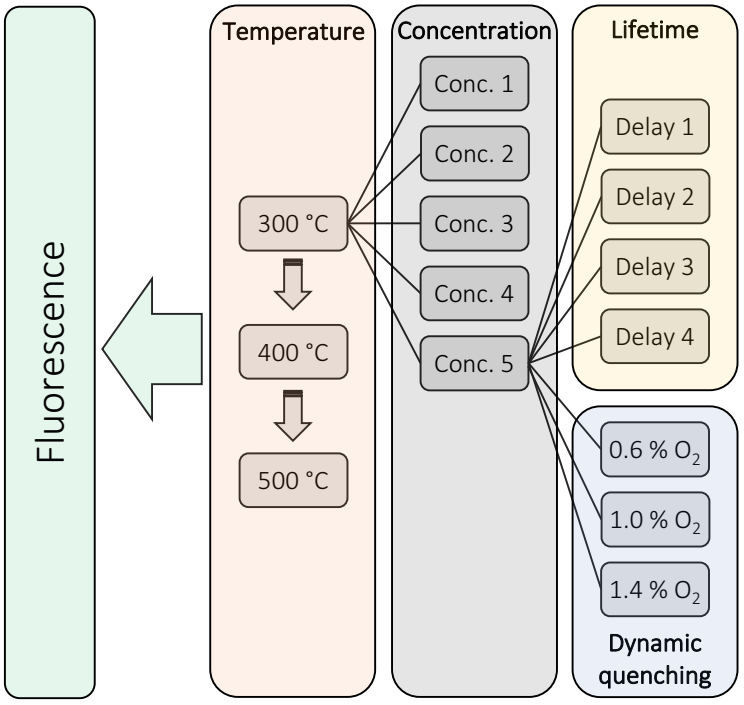

Figure 9.3: *Experimental procedure for each compound.*

9.3 Results

Results are divided into 3 sections: analysis of individual compounds, verification with synthetic mixtures, and pyrolysis experiments.

9.3.1 Individual compounds

From the 36 conditions measured for each compound, 3 different set of data can be obtained for each temperature: intensity-concentration correlation, temporal decay (lifetime), and influence of dynamic quenching (O_2). Each condition was repeated 40 times to ensure repeteability of the results. Fig. 9.4 shows an example of the 36 conditions measured for naphthalene. By analyzing the emission spectrum for each condition, the influence of each parameter relevant to this spectroscopic principle can be determined. The fluorescence emission spectra at 300, 400, and 500 °C with a concentration of 200 mg/m^3 are shown in Fig. 9.4 (a). In this case, the influence of temperature on the spectrum can be observed. Besides the evident decrease in intensity, there is also a slight red-shift (i.e., shift to longer wavelengths) and a broadening of the spectrum. This effect is already well known and has been reported in the literature [108]. However, its determination in this case is essential for quantification in a transient process.

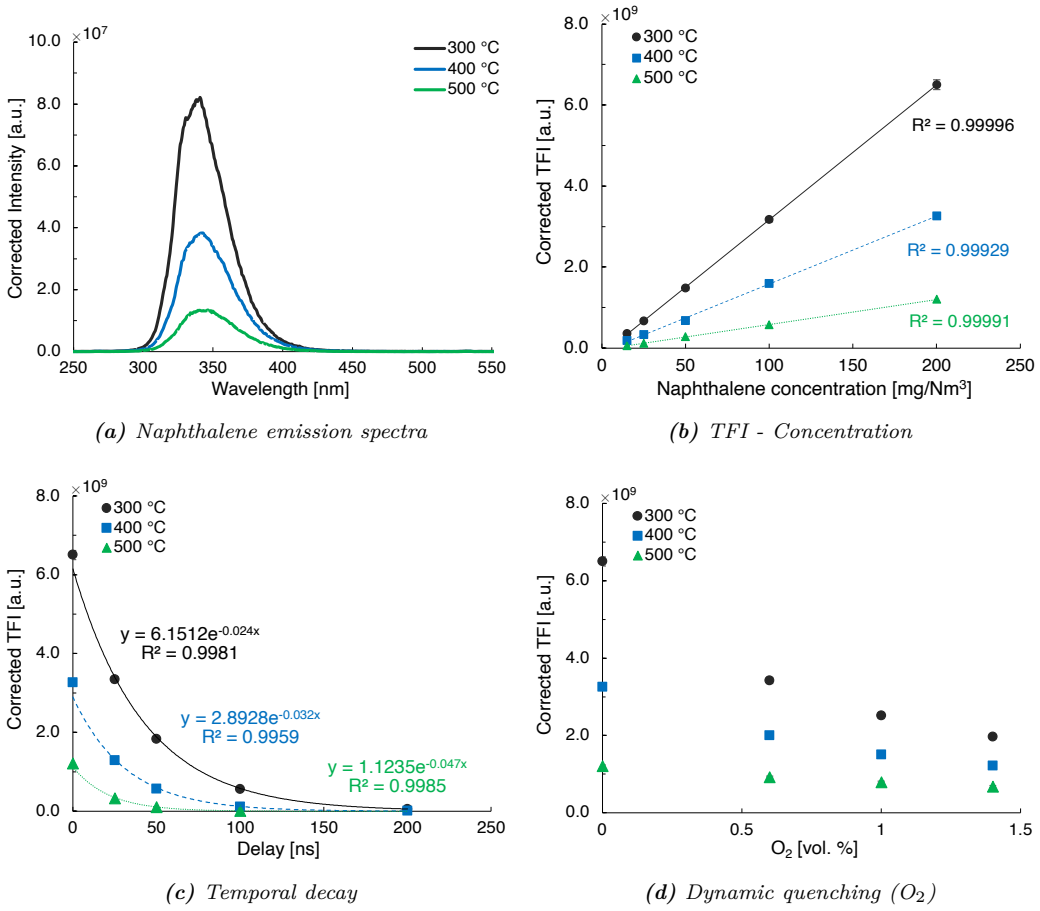

(a) Naphthalene emission spectra *(b) TFI - Concentration*

(c) Temporal decay *(d) Dynamic quenching (O_2)*

Figure 9.4: *Data set for naphthalene. (a) Fluorescence emission spectra with a concentration of 200 mg/Nm^3. (b) Correlation between total fluorescence intensity (TFI) and concentration. (c) Temporal decay with a concentration of 200 mg/Nm^3. (d) Dynamic quenching decay with a concentration of 200 mg/Nm^3. Error bars represent the standard deviation.*

In addition to considering the shape of the spectrum for each condition, another fundamental parameter for quantification is the intensity. In this case, as previously introduced, it is determined by the TFI (i.e., the area below the spectrum). By means of the TFI, the linear correlation between the fluorescence emission and the concentration can be obtained. Fig. 9.4 (b) shows the linear fitting of the TFI as a function of concentration for each temperature. It is important to note that each TFI measurement point in the graph represents the average of 40 repetitions. Error bars are also represented, however, due to the high repeatability, their values are not visible. This is generally the case for most species with high fluorescence signals (PAHs and BTX), with errors below 5 %. For species with lower intensity emissions (e.g., aromatic carbonyls) the error is larger.

Through the TFI, the temporal decay and the effect that oxygen has on the fluorescence intensity can be determined. Fig. 9.4 (b) shows the different temporal profiles for each temperature for a concentration of 200 mg/Nm^3. As explained above,

lifetime should be independent of concentration, however, it does depend on temperature. In fact, in general, the higher the temperature, the lower the lifetime. This is clearly seen by fitting the results with an exponential function (see Fig. 9.4 (b)). With respect to oxygen quenching, a greater influence is seen at lower temperatures, in accordance with the longer lifetime, Fig. 9.4 (d). That is, the longer the time in the excited state (longer lifetime) the more time the oxygen molecules will have to interact with the excited molecules and therefore the higher the probability of deactivation by collisional quenching.

Similar results were obtained for species of the same group, i.e. PAHs. In the case of phenanthrene, a lower temperature quenching effect was observed, however, the fluorescence intensity was very similar to that of naphthalene, as well as the lifetime and oxygen quenching. Pyrene showed higher fluorescence intensity, about four times more than for naphthalene and phenanthrene, and also longer lifetimes. On the other hand, fluoranthene showed shorter lifetimes and therefore was less affected by oxygen. Despite the differences, these compounds, measured in the same concentration range (15 - 200 mg/Nm^3), exhibited results in the same order of magnitude.

From the phenolics group, guaiacol and m-cresol were analyzed. The data set for guaiacol is shown in Fig. 9.5. In this case, to reach the same fluorescence intensity levels (or in the same order of magnitude), much higher concentrations were used, between 2500 - 15000 mg/Nm^3. This highlights the high fluorescence efficiency of polyaromatic species compared to other groups. Fig. 9.5 (a) shows the emission spectrum of guaiacol at different temperatures. Together with Fig. 9.5 (b) it can be seen the great influence that temperature has on the quantum yield, where at 500 °C practically no signal was observed (two orders of magnitude less than for 300 °C). Moreover, this group is characterized by very short lifetimes, in fact, even with a delay of 15 ns, no signal was detected (see Fig. 9.5 (c)). The low lifetime leads to almost no influence of oxygen. Similar results have been obtained with m-cresol, although the fluorescence intensity was an order of magnitude lower for similar concentrations.

From the one-ring aromatic hydrocarbons group (BTX), toluene and xylene were analyzed. The toluene data set is shown in Fig. 9.6. Higher concentrations were used to obtain intensities comparable to those detected with the previous groups. Measurements were performed with concentrations between 6000 mg/Nm^3 and 60000 mg/Nm^3 (6 - 60 g/Nm^3). The influence of the different parameters (temperature, delay, and the presence of oxygen) is very similar to that observed for

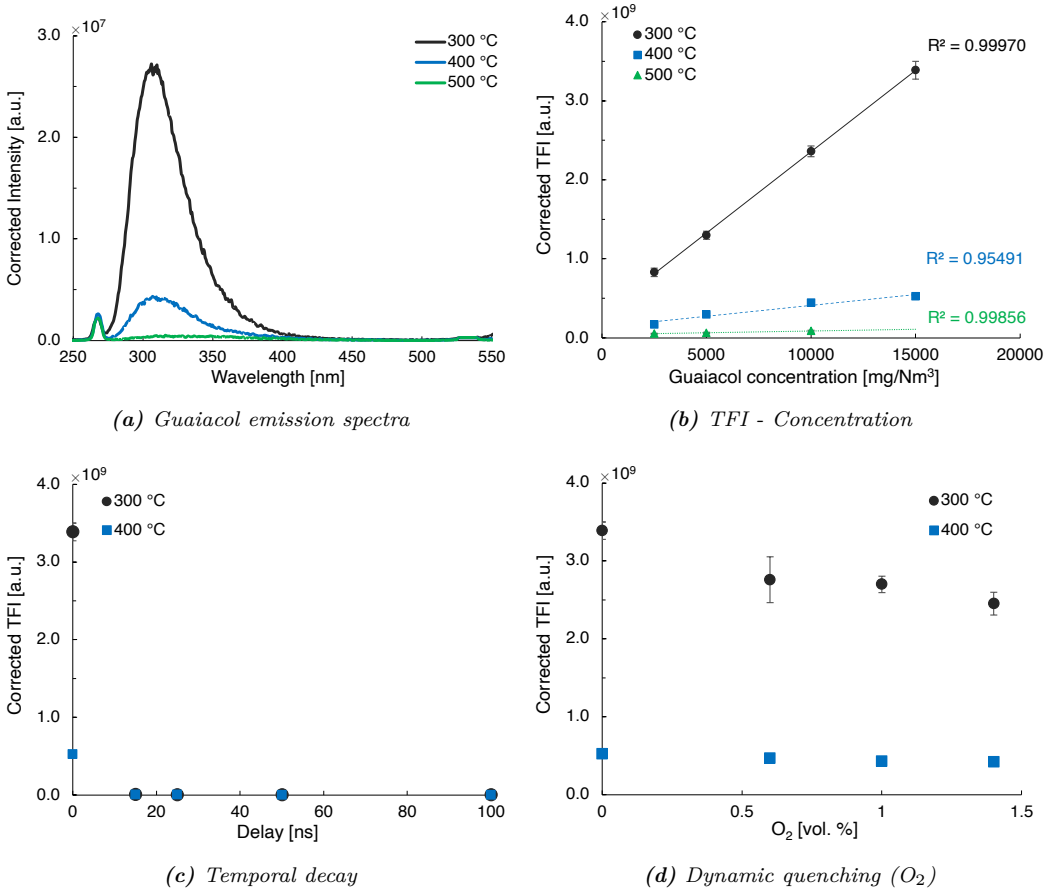

(a) Guaiacol emission spectra

(b) TFI - Concentration

(c) Temporal decay

(d) Dynamic quenching (O_2)

Figure 9.5: *Data set for guaiacol. (a) Fluorescence emission spectra with a concentration of 10000 mg/Nm^3. (b) Correlation between total fluorescence intensity (TFI) and concentration. (c) Temporal decay with a concentration of 15000 mg/Nm^3. (d) Dynamic quenching decay with a concentration of 15000 mg/Nm^3. Error bars represent the standard deviation.*

the phenolics group. Temperature has a strong quenching effect on the fluorescence emission (see Fig. 9.6 (a)). Although in this case, at 500 °C it is still possible to identify the fluorescence spectrum. Furthermore, as shown in Fig. 9.6 (c), the lifetime is very short for all temperatures, with no appreciable fluorescence when applying a delay of 25 ns. Accordingly, oxygen has a little influence at low temperatures, and almost no influence at 400 °C and 500 °C (Fig. 9.6 (d)). It is important to note that, due to the high concentrations, a saturation point in the fluorescence intensity has been detected. This is reflected in the linear correlations between the different TFI measurement points at 300 °C in Fig. 9.6 (b). The dashed line represents the linear correlation considering concentrations of 10000 mg/Nm^3 and 20000 mg/Nm^3. The solid line also takes into account the measurement made with 40000 mg/Nm^3. Therefore, it is evident that for higher concentrations, the linearity between concentration and fluorescence intensity is no longer fulfilled. However, such large concentrations of these species in the employed pyrolysis conditions are not expected.

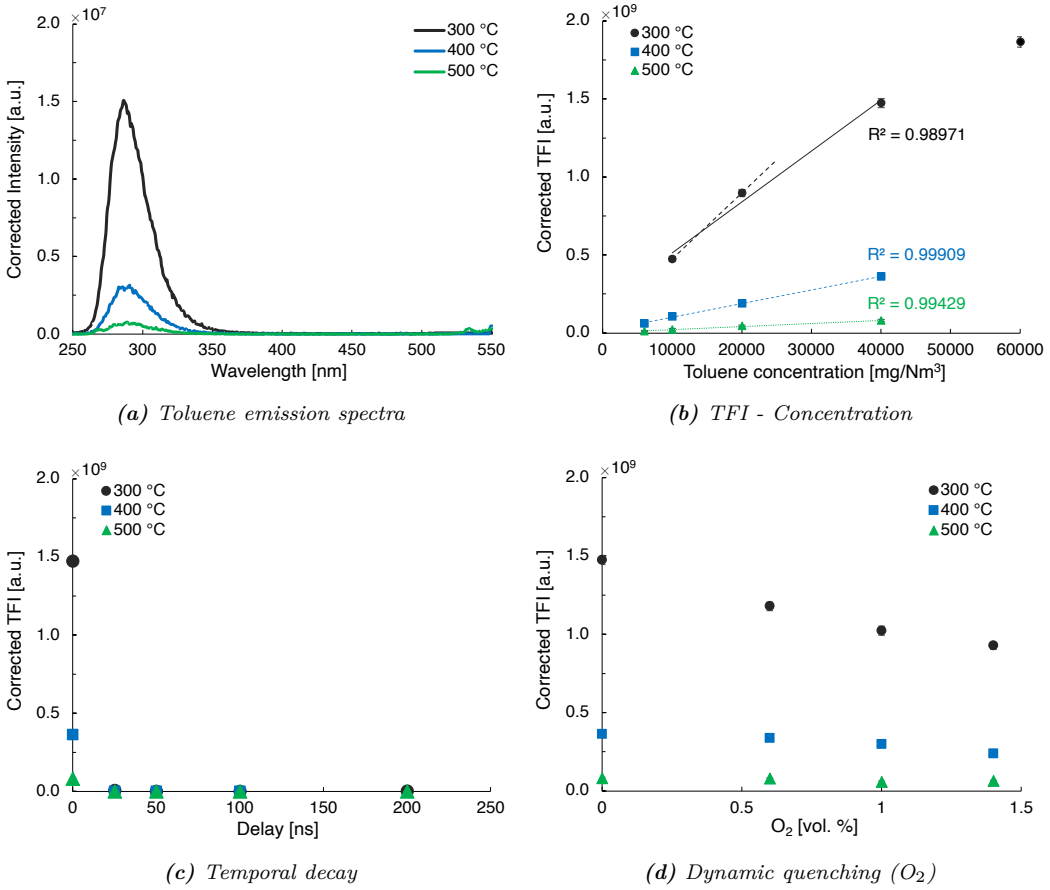

(a) Toluene emission spectra *(b) TFI - Concentration*

(c) Temporal decay *(d) Dynamic quenching (O_2)*

Figure 9.6: *Data set for toluene. (a) Fluorescence emission spectra with a concentration of 20000 mg/Nm^3. (b) Correlation between total fluorescence intensity (TFI) and concentration. (c) Temporal decay with a concentration of 40000 mg/Nm^3. (d) Dynamic quenching decay with a concentration of 40000 mg/Nm^3. Error bars represent the standard deviation.*

Aromatic carbonyls (aromatic ketones and aromatic aldehydes) were the last group of compounds that emitted fluorescence at the selected excitation wavelength. Three compounds were measured: benzophenone, benzaldehyde, and 2-hydroxyacetophenone. For the latter no signal was detected, despite introducing concentrations up to 40000 mg/Nm^3. As a verification, the accumulation of the camera was changed from 50 to 200 (number of laser pulses that produce a spectrum, i.e.,the more pulses, the more fluorescence). With this configuration, a signal in the same emission range as for the other two was very slightly discernible. This shows the low quantum yield of this compound. Under the conditions used in the pyrolysis experiments, this compound is therefore not expected to influence the fluorescence signal. Both benzaldehyde and benzophenone showed detectable emission. The data set for benzophenone is shown in Fig. 9.7. As already introduced in Section 2.2.1, the substitution of a carbonyl group (C=O) on the aromatic ring promotes the lower energy transition $n \rightarrow \pi^*$ due to the presence of the double-bonded oxygen,

and inhibits fluorescence. As can be seen in Fig. 9.7 (a), with a concentration of 9000 mg/Nm^3, the emission spectrum is an order of magnitude smaller than for previous groups. That is, the group of aromatic carbonyls emits the least fluorescence. This is mainly related to their low quantum yield, since, as shown in Fig. 2.13, the absorption cross section is in the same range as for phenolics.

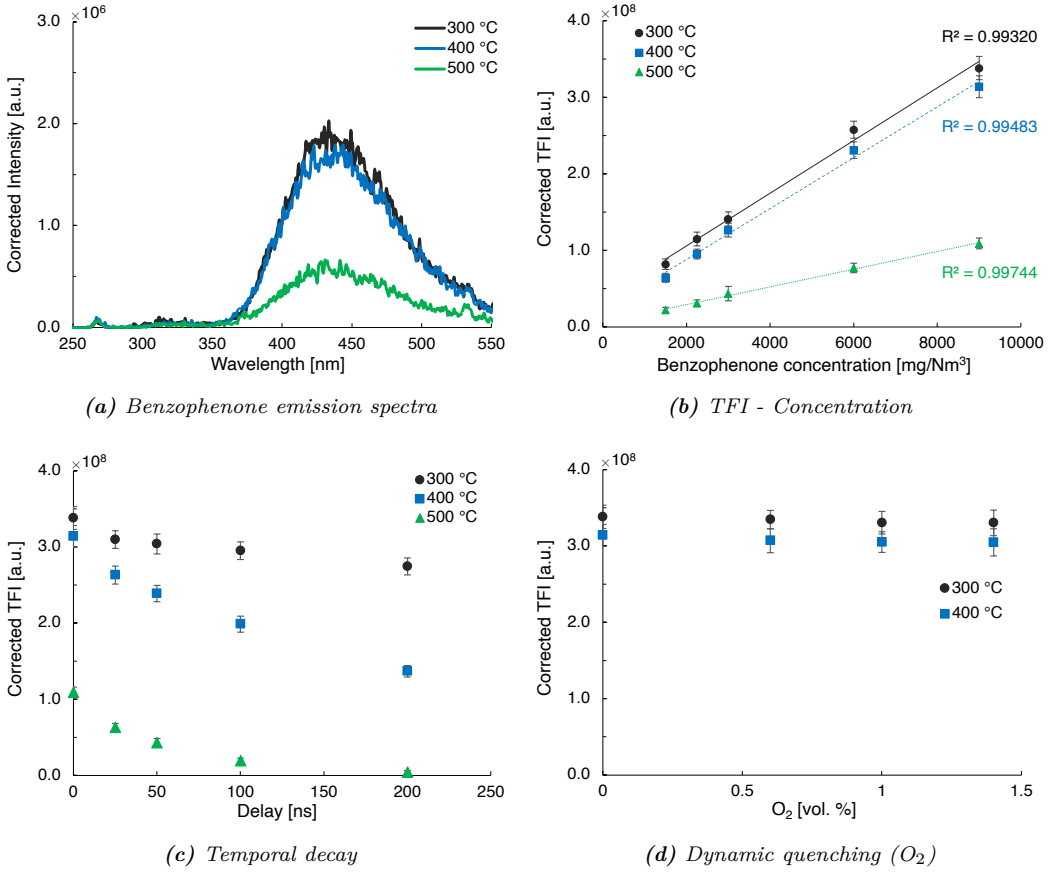

(a) Benzophenone emission spectra

(b) TFI - Concentration

(c) Temporal decay

(d) Dynamic quenching (O_2)

Figure 9.7: *Data set for benzophenone. (a) Fluorescence emission spectra with a concentration of 9000 mg/Nm^3. (b) Correlation between total fluorescence intensity (TFI) and concentration. (c) Temporal decay with a concentration of 9000 mg/Nm^3. (d) Dynamic quenching decay with a concentration of 9000 mg/Nm^3. Error bars represent the standard deviation.*

Fig. 9.7 (c) shows the long lifetime of benzophenone. At 300 °C with a delay of 200 ns the signal intensity barely decreased. Benzaldehyde also exhibited this behavior. Several studies claim that these aromatic carbonyl compounds emit only phosphorescence due to the high efficiency of intersystem crossing $S_1 \rightarrow T_1$ [185,186]. Other works, however, reported that the luminescence emission signal comes from a combination of phosphorescence and delayed fluorescence, or directly from thermally activated delayed fluorescence [187]. Unlike most compounds, in which the triplet state (T_1) has a lower energy than the first singlet excited state (S_1), in the case of aromatic carbonyls both have similar energies, so the emission spectrum would be in the same range (differences in emission shown in [188]). This fact would promote

isoenergetic intersystem crossing to the T_1 excited state and its subsequent emission, in the form of phosphorescence. Therefore, based on the literature and the long lifetimes measured at high temperatures, it is possible that the emission spectrum is due to a combination of both fluorescence and phosphorescence.

Regarding the furans group, neither furfural nor furan showed detectable emission signals, both measured at concentrations up to 100 g/Nm^3 in the gas-phase and even in liquid phase (as verification). In general, heterocyclic compounds, such as pyridine, furan, or thiophene, are reported to not emit fluorescence [111]. It is important to highlight that, in this case, due to their high absorption cross section (shown in Fig. 2.13, Section 2.2.1), which in the case of furfural is even in the same range as PAHs, laser absorption was observed. However, any compound emitted fluorescence. This confirms the low quantum yields of these species under the conditions employed. On the other hand, the fusion of cyclic aromatic rings to heterocyclic nucleus, is reported to increase the molar absorptivity of the absoption band [111]. Even though the lifetimes are reported to be shorter compared to unsubstituted benzene ring, fluorescence can be detected for such compounds [111]. The nature of dibenzofuran, being a furanic nucleus linked to two benzene rings, meets the characteristics described. The data set for this compound is shown in Fig. 9.8. The high fluorescence intensity emitted for concentrations between 500 and 1500 mg/Nm^3 can be observed in Fig. 9.8 (b). Furthermore, as reported in the literature, it exhibited a very short lifetime. With a delay of 25 ns almost no fluorescence signal was detected (see Fig. 9.8 (c)). As previously mentioned, due to this short lifetime, the influence of oxygen was very weak. So the fact is that, when analyzing its fluorescence behavior in terms of emission spectrum and intensity, it resembles much more the one-ring aromatic hydrocarbons group, rather than the furans group.

The remaining aromatic and aliphatic compounds measured did not exhibit any fluorescence emission. Among all of them, the ones with the highest absorption cross-section are the quinones. Therefore, the fact that no emission was detected should be more related to their low quantum yield. Aliphatic compounds have very low absorption bands, so their emission at the selected wavelength is very unlikely, especially at atmospheric pressures and high temperatures. However, due to the high concentration of such species in the pyrolysis process, this fact needed to be confirmed. Both aliphatic ketones and aldehydes tend to emit fluorescence with excitation wavelengths longer than 300 nm [115, 189, 190]. In fact, formaldehyde, a primary pyrolysis product, is mainly exited at 355 nm [190].

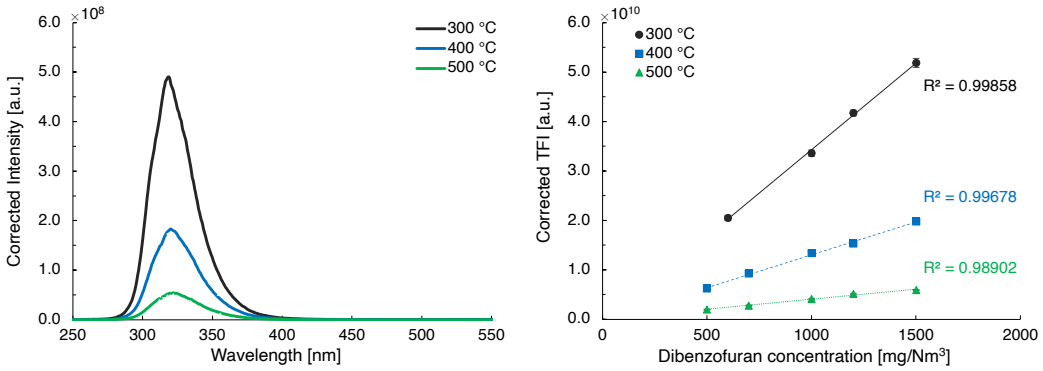

(a) Dibenzofuran emission spectra *(b) TFI - Concentration*

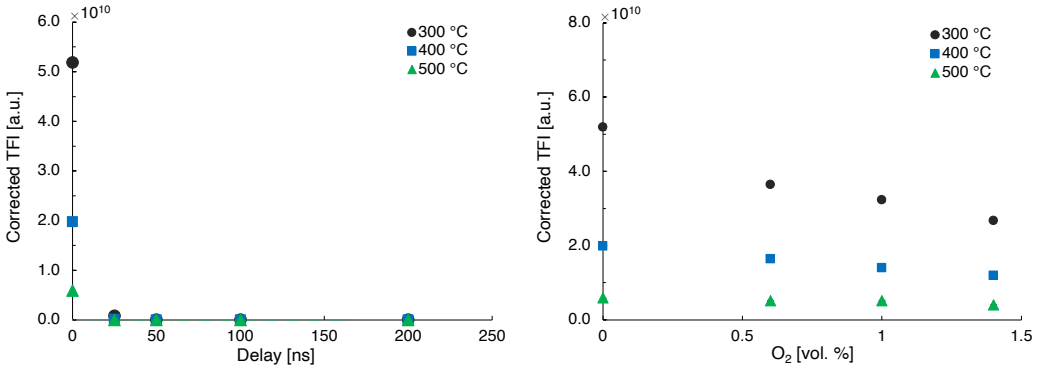

(c) Temporal decay *(d) Dynamic quenching (O_2)*

Figure 9.8: *Data set for dibenzofuran. (a) Fluorescence emission spectra with a concentration of 1000 mg/Nm³. (b) Correlation between total fluorescence intensity (TFI) and concentration. (c) Temporal decay with a concentration of 1500 mg/Nm³. (d) Dynamic quenching decay with a concentration of 1500 mg/Nm³. Error bars represent the standard deviation.*

Therefore, from the individual results of up to 23 representative compounds, we can conclude that only aromatic compounds will emit detectable fluorescence under the conditions employed. Among them, only PAHs, BTX, phenolics, and aromatic carbonyls could contribute to the fluorescence signal during pyrolysis. The correlation between signal intensity and concentration of the compounds at 300 °C is shown in Fig. 9.9. Both parameters are plotted on a logarithmic scale to make them comparable on the same graph. As shown by the individual results, polyaromatic compounds emit the most intense fluorescence even at much lower concentrations than the other groups. The next group would be the phenolics, which in order to reach the signal intensity of polyaromatics would require concentrations at least two orders of magnitude higher, although they could already contribute to the emission at relatively low concentrations. Taking into account that phenolics are one of the main products in the decomposition of lignin, their potential influence on the emission spectrum has to be considered, especially at lower temperatures, since their quenching effect with increasing temperatures is very high. One-ring aromatic hydrocarbons (BTX)

also exhibited similar fluorescence behavior to phenolics, and their major contribution should be more noticeable at low temperatures (high temperature-quenching effect). However, these are expected to be products of secondary reactions, so their release at low temperatures would be unlikely. Finally, it has been found that aromatic carbonyls must be present in high concentrations to reach emission levels of polyaromatics. Specifically, they would need concentrations 3 or 4 orders of magnitude higher. Although, as we have seen, at lower concentrations they can already contribute to the emission spectrum. Moreover, they do not exhibit large quenching effect due to high temperatures, therefore, their presence throughout the process can be detected.

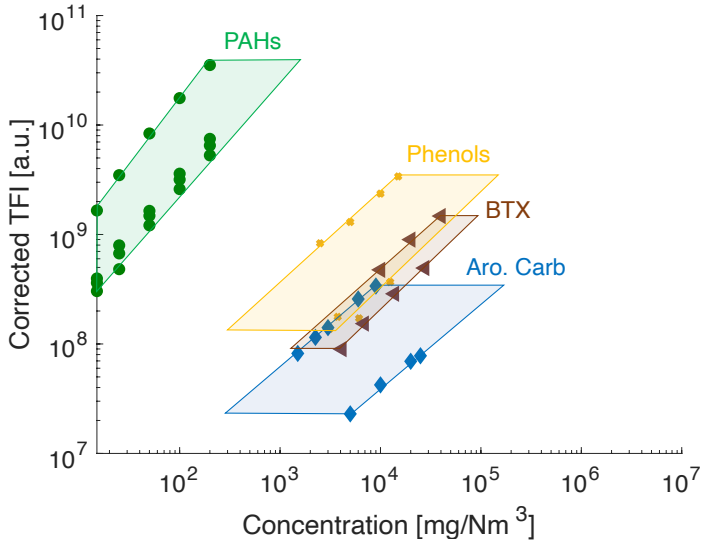

Figure 9.9: *Total fluorescence intensity (TFI) as a function of the concentration at 300 °C for all measured compounds clustered in groups."Aro. Carb"stands for aromatic carbonyls.*

In addition to the intensity of the emission spectrum, as mentioned above, it is important to determine the emission range. Fig. 9.10 shows the individual spectra of each compound together with their average spectra at 300 °C. The selected concentration for each compound in Fig. 9.10 is different in order to obtain comparable results. As can be seen, BTX and phenolics emit fluorescence at wavelengths between 280 and 350 nm. In this group we have to include also species such as dibenzofuran. When increasing the number of aromatic rings bonded together, the emitted light shifts to longer wavelengths, starting with naphthalene, with a maximum peak at 340 nm, until fluoranthene, with a broad spectrum between 400 - 550 nm. The latter is also coincident with the fluorescence emission of aromatic carbonyls. Due to the superposition of these compounds, especially at long wavelengths (with carbonyls and fluoranthene) and short wavelengths (with the one-ring aromatics), an exact quali-

tative analysis cannot be achieved only by the sum of individual compounds alone. Therefore, different LIF-relevant parameters (lifetime, quenching) needed to be considered for the determination of the compounds that can potentially contribute to the total spectrum.

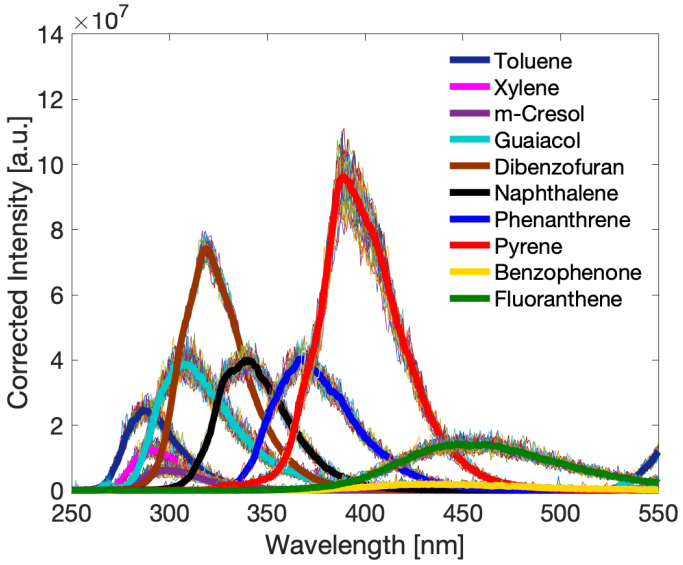

Figure 9.10: *Individual spectra and average spectrum of different species at 300 °C. For the spectra to be comparable, the concentration is different for each of them.*

9.3.2 Synthetic mixtures

The analysis of the pyrolysis fluorescence spectra as a function of individual species is based on the fact that the fluorescence emission of a mixture of compounds can be determined from the sum of the individual spectrum of each compound under the same conditions. However, as it has been shown in the previous section, due to the different species emitting in a similar wavelength range, it is necessary to analyze not only the fluorescence spectrum for one condition (e.g., same temperature, same delay), but also other LIF-relevant parameters which will have a different influence on the individual compounds. By combining the results under different conditions, a more accurate qualitative and quantitative analysis can be performed.

Before determining the possible approach for analyzing the pyrolysis fluorescence spectra on the basis of the individual results of each compound, it is necessary to verify whether synthetic mixtures of compounds behave in the same way as the sum of the individual compounds for all measured conditions. For this purpose, different mixtures were prepared and measured. Tab. 9.2 shows a summary of them, as well

Table 9.2: *Summary of synthetic mixtures and conditions.*

Mixture	Figure		Conc.	Solvent	Concentration compounds [mg/m^3]				Temperature [°C]	Delay [ns]	O_2 [%]
					Toluene						
Mixture 1	Fig. 9.11	(a)	1.1	Cyclohexane	10000.00				300	0	0
		(b)	1.2	Cyclohexane	40000.00				300	0	0
					Naphthalene	Phenanthrene	Benzaldehyde	H-acetophe*			
Mixture 2	Fig. 9.12	(a)	2.1	Cyclohexane	15.00	15.40	4183.95	1147.11	300	0	0
					Naphthalene	Pyrene					
Mixture 3	Fig. 9.13	(a)	3.1	Cyclohexane	15.00	15.40			300	0	0
		(b)	3.1	Cyclohexane	25.00	24.92			400	0	0
		(c)	3.2	Cyclohexane	100.00	99.68			300	50	0
		(d)	3.2	Cyclohexane	100.00	99.68			300	200	0
					Toluene	Naphthalene	Fluoranthene				
Mixture 4	Fig. 9.14	(a)	4.1	Cyclohexane	4290.46	15.00	15.14		300	0	0
		(b)	4.1	Cyclohexane	21452.32	75.00	75.72		400	0	0
		(c)	4.3	Cyclohexane	14301.54	50.00	50.48		300	0	0.6
		(d)	4.3	Cyclohexane	14301.54	50.00	50.48		300	0	1.4
					Naphthalene	Phenanthrene	Pyrene				
Mixture 5	Fig. 9.15	(a)	5.1	Cyclohexane	25.00	21.83	6.08		300	0	0
		(b)	5.1	Cyclohexane	25.00	21.83	6.08		400	0	0
		(c)	5.2	Cyclohexane	75.00	65.49	18.23		300	25	0
		(d)	5.2	Cyclohexane	75.00	65.49	18.23		400	25	0
		(e)	5.2	Cyclohexane	75.00	65.49	18.23		300	0	1.0
		(f)	5.2	Cyclohexane	75.00	65.49	18.23		400	0	1.0

(*) Hydroxyacetophenone

as some of the conditions employed. As for individual compounds, the different concentrations for each mixture was obtained by varying the injection rate of the syringe pump. It is important to note that more conditions than the ones presented in the table and figures were measured, however, only part of them are shown for the sake of simplicity.

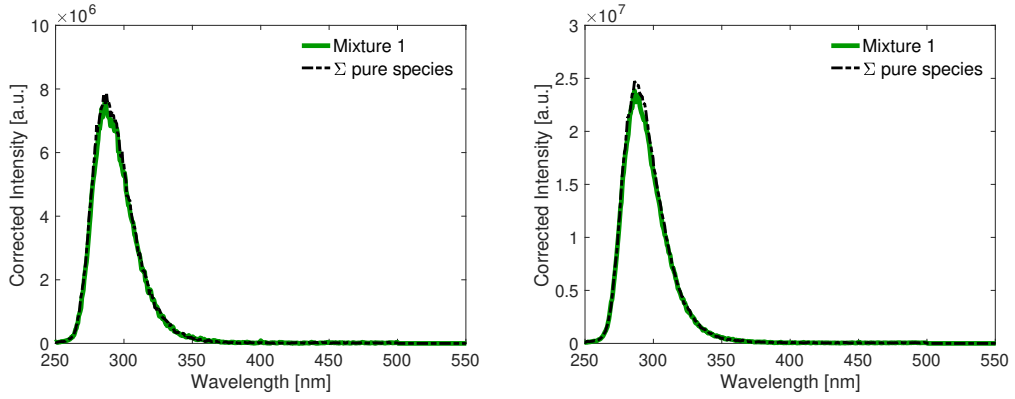

(a) *300 °C; Conc: 1.1; D: 0 ns; O_2: 0 %* ***(b)*** *300 °C; Conc: 1.2; D: 0 ns; O_2: 0 %*

Figure 9.11: *Comparison between the fluorescence spectra of Mixture 1 (Cyclohexane + Toluene) and pure toluene at 300 °. Concentration and conditions are given in Tab. 9.2.*

The first verification was performed to determine the influence of the solvent content. For this purpose, a mixture of cyclohexane (solvent used also for the individual compounds) with toluene at 50 vol.% was prepared. The comparison between the mixture (Mixture 1) and pure toluene is presented in Fig. 9.11. Two differ-

ent measurements were performed with the lowest (Fig. 9.11 (a), 10000 mg/Nm^3) and the highest (Fig. 9.11 (b), 40000 mg/Nm^3) toluene concentration. As it can be observed, the presence of cyclohexane had negligible effects on the fluorescence spectrum. When considering the total fluorescence intensity, the errors are below 4%.

The second mixture was prepared to study the potential influence that other species (capable of absorbing light but unable to emit fluorescence) could have on the fluorescence signal. As observed in the previous section, many species with low quantum yields but high absorption cross sections are produced during pyrolysis. For this purpose, besides different compounds capable of emitting fluorescence (naphthalene, phenanthrene, and benzaldehyde), hydroxyacetophenone, which did not exhibit any fluorescence although having absorption cross sections at similar levels as phenolics [112], was also introduced (Mixture 2 in Tab. 9.2). The comparison between the emission spectra of the mixture and the sum of the individual species (naphthalene, phenanthrene and benzaldehyde) is shown in Fig. 9.12. As it can be observed, there is very good agreement between both, meaning that the presence of hydroxyacetophenone did not affect the fluorescence signal. It should be noted, however, that a very high concentration of species absorbing energy without emitting it could have a negative effect on the linear correlation between fluorescence and concentration if the energy of the excitation source is not sufficient. However, previous verification of the linearity between the fluorescence signal and the laser energy was performed for the case with the highest concentration of pyrolysis volatiles.

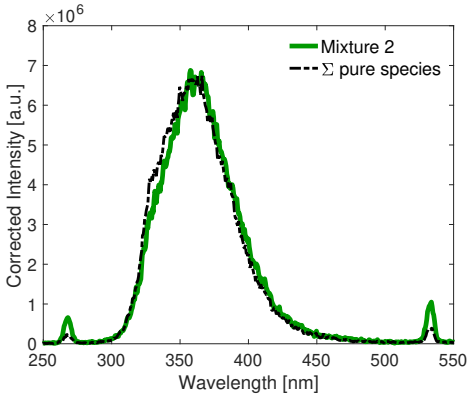

(a) 300 °C; Conc: 2.1; D: 0 ns; O_2: 0 %

Figure 9.12: *Comparison between the fluorescence spectrum of Mixture 2 (Naphthalene + Phenanthrene + Benzaldehyde + Hydroxyacetophenone) and the fluorescence spectrum obtained by the sum of the spectra of individual species. Concentration and conditions are given in Tab. 9.2.*

Two more mixtures were prepared to verify also the influence of temperature, delay and O_2 quenching. The first one was prepared with naphthalene and pyrene (Mix-

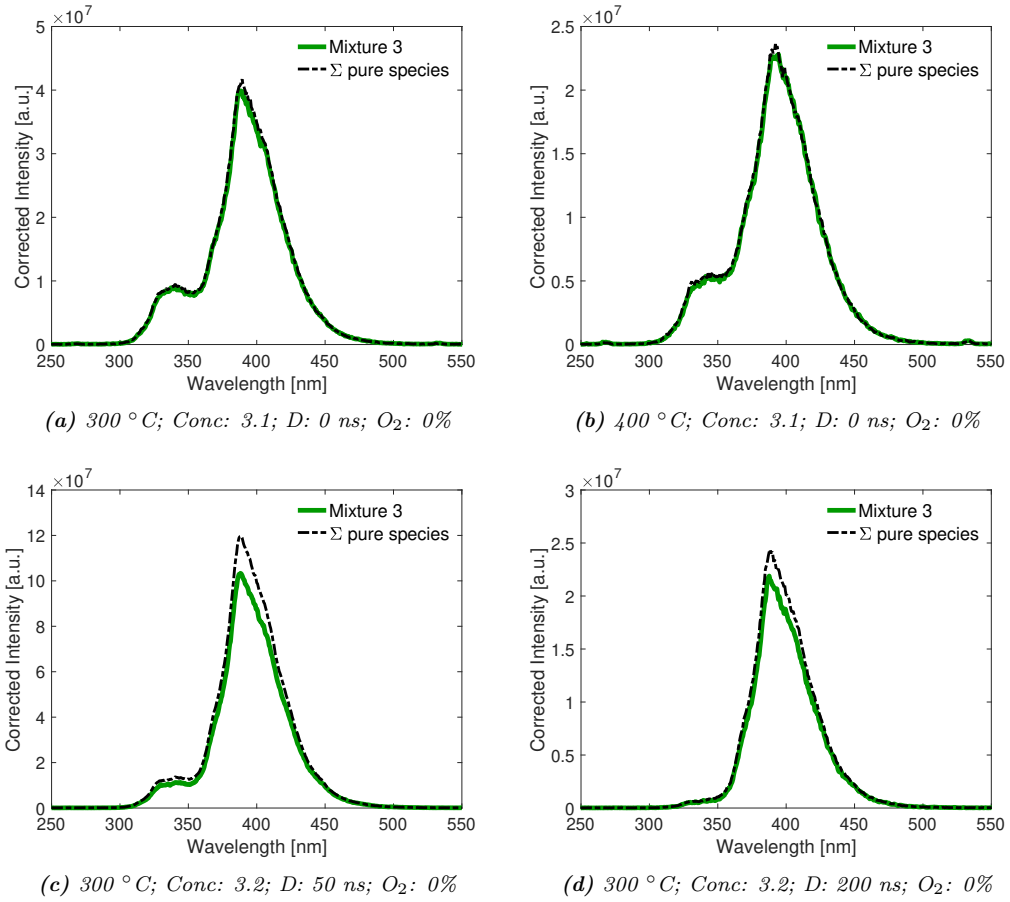

(a) 300 °C; Conc: 3.1; D: 0 ns; O_2: 0%

(b) 400 °C; Conc: 3.1; D: 0 ns; O_2: 0%

(c) 300 °C; Conc: 3.2; D: 50 ns; O_2: 0%

(d) 300 °C; Conc: 3.2; D: 200 ns; O_2: 0%

Figure 9.13: *Comparison between the fluorescence spectrum of Mixture 3 (Naphthalene + Pyrene) and the fluorescence spectrum obtained by the sum of the spectra of individual species. Concentration and conditions are given in Tab. 9.2.*

ture 3). Some results are shown in Fig. 9.13. The concentrations and conditions employed are given in Tab. 9.2. Very good agreement was observed for different concentrations (results not shown) and temperatures, Fig. 9.13 (a) and (b). In the case of the experiments with delay, Fig. 9.13 (c) and (d), a small overestimation was observed in the case of the spectrum obtained from the individual species. The effect of O_2 quenching was studied with a mixture of toluene, naphthalene, and fluoranthene (Mixture 4). The results are presented in Fig. 9.14. A good agreement was obtained for all cases. In the case of using different temperatures and concentrations, Fig. 9.14 (a) and (b), only a small deviation was observed in the spectral range belonging to fluoranthene. In Fig. 9.14 (c) and (d), despite different deviations in each of the species, the errors obtained for the total fluorescence intensity, which takes into account the whole spectral range, are only 6 and 12 %, respectively.

Finally, a mixture was prepared based on the fluorescence spectra obtained during pyrolysis experiments. As shown in previous chapters, the maximum peak of the

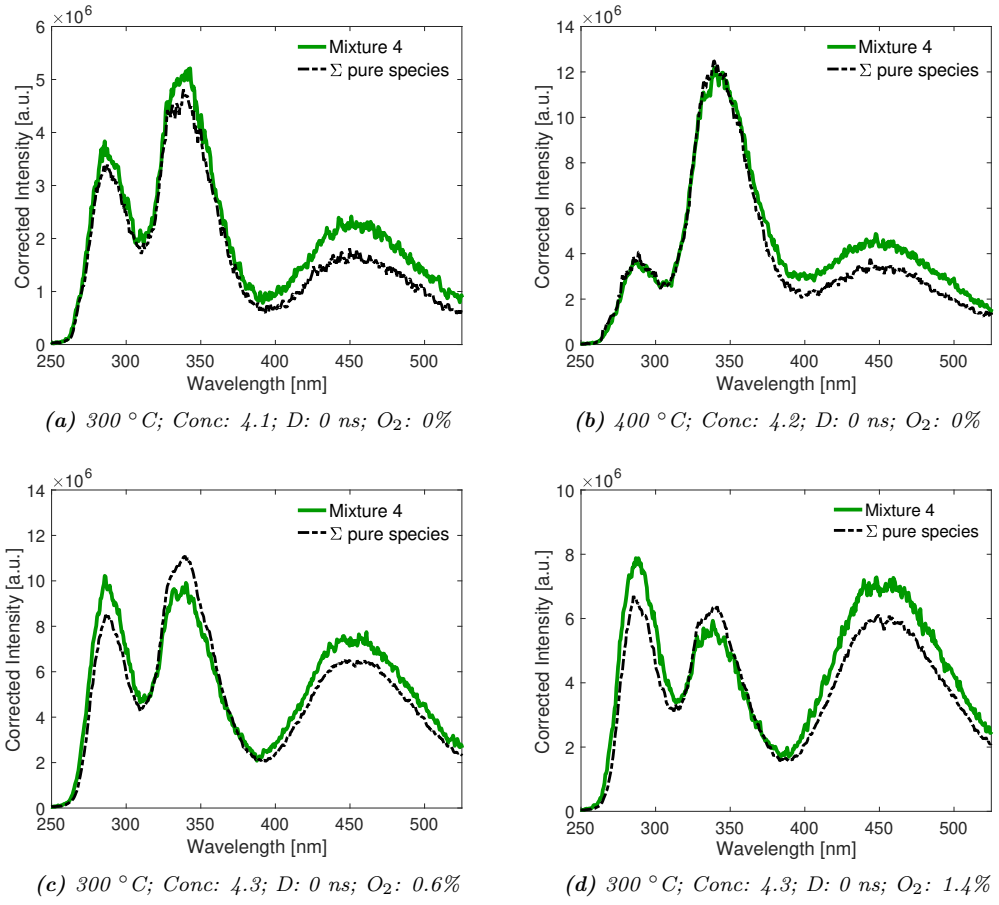

(a) 300 °C; Conc: 4.1; D: 0 ns; O_2: 0%

(b) 400 °C; Conc: 4.2; D: 0 ns; O_2: 0%

(c) 300 °C; Conc: 4.3; D: 0 ns; O_2: 0.6%

(d) 300 °C; Conc: 4.3; D: 0 ns; O_2: 1.4%

Figure 9.14: *Comparison between the fluorescence spectrum of Mixture 4 (Toluene + Naphthalene + Fluoranthene) and the fluorescence spectrum obtained by the sum of the spectra of individual species. Concentration and conditions are given in Tab. 9.2.*

spectra during pyrolysis was between 350 and 400 nm. This spectral range corresponds mainly to 2-, 3-, and 4-ring aromatic species. Therefore, Mixture 5 was prepared with naphthalene, phenanthrene, and pyrene. Concentrations and conditions employed are listed in Tab. 9.2. For this case, the influence of all LIF-relevant parameters was measured: concentration, temperature, delay, and O_2 quenching. Part of the results are shown in Fig. 9.15. As for the previous mixtures, very good agreement was found for all cases, especially with respect to concentration, temperature, and O_2-quenching. In the case of the experiments performed with delay, an overestimation of the spectrum calculated on the basis of the individual species was again observed. The deviation of the total fluorescence intensity (TFI) was, in this case, of around 15%. This effect should be considered when analyzing the pyrolysis experiments.

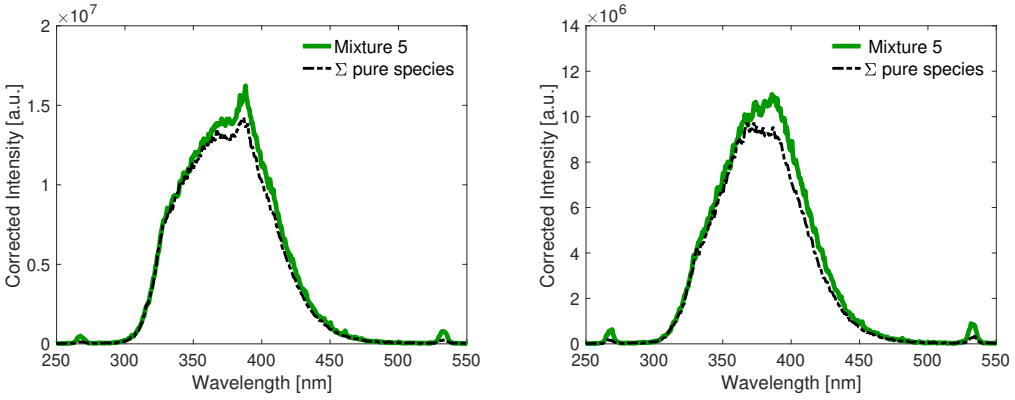

(a) 300 °C; Conc: 5.1; D: 0 ns; O_2: 0%

(b) 400 °C; Conc: 5.1; D: 0 ns; O_2: 0%

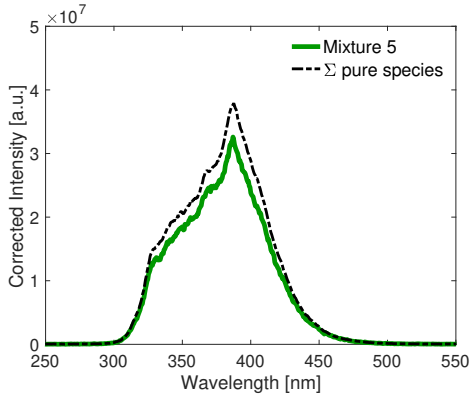

(c) 300 °C; Conc: 5.2; D: 25 ns; O_2: 0%

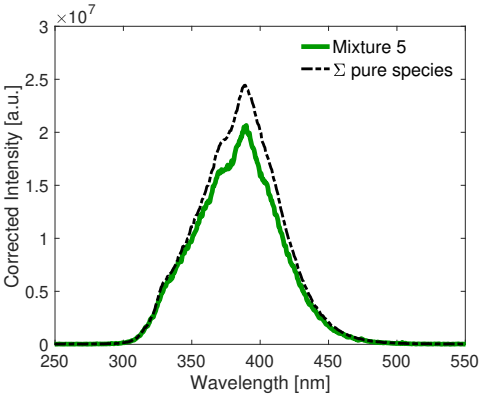

(d) 400 °C; Conc: 5.2; D: 25 ns; O_2: 0%

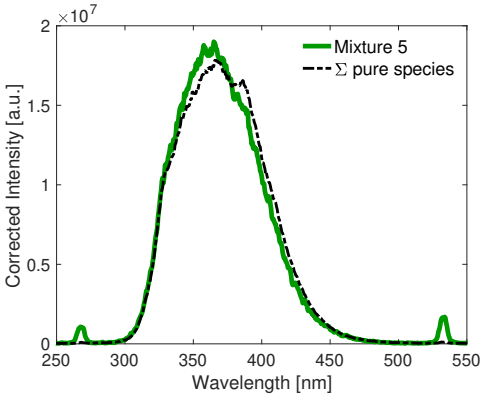

(e) 300 °C; Conc: 5.2; D: 0 ns; O_2: 1.0%

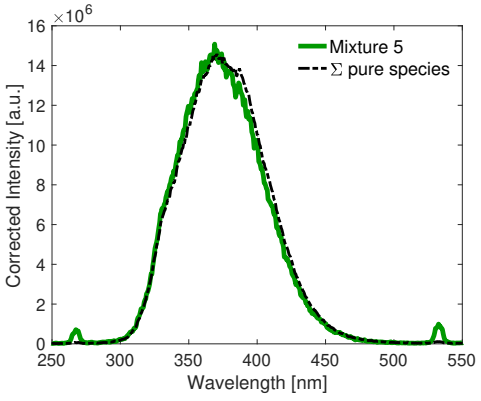

(f) 400 °C; Conc: 5.2; D: 0 ns; O_2: 1.0%

Figure 9.15: *Comparison between the fluorescence spectrum of Mixture 5 (Naphthalene + Phenanthrene + Pyrene) and the fluorescence spectrum obtained by the sum of the spectra of individual species. Concentration and conditions are given in Tab. 9.2.*

9.3.3 Pyrolysis experiments

After analysis of the fluorescence behavior of the different individual compounds, and verification with synthetic mixtures, pyrolysis experiments were performed varying all the previously calibrated parameters. Tab. 9.3 shows each of the conditions employed and the materials used. Each condition was also repeated twice. The experimental campaign is based on Chapter 8, in which a semi-quantitative characterization of the total amount of fluorescence-emitting species formed during pyrolysis of woody biomass was obtained based on the behavior of each of its macrocomponents. Therefore, experiments were performed not only with wood, but also with cellulose, xylan, and lignin. With the calibration of up to 23 representative species (of which 11 emitted detectable fluorescence) it is intended to explore potential improvements in qualitatively and quantitatively determining the individual species that form the emission spectrum. Moreover, the introduction of new excitation wavelengths (320 and 380 nm) could contribute to better identification and differentiation of species.

However, analyzing each spectrum individually on the basis of all the parameters used is a very challenging. An example of a fluorescence spectrum during pyrolysis of beech wood at the time when the temperature reaches 400 °C is shown in Fig. 9.16. The spectrum at this temperature has been chosen to be directly comparable with the measured conditions of the individual compounds without interpolation.

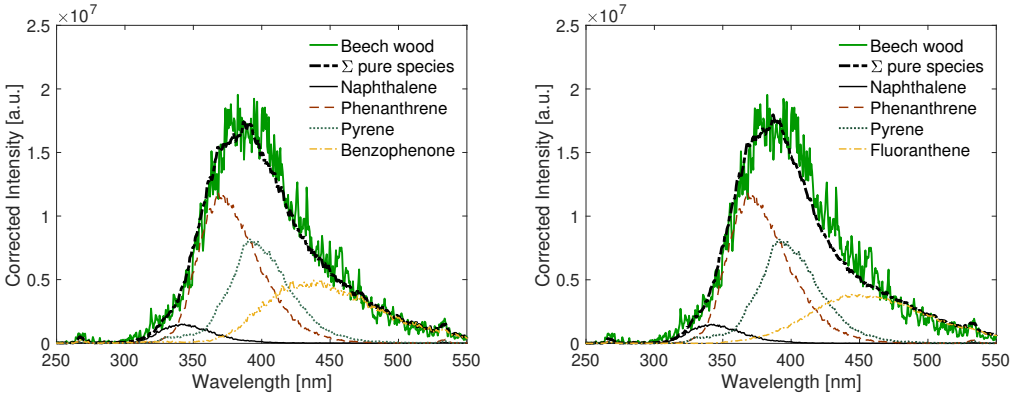

(a) Fitting with Benzophenone *(b) Fitting with Fluoranthene*

Figure 9.16: *Comparison between the fluorescence spectrum of beech wood at 400 °C and the fluorescence spectrum obtained by the sum of the spectra of individual species.*

As it can be observed, only by considering the emission spectrum (at the appropriate temperature and by adjusting the concentration value), two different quantitative solutions can be obtained. One of them, Fig. 9.16 (a), by linear combination of the individual spectra of naphthalene, phenanthrene, pyrene, and benzophenone.

Being the concentrations obtained: 10 mg/Nm^3 for naphthalene, 40 mg/Nm^3 for phenanthrene, 10 mg/Nm^3 for pyrene, and 25000 mg/Nm^3 for benzophenone. In Fig. 9.16 (b), however, a similar spectrum can be also obtained by: 10 mg/Nm^3 for naphthalene, 40 mg/Nm^3 for phenanthrene, 12 mg/Nm^3 for pyrene, and 75 mg/Nm^3 for fluoranthene. This is just one example that highlights the need to employ different parameters in order to achieve a more accurate characterization of the possible compounds that can contribute to the fluorescence signal in the same wavelength range. However, as previously introduced, each parameter influences each compound in a different way, and the only linear correlation is the one obtained between concentration and signal intensity. The number of variables to consider with different correlations with signal intensity for each compound, which in turn depend on each other (temperature-lifetime; temperature-O_2-quenching), increases the mathematical complexity for solving the problem.

A possible approach for data analysis is the use of advanced computational methods such as those employed in neural networks. With the development of a neural network, through certain known parameters (inputs), in this case: temperature, delay, O_2 concentration, and the pyrolysis spectrum, the concentrations of the individual species that compose the input spectrum could be obtained. However, to achieve an accurate prediction in this kind of computational methods, it is necessary to include a large amount of data. Depending on the application and its difficulty, it may vary from several thousands to several millions of data points for optimal performance. Although at first sight it may seem that a large amount of data has been obtained from the calibration of pure species (11 species emitting fluorescence x 36 conditions x 40 repetitions = 15840 spectra), it may be insufficient in order to accurately predict the concentration of 11 different compounds. Obtaining sufficient data by preparing mixtures experimentally would be a very difficult and time-consuming task. Experimental calibration, taking into account that it should be performed for each wavelength and should be repeated every so often, renders it a very inefficient method. However, these data could be obtained from the individual results of each compound, not only with the direct use of each one of them, but also with the creation of a large number of combinations obtained from them. That is, based on the results presented in the previous section, in which it was possible to describe the fluorescence behavior of the synthetic mixtures as a function of the individual compounds, by calculating artificial mixtures, which would represent mixtures of real compounds, the necessary amount of data could be obtained to train the neural network in an effective way.

Table 9.3: *Summary of pyrolysis experiments performed after calibration.*

Material	Initial Mass [g]	Heating rate [°C/min]	Final temperature [°C]	Wavelength [nm]	Delay [ns]	O_2 [%]
Beech wood	1	10	600	266	0	0
					10	0
					25	0
					0	0.3
					0	0.6
					0	1.0
				320	0	0
				380	0	0
Cellulose	1	10	600	266	0	0
					10	0
					25	0
					0	0.3
					0	0.6
				320	0	0
				380	0	0
Xylan	1	10	600	266	0	0
					10	0
					25	0
					0	0.3
					0	0.6
				320	0	0
				380	0	0
Lignin	1	10	600	266	0	0
					10	0
					25	0
					0	0.3
					0	0.6
				320	0	0
				380	0	0

The development of a neural network based on these experimental results is being carried out in the Laboratory of Process Automation Systems at the Department of Chemical and Biochemical Engineering of the Technische Universität Dortmund within the framework of a scientific collaboration. The analysis of the pyrolysis experiments by means of a neural network, previously trained with the individual compounds and artificial mixtures, represents the current work in progress and needs to be further developed.

Chapter 10

Summary and outlook

The main objective of this work was to contribute to improve the understanding of the pyrolysis conversion of lignocellulosic biomass. To this end, three of the main open questions with regard to the actual pyrolysis mechanism were studied in several publications: the influence of heterogeneous secondary reactions (triggered by intra-particle transport limitations), the formation of aromatic species, and the influence of inorganics.

The first step was the development of a particle-level reactor in which mass and temperature in the center of the particle could be measured on-line in order to study the time-dependent evolution of the slow pyrolysis process. The investigation of transport-controlled regimes, with the utilization of thermally-thick wood particles, allowed to focus on the presence of heterogeneous secondary reactions by increasing the retention time of the volatiles within the solid matrix. Furthermore, advanced laser-based spectroscopic techniques were employed to gain further insights into the complex pyrolysis mechanism in an on-line, in-situ, and non-intrusive manner. LIF spectroscopy was employed to track, qualitatively and semi-quantitatively, the evolution of mainly aromatic species. IRLAS was applied, through a external scientific collaboration, to quantitative characterize permanent gases and water vapor. Different pyrolysis behaviors were found between two different types of woody biomass, beech and pine (as representative of hard- and softwood), which could not solely be explained by their differences in organic composition. For beech wood, an exothermic peak during the main devolatilization stage was associated to a temporal overlapping of primary decomposition of cellulose and lignin together with the presence of heterogeneous secondary reactions of primary volatiles, leading to the formation of aromatic species. For pine, in contrast, an endothermic region was observed during the main devolatilization stage, associated with the primary decomposition

of cellulose. The exothermic peak, in this case, was delayed (at higher temperatures) and coincident with lignin decomposition and release of aromatic compounds. This fact indicated that heterogeneous reactions of the primary products, leading to PAHs formation, occurred at the same time with further changes in the lignin structure and resulted in an enhancement of the exothermic reactions. Preliminary experiments performed with leached beech wood particles showed similar results, indicating the presence of inorganics as one of the possible reason for such differences. Both chemical and physical properties showed, therefore, to play a significant role in the different reaction pathways. With the implementation of the employed experimental conditions in a particle model, which included a detailed pyrolysis reaction scheme, the capabilities and limitations of numerical and experimental results were revealed. The model, which quantified the extent of heterogeneous charring reactions in the form of adjustable parameters, was able to predict both mass loss and temperature evolution, as well as H_2O and CO release. However, the delayed CH_4 release, which was previously attributed to lignin devolatilization, was not properly described. Moreover, delayed emission of aromatic compounds, detected by LIF, with respect to the release of light- and heavy-condensables (from the numerical results), revealed their origin from secondary reactions and the need to include their formation in more detailed pyrolysis mechanisms.

To further investigate the origin of the difference between the pyrolysis behavior of beech and pine, the former was washed with H_2O and HCl in order to reach different levels of inorganic content. The removal of inorganics from beech wood, resulted in a pyrolytic behavior similar to that of pine, with a delayed lignin decomposition. Moreover, this was accompanied by the release of CH_4, a second peak in the release of CO, a delay/widening of the TFI curve (tracking the production and emission of fluorescence-emitting species), and a strong change in the process thermochemistry (very similar to the one for pine). Such trends were confirmed by off-line GC-MS analysis, with higher major carbohydrates and lower phenol yields when AAEM were reduced. These facts, together with the similarities in K content between pine and washed beech wood, supported the hypothesis that the differences between both types of woods (original beech and pine) could be attributed to the varying content in inorganic species, especially K, rather than to their differences in structure and organic composition.

Due to the results obtained, beech wood particles were doped with KCl to specifically study the effect of potassium on the pyrolytic behavior of wood. Addition of K catalyzed the pyrolysis process and especially affected both cellulose and lignin

devolatilization by shifting the maximum of the conversion rate towards lower temperatures. The overlap of both macrocomponents decomposition was accompanied by strong exothermicity and the release of fluorescence-emitting species, indicating an enhancement of heterogeneous secondary reactions. Its combined impact with the presence of transport limitations was also addressed at medium heating rates. The catalytic effect of K on charring reactions, leading to higher char and H_2O yields, was confirmed. Besides, both CH_4 and CO production were suppressed upon addition of K. The observed exothermicity at particle level was confirmed to be a combination of both phenomena, i.e., the presence of both inorganics and transport limitations.

A comprehensive analysis based on the main macrocomponents of biomass (hemicellulose, cellulose, and lignin) was performed to determine the origin of the combined influence of both transport resistances and inorganic species on the pyrolysis mechanism. The development of a new particle-level reactor together with the implementation of new (on-line GC-TCD) and improved (LIF spectroscopic system) analytical techniques, allowed the characterization of permanent gases and the semi-quantification of the total amount of fluorescence-emitting species, respectively. After an experimental campaign of more than 100 experiments, made with different materials (raw, washed, and doped) and different initial masses, it was concluded that inorganic species, in the presence of intra-particle transport resistances, catalyze mainly cellulose decomposition, changing the thermochemistry of the process to a more exothermic regime and increasing char and gas yields (mainly CO_2) due to a preference for the fragmentation reaction pathway. Based on the results obtained for cellulose, a reaction mechanism was proposed. The higher temperatures promoted from the effect of K and intra-particle resistances on cellullose, leaded to an overlap and narrowing of the three macrocomponents devolatilization during pyrolysis of wood. The inhibition of CO at high temperatures with increasing inorganic content was related to the preference for deoxygenation through both CO_2 and H_2O. With respect to PACs formation, lignin was found to be the main source during the main devolatilization stage. However, at higher temperatures, when no further mass loss was detected, PACs mainly derived from holocellulose through similar reaction mechanism as for CH_4 formation, based on their similar release patterns. Moreover, the inhibition of both upon addition of inorganics revealed a competition between charring and PACs formation. These results have been crucial to contribute to the further understanding of the influence of inorganics, the presence of heterogeneous

secondary reactions, and the formation of aromatic compounds, three of the main open questions with respect to the actual pyrolysis mechanism.

Furthermore, in order to explore potential improvements on both selectivity and sensitivity of laser-induced fluorescence spectroscopy when applied to pyrolysis characterization, a calibration of the system with up to 23 representative compounds was performed. With the collection of 15840 fluorescence spectra under 400 different conditions, deriving from 11 pyrolysis products, it could be concluded that only aromatic compounds could emit detectable fluorescence under the conditions employed. Moreover, among them, only PAHs, BTX, phenols, and aromatic carbonyls could contribute to the fluorescence signal during pyrolysis. The correlation between concentration and fluorescence intensity at different temperatures was determined for each group. Together with the analysis of their fluorescence lifetime and O_2-quenching, it is aimed to achieve a better qualitative and quantitative characterization of the fluorescence-emitting species. It would be the first time that quantitative LIF-analysis is performed in pyrolysis. Moreover, due to the large database obtained with individual species together with the possible calculation of artificial mixtures, after a previous validation with real mixtures, a neural network will be developed to perform the analysis. The possibility of developing such advanced computational method applied to this field, would allow the application of this spectroscopic principle (and others) in a much more efficient way by only calibrating pure species. The characterization of other pyrolysis products would also be possible by using other wavelengths, for which the developed model would also be valid.

10.1 Future work

The future development perspectives of this research encompasses on several aspects. On the one hand, the extensive experimental results can be used for the improvement and further development of the pyrolysis mechanism, both for the inclusion of the influence of inorganics and heterogeneous secondary reactions, in this case, by means of Arrhenius equations. In this way their influence would be determined by process parameters such as temperature. The quantification of aromatic species (such as PAHs and BTX) by means of LIF will also be crucial for their inclusion in more developed pyrolysis schemes.

On the other hand, pyrolysis conditions could be extended. In fact, the new particle-level reactor was developed with a view to performing experiments at medium and

fast heating rates. This is possible through the installation of a hydraulic opening and closing system and a retractable cooling chamber. The realization of this type of experiments at faster heating rates and higher temperatures would also allow the study of secondary reactions in the gas phase. For this purpose, an ex-situ measurement cell already exists in which the results obtained in-situ by means of both laser-based spectroscopic techniques (IRLAS and LIF) could be compared. In the case of LIF, however, it would be necessary the installation of an automatic flipping mirror in order to not lose the alignment of the laser beam in the main reactor cell. The utilization of a beam splitter would also be possible after validation of sufficient laser energy for both measurement cells.

Regarding the LIF spectroscopic system, the utilization of different wavelengths would be necessary in order to focus on other pyrolysis products. For instance, to work with shorter wavelengths (< 230 nm) would promote different electronic transitions, such as $n \rightarrow \sigma^*$, and characterization of other pyrolysis species, such as alcohols, may be possible. To work with longer wavelengths (> 355 nm) would allow to characterize some aliphatic carbonyls. The neural network that will be developed for 266 nm, could also be used for these conditions.

Appendix A

Publications

In the following Appendix A, peer-reviewed publications, and oral and visual presentations are listed.

A.1 Publications related to this thesis

1. Pyrolysis behavior of thermally thick wood particles: time-resolved characterization with laser based in-situ diagnostics. N. Lang, C. Rupp, **H. Almuina-Villar**, A. Dieguez-Alonso, F. Behrendt, and J. Röpcke. *Fuel*, 210 (Supplement C): 371-379, 2017. https://doi.org/10.1016/j.fuel.2017.08.077

2. Laser-Based Spectroscopy Diagnosis and Detailed Numerical Models to Gain Understanding on the Slow Pyrolysis Behavior of Thermally Thick Wood Particles. **H. Almuina-Villar**, A. Anca-Couce, N. Lang, J. Röpcke, F. Behrendt, and A. Dieguez-Alonso. *Chemical Engineering Transactions*, 65: 109-114, 2018. https://doi.org/10.3303/CET1865019

3. Application of laser-based diagnostics for characterization of the influence of inorganics on the slow pyrolysis of woody biomass. **H. Almuina-Villar**, N. Lang, A. Anca-Couce, J. Röpcke, F. Behrendt, and A. Dieguez-Alonso. *Journal of Analytical and Applied Pyrolysis*, 140: 125-136, 2019. https://doi.org/10.1016/j.jaap.2019.03.004

4. Combined Influence of Inorganics and Transport Limitations on the Pyrolytic Behaviour of Woody Biomass. **H. Almuina-Villar**, P. Sommersacher, S. Retschitzegger, A. Anca-Couce, and A. Dieguez-Alonso. *Chemical Engineering Transactions*, 80: 73-78, 2020. https://doi.org/10.3303/CET2080013

5. Synergistic influence of inorganics and intra-particle transport resistances on the pyrolysis mechanism of woody biomass based on its macrocomponents. **H. Almuina-Villar**, C. M. Grottola, F. Hempel, N. Lang, J.-P. H. van Helden, F. Behrendt, and A. Dieguez-Alonso. In preparation for submission to *Energy Conversion and Management*.

A.2 Other publications

6. Experimental investigation on biomass shrinking and swelling behaviour: Particles pyrolysis and wood logs combustion. G. Caposciutti, **H. Almuina-Villar**, A. Dieguez-Alonso, T. Gruber, J. Kelz, U. Desideri, C. Hochenauer, R. Scharler, and A. Anca-Couce. *Biomass and Bioenergy*, 123: 1–13, 2019. https://doi.org/10.1016/j.biombioe.2019.01.044

7. Correlations between tar content and permanent gases as well as reactor temperature in a lab-scale fluidized bed biomass gasifier applying different feedstock and operating conditions. L. von Berg, G. Pongratz, A. Pilatov, **H. Almuina-Villar**, C. Hochenauer, R. Scharler, and A. Anca-Couce.*Fuel*, 305: 121531, 2021. https://doi.org/10.1016/j.fuel.2021.121531

8. Assessment of measurement methods to characterize the producer gas from biomass gasification with steam in a fluidized bed. A. Anca-Couce, L. von Berg, G. Pongratz, R. Scharler, C. Hochenauer, M. Geusebroek, J. Kuipers, C. M. Vilela, T. Kraia, K. Panopoulos, I. Funcia, A. Dieguez-Alonso, **H. Almuina-Villar**, N. Kienzl, and S. Martini. Submitted to *Biomass and Bioenergy*, 2021.

A.3 Oral and visual presentations

1. Laser-based spectroscopy diagnosis and detailed numerical models to gain understanding on the slow pyrolysis behavior of thermally thick wood particles. **H. Almuina-Villar**, A. Anca-Couce, N. Lang, J. Röpcke, F. Behrendt, A. Dieguez-Alonso. International Conference on Biomass, Bologna, Italy, June 2018.

2. Laser-based spectroscopy techniques applied to pyrolysis. **H. Almuina-Villar**, A. Dieguez-Alonso, N. Lang, J. Röpcke, F. Behrendt. 37th International Symposium on Combustion, Dublin, Ireland, July 2018.

Bibliography

[1] European Commission. Eu climate action and the european green deal. Website. Online available at: https://ec.europa.eu/clima/policies/eu-climate-action_en. Last accesed 01-October-2021.

[2] European Commission. Energy. Renewable energy targets. Website. Online available at: https://ec.europa.eu/energy/topics/renewable-energy/directive-targets-and-rules/renewable-energy-targets_en. Last accesed 01-October-2021.

[3] European Commission. Energy. Renewable energy directive. Website. Online available at: https://ec.europa.eu/energy/topics/renewable-energy/directive-targets-and-rules/renewable-energy-directive_en. Last accesed 01-October-2021.

[4] European Commission. Energy. Renewable energy. Solar power. Website. Online available at: https://ec.europa.eu/energy/topics/renewable-energy/solar-power_en. Last accesed 02-October-2021.

[5] P. McKendry. Energy production from biomass (part 1): overview of biomass. *Bioresource Technology*, 83(1):37–46, 2002. Reviews Issue. doi:10.1016/S0960-8524(01)00118-3.

[6] A. Dieguez-Alonso. *Fixed-bed biomass pyrolysis: mechanisms and biochar production*. PhD thesis, Technische Universität Berlin, 2015. ISBN online: 978-3-945682-22-7.

[7] S. V. Vassilev, D. Baxter, L. K. Andersen, and C. G. Vassileva. An overview of the chemical composition of biomass. *Fuel*, 89(5):913–933, 2010. doi:10.1016/j.fuel.2009.10.022.

[8] A. Anca-Couce. Reaction mechanisms and multi-scale modelling of lignocellulosic biomass pyrolysis. *Progress in Energy and Combustion Science*, 53:41–79, 2016. doi:10.1016/j.pecs.2015.10.002.

[9] European Commission. Energy. Renewable energy. Biomass. Website. Online available at: https://ec.europa.eu/energy/topics/renewable-energy/biomass_en#eu-rules-on-sustainable-biomass. Last accesed 02-October-2021.

[10] P. McKendry. Energy production from biomass (part 2): conversion technologies. *Bioresource Technology*, 83(1):47–54, 2002. Reviews Issue. doi:10.1016/S0960-8524(01)00119-5.

[11] P. Basu. Chapter 1 - Introduction. In P. Basu, editor, *Biomass Gasification and Pyrolysis*, pages 1–25. Academic Press, Boston, 2010. doi:10.1016/B978-0-12-374988-8.00001-5.

[12] Y. Dahman, K. Syed, S. Begum, P. Roy, and B. Mohtasebi. 14 - Biofuels: Their characteristics and analysis. In D. Verma, E. Fortunati, S. Jain, and X. Zhang, editors, *Biomass, Biopolymer-Based Materials, and Bioenergy*, Woodhead Publishing Series in Composites Science and Engineering, pages 277–325. Woodhead Publishing, 2019. doi:10.1016/B978-0-08-102426-3.00014-X.

[13] B. Abdullah, S. A. F. Syed Muhammad, Z. Shokravi, S. Ismail, K. A. Kassim, A. N. Mahmood, and M. M. A. Aziz. Fourth generation biofuel: A review on risks and mitigation strategies. *Renewable and Sustainable Energy Reviews*, 107:37–50, 2019. doi:10.1016/j.rser.2019.02.018.

[14] P. Basu. Chapter 3 - Pyrolysis and Torrefaction. In P. Basu, editor, *Biomass Gasification and Pyrolysis*, pages 65–96. Academic Press, Boston, 2010. doi:10.1016/B978-0-12-374988-8.00003-9.

[15] F. Behrendt, Y. Neubauer, M. Oevermann, B. Wilmes, and N. Zobel. Direct liquefaction of biomass. *Chemical Engineering & Technology*, 31(5):667–677, 2008. doi:10.1002/ceat.200800077.

[16] A. Funke and F. Ziegler. Hydrothermal carbonization of biomass: A summary and discussion of chemical mechanisms for process engineering. *Biofuels, Bioproducts and Biorefining*, 4(2):160–177, 2010. doi:10.1002/bbb.198.

[17] T. Nussbaumer. Overview on Technologies for Biomass Combustion and Emission Levels of Particulate Matter, prepared for Swiss Federal Office for the Environment (FOEN) as a contribution to the Expert Group on Techno-Economic Issues (EGTEI) under the Convention on Long-Range Transboundary Air Pollution (CLRTAP). Technical report, Verenum. Ingenieurbüro für Verfahrens-, Energie- und Umwelttechnik, June 2010.

[18] A.V. Bridgwater. Review of fast pyrolysis of biomass and product upgrading. *Biomass and Bioenergy*, 38:68–94, 2012. doi:10.1016/j.biombioe.2011.01.048.

[19] C. Di Blasi. Combustion and gasification rates of lignocellulosic chars. *Progress in Energy and Combustion Science*, 35(2):121–140, 2009. doi:10.1016/j.pecs.2008.08.001.

[20] S. Wang, G. Dai, H. Yang, and Z. Luo. Lignocellulosic biomass pyrolysis mechanism: A state-of-the-art review. *Progress in Energy and Combustion Science*, 62:33–86, 2017. doi:10.1016/j.pecs.2017.05.004.

[21] P. Giudicianni, V. Gargiulo, C. M. Grottola, M. Alfè, A. I. Ferreiro, M. A. A. Mendes, M. Fagnano, and R. Ragucci. Inherent metal elements in biomass pyrolysis: A review. *Energy & Fuels*, 35(7):5407–5478, 2021. doi:10.1021/acs.energyfuels.0c04046.

[22] K. Weber and P. Quicker. Properties of biochar. *Fuel*, 217:240–261, 2018. doi:10.1016/j.fuel.2017.12.054.

[23] D. Mohan, C. U. Pittman, and P. H. Steele. Pyrolysis of wood/biomass for bio-oil: a critical review. *Energy & Fuels*, 20(3):848–889, 2006. doi:10.1021/ef0502397.

[24] R. J. Evans and T. A. Milne. Molecular characterization of the pyrolysis of biomass. *Energy & Fuels*, 1(2):123–137, 1987. doi:10.1021/ef00002a001.

[25] R. J. Evans and T. A. Milne. Molecular characterization of the pyrolysis of biomass. 2. applications. *Energy & Fuels*, 1(4):311–319, 1987. doi:10.1021/ef00004a001.

[26] T. A. Milne, R. J. Evans, and N. Abatzaglou. Biomass Gasifier "Tars": Their Nature, Formation, and Conversion. *Tech. rep., National Renewable Energy Laboratory*, 1998. doi:10.2172/3726.

[27] A. Gómez-Barea and B. Leckner. Modeling of biomass gasification in fluidized bed. *Progress in Energy and Combustion Science*, 36(4):444–509, 2010. doi:10.1016/j.pecs.2009.12.002.

[28] A. Dieguez-Alonso, A. Anca-Couce, N. Zobel, and F. Behrendt. Understanding the primary and secondary slow pyrolysis mechanisms of holocellulose, lignin and wood with laser-induced fluorescence. *Fuel*, 153:102–109, 2015. doi:10.1016/j.fuel.2015.02.097.

[29] A. Dieguez-Alonso, A. Anca-Couce, and N. Zobel. On-line tar characterization from pyrolysis of wood particles in a technical-scale fixed-bed reactor by applying laser-induced fluorescence (LIF). *Journal of Analytical and Applied Pyrolysis*, 102:33–46, 2013. doi:10.1016/j.jaap.2013.04.005.

[30] N. Zobel and A. Anca-Couce. Slow pyrolysis of wood particles: Characterization of volatiles by laser-induced fluorescence. *Proceedings of the Combustion Institute*, 34(2):2355–2362, 2013. doi:10.1016/j.proci.2012.06.130.

[31] S. V. Vassilev, D. Baxter, L. K. Andersen, C. G. Vassileva, and T. J. Morgan. An overview of the organic and inorganic phase composition of biomass. *Fuel*, 94:1–33, 2012. doi:10.1016/j.fuel.2011.09.030.

[32] P. Basu. Chapter 2 - Biomass characteristics. In P. Basu, editor, *Biomass Gasification and Pyrolysis*, pages 27–63. Academic Press, Boston, 2010. doi:10.1016/B978-0-12-374988-8.00002-7.

[33] Pushkaraj R. Patwardhan, Robert C. Brown, and Brent H. Shanks. Product distribution from the fast pyrolysis of hemicellulose. *ChemSusChem*, 4(5):636–643, 2011. doi:10.1002/cssc.201000425.

[34] E. Ranzi, A. Cuoci, T. Faravelli, A. Frassoldati, G. Migliavacca, S. Pierucci, and S. Sommariva. Chemical kinetics of biomass pyrolysis. *Energy Fuels*, 22(6):4292–4300, 2008. doi:10.1021/ef800551t.

[35] S. Wang, B. Ru, H. Lin, W. Sun, and Z. Luo. Pyrolysis behaviors of four lignin polymers isolated from the same pine wood. *Bioresource Technology*, 182:120–127, 2015. doi:10.1016/j.biortech.2015.01.127.

[36] P. Giudicianni, A. I. Ferreiro, V. Gargiulo, M. Alfe, M. Costa, M. Rabacal, and R. Ragucci. Effect of kcl doping on the slow pyrolysis of lignin. *Chemical Engineering Transactions*, 80:109–114, Jun. 2020. doi:10.3303/CET2080019.

[37] D. J. Nowakowski and J. M. Jones. Uncatalysed and potassium-catalysed pyrolysis of the cell-wall constituents of biomass and their model compounds. *Journal of Analytical and Applied Pyrolysis*, 83(1):12–25, 2008. doi:10.1016/j.jaap.2008.05.007.

[38] E. Jakab, O. Faix, F. Till, and T. Székely. The effect of cations on the thermal decomposition of lignins. *Journal of Analytical and Applied Pyrolysis*, 25:185–194, 1993. Proceedings of the 10th International Conference on Fundamental Aspects, Processes and Applications of Pyrolysis. doi:10.1016/0165-2370(93)80039-3.

[39] E. Jakab, O. Faix, and F. Till. Thermal decomposition of milled wood lignins studied by thermogravimetry/mass spectrometry. *Journal of Analytical and Applied Pyrolysis*, 40-41:171–186, 1997. doi:10.1016/S0165-2370(97)00046-6.

[40] P. E. A. Debiagi, C. Pecchi, G. Gentile, A. Frassoldati, A. Cuoci, T. Faravelli, and E. Ranzi. Extractives extend the applicability of multistep kinetic scheme of biomass pyrolysis. *Energy & Fuels*, 29(10):6544–6555, 2015. doi:10.1021/acs.energyfuels.5b01753.

[41] A. Trendewicz, R. Evans, A. Dutta, R. Sykes, D. Carpenter, and R. Braun. Evaluating the effect of potassium on cellulose pyrolysis reaction kinetics. *Biomass and Bioenergy*, 74:15–25, 2015. doi:10.1016/j.biombioe.2015.01.001.

[42] E. Ranzi, M. Corbetta, F. Manenti, and S. Pierucci. Kinetic modeling of the thermal degradation and combustion of biomass. *Chemical Engineering Science*, 110:2–12, 2014. Mackie-2013 "Pushing the boundaries". doi:10.1016/j.ces.2013.08.014.

[43] M. Corbetta, A. Frassoldati, H. Bennadji, K. Smith, M. J. Serapiglia, G. Gauthier, T. Melkior, E. Ranzi, and E. M. Fisher. Pyrolysis of centimeter-scale woody biomass particles: Kinetic modeling and experimental validation. *Energy & Fuels*, 28(6):3884–3898, 2014. doi:10.1021/ef500525v.

[44] A. Anca-Couce, R. Mehrabian, R. Scharler, and I. Obernberger. Kinetic scheme of biomass pyrolysis considering secondary charring reactions. *Energy Conversion and Management*, 87:687–696, 2014. doi:10.1016/j.enconman.2014.07.061.

[45] A. Anca-Couce, P. Sommersacher, and R. Scharler. Online experiments and modelling with a detailed reaction scheme of single particle biomass pyrolysis. *Journal of Analytical and Applied Pyrolysis*, 127:411 – 425, 2017. doi:10.1016/j.jaap.2017.07.008.

[46] T. Hosoya, H. Kawamoto, and S. Saka. Pyrolysis behaviors of wood and its constituent polymers at gasification temperature. *Journal of Analytical and Applied Pyrolysis*, 78(2):328–336, 2007. doi:10.1016/j.jaap.2006.08.008.

[47] Q. Liu, Z. Zhong, S. Wang, and Z. Luo. Interactions of biomass components during pyrolysis: A tg-ftir study. *Journal of Analytical and Applied Pyrolysis*, 90(2):213–218, 2011. doi:10.1016/j.jaap.2010.12.009.

[48] S. Wang, X. Guo, K. Wang, and Z. Luo. Influence of the interaction of components on the pyrolysis behavior of biomass. *Journal of Analytical and Applied Pyrolysis*, 91(1):183–189, 2011. doi:10.1016/j.jaap.2011.02.006.

[49] J. Zhang, Y. S. Choi, C. G. Yoo, T. H. Kim, R. C. Brown, and B. H. Shanks. Cellulose–hemicellulose and cellulose–lignin interactions during fast pyrolysis. *ACS Sustainable Chemistry & Engineering*, 3(2):293–301, 2015. doi:10.1021/sc500664h.

[50] C. Di Blasi. Comparison of semi-global mechanisms for primary pyrolysis of lignocellulosic fuels. *Journal of Analytical and Applied Pyrolysis*, 47(1):43–64, 1998. doi:10.1016/S0165-2370(98)00079-5.

[51] J. E. White, W. J. Catallo, and B. L. Legendre. Biomass pyrolysis kinetics: A comparative critical review with relevant agricultural residue case studies. *Journal of Analytical and Applied Pyrolysis*, 91(1):1–33, 2011. doi:doi.org/10.1016/j.jaap.2011.01.004.

[52] T. Faravelli, A. Frassoldati, and E. M. Ranzi. Modellazione dettagliata della pirolisi di biomasse: Modelli cinetici di de volatilizzazione. *La Rivista dei Combustibili e dell'Industria Chimica*, 61(5):249–270, 2007. URL: http://hdl.handle.net/11311/515086.

[53] T. Faravelli, A. Frassoldati, G. Migliavacca, and E. Ranzi. Detailed kinetic modeling of the thermal degradation of lignins. *Biomass and Bioenergy*, 34(3):290–301, 2010. doi:10.1016/j.biombioe.2009.10.018.

[54] M. B. Pecha, J. I. M. Arbelaez, M. Garcia-Perez, F. Chejne, and P. N. Ciesielski. Progress in understanding the four dominant intra-particle phenomena of lignocellulose pyrolysis: chemical reactions, heat transfer, mass transfer, and phase change. *Green Chemistry*, 21:2868–2898, 2019. doi:10.1039/C9GC00585D.

[55] E. Ranzi, A. Frassoldati, R. Grana, A. Cuoci, T. Faravelli, A. P. Kelley, and C. K Law. Hierarchical and comparative kinetic modeling of laminar flame speeds of hydrocarbon and oxygenated fuels. *Progress in Energy and Combustion Science*, 38(4):468–501, 2012. doi:10.1016/j.pecs.2012.03.004.

[56] A. Broido. Kinetics of solid-phase cellulose pyrolysis. In F Shafizadeh, Kyosti V. Sarkanen, and David A. Tillman, editors, *Thermal Uses and Properties of Carbohydrates and Lignins*, pages 19–36. Academic Press, 1976. doi:10.1016/B978-0-12-637750-7.50006-6.

[57] F. Shafizadeh. Introduction to pyrolysis of biomass. *Journal of Analytical and Applied Pyrolysis*, 3(4):283–305, 1982. doi:10.1016/0165-2370(82)80017-X.

[58] J. Piskorz, D. St.A.G. Radlein, D. S. Scott, and S. Czernik. Pretreatment of wood and cellulose for production of sugars by fast pyrolysis. *Journal of Analytical and Applied Pyrolysis*, 16(2):127–142, 1989. doi:10.1016/0165-2370(89)85012-0.

[59] M. J. Antal Jr. and G. Varhegyi. Cellulose pyrolysis kinetics: The current state of knowledge. *Industrial & Engineering Chemistry Research*, 34(3):703–717, 1995. doi:10.1021/ie00042a001.

[60] V. Mamleev, S. Bourbigot, M. Le Bras, and J. Yvon. The facts and hypotheses relating to the phenomenological model of cellulose pyrolysis: Interdependence of the steps. *Journal of Analytical and Applied Pyrolysis*, 84(1):1–17, 2009. doi:10.1016/j.jaap.2008.10.014.

[61] E. Leng, Y. Wang, X. Gong, B. Zhang, Y. Zhang, and M. Xu. Effect of kcl and cacl2 loading on the formation of reaction intermediates during cellulose fast pyrolysis. *Proceedings of the Combustion Institute*, 36(2):2263–2270, 2017. doi:10.1016/j.proci.2016.06.167.

[62] A. I. Ferreiro, M. Rabaçal, M. Costa, P. Giudicianni, C. M. Grottola, and R. Ragucci. Modeling the impact of the presence of kcl on the slow pyrolysis of cellulose. *Fuel*, 215:57–65, 2018. doi:https://doi.org/10.1016/j.fuel.2017.11.019.

[63] E. Leng, M. Costa, X. Gong, A. Zheng, S. Liu, and M. Xu. Effects of kcl and cacl2 on the evolution of anhydro sugars in reaction intermediates during cellulose fast pyrolysis. *Fuel*, 251:307–315, 2019. doi:10.1016/j.fuel.2019.04.006.

[64] G. Várhegyi, P. Szabó, W. S.-L. Mok, and M.J. Antal Jr. Kinetics of the thermal decomposition of cellulose in sealed vessels at elevated pressures. effects of the presence of water on the reaction mechanism. *Journal of Analytical and Applied Pyrolysis*, 26(3):159–174, 1993. doi:10.1016/0165-2370(93)80064-7.

[65] J.L. Banyasz, S. Li, J. Lyons-Hart, and K.H. Shafer. Gas evolution and the mechanism of cellulose pyrolysis. *Fuel*, 80(12):1757–1763, 2001. doi:10.1016/S0016-2361(01)00060-6.

[66] Y. Lin, J. Cho, G. A. Tompsett, P. R. Westmoreland, and G. W. Huber. Kinetics and mechanism of cellulose pyrolysis. *The Journal of Physical Chemistry C*, 113(46):20097–20107, 2009. doi:10.1021/jp906702p.

[67] P. R. Patwardhan, J. A. Satrio, R. C. Brown, and B. H. Shanks. Influence of inorganic salts on the primary pyrolysis products of cellulose. *Bioresource Technology*, 101(12):4646 – 4655, 2010. doi:10.1016/j.biortech.2010.01.112.

[68] Y. Le Brech, T. Ghislain, S. Leclerc, M. Bouroukba, L. Delmotte, N. Brosse, C. Snape, P. Chaimbault, and A. Dufour. Effect of potassium on the mechanisms of biomass pyrolysis studied using complementary analytical techniques. *ChemSusChem*, 9(8):863–872, 2016. doi:10.1002/cssc.201501560.

[69] X. Zhou, W. Li, R. Mabon, and L. J. Broadbelt. A mechanistic model of fast pyrolysis of hemicellulose. *Energy Environ. Sci.*, 11:1240–1260, 2018. doi:10.1039/C7EE03208K.

[70] C. Di Blasi and M. Lanzetta. Intrinsic kinetics of isothermal xylan degradation in inert atmosphere. *Journal of Analytical and Applied Pyrolysis*, 40-41:287–303, 1997. doi:10.1016/S0165-2370(97)00028-4.

[71] G. Varhegyi, M. J. Antal, T. Szekely, and P. Szabo. Kinetics of the thermal decomposition of cellulose, hemicellulose, and sugarcane bagasse. *Energy & Fuels*, 3(3):329–335, 1989. doi:10.1021/ef00015a012.

[72] D.K. Shen, S. Gu, and A.V. Bridgwater. Study on the pyrolytic behaviour of xylan-based hemicellulose using TG–FTIR and Py–GC–FTIR. *Journal of*

Analytical and Applied Pyrolysis, 87(2):199–206, 2010. doi:10.1016/j.jaap.2009.12.001.

[73] J. Wang, M. Asmadi, and H. Kawamoto. The effect of uronic acid moieties on xylan pyrolysis. *Journal of Analytical and Applied Pyrolysis*, 136:215–221, 2018. doi:10.1016/j.jaap.2018.10.002.

[74] P. Giudicianni, V. Gargiulo, C. M. Grottola, M. Alfè, and R. Ragucci. Effect of alkali metal ions presence on the products of xylan steam assisted slow pyrolysis. *Fuel*, 216:36–43, 2018. doi:10.1016/j.fuel.2017.11.150.

[75] P. Giudicianni, V. Gargiulo, M. Alfè, R. Ragucci, A.I. Ferreiro, M. Rabaçal, and M. Costa. Slow pyrolysis of xylan as pentose model compound for hardwood hemicellulose: A study of the catalytic effect of na ions. *Journal of Analytical and Applied Pyrolysis*, 137:266–275, 2019. doi:10.1016/j.jaap.2018.12.004.

[76] Shuai Zhou, Brennan Pecha, Michiel van Kuppevelt, Armando G. McDonald, and Manuel Garcia-Perez. Slow and fast pyrolysis of douglas-fir lignin: Importance of liquid-intermediate formation on the distribution of products. *Biomass and Bioenergy*, 66:398–409, 2014. doi:10.1016/j.biombioe.2014.03.064.

[77] C. Di Blasi, A. Galgano, and C. Branca. Effects of potassium hydroxide impregnation on wood pyrolysis. *Energy & Fuels*, 23(2):1045–1054, 2009. doi:10.1021/ef800827q.

[78] S. B. Nordin, J. O. Nyren, and E. L. Back. An indication of molten cellulose produced in a laser beam. *Textile Research Journal*, 44(2):152–154, 1974. doi:10.1177/004051757404400211.

[79] F. J. Kilzer and A. Broido. Speculations on the nature of cellulose pyrolysis. *Pyrodinamics*, 2:151–163, 1965.

[80] A. Dufour, M. Castro-Diaz, N. Brosse, M. Bouroukba, and C. Snape. The origin of molecular mobility during biomass pyrolysis as revealed by in situ 1H NMR spectroscopy. *ChemSusChem*, 5(7):1258–1265, 2012. doi:10.1002/cssc.201100442.

[81] N. Zobel and A. Anca-Couce. Influence of intraparticle secondary heterogeneous reactions on the reaction enthalpy of wood pyrolysis. *Journal of Analytical and Applied Pyrolysis*, 116:281–286, 2015. doi:10.1016/j.jaap.2015.08.019.

[82] S. Ciuta, F. Patuzzi, M. Baratieri, and M. J. Castaldi. Biomass energy behavior study during pyrolysis process by intraparticle gas sampling. *Journal of Analytical and Applied Pyrolysis*, 108(Supplement C):316 – 322, 2014. doi:10.1016/j.jaap.2014.04.012.

[83] W. C. Park, A. Atreya, and H. R. Baum. Experimental and theoretical investigation of heat and mass transfer processes during wood pyrolysis. *Combustion and Flame*, 157(3):481–494, 2010. doi:10.1016/j.combustflame.2009.10.006.

[84] G. Gauthier, T. Melkior, S. Salvador, M. Corbetta, A. Frassoldati, S. Pierucci, E. Ranzi, H. Bennadjid, and E.M. Fisher. Pyrolysis of thick biomass particles: Experimental and kinetic modelling. *Chemical Engineering Transactions*, 32:601–606, 2013. doi:10.3303/CET1332101.

[85] K. Norinaga, T. Shoji, S. Kudo, and J.-I. Hayashi. Detailed chemical kinetic modelling of vapour-phase cracking of multi-component molecular mixtures derived from the fast pyrolysis of cellulose. *Fuel*, 103:141–150, 2013. doi:10.1016/j.fuel.2011.07.045.

[86] H. Bennadji, K. Smith, S. Shabangu, and E. M. Fisher. Low-temperature pyrolysis of woody biomass in the thermally thick regime. *Energy & Fuels*, 27(3):1453–1459, 2013. doi:10.1021/ef400079a.

[87] H. Bennadji, K. Smith, M. J. Serapiglia, and E. M. Fisher. Effect of particle size on low-temperature pyrolysis of woody biomass. *Energy & Fuels*, 28(12):7527–7537, 2014. doi:10.1021/ef501869e.

[88] L. Wang, Ø. Skreiberg, M. Gronli, G. P. Specht, and M. J. Antal. Is elevated pressure required to achieve a high fixed-carbon yield of charcoal from biomass? part 2: The importance of particle size. *Energy & Fuels*, 27(4):2146–2156, 2013. doi:10.1021/ef400041h.

[89] A. Anca-Couce, A. Dieguez-Alonso, N. Zobel, A. Berger, N. Kienzl, and F. Behrendt. Influence of heterogeneous secondary reactions during slow pyrolysis on char oxidation reactivity of woody biomass. *Energy & Fuels*, 31(3):2335–2344, 2017. doi:10.1021/acs.energyfuels.6b02350.

[90] CEN/TC BT/TF 143. Biomass Gasification – Tar and Particles in Product Gases – Sampling and Analysis, 2004.

[91] M. Staš, D. Kubička, J. Chudoba, and M. Pospíšil. Overview of analytical methods used for chemical characterization of pyrolysis bio-oil. *Energy & Fuels*, 28(1):385–402, 2014. doi:10.1021/ef402047y.

[92] D.C. Harris and C.A. Lucy. *Quantitative Chemical Analysis*. W. H. Freeman, 2019.

[93] C. Branca, P. Giudicianni, and C. Di Blasi. Gc/ms characterization of liquids generated from low-temperature pyrolysis of wood. *Industrial & Engineering Chemistry Research*, 42(14):3190–3202, 2003. doi:10.1021/ie030066d.

[94] C. Zhang, L. Chao, Z. Zhang, L. Zhang, Q. Li, H. Fan, S. Zhang, Q. Liu, Y. Qiao, Y. Tian, Y. Wang, and X. Hu. Pyrolysis of cellulose: Evolution of functionalities and structure of bio-char versus temperature. *Renewable and Sustainable Energy Reviews*, 135:110416, 2021. doi:10.1016/j.rser.2020.110416.

[95] R. Bassilakis, R.M. Carangelo, and M.A. Wójtowicz. TG-FTIR analysis of biomass pyrolysis. *Fuel*, 80(12):1765–1786, 2001. doi:10.1016/S0016-2361(01)00061-8.

[96] W. de Jong, A. Pirone, and M.A. Wójtowicz. Pyrolysis of miscanthus giganteus and wood pellets: TG-FTIR analysis and reaction kinetics. *Fuel*, 82(9):1139–1147, 2003. doi:10.1016/S0016-2361(02)00419-2.

[97] H. Yang, R. Yan, H. Chen, D. H. Lee, and C. Zheng. Characteristics of hemicellulose, cellulose and lignin pyrolysis. *Fuel*, 86(12):1781–1788, 2007. doi:10.1016/j.fuel.2006.12.013.

[98] T. Siengchum, M. Isenberg, and S. S.C. Chuang. Fast pyrolysis of coconut biomass – an FTIR study. *Fuel*, 105:559–565, 2013. doi:10.1016/j.fuel.2012.09.039.

[99] C. Hao, S. Wu, and C. Liu. Study on the mechanism of the pyrolysis of a lignin monomeric model compound by in situ ftir. *BioResources*, 9(3):4441–4448, 2014.

[100] M. Tacke, F. Wienhold, R. Grisar, H. Fischer, and F.-J. Lübken. The use of tunable diode laser absorption spectroscopy for atmospheric measurements. In R.A. Meyers, editor, *Encyclopedia of Analytical Chemistry*, volume 3 of *Chemical Analysis Series*, chapter Section Environment: Trace Gas Monitoring, page 2033. Wiley, Chichester, UK, 2000.

[101] P. Werle, F. Slemr, K. Maurer, R. Kormann, R. Mücke, and B. Jänker. Near- and mid-infrared laser-optical sensors for gas analysis. *Optics and Lasers in Engineering*, 37(2):101–114, 2002. Optical Methods in Earth Sciences. doi:10.1016/S0143-8166(01)00092-6.

[102] J. Röpcke, G. Lombardi, A. Rousseau, and P. B. Davies. Application of mid-infrared tuneable diode laser absorption spectroscopy to plasma diagnostics: a review. *Plasma Sources Science and Technology*, 15(4):S148–S168, 2006. doi:10.1088/0963-0252/15/4/s02.

[103] H. I. Schiff, G. I. Mackay, and J. Bechara. The use of tunable diode laser absorption spectroscopy for atmospheric measurements. *Research on Chemical Intermediates*, 20:525–556, 1994. doi:10.1163/156856794X00441.

[104] P. A. Martin. Near-infrared diode laser spectroscopy in chemical process and environmental air monitoring. *Chem. Soc. Rev.*, 31:201–210, 2002. doi:10.1039/B003936P.

[105] K. Clemitshaw. A review of instrumentation and measurement techniques for ground-based and airborne field studies of gas-phase tropospheric chemistry. *Critical Reviews in Environmental Science and Technology*, 34(1):1–108, 2004. doi:10.1080/10643380490265117.

[106] M. S. Zahniser, D. D. Nelson, B. McManus, P. L. Kebabian, D. Lloyd, D. Fowler, D. S. Jenkinson, J. L. Monteith, and M. H. Unsworth. Measurement of trace gas fluxes using tunable diode laser spectroscopy. *Philosophical Transactions of the Royal Society of London. Series A: Physical and Engineering Sciences*, 351(1696):371–382, 1995. doi:10.1098/rsta.1995.0040.

[107] T. Mouton, X. Mercier, and P. Desgroux. Isomer discrimination of PAHs formed in sooting flames by jet-cooled laser-induced fluorescence: application to the measurement of pyrene and fluoranthene. *Applied Physics B*, 122:123, 2016. doi:10.1007/s00340-016-6397-9.

[108] F. Ossler, T. Metz, and M. Aldén. Picosecond laser-induced fluorescence from gas-phase polycyclic aromatic hydrocarbons at elevated temperatures. i. cell measurements. *Applied Physics B*, 72:465–478, 2001. doi:10.1007/s003400100519.

[109] J. R. Lakowicz. *Principles of Fluorescence Spectroscopy*. Springer, 3rd edition, 2006. doi:10.1007/978-0-387-46312-4.

[110] D.C. Harris. *Quantitative Chemical Analysis*. W. H. Freeman and Company, 8th edition, 2010.

[111] D. A. Skoog, F. J. Holler, and S. R. Crouch. *Principles of instrumental analysis*. Thomson, Brooks/Cole, 6th edition, 2007.

[112] H. Keller-Rudek, G. K. Moortgat, R. Sander, and R. Sörensen. The MPI-Mainz UV/VIS spectral atlas of gaseous molecules of atmospheric interest. *Earth Syst. Sci. Data*, 5, 2013. Last accesed: 01.09.2021. doi:10.5194/essd-5-365-2013.

[113] L. J. Jandris and R. Ken Forcé. Determination of polynuclear aromatic hydrocarbons in vapor phases by laser-induced molecular fluorescence. *Analytica Chimica Acta*, 151:19 – 27, 1983. doi:10.1016/S0003-2670(00)80057-4.

[114] J. Borgmeyer and F. Behrendt. On-line tar monitoring using light-induced fluorescence: A setup for continuous operation in a biomass gasification plant environment. *Optics and Laser Technology*, 123:105906, 2020. doi:10.1016/j.optlastec.2019.105906.

[115] C. Brackmann, M. Aldén, P. E. Bengtsson, K. O. Davidsson, and J. B. C. Pettersson. Optical and mass spectrometric study of the pyrolysis gas of wood particles. *Applied Spectroscopy*, 57(2):216–222, 2003. doi:10.1366/000370203321535141.

[116] F. Ferreira da Silva, E. Lange, P. Limão-Vieira, N.C. Jones, S.V. Hoffmann, M.-J. Hubin-Franskin, J. Delwiche, M.J. Brunger, R. Neves, M. Lopes, E. Oliveira, R. da Costa, M. Varella, M. Bettega, F. Blanco, G. Garcia, M. Lima, and D.B. Jones. Electronic excitation of furfural as probed by high-resolution vacuum ultraviolet spectroscopy, electron energy loss spectroscopy, and ab initio calculations. *The Journal of Chemical Physics*, 143, 2015. doi:10.1063/1.4932603.

[117] E. Roth, A. Chakir, and A Ferhati. Study of a benzoylperoxy radical in the gas phase: Ultraviolet spectrum and c6h5c(o)o2 + ho2 reaction between 295 and 357 k. *The Journal of Physical Chemistry A*, 114(38):10367–10379, 2010. doi:10.1021/jp1021467.

[118] M. Taniguchi and J. S. Lindsey. Database of absorption and fluorescence spectra of >300 common compounds for use in photochemcad. *Photochemistry and Photobiology*, 94(2):290–327, 2018. doi:10.1111/php.12860.

[119] R. Sun, N. Zobel, Y. Neubauer, C. Cardenas Chavez, and F. Behrendt. Analysis of gas-phase polycyclic aromatic hydrocarbon mixtures by laser-induced fluorescence. *Optics and Lasers in Engineering*, 48(12):1231–1237, 2010. doi:10.1016/j.optlaseng.2010.06.009.

[120] M. de Joannon, R. Ragucci, A. Cavaliere, and A. Ciajolo. Identification of oxygenated compounds in combustion systems. *Chemosphere*, 42(5):843–851, 2001. Proceedings of the 6th Intl Congress on Toxic combustion. doi:10.1016/S0045-6535(00)00259-9.

[121] J. H. Richardson and M. E. Ando. Sub-part-per-trillion detection of polycyclic aromatic hydrocarbons by laser induced molecular fluorescence. *Analytical Chemistry*, 49(7):955–959, 1977. doi:10.1021/ac50015a021.

[122] J.W. Robinson and J.D. Dake. Remote sensing of air pollutants by laser-induced infrared fluorescence—a review. *Analytica Chimica Acta*, 71(2):277 – 288, 1974. doi:10.1016/S0003-2670(01)85431-3.

[123] L. D'Ottone, P. Campuzano-Jost, D. Bauer, and A. J. Hynes. A pulsed laser photolysis-pulsed laser induced fluorescence study of the kinetics of the gas-phase reaction of oh with no2. *The Journal of Physical Chemistry A*, 105(46):10538–10543, 2001. doi:10.1021/jp012250n.

[124] A. Bruno, F. Ossler, C. de Lisio, P. Minutolo, N. Spinelli, and A. D'Alessio. Detection of fluorescent nanoparticles in flame with femtosecond laser-induced

fluorescence anisotropy. *Opt. Express*, 16(8):5623–5632, Apr 2008. doi:10.1364/OE.16.005623.

[125] M. Sirignano, A. Collina, M. Commodo, P. Minutolo, and A. D'Anna. Detection of aromatic hydrocarbons and incipient particles in an opposed-flow flame of ethylene by spectral and time-resolved laser induced emission spectroscopy. *Combustion and Flame*, 159(4):1663 – 1669, 2012. doi:10.1016/j.combustflame.2011.11.005.

[126] S. Karellas and J. Karl. Analysis of the product gas from biomass gasification by means of laser spectroscopy. *Optics and Lasers in Engineering*, 45(9):935 – 946, 2007. doi:10.1016/j.optlaseng.2007.03.006.

[127] C. Baumhakl and S. Karellas. Tar analysis from biomass gasification by means of online fluorescence spectroscopy. *Optics and Lasers in Engineering*, 49(7):885 – 891, 2011. doi:10.1016/j.optlaseng.2011.02.015.

[128] K. Kohse-Höinghaus. *Applied Combustion Diagnostics*. Applied Combustion Diagnostics. Taylor & Francis, 2002.

[129] M.J. Prins, Z.S. Li, R.J.M. Bastiaans, J.A. van Oijen, M. Aldén, and L.P.H. de Goey. Biomass pyrolysis in a heated-grid reactor: Visualization of carbon monoxide and formaldehyde using laser-induced fluorescence. *Journal of Analytical and Applied Pyrolysis*, 92(2):280–286, 2011. doi:10.1016/j.jaap.2011.06.008.

[130] I. Milosavljevic, V. Oja, and E. M. Suuberg. Thermal effects in cellulose pyrolysis: relationship to char formation processes. *Industrial & Engineering Chemistry Research*, 35(3):653–662, 1996. doi:10.1021/ie9504381.

[131] C. Di Blasi. Modeling chemical and physical processes of wood and biomass pyrolysis. *Progress in Energy and Combustion Science*, 34(1):47–90, 2008. doi:10.1016/j.pecs.2006.12.001.

[132] J. J. Manyà, M. A. Ortigosa, S. Laguarta, and J. A. Manso. Experimental study on the effect of pyrolysis pressure, peak temperature, and particle size on the potential stability of vine shoots-derived biochar. *Fuel*, 133:163–172, 2014. doi:10.1016/j.fuel.2014.05.019.

[133] L. Wang, Ø. Skreiberg, S. Van Wesenbeeck, M. Grønli, and M. J. Antal. Experimental study on charcoal production from woody biomass. *Energy & Fuels*, 30(10):7994–8008, 2016. doi:10.1021/acs.energyfuels.6b01039.

[134] J. Rath, M.G. Wolfinger, G. Steiner, G. Krammer, F. Barontini, and V. Cozzani. Heat of wood pyrolysis. *Fuel*, 82(1):81–91, 2003. doi:10.1016/S0016-2361(02)00138-2.

[135] J. Röpcke, P. B. Davies, N. Lang, A. Rousseau, and S. Welzel. Applications of quantum cascade lasers in plasma diagnostics: a review. *Journal of Physics D: Applied Physics*, 45(42):423001, 2012. doi:10.1088/0022-3727/45/42/423001.

[136] J. H. van Helden, N. Lang, U. Macherius, H. Zimmermann, and J. Röpcke. Sensitive trace gas detection with cavity enhanced absorption spectroscopy using a continuous wave external-cavity quantum cascade laser. *Appl. Phys. Lett.*, 103(3):131114, 2013. (Addendum: Appl. Phys. Lett. 104 (2014) 099901, doi: 10.1063/1.4867243). doi:10.1063/1.4823545.

[137] A. S. C. Nave, B. Baudrillart, S. Hamann, F. Bénédic, G. Lombardi, A. Gicquel, J. H. van Helden, and J. Röpcke. Spectroscopic study of low pressure, low temperature h2–CH4–CO2microwave plasmas used for large area deposition of nanocrystalline diamond films. part i: on temperature determination and energetic aspects. *Plasma Sources Science and Technology*, 25(6):065002, 2016. doi:10.1088/0963-0252/25/6/065002.

[138] J. Röpcke, L. Mechold, M. Käning, J. Anders, F. G. Wienhold, D. Nelson, and M. Zahniser. IRMA: A tunable infrared multicomponent acquisition system for plasma diagnostics. *Rev. Sci. Instrum.*, 71(10):3706, 2000. doi:10.1063/1.1290041.

[139] L.S. Rothman, I.E. Gordon, Y. Babikov, A. Barbe, D. Chris Benner, P.F. Bernath, M. Birk, L. Bizzocchi, V. Boudon, L.R. Brown, A. Campargue, K. Chance, E.A. Cohen, L.H. Coudert, V.M. Devi, B.J. Drouin, A. Fayt, J.-M. Flaud, R.R. Gamache, J.J. Harrison, J.-M. Hartmann, C. Hill, J.T. Hodges, D. Jacquemart, A. Jolly, J. Lamouroux, R.J. Le Roy, G. Li, D.A. Long, O.M. Lyulin, C.J. Mackie, S.T. Massie, S. Mikhailenko, H.S.P. Müller, O.V. Naumenko, A.V. Nikitin, J. Orphal, V. Perevalov, A. Perrin, E.R. Polovtseva, C. Richard, M.A.H. Smith, E. Starikova, K. Sung, S. Tashkun, J. Tennyson, G.C. Toon, Vl.G. Tyuterev, and G. Wagner. The hitran2012 molecular spectroscopic database. *Journal of Quantitative Spectroscopy and Radiative Transfer*, 130:4–50, 2013. HITRAN2012 special issue. doi:10.1016/j.jqsrt.2013.07.002.

[140] D. D. Nelson, J. H. Shorter, J. B. McManus, and M. S. Zahniser. Sub-part-per-billion detection of nitric oxide in air using a thermoelectrically cooled mid-infrared quantum cascade laser spectrometer. *Applied Physics B*, 75(2):343, 2002. doi:10.1007/s00340-002-0979-4.

[141] M. G. Grønli, G. Várhegyi, and C. Di Blasi. Thermogravimetric analysis and devolatilization kinetics of wood. *Industrial & Engineering Chemistry Research*, 41(17):4201–4208, 2002. doi:10.1021/ie0201157.

[142] K. Slopiecka, P. Bartocci, and F. Fantozzi. Thermogravimetric analysis and kinetic study od poplar wood pyrolysis. In *Third International Conference on Applied Energy.*, pages 1687 – 1698, 2011. 16-18 May 2011 - Perugia, Italy.

[143] A. Anca-Couce, N. Zobel, A. Berger, and F. Behrendt. Smouldering of pine wood: Kinetics and reaction heats. *Combustion and Flame*, 159(4):1708–1719, 2012. doi:10.1016/j.combustflame.2011.11.015.

[144] A. P. Schinkel. *Zur Bildung und Degradation von Teeren aus der Pyrolyse nachwachsender Rohstoffe*. PhD thesis, Universitaet Kassel, 2008. ISBN online: 978-3-89958-709-4.

[145] M. L. Boroson, J. B. Howard, J. P. Longwell, and W. A. Peters. Heterogeneous cracking of wood pyrolysis tars over fresh wood char surfaces. *Energy & Fuels*, 3(6):735–740, 1989. doi:10.1021/ef00018a014.

[146] L. Fagernäs, E. Kuoppala, K. Tiilikkala, and A. Oasmaa. Chemical composition of birch wood slow pyrolysis products. *Energy & Fuels*, 26(2):1275–1283, 2012. doi:10.1021/ef2018836.

[147] C. Di Blasi, C. Branca, and A. Galgano. On the experimental evidence of exothermicity in wood and biomass pyrolysis. *Energy Technology*, 5(1):19–29, 2017. doi:10.1002/ente.201600091.

[148] R.S. Miller and J. Bellan. A generalized biomass pyrolysis model based on superimposed cellulose, hemicellulose and lignin kinetics. *Combustion Science and Technology*, 126(1-6):97–137, 1997. doi:10.1080/00102209708935670.

[149] N. Lang, C. Rupp, H. Almuina-Villar, A. Dieguez-Alonso, F. Behrendt, and J. Röpcke. Pyrolysis behavior of thermally thick wood particles: Time-resolved characterization with laser based in-situ diagnostics. *Fuel*, 210:371–379, 2017. doi:10.1016/j.fuel.2017.08.077.

[150] A. Anca-Couce and R. Scharler. Modelling heat of reaction in biomass pyrolysis with detailed reaction schemes. *Fuel*, 206:572–579, 2017. doi:10.1016/j.fuel.2017.06.011.

[151] M. L. Boroson, J. B. Howard, J. P. Longwell, and W. A. Peters. Product yields and kinetics from the vapor phase cracking of wood pyrolysis tars. *AIChE Journal*, 35(1):120–128, 1989. doi:10.1002/aic.690350113.

[152] P. Morf, P. Hasler, and T. Nussbaumer. Mechanisms and kinetics of homogeneous secondary reactions of tar from continuous pyrolysis of wood chips. *Fuel*, 81(7):843–853, 2002. doi:10.1016/S0016-2361(01)00216-2.

[153] A.G. Liden, F. Berruti, and D.S. Scott. A kinetic model for the production of liquids from the flash pyrolysis of biomass. *Chemical Engineering Communications*, 65(1):207–221, 1988. doi:10.1080/00986448808940254.

[154] X. Shi, F. Ronsse, and J. G. Pieters. Finite element modeling of intraparticle heterogeneous tar conversion during pyrolysis of woody biomass particles. *Fuel Processing Technology*, 148:302–316, 2016. doi:10.1016/j.fuproc.2016.03.010.

[155] A. K. Sadhukhan, P. Gupta, and R. K. Saha. Modelling of pyrolysis of large wood particles. *Bioresource Technology*, 100(12):3134–3139, 2009. doi:10.1016/j.biortech.2009.01.007.

[156] A. K. Sadhukhan, P. Gupta, and R. K. Saha. Modelling and experimental studies on pyrolysis of biomass particles. *Journal of Analytical and Applied Pyrolysis*, 81(2):183–192, 2008. doi:10.1016/j.jaap.2007.11.007.

[157] P. Ahuja, S. Kumar, and P. C. Singh. A model for primary and heterogeneous secondary reactions of wood pyrolysis. *Chemical Engineering & Technology*, 19(3):272–282, 1996. doi:10.1002/ceat.270190312.

[158] P. T. Williams and P. A. Horne. The role of metal salts in the pyrolysis of biomass. *Renewable Energy*, 4(1):1–13, 1994. doi:10.1016/0960-1481(94)90058-2.

[159] N. Kuzhiyil, D. Dalluge, X. Bai, K. H. Kim, and R. C. Brown. Pyrolytic sugars from cellulosic biomass. *ChemSusChem*, 5(11):2228–2236, 2012. doi:10.1002/cssc.201200341.

[160] C. Di Blasi, C. Branca, and A. Galgano. Role of the potassium chemical state in the global exothermicity of wood pyrolysis. *Industrial & Engineering Chemistry Research*, 57(34):11561–11571, 2018. doi:10.1021/acs.iecr.8b02047.

[161] F. Guo, Y. Liu, Y. Wang, X. Li, T. Li, and C. Guo. Pyrolysis kinetics and behavior of potassium-impregnated pine wood in tga and a fixed-bed reactor. *Energy Conversion and Management*, 130:184–191, 2016. doi:10.1016/j.enconman.2016.10.055.

[162] H. Almuina-Villar, A. Anca-Couce, N. Lang, J. Röpcke, F. Behrendt, and A. Dieguez-Alonso. Laser-based spectroscopy diagnosis and detailed numerical models to gain understanding on the slow pyrolysis behavior of thermally thick wood particles. *Chemical Engineering Transactions*, 65:109 – 114, 2018. doi:10.3303/CET1865019.

[163] J. B. Wooten, J. I. Seeman, and M. R. Hajaligol. Observation and characterization of cellulose pyrolysis intermediates by 13c CPMAS NMR. a new mechanistic model. *Energy & Fuels*, 18(1):1–15, 2004. doi:10.1021/ef0300601.

[164] M. Orain, P. Baranger, B. Rossow, and F. Grisch. Fluorescence spectroscopy of naphthalene at high temperatures and pressures: implications for fuel-concentration measurements. *Applied Physics B*, 102(1):163–172, 2011. doi:10.1007/s00340-010-4353-7.

[165] H. Grosch, Z. Sárossy, H. Egsgaard, and A. Fateev. Uv absorption cross-sections of phenol and naphthalene at temperatures up to 500°c. *Journal of Quantitative Spectroscopy and Radiative Transfer*, 156:17–23, 2015. doi:10.1016/j.jqsrt.2015.01.021.

[166] A. Thöny and M. J. Rossi. Gas-phase uv spectroscopy of anthracene, xanthone, pyrene, 1-bromopyrene and 1,2,4-trichlorobenzene at elevated temperatures. *Journal of Photochemistry and Photobiology A: Chemistry*, 104(1):25–33, 1997. doi:10.1016/S1010-6030(96)04575-3.

[167] L. R. Allain, D. N. Stratis, B. M. Cullum, J. Mobley, M. R. Hajaligol, and T. Vo-Dinh. Real-time detection of pah mixtures in the vapor phase at high temperatures. *Journal of Analytical and Applied Pyrolysis*, 66(1):145–154, 2003. doi:10.1016/S0165-2370(02)00110-9.

[168] M. Hajaligol, B. Waymack, and D. Kellogg. Low temperature formation of aromatic hydrocarbon from pyrolysis of cellulosic materials. *Fuel*, 80(12):1799–1807, 2001. doi:10.1016/S0016-2361(01)00063-1.

[169] T. E. McGrath, W.G. Chan, and M. R. Hajaligol. Low temperature mechanism for the formation of polycyclic aromatic hydrocarbons from the pyrolysis of cellulose. *Journal of Analytical and Applied Pyrolysis*, 66(1):51–70, 2003. doi:10.1016/S0165-2370(02)00105-5.

[170] T. E. McGrath, J. B. Wooten, W. Geoffrey Chan, and M. R. Hajaligol. Formation of polycyclic aromatic hydrocarbons from tobacco: The link between low temperature residual solid (char) and PAH formation. *Food and Chemical Toxicology*, 45(6):1039–1050, 2007. doi:10.1016/j.fct.2006.12.010.

[171] A. Dieguez-Alonso, A. Funke, A. Anca-Couce, A. G. Rombolà, G. Ojeda, J. Bachmann, and F. Behrendt. Towards biochar and hydrochar engineering—influence of process conditions on surface physical and chemical properties, thermal stability, nutrient availability, toxicity and wettability. *Energies*, 11(3), 2018. doi:10.3390/en11030496.

[172] S. Hu, L. Jiang, Y. Wang, S. Su, L. Sun, B. Xu, L. He, and J. Xiang. Effects of inherent alkali and alkaline earth metallic species on biomass pyrolysis at different temperatures. *Bioresource Technology*, 192:23–30, 2015. doi:10.1016/j.biortech.2015.05.042.

[173] M. H. Shah, L. Deng, H. Bennadji, and E. M. Fisher. Pyrolysis of potassium-doped wood at the centimeter and submillimeter scales. *Energy & Fuels*, 29(11):7350–7357, 2015. doi:10.1021/acs.energyfuels.5b01776.

[174] H. Almuina-Villar, N. Lang, A. Anca-Couce, J. Röpcke, F. Behrendt, and A. Dieguez-Alonso. Application of laser-based diagnostics for characterization of the influence of inorganics on the slow pyrolysis of woody biomass. *Journal*

of Analytical and Applied Pyrolysis, 140:125–136, 2019. doi:10.1016/j.jaap.2019.03.004.

[175] P. Sommersacher, N. Kienzl, T. Brunner, and I. Obernberger. Simultaneous online determination of s, cl, k, na, zn, and pb release from a single particle during biomass combustion. part 1: Experimental setup–implementation and evaluation. *Energy & Fuels*, 29(10):6734–6746, 2015. doi:10.1021/acs.energyfuels.5b00621.

[176] P. Sommersacher, N. Kienzl, T. Brunner, and I. Obernberger. Simultaneous online determination of s, cl, k, na, zn, and pb release from a single particle during biomass combustion. part 2: Results from test runs with spruce and straw pellets. *Energy & Fuels*, 30(4):3428–3440, 2016. doi:10.1021/acs.energyfuels.5b02766.

[177] A. Demirbaş. Gaseous products from biomass by pyrolysis and gasification: effects of catalyst on hydrogen yield. *Energy Conversion and Management*, 43(7):897–909, 2002. doi:10.1016/S0196-8904(01)00080-2.

[178] H. Almuina-Villar, P. Sommersacher, S. Retschitzegger, A. Anca-Couce, and A. Dieguez-Alonso. Combined influence of inorganics and transport limitations on the pyrolytic behaviour of woody biomass. *Chemical Engineering Transactions*, 80:73–78, 2020. doi:10.3303/CET2080013.

[179] G. Caposciutti, H. Almuina-Villar, A. Dieguez-Alonso, T. Gruber, J. Kelz, U. Desideri, C. Hochenauer, R. Scharler, and A. Anca-Couce. Experimental investigation on biomass shrinking and swelling behaviour: Particles pyrolysis and wood logs combustion. *Biomass and Bioenergy*, 123:1–13, 2019. doi:10.1016/j.biombioe.2019.01.044.

[180] I.E. Gordon, L.S. Rothman, C. Hill, R.V. Kochanov, Y. Tan, P.F. Bernath, M. Birk, V. Boudon, A. Campargue, K.V. Chance, B.J. Drouin, J.-M. Flaud, R.R. Gamache, J.T. Hodges, D. Jacquemart, V.I. Perevalov, A. Perrin, K.P. Shine, M.-A.H. Smith, J. Tennyson, G.C. Toon, H. Tran, V.G. Tyuterev, A. Barbe, A.G. Császár, V.M. Devi, T. Furtenbacher, J.J. Harrison, J.-M. Hartmann, A. Jolly, T.J. Johnson, T. Karman, I. Kleiner, A.A. Kyuberis, J. Loos, O.M. Lyulin, S.T. Massie, S.N. Mikhailenko, N. Moazzen-Ahmadi, H.S.P. Müller, O.V. Naumenko, A.V. Nikitin, O.L. Polyansky, M. Rey, M. Rotger, S.W. Sharpe, K. Sung, E. Starikova, S.A. Tashkun, J. Vander Auwera, G. Wagner, J. Wilzewski, P. Wcisło, S. Yu, and E.J. Zak. The hitran2016 molecular spectroscopic database. *Journal of Quantitative Spectroscopy and Radiative Transfer*, 203:3–69, 2017. HITRAN2016 Special Issue. doi:10.1016/j.jqsrt.2017.06.038.

[181] J. Cho, J. M. Davis, and G. W. Huber. The intrinsic kinetics and heats of reactions for cellulose pyrolysis and char formation. *ChemSusChem*, 3(10):1162–1165, 2010. doi:10.1002/cssc.201000119.

[182] T. R. Carlson, J. Jae, Y.-C. Lin, G. A. Tompsett, and G. W. Huber. Catalytic fast pyrolysis of glucose with hzsm-5: The combined homogeneous and heterogeneous reactions. *Journal of Catalysis*, 270(1):110–124, 2010. doi:10.1016/j.jcat.2009.12.013.

[183] V. Gargiulo, P. Giudicianni, M. Alfè, and R. Ragucci. About the influence of doping approach on the alkali metal catalyzed slow pyrolysis of xylan. *Journal of Chemistry*, 2019:9392571, 2019. doi:10.1155/2019/9392571.

[184] Wen-Liang Wang, Xue-Yong Ren, Lu-Fei Li, Jian-Min Chang, Li-Ping Cai, and Jing Geng. Catalytic effect of metal chlorides on analytical pyrolysis of alkali lignin. *Fuel Processing Technology*, 134:345–351, 2015. doi:10.1016/j.fuproc.2015.02.015.

[185] T. Itoh. The evidence showing that the intersystem crossing yield of benzaldehyde vapour is unity. *Chemical Physics Letters*, 151(1):166–168, 1988. doi:10.1016/0009-2614(88)80089-7.

[186] N. Ohmori, T. Suzuki, and M. Ito. Why does intersystem crossing occur in isolated molecules of benzaldehyde, acetophenone, and benzophenone? *The Journal of Physical Chemistry*, 92(5):1086–1093, 1988. doi:10.1021/j100316a019.

[187] Z.-P. Lin and W. A. Aue. Gas-phase luminescence of aromatic carbonyl compounds in excited nitrogen at atmospheric pressure. *Canadian Journal of Chemistry*, 78(1):95–117, 2000. doi:10.1139/v99-203.

[188] A. M. Turek, G. Krishnamoorthy, K. Phipps, and J. Saltiel. Resolution of benzophenone delayed fluorescence and phosphorescence with compensation for thermal broadening. *The Journal of Physical Chemistry A*, 106(25):6044–6052, 2002. doi:10.1021/jp0200122.

[189] M. P. O'Sullivan and A. C. Testa. Fluorescence of aliphatic ketones. *Journal of the American Chemical Society*, 92(20):5842–5844, 1970. doi:10.1021/ja00723a005.

[190] C. Brackmann, J. Nygren, X. Bai, Z. Li, H. Bladh, B. Axelsson, I. Denbratt, L. Koopmans, P.-E. Bengtsson, and M. Aldén. Laser-induced fluorescence of formaldehyde in combustion using third harmonic nd:yag laser excitation. *Spectrochimica Acta Part A: Molecular and Biomolecular Spectroscopy*, 59(14):3347–3356, 2003. doi:10.1016/S1386-1425(03)00163-X.